Winter 12-21-2011

Living Radical Polymerization Catalysts: Synthesis, Application, and Utilization of Polymer Products in the Synthesis of Metal Nanoparticles

Sara E. Hayik
University of Pennsylvania, nsara@sas.upenn.edu

Living Radical Polymerization Catalysts: Synthesis, Application, and Utilization of Polymer Products in the Synthesis of Metal Nanoparticles

Abstract
Living Radical Polymerization Catalysts: Synthesis, Application, and Utilization of Polymer Products in the Synthesis of Metal Nanoparticles

Sara Elizabeth Hayik

Supervisor: Professor Bradford B. Wayland

Living radical polymerization techniques are powerful tools for prepared specialty polymer products used in applications from biotechnology to electronics. Development of catalysts for the different methods is important for increased versatility. The goals of this research were to develop new radical addition-fragmentation chain transfer (RAFT) and cobalt mediated radical polymerization (CMRP) catalysts and utilize polymers produced through controlled radical polymerization techniques for the synthesis of metal nanoparticles. Vanadium complexes were designed to mimic conventional RAFT chain transfer agents and tested in the polymerization of methylacrylate (MA) and styrene. These complexes proved unsuitable for use as RAFT catalysts. Several cobalt complexes, using salen and salen derivative ligands, were prepared and tested as CMRP catalysts for the polymerization of MA and vinyl acetate (VAc). (R,R)-N,N'-Bis(3,5-di-tert-butylsalicylidene)-1,2-cyclohexanediamino Cobalt (II) proved to be the most promising candidate for both polymers. MA was prepared with PDIs 1.32 and under while the VAc PDIs were under 1.50. In both cases, observations suggesting a controlled polymerization were reported. PDMAEMA synthesized using a RAFT polymerization was used to stabilize and control the formation of platinum, gold, and palladium nanoparticles. Protonation of the polymer chains using succinic acid or acidic metal complexes allowed for ionic cross-linking by the metal anions, which is observed through DLS analysis. Reduction of the metal complexes was then performed within the nanogel and the rapid stabilization by the polymer results in small well defined particles. Well defined particles were produced for each metal with different size ranges for each. Nanogel formation is critical mechanism for control in each system and was seen only in systems containing dianionic species

Degree Type
Dissertation

Degree Name
Doctor of Philosophy (PhD)

Graduate Group
Chemistry

First Advisor
Dr Bradford B. Wayland

Keywords
living radical polymerization, metal nanoparticles, polymerization, nanogel, LRP catalysts

Subject Categories
Inorganic Chemistry

LIVING RADICAL POLYMERIZATION CATALYSTS: SYNTHESIS, APPLICATION, AND UTILIZATION OF POLYMER PRODUCTS IN THE SYNTHESIS OF METAL NANOPARTICLES

Sara Elizabeth Hayik

A DISSERTATION

In

Chemistry

Presented to the Faculties of the University of Pennsylvania

In

Partial Fulfillment of the Requirements for the

Degree of Doctor of Philosophy

2011

Supervisor of Dissertation

_____

Bradford B. Wayland, Professor of Chemistry

Graduate Group Chairperson

_____

Gary A. Molander, Professor of Chemistry

Dissertation Committee

Larry G. Sneddon, Professor of Chemistry

Christopher Murray, Professor of Chemistry

So-Jung Park, Assistant Professor of Chemistry

LIVING RADICAL POLYMERIZATION CATALYSTS: SYNTHESIS, APPLICATION, AND UTILIZATION OF POLYMER PRODUCTS IN THE SYNTHESIS OF METAL NANOPARTICLES

Dedication

To my family and friends,

I would have never made it without you.

Acknowledgements

First I would like to thank my dissertation advisor Dr. Bradford Wayland. Dr. Wayland allowed me the freedom to grow as scientist, teacher and person. I am extremely grateful for his guidance throughout my graduate experience and for the introduction to a field in which I had no experience. Dr. Wayland provided me with the opportunity to find a path to teaching without which I would never have found what I believe is my true calling.

I would also like to thank Dr. Mike Fryd who provided both personal and scientific support. Mike introduced me to the world of nanotechnology and was always there to challenge my assumptions. Mike's optimism was always welcome in the face of unexpected results. This characteristic has forever changed my scientific viewpoint leading me down the path of how and why versus just looking at the whats.

I sincerely appreciate all of the time that my dissertation committee has given to my endeavor. Dr. Larry Sneddon, Dr. So-jung Park, and Dr. Chris Murray have all provided me with an excellent support system and have asked excellent and challenging questions. I would also like to thank Dr. Michael Therien who served on my committee in the early stages of my work.

The support staff of the University of Pennsylvania Chemistry department is superb. I would especially like to thank Bruce and Rico for always being there to fix the lab, move heavy items, or just for a talk. Mandy Swope provided an incredible amount of guidance as I planned these final few steps and without her I would have been helpless. Andre and Cong were always there to brighten my day on trips to the stockroom and Tommy Nguyen kept all of my teaching responsibilities in line.

Dr Susan Phillips provided me with incredible teaching freedom. I will forever be extremely grateful for this opportunity. I entered graduate school terrified of teaching and left a teacher. Sue's incredible support and trust gave me this confidence and completely changed my future.

I could not have asked for better classmates without whom I do not believe I could have made it through the trials and tribulations of the last few years. Dr. Dan Himmelberger, Dr. Julie

Aaron, Dr. Ian Farrell, Diana (Cabral) Challen provided me with some of my best times at Penn at lunches, Dining Days, Livestrong, and the many wonderful celebrations including my wedding. Dr Fernando Jove, Dr. Sounak Sarkar, and Dr Chi-How Peng were fantastic groupmates. I would also like to thank the members of the Sneddon group especially Ariane Perez-Gavilin and Emily Berkley, who provided me with both entertainment and help throughout my stay on the third floor. Jen Scricco welcomed me into the group and guided me in the infancy of my research. I would like to express my sincere gratitude to Amanda Kamps who performed the TEM imagining of my nanoparticle without which my work would not have been complete. I would also like to thank Amanda and Sean for all of the hours of nerd games. I would like to thank Dr. Andre Isaacs, Xi-Jun Chen, Rob Hickey, Dierdre Sandrock, Ben Dyme, and Daniell Reifsnyder for their friendship.

The love of chemistry does not begin in college so I would like to thank Mrs Teri Miller for introducing me to chemistry in high school. Mrs. Miller's excitement and wonderful teaching gave me the spark to further pursue the field. The opportunities I was given in high school were well beyond the expected and for that I am extremely grateful. I am also so appreciative of her patience since I know I was not always the best student.

Dr. Edward Rajaseelan took the spark and turned it into a flame during my time at Millersville University. I have never met a teacher who is his equal and I can only hope to someday be a fraction of what he was to me to my own students. Dr. R. saw in me what I did not see in myself and for that I am forever grateful.

I would like to thank my family who have always supported me. My in-laws Joe and Winnie have been supportive of both Seth and I throughout the graduate school process. A love of science, exploration, and science were seeded early in me by my Grandma Nichols, persistence seems to be a family trait handed down through my GrammyDoris, and all of my grandparents have provided unwavering support of my somewhat untraditional path. My parents, Sheila and Dave, may never have understood what I was doing scientifically but were always there for me in the ups and downs of graduate school. My brothers, Keith and Jeremy, never let

me get a big head but were always there especially Keith who saved me from so very many car disasters. Yes I am finally done with that paper everyone!

Finally I would like to thank Seth who has been the proofreader, the motivator, the sounding board, and every other niche I have needed filled. I know I have not always made it easy for him but I know I would have never made it this far without his patience, guidance, and most of all his love. I will also always appreciate him letting us get our three cats who have been ever so helpful writing my dissertation. Seth has always let me go with my crazy projects no matter the inconvenience, including the huge piles of dissertation materials all over the house. Seth and I have grown up as a couple together from awkward teenagers to what feels like an old married couple. We have come so far and made it through so much and I cannot wait to see what our future holds. Thank you, thank you, thank you!

Abstract

LIVING RADICAL POLYMERIZATION CATALYSTS: SYNTHESIS, APPLICATION, AND UTILIZATION OF POLYMER PRODUCTS IN THE SYNTHESIS OF METAL NANOPARTICLES

Sara Elizabeth Hayik

Supervisor: Professor Bradford B. Wayland

Living radical polymerization techniques are powerful tools for prepared specialty polymer products used in applications from biotechnology to electronics. Development of catalysts for the different methods is important for increased versatility. The goals of this research were to develop new radical addition-fragmentation chain transfer (RAFT) and cobalt mediated radical polymerization (CMRP) catalysts and utilize polymers produced through controlled radical polymerization techniques for the synthesis of metal nanoparticles. Vanadium complexes were designed to mimic conventional RAFT chain transfer agents and tested in the polymerization of methylacrylate (MA) and styrene. These complexes proved unsuitable for use as RAFT catalysts. Several cobalt complexes, using salen and salen derivative ligands, were prepared and tested as CMRP catalysts for the polymerization of MA and vinyl acetate (VAc). (R,R)-N,N'-Bis(3,5-di-tert-butylsalicylidene)-1,2-cyclohexanediamino Cobalt (II) proved to be the most promising candidate for both polymers. MA was prepared with PDIs 1.32 and under while the VAc PDIs were under 1.50. In both cases, observations suggesting a controlled polymerization were reported. PDMAEMA synthesized using a RAFT polymerization was used to stabilize and control the formation of platinum, gold, and palladium nanoparticles. Protonation of the polymer chains using succinic acid or acidic metal complexes allowed for ionic cross-linking by the metal anions, which is observed

through DLS analysis. Reduction of the metal complexes was then performed within the nanogel and the rapid stabilization by the polymer results in small well defined particles. Well defined particles were produced for each metal with different size ranges for each. Nanogel formation is critical mechanism for control in each system and was seen only in systems containing dianionic species

Table of Contents

List of Tables

List of Figures

List of Schemes

Chapter 1 - A Summary of Living Radical Polymerization (LRP) Mechanisms, Catalysts, and Applications

1.1 Introduction

Research in living polymerization stretches back to the 1950's when Szwarc discovered living anionic polymerization[1-4]. For more than a decade Szwarc's technique was the only known living process. However, since the mid-1970's advancements in controlled polymerization have resulted in the development of a variety of processes. Interest in Living Radical Polymerization (LRP) has surged recently due to increased demand for polymers with well-defined properties. Polymers with narrow molecular weight distribution (M_w/M_n), incorporation of interesting functional groups, and exotic structures have been synthesized utilizing LRP. This level of control allows for the design of novel polymers for use in the fields of medicine[1], nanotechnology[5], and biochemistry[6, 7]. The desire for the application of this process to a wide variety of systems has led to the development of several different approaches to LRP including atom transfer radical polymerization (ATRP), reversible addition-fragmentation chain transfer (RAFT), nitroxide-mediated polymerization (NMP), and cobalt-mediated radical polymerization (CMRP). All of these processes address the limitations of free radical polymerization, low control of molecular weight distribution and structure, and serve to complement each other by providing techniques for a wide variety of conditions.

1.1.1 Free Radical Polymerization

Free radical polymerization is one of the most important commercial processes for the synthesis of high molecular weight polymers[8-10]. Several factors are responsible for the technique's leading role in industrial synthesis of polymers: functional group tolerance in both the solvent and monomer, adaptability to a wide range of reaction conditions, simplicity and low cost compared to other techniques, and the ability to polymerize diverse monomers[9, 11, 12]. Conversely, conventional free radical polymerization has significant limitations as well: low control over molecular weight distribution, inability to produce low molecular weight polymers, poor control over macromolecule architecture, and lack of control over copolymer composition[11]. Radical polymerization is characterized by three distinct processes: initiation, propagation, and termination, Scheme 1. 1[9, 13]. Initiation in free radical polymerization is generally performed

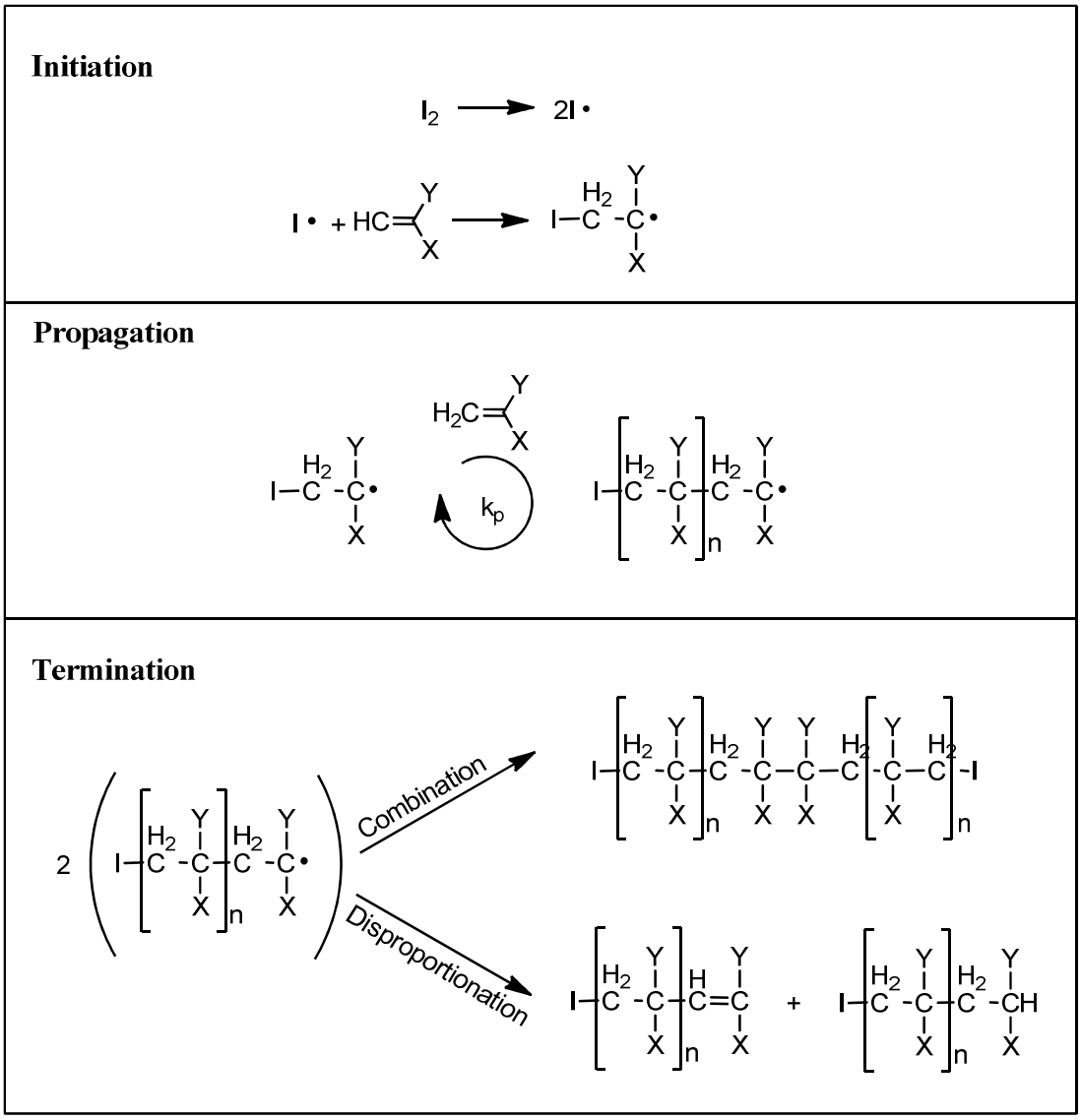

Scheme 1. 1 - Free Radical Polymerization General Mechanism

through the formation of primary radicals by either thermal or photochemical decomposition[14].

The choice of initiator will depend on monomer, solvent, and temperature[14]. Traditionally polymers are considered to form in an exclusively head-to-tail formation as is indicated in general polymer formulas $(CH_2CXY)_n$. However, the materials produced in the manner have physical properties that vary significantly from polymers prepared from other methods such as ionic polymerization. These behavioral differences indicate that the general polymer formulas do not provide sufficient information to predict physical properties of the materials. Initiators play a crucial role in the formation of the polymer chain and also determine the endgroups that will be present in some of the chains[14], therefore, playing a major role in the ultimate physical characteristics of the material. The initiation phase in free radical polymerization, Scheme 1. 1, is comprised of two steps. The first is the homolytic cleavage of the initiator through homolysis or photolysis. Second, the primary radical forms an initiating radical through combination with a monomer unit.

While the initiation step of the polymerization appears to be very simplistic, the production of initiating radicals is governed by a complex set of interactions between the primary radicals and their environment. Generally the efficiency of any given initiator is thought to be the fraction of the radicals produced that escape the solvent cage and can proceed to participate in the polymerization reaction[14]. This takes into account the radicals lost in the production of byproducts through reaction of the radicals with themselves, in some instances this will result in the reformation of the initiator which will not create byproducts but will reduce the rate of radical generation. However, this view does not take into account the loss of primary radicals due to other side reactions. For each monomer, the initiator is chosen to minimize the most common side-reactions, Scheme 1. 2; abstraction, aromatic substitution, and β-scission resulting in the formation of secondary radicals[14]. This will also determine the amount of tail or head addition that will occur. These factors can then be utilized to tailor the product and minimize formation of undesirable byproducts. Other factors influencing the fate of the radicals during the initiation stage are the solvent and temperature of the system. Introduction of solvent to a polymerization

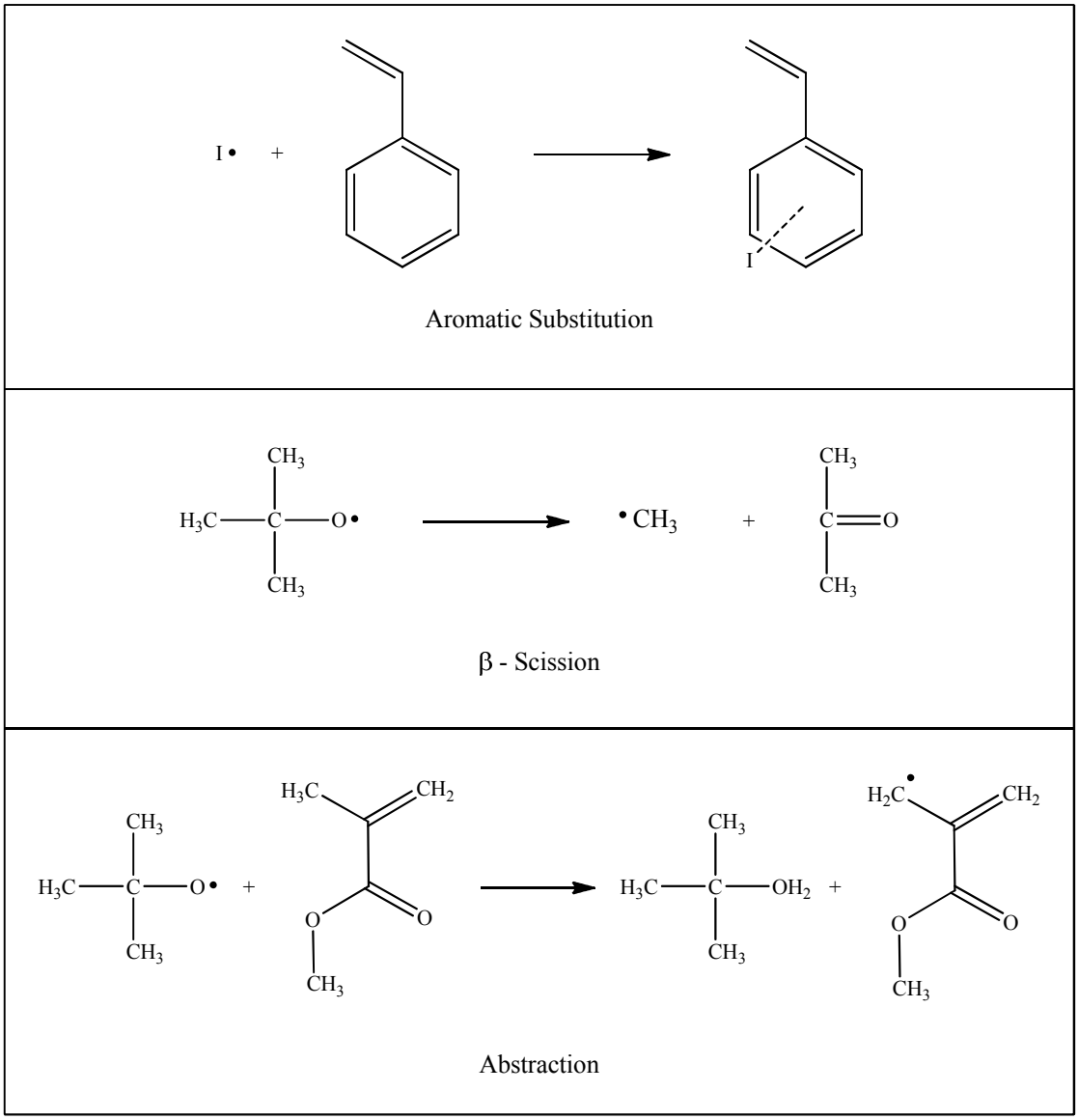

Scheme 1. 2 - Common Free Radical Side Reactions

system will result in lower viscosity which will decrease the importance of the cage reactions, the radical can escape the cage more easily at lower viscosities, but, it can also lead to the formation of solvent rather than monomer derived radicals, altering the final composition and physical properties of the material[14]. Cage effects as well as the importance of the different side reactions are greatly influenced by the temperature of the system. Increasing the temperature of the system will improve the ability of the radical to exit the solvent cage improving the efficiency. However, higher temperatures can also favor side-reactions that form detrimental products.

Once the initiating radical is successfully formed, the radical will enter the propagation stage. Through addition of monomer to the propagating radical, radical polymer chains are formed[15]. Head-to-tail addition is most favored but all other additions are also likely to occur, Scheme 1. 3[12, 14, 15]. Adding to the complexity of the formation of the polymer chain, 1,1- di or monosubstituted monomers can form stereoisomers as they add to the chain[16]. Each propagating radical typically begins in a sp^2 configuration and is therefore achiral[12]. Addition of the monomer unit will determine the configuration and the tacticity of the polymer. Tacticity of the polymer is most commonly determined experimentally through proton NMR since the chemical shift will be affected by the two neighboring monomer units[16]. This allows for the determination of the ratio of possible triads (mm, rr, or mr) to be calculated. Monomer structure can play a role in the tacticity of the polymer product, typically radical polymerization produces an excess of syndiotactic groups, however, monomers with bulky substituents favor isotactic formation[14, 16]. Propagation rates (k_p) vary greatly between monomers and is affected by the polymer chain length. Overall, monomers with hydrogen as the α-substituent tend to have significantly larger k_ps than those with other types of substituents. Within monomer groups of similar substituent type, those with large activation energies (E_a) show low rates of propagation due to the increased stability of the propagating radicals[14]. Certain monomers, eg. HEMA and MAA, have proven to be solvent and concentration dependent which indicates there is a significant effect from inter and intramolecular hydrogen-bonding. This process will continue until termination of the chains occurs. Traditionally, the k_p is considered independent of polymer chain length, however, evidence points to a significant

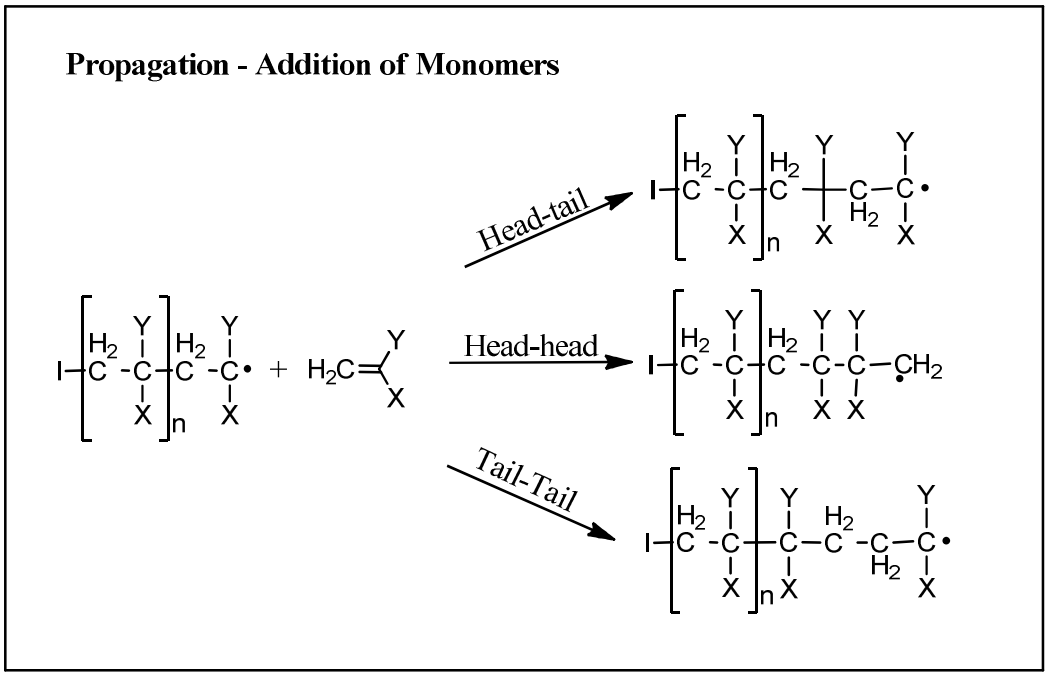

Scheme 1. 3 - Mechanisms of Addition of Monomers to Polymer Chain

difference between overall k_p and the calculated rate of small radical reactions with monomers. As the polymer chain grows the radical end will become buried within the polymer coil, resulting in the radical contacting monomer molecules less often, therefore, the effective monomer concentration for the radical is lowered. This will effectively lower the k_p since the monomer-radical interaction occurs less frequently.

Combination and disproportionation, Scheme 1. 1, are the two main routes of irreversible radical termination[9, 13, 15]. Both of these processes involve reactions between two polymer chain radicals. Combination occurs when two polymer radicals or a polymer radical and an initiator derived radical, Scheme 1. 4, combine to create a single polymer chain. In the disproprotionation mechanism, one polymer radical abstracts a hydrogen from the second leaving one chain terminated with a vinyl endgroup and the second with alkane[13]. Minimization of the termination mechanism is achieved by controlling the reaction conditions in order to make radical propagation more favorable than termination. Viscosity of the medium is extremely important in determining the rate of termination (k_t); as it increases, the ability of the radical ends to come together decreases lowering the k_t[17]. High viscosity systems create an environment where the radical ends, which are generally buried within the polymer coil, diffuse more slowly through the reaction medium greatly increasing the time it will require to meet another radical end[9]. Alternatively, inhibition of the polymerization reaction can be responsible for the deactivation of propagating radicals. Species which act as inhibitors are typically low molecular weight molecules that form stable radical species, stable radicals, and transition metal salts[14]. Combination of propagating radicals or initiator derived species deactivate the radicals and in the case of the propagating radicals forming dead polymer chains, Scheme 1. 4. All of these processes remove radicals from the polymerization system limiting chain growth and only through minimization of k_t and inhibition will propagation continue producing more higher molecular weight polymer chains.

During free radical polymerization there is no control of the propagating or initiator derived radicals. Propagating radicals are extremely short lived, generally about 5-10 seconds[10],

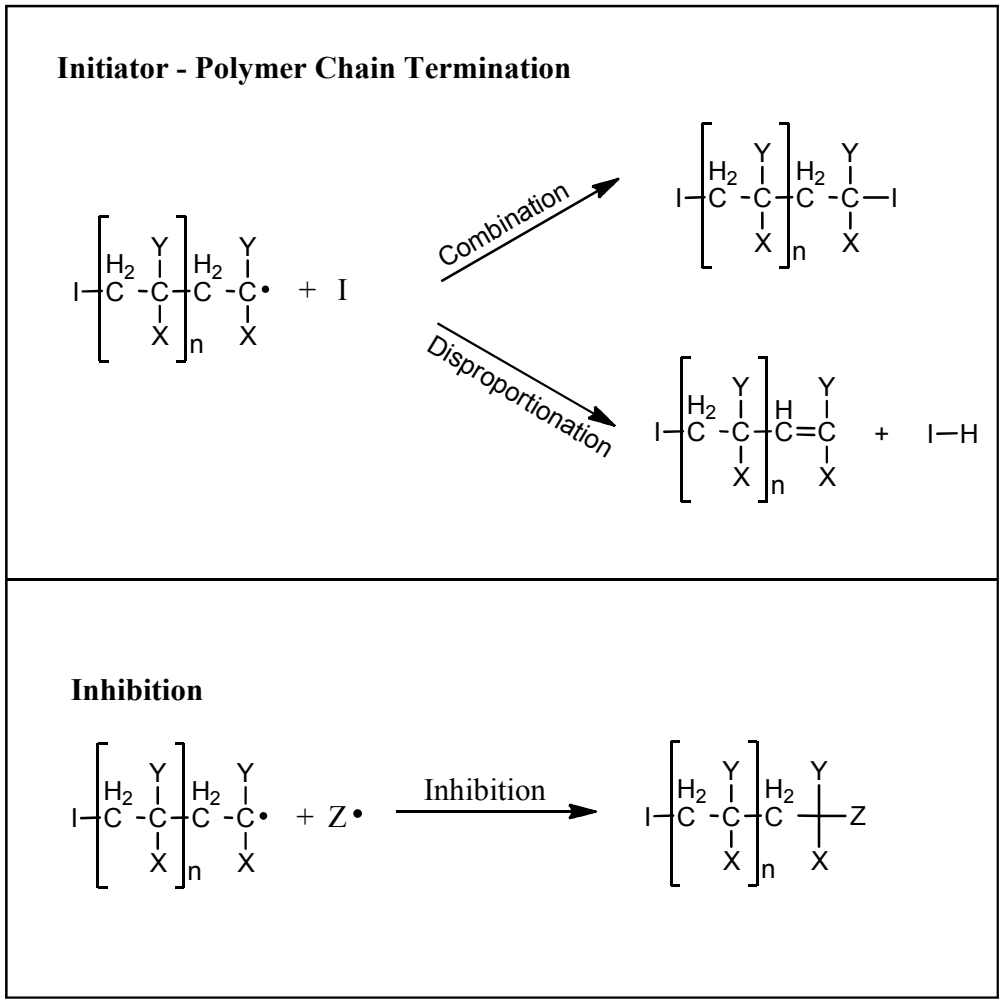

Scheme 1. 4 - Initiator Termination and Inhibition Mechanisms

and occur in low concentration, typically about 10^{-7}M, in these processes[10]; therefore, throughout the entire polymerization, chains are being formed, terminated, and propagated. This results in a wide range of molecular weights within the material and random orientation of the monomer units within the chain greatly affecting the physical properties of the polymer produced. Conversely, in idealized living radical polymerization first all of the chains are initiated, then propagate at the same rate, survive the entire polymerization, and can begin the propagation stage again with the addition of more monomers,[9, 10] resulting in narrow molecular weight distributions and provides well defined polymer structures including the ability to synthesize block copolymers and quantitative retention of end-groups. Polymers synthesized in this manner can be tailored for each application to obtain materials with very specific physical properties.

1.1.2 Degenerative Transfer (DT) and Reversible Termination (RT)

Central to the LRP processes are DT and RT[18, 19]. The different synthetic methods can be divided roughly into mechanisms that either utilize DT or RT as the key to the living character of the system[18]. In both systems, a dormant species is used as storage for the latent propagating radicals[19]. For a radical polymerization to be "living" in character, a dynamic equilibrium between propagating radicals and dormant species must exist. LRP techniques take advantage of the ability of certain species to reversibly deactivate propagating radicals[18]. Through deactivation, only a very small quantity of active radicals are ever present in the system allowing for controlled growth of the polymer chains[9]. Both mechanisms rely on the storage of propagating radicals in a dormant species, these radicals have a relatively fast interchange with the radicals from the solution.

The RT mechanism is differentiated from the DT pathway by the radical source and control of the propagating radicals[19], Scheme 1. 5 A[18, 20, 21]. RT relies exclusively on the dormant complex for its radical source[20]. The process occurs by either homolytic dissociation, Scheme 1. 5 A.1, or atom transfer, Scheme 1. 5 A.2, depending on the particular polymerization method[21]. A virtually constant low concentration of propagating radicals is maintained by a quasi-equilibria

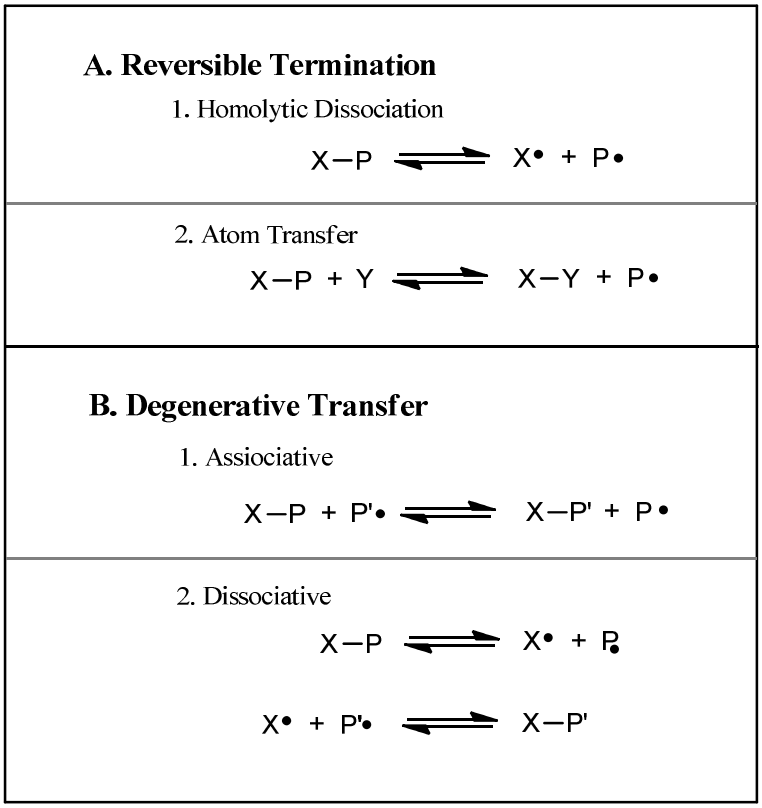

Scheme 1. 5 - RT and DT Mechanisms

between freely diffusing radicals and the latent radicals in the dormant species[12]. This concentration will slowly decline as small amounts of the propagating radicals irreversibly terminate. The disproportionately small bimolecular termination rate results in radicals, both in the dormant and freely diffusing species, with exceptionally long lifespan; this process is known as the persistent radical effect (PRE)[20, 22, 23] and the control of the radicals by the dormant complex contributes to the living character of the polymerization.

DT processes are distinguished by the injection of radicals from an external source, such as azo initiators V-70 and AIBN[19]. A continual influx of radicals is injected into the system by initiators, Scheme 1. 5 B. This is the main source of radicals in the system so the radical concentration is almost entirely determined by the decay rate of the initiator. Therefore, varying the initiator is a source of control for the polymerization since there is a wide range of decay rates for commercially available initiators. During the DT mechanism, monomers are initiated by radicals from the external radical source. These radicals then exchange with the latent radicals in the dormant complex[15, 19]. This interchange between the active and dormant species is what makes this a degenerative process. DT occurs when propagating radicals in solution interchange with the latent radical in the dormant complex. While this exchange is typically associative[19], Scheme 1. 5 B.1, it also occur through a two step dissociative process[19], Scheme 1. 5 B.2. The latent and propagating radical should only differ by their chain lengths. Therefore, the exchange process approaches degeneracy, $\Delta G^{\circ} \approx 0$, and the equilibrium constant nears unity. The concentration of radicals is almost entirely determined by the concentration of the external radical so the rate of entry into the solution and the rate of termination of the radicals determine the amount of radicals in the system at any given time. Radical concentrations and polymerization rates approach those of uncontrolled free radical polymerization. Therefore, the PRE cannot contribute to the living character in DT processes.

1.1.3 Role of RT and DT Processes in the Living Character of Radical Polymerization

Living character in the RT process results from the PRE[12, 20, 22]. When a stable chemical species binds reversibly with a propagating radical, the concentration of the radicals is controlled by the dormant species. Each dormant complex is capable of releasing the latent radical for

further growth of the polymer chain[12, 15]. This process extends the lifetime of a propagating radical from the second timescale in a typical free radical polymerization to the ability to restart a polymerization reaction by the addition of monomer to a dormant species after several days[20]. The ability to continue polymerization in this manner is the "living" character of the polymerization. During the reaction, any radicals that are terminated will reduce the number of living radicals since they are not held within the dormant complex the chain can no longer grow[21]. Therefore, in a RT process the living character fraction at any time during the reaction is determined by the ratio of the dormant complex at time, t, to the initial concentration of dormant complexes.

DT processes do not rely on the PRE since the rate of the radical interchange in this mechanism is many times faster than that found in RT[12, 19, 24]. Instead the dormant complex is the main source of the living character of this process. Radicals from both the dormant complex and the external radical source play a role in the DT mechanism. During this process, the dormant complex concentration remains but the number of growing polymer chains is equivalent to the initial number of latent radicals in the dormant complex as well as the number of radicals in the solution which are initiated by the external radical source[19, 24]. For the radicals to be considered "living" in this system the latent radicals in the dormant complex must enter the solution, propagate with monomers, and return to the dormant complex repeatedly throughout the polymerization reaction[15, 25]. By injecting radicals from an external source new radicals will interchange with the latent radicals in the dormant complex[24]. Introduction of these radicals to the solution allows for termination of the radical. Thus, the number of fully living radicals will decrease with the introduction of radicals from the external source. Therefore, it is imperative that the minimum amount of radicals from the external source are injected to maintain the maximum number of fully living chains. As a DT process RAFT polymerizations generally call for a ratio of radicals injected from an external source to latent radicals in the initial dormant complex to be approximately 1 to 10. This ensures that at least 90% of the latent radicals in the initial complex should survive in the dormant complex after the radicals driving the polymerization process fully terminate. However, it has been demonstrated that even at larger ratios of external radicals to the dormant complex a majority of the monomer radicals end up in the latent living

polymer chains in the dormant complex. In this study, methyl acrylate (MA) polymerization is mediated by the Co(TMP) complex. The external radical source is V-70 and the ratio of external radicals released into solution to dormant species is approximately one to one[19, 26]. Observations from this study indicate that while there are two polymer chains possible for each dormant complex, the experimental number average molecular weight approaches the expected value for one living chain per cobalt center and low polydispersity (PDI)[19]. This indicates that the majority of the living radical chains are stored as latent radicals in the dormant species[19]. Preferential propagation of the larger latent chains occurs and termination appears to be predominantly restricted to the small initiator derived radicals.

1.2 Nitroxide-mediated Polymerization (NMP)

The discovery of the ability of nitroxides to control polymerizations was an product of experiments by David H. Solomon as an outgrowth of radical trapping experiments[27]. Initially, 2,2,6,6-tetramethylpiperidinyl-1-oxy (TEMPO) was used to trap carbon centered radials in order to study the mechanism of the initiation step of free radical polymerization reactions[11]. TEMPO was chosen since alkoxyamines are known inhibitors of polymerization and are used as polymer stabilizers[27]. Therefore, the addition of the TEMPO molecule to the carbon centered radical will result in a stable molecule that cannot react further effectively trapping the radical. TEMPO is also ideal since the combination occurs at diffusion-controlled rates ensuring that the radicals will be trapped in the initiation stage prior to further progress in the polymerization reaction.

Solomon continued to develop various alkoxyamines as radical trapping agents and experiments indicated that with appropriate molecular structure dissociation can occur, resulting in low molecular weight oligomers[11]. The first description of the NMP process is found in Solomon's 1984 patent[28] which describes several nitroxides and alkoxyamines behavior in producing oligomers and the possibility of creating conditions that would lead to polymerization. While the idea of NMP had been described at this point low molecular weight polymers had yet to be produced via this method. Indeed until the work of Michael K. Georges in 1993, very little progress was made in developing this process.

Georges was able to utilize the NMP technique to synthesize polystyrene with a relatively low polydispersity using nitroxides as the stable free radical[29]. In this work, TEMPO was used as the nitroxide and benzyl peroxide (BPO) as the initiator. The benefits of using TEMPO as the stabile free radical are weaker bonds with the propagating styrene chains than iniferters, promotion of the dissociation of peroxide initiators, and the fact that they are free radical inhibitors[11]. Weak bonds with the propagating styrene chains will allow for the dissociation of the styrene chain from the TEMPO molecule allowing for further polymerization to occur, increased peroxide dissociation will promote initiation of polymer chains at the same time and inhibition of free radicals lowers the chance of initiation of chains late in the polymerization process. All of these behaviors help promote the formation of low polydispersity products.

1.2.1 Importance of Nitroxide Structure

Nitroxides and alkoxyoxides with a wide variety of structures have been studied to ascertain their ability for application in NMP. Using both experimental and theoretical work, some generalizations can be made regarding the correlation between structure and behavior of these molecules.[14] Using the general mechanism shown in Scheme 1. 6, different structural components can be analyzed according to their impact on the mechanism. When analyzing the mechanism shown in Scheme 1. 6 it is apparent that the environment around the C-O bond of the deactivated species will be crucial for determining the lability of the bond[14, 30]. This environment is determined by the nitroxide being utilized for the reactions. Several key factors will determine this environment including steric[30, 31], fragment polarity[30], radical stability[30], and available hydrogen bonding[14]. Each of the prior aspects can be looked at to determine the impact on activation and deactivation processes of the mechanism.

Looking that the steric influences it is apparent that increasing the steric hindrance around the C-O bond will cause a weakening increasing the activation rate of the mechanism[31]. This occurs due to the repulsions caused by the increased number of atoms around the C-O

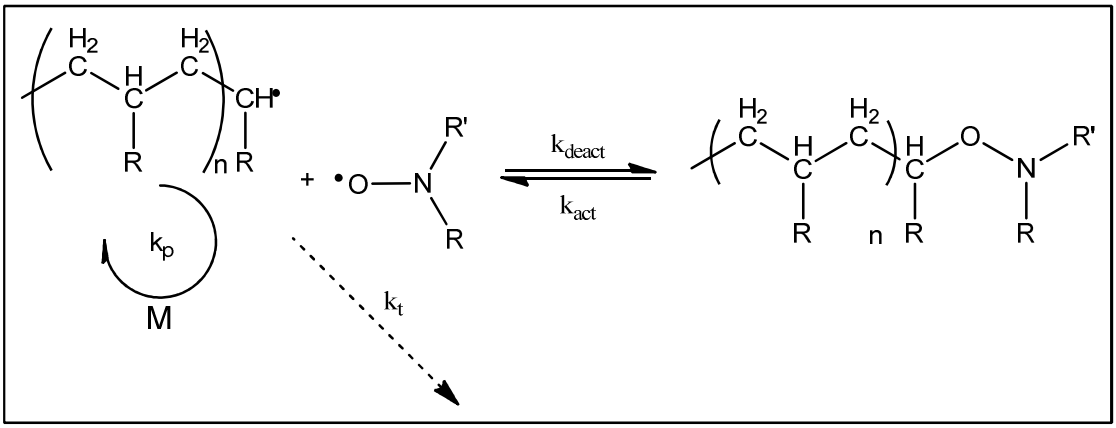

Scheme 1. 6 - General NMP Mechanism

bond from the nitroxide species which will decrease the stability of the molecule formed through the bonding of the two radicals[30].

Radical stability can play a major role in the rate of activation versus deactivation and this effect is seen more greatly in secondary and tertiary nitroxides. When the activation process occurs C-O bond homolysis of the deactivated species is observed resulting in the formation of two radical species. The stability of these radicals then determines the rate at which the deactivation process will progress since the more stable the radical the longer the possible lifespan[30]. Nitroxides are extremely stable free radicals as exemplified by their ability to act as stabilizers for polymers[11]. As a stabilizer, the radical must have a long lifespan so that they may trap any other radicals that are introduced to the system and may cause adverse effects. From this behavior, it is apparent that the rate of deactivation should be very high with increased radical stability since the persistent radical will immediately react when it encounters another appropriate radical species[30]. In the case of nitroxides, the ideal radical species are carbon centered like those found in polymerization reactions.

Groups on the fragments can contribute greatly to the polarity affecting the strength of the C-O bond being formed in the deactivation process. Electron withdrawing groups on either fragment weaken the bond which in turn favors disproportionation and increases the activation rate[30, 32]. If instead electron donating groups are present, the opposite influence on the rate is expected. Another factor which concerns the identity of the groups on the fragments, is the contribution from hydrogen bonding between the nitroxide radical and the polymer radical. If there are hydroxyl groups on one of the fragments hydrogen bonding is then possible between the oxygen and the hydrogen atoms present in the molecules[14]. Hydrogen bonding will increase the stability of the deactivated species therefore decreasing the activation rate for the mechanism.

All of the factors described indicate the importance of the structure of both the monomer and nitroxide radicals. Figure 1. 1 shows a the structure of a variety of representative nitroxide molecules that have been studied to determine the rates of activation and deactivation. In this table, several properties are being shown. Each column represents increasing numbers of

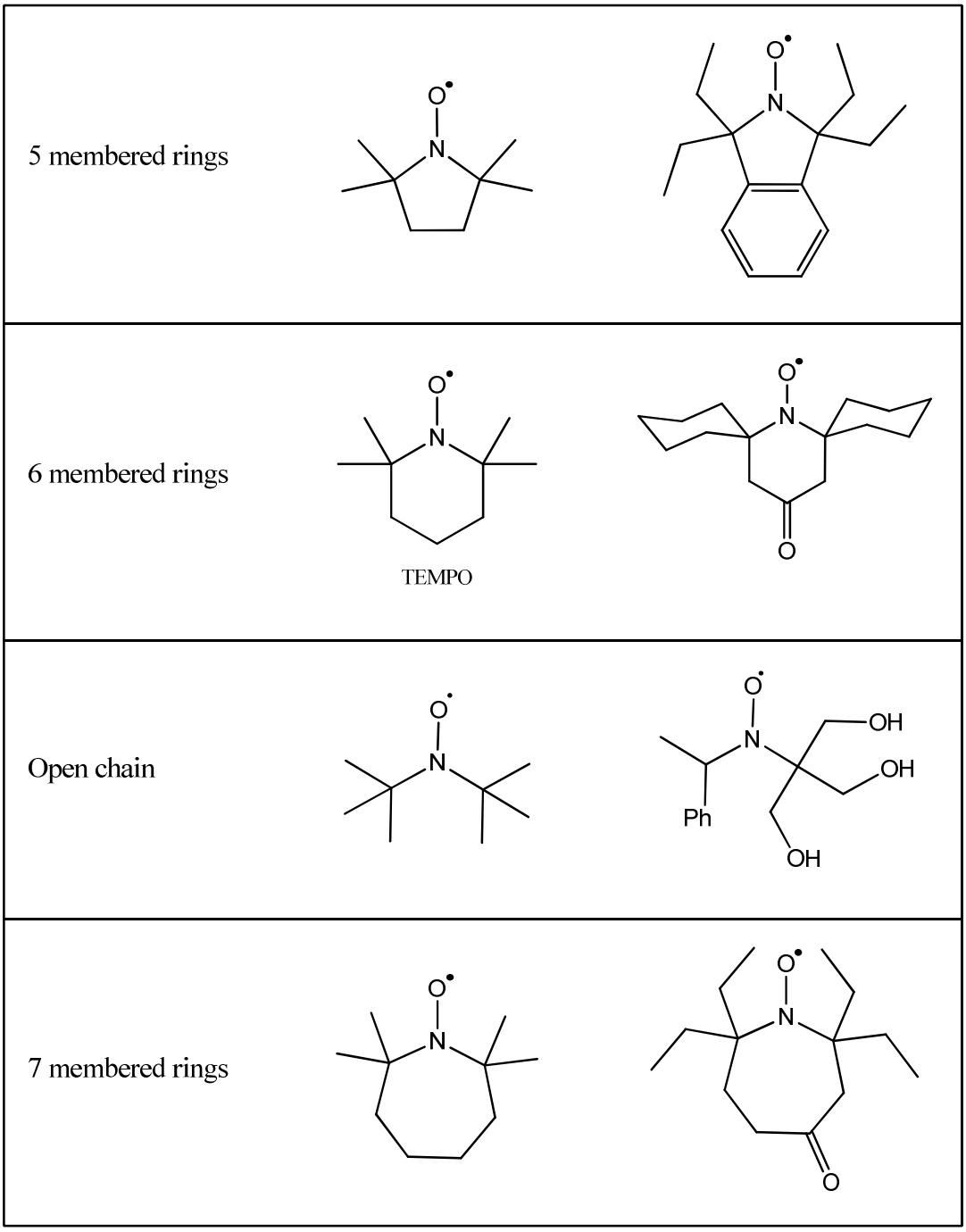

Figure 1. 1 - Nitroxides for the NMP Method

carbon atoms within the ring containing the nitroxide moiety. The third row is an exception and shows two open chain molecules. In the first column of structures, only the number of atoms in the ring are changing between the molecules while there is less similarity between the structures shown in the second column. Looking at the rows in Figure 1. 1, the first molecule is less complex and less sterically hindered than the second in each row. Rate of activation is seen to increase with increasing carbon number and moving down the first column where this is the only variable it has been experimentally determined to follow this trend. The open chain is placed in increasing rate of activation as well in this table[14, 31]. If the rates of activation are compared across the rows shown in Figure 1. 1, an increase is expected for all but the open chain row. In each of these cases, the sterics around the nitroxide moiety are increased which generally increases the rate of activation by weakening the C-O bond[14]. The open chain row is expected to be an exception due to the 3 hydroxide groups which are present, since these groups can form hydrogen bonds the increase in the rate of activation from the increased steric bulk may be offset by the decrease due to hydrogen bonding. Given the available factors which can be tuned on the nitroxide radical, it is possible to synthesize specialized compounds in order to optimize the rate of activation for the monomer being utilized.

1.2.2 NMP Mechanism

Discussion of the mechanism which drives NMP must be focused on its central kinetic mechanism the persistent radical effect (PRE)[20, 22, 23, 33]. As mentioned in Section 1.1.2, the PRE relies on small amounts of radicals existing at all times through homolytic dissociation of dormant species into stable radicals which can then interchange allowing for polymer growth. For the initiation of polymerization in the NMP method unimolecular initiators allow for detailed identification of the initiation species and concentration calculations[33, 34]. Development of initiator molecules focused on the chain end functional group, an alkoxyamine[28], which is seen in dormant species found in reactions utilizing bimolecular initiator species. Addition of small organic groups, which form stable radicals, to nitroxides such as those shown in Figure 1. 1, results in alkoxyamine derivatives with weak C-O bonds between the two groups. During the initiation step,

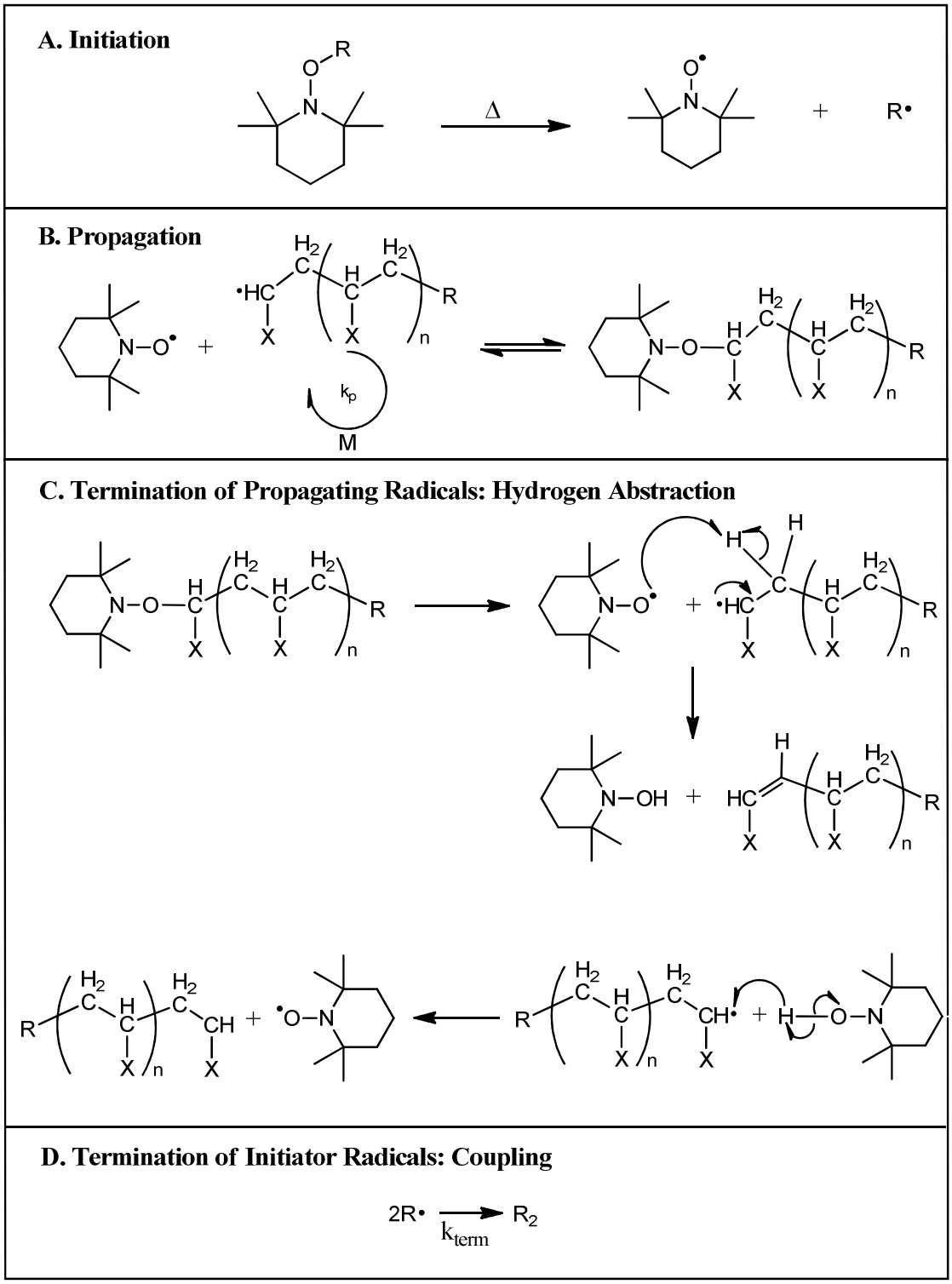

Scheme 1. 7 - Detailed NMP Mechanism

shown in Scheme 1. 7A, the weak C-O bond is homolytically cleaved through the addition of thermal energy resulting in two radical species[33, 34]. Throughout the polymerization the nitroxyl radical is considered the mediating radical, which will form the dormant species through the creation of a weak carboxyamine linkage with polymer chain radicals resulting in the living characteristic of the system. After the formation of the primary radicals from the initiator species, several fates are available and their likelihood is dependent on the degree of polymerization which has already occurred in the reaction mixture. Early in the reaction, facile movement of the radical species occurs allowing for radical-radical coupling, Scheme 1. 7D, as a major termination mechanism for small radical or oligomers, resulting in the loss of two radicals[33, 34]. As the reaction progresses, the viscosity of the medium increases due to the growing polymer chain. This increased viscosity hinders the movement of the radicals which decreases the probability of loss of radicals through coupling, therefore, the greatest loss of propogating radicals is seen early in the reaction[33].

Ideally, the majority of the radicals formed from the thermolysis of the initiator in step A enter the propagation stage of the polymerization, Scheme 1. 7B. During the propagation stage an equilibrium is formed between the dormant species and the mediating and propagating radical pair. When the dormant molecule cleaves homolytically at the carboxyl group, the radical pair separates with the propagating radical entering into the polymerization step. Eventually the polymer radical chain encounters the mediating nitroxyl group and reforms the dormant molecule. The rate at which the equilibrium will occur is determined by the strength of the C-O bond as well as the stability of the radicals being formed. In order to have linear growth of the polymer chains resulting in a low PDI, the equilibrium must be balanced through appropriate choice of monomer and initiator to form a labial C-O bond that is still strong enough to form the dormant species on a regular basis[34].

Another fate of the radicals formed in the initiation and propagation steps of the polymerization, is hydrogen abstraction[14], Scheme 1. 7C. The result of this process is the termination of two growing polymer chains and loss of living behavior. Hydrogen abstraction can occur at any point during the polymerization or after the polymerization is completed resulting in

chain end degradation[33]. During this reaction the alkoxyamine chain end degrades into the nitroxyl and polymer radical species. The nitroxyl radical then abstracts a hydrogen from the polymer radical forming a hydroxylamine and a polymer chain with a C-C double bond as the end group[33]. At this point in the chain end degradation, the living character of one polymer chain is deactivated through loss of the mediating radical as the end group. At this point the dormant species is now the hydroxylamine where the O-H bond is labile and the molecule is reactive in further reactions. Within this system, the hydroxylamine interacts with another polymer chain, this time in the radical form. The hydrogen on the hydroxylamine is abstracted by the polymer radical reforming the nitroxyl radical and a saturated polymer chain[33]. While the mediating radical is regenerated another growing polymer chain is sacrificed decreasing the living character of the polymer system. This termination process is particularly important when considering graft and block copolymers since it can occur after the initial polymerization is halted resulting in polymer chains which are not receptive to another polymer being added to the chain.

1.2.3 Advantages of NMP

While NMP is not ideal in every instance and has weaknesses associated with the high temperatures required[33], long reaction times[33], inability to control methacrylate[34] and vinyl acetate based monomers, and failure to proceed to high conversion, it has proven advantageous in several regards. One of the most important benefits of NMP is the ability to synthesize polymers with very high purity[34]. Systems utilizing metal complexes for living polymerization have a high likelihood of being contaminated if the monomer is reactive with the metal incorporating the complex along the chain instead of as the chain end group[34]. For polymers which are intended to be used in medical or electronic applications, these impurities can be catastrophic. Therefore, the NMP method allows for the synthesis of these polymers without possible metal contamination making it extremely useful for these applications. Another area where NMP has proved extremely useful is in the preparation of polymers from 1,3-dienes[34]. Until recently, no other living polymerization technique was able to create homopolymer or block copolymers from this class of monomers making NMP essential for synthesis of these materials. NMP methods are generally simple preparations which is especially useful for the synthesis of polystyrene which has proved

relatively difficult with other living radical polymerization systems[31, 34]. This ease of has kept NMP as the preferential synthetic method for well defined polystyrene[34]. While no one single NMP system has proven useful for all monomer classes, increased variability should be able to be obtained in order to form different block or graft copolymers though reversible alteration of the nitroxyl group after the first polymerization is completed to create a suitable environment for the polymerization of a second dissimilar monomer. In many cases, other living polymerization methods are now becoming competitive in these areas however, NMP has been useful while these techniques have matured.

1.3 Atom Transfer Radical Polymerization (ATRP)

Initial reports of ATRP were published in 1995 by two groups both pursuing an extension of atom transfer radical addition (ATRA) which had been developed decades earlier[14, 35-38]. Development of ATRA to ATRP by mechanistic necessity focused in developing a system where the substrate radicals are similar in stability to the radicals formed initially by the transfer of a halide to a metal complex catalyst[14, 18]. In traditional ATRA, the substrate radical, formed through the reaction shown in Scheme 1. 8B, has low stability so the formation of the halogenated organic compound, step C in Scheme 1. 8, terminates the overall reaction[18]. In order for polymerization to progress, the monomer must instead form an equilibrium in step C and therefore, the stability of the substrate must be similar to the initial radical formed in step A of Scheme 1. 8[14, 18]. Using this approach initial reports by Sawamote in 1995 showed the use of ruthenium catalysts[39] while Wang and Matyjaszweski utilized copper as catalysts[40, 41]. As research has progressed in this area of LRP several other transition metals[14, 42-46] have been explored but copper complexes have remained the most popular due to its immense versatility in use of monomers, solvents, and bulk reaction conditions[7, 18, 47]. ATRP is proving immensely useful due to the extensive tunability of the metal catalysts as well as reaction condition which allows a wide variety of polymers and copolymers to be synthesized from monomers with an extensive diversity of functional groups.

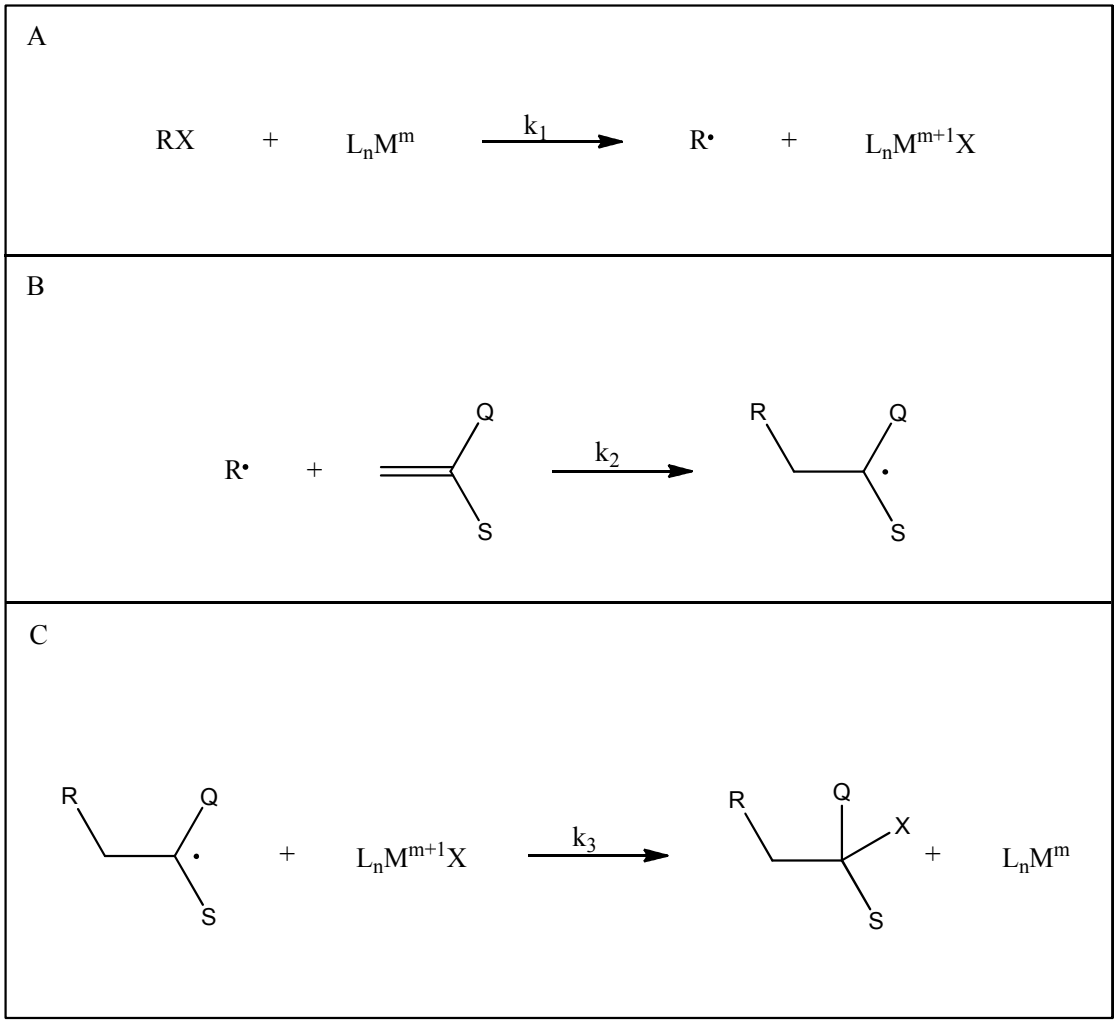

Scheme 1. 8- ATA Mechanism

1.3.1 Importance of Structures of Metal Catalysts

A multitude of transition metal complexes are used as catalysts for the ATRP process, examples shown in Figure 1. 2. The ligands used for these complexes are chosen in order to fulfill several requirements necessary for increased efficacy as an ATRP catalyst. Solubility is factor that is considered when determining which ligands to use on the metal center since the complex must be in solution for catalytic activity to occur[7, 18]. Often ligands with large nonpolar groups are necessary in order to solubilize the transition metal catalysts in the nonpolar reaction medium that is typically necessary for the polymerization reaction[18]. While the solubility of the metal complex is important, the effect of the ligand on the reducing power of the metal must also be considered.

Examination of the ATRA mechanism indicates the importance of the redox potential of the catalyst since a change of oxidation state is observed in halogenation and dehalogenation of the metal complex, steps A and C in Scheme 1. 8[46]. Changes in the redox potential through use of different ligands affects the activity of the catalyst and the rate of activation and deactivation of the propagating radical[14]. Increases in activity are observed when the high oxidation species is stabilized through ligand effects since the dormant complex is less favored allowing the polymerization to proceed for longer periods[7, 48]. Ligand geometry plays a significant role in the activity of the metal catalyst since different oxidation states favor different geometries[7, 12, 48]. Therefore, if the ligand geometry is similar to the favored geometry of that oxidation state the complex is stabilized.

Several other ligand features show trends of increasing catalyst activity when considering the most common copper based catalysts. In the case of multidentate ligands, activity is seen to increase when going from bi- to tri- to tetradentate ligand[7, 14]. Increasing the number of coordinated nitrogen groups is also associated with an increase in the activity of the species[12, 14]. If the electron donating ability increases, the activity is seen to increase even further[18, 49-51]. Utilizing structural features of the ligands coordinated to the transition metal allows for the

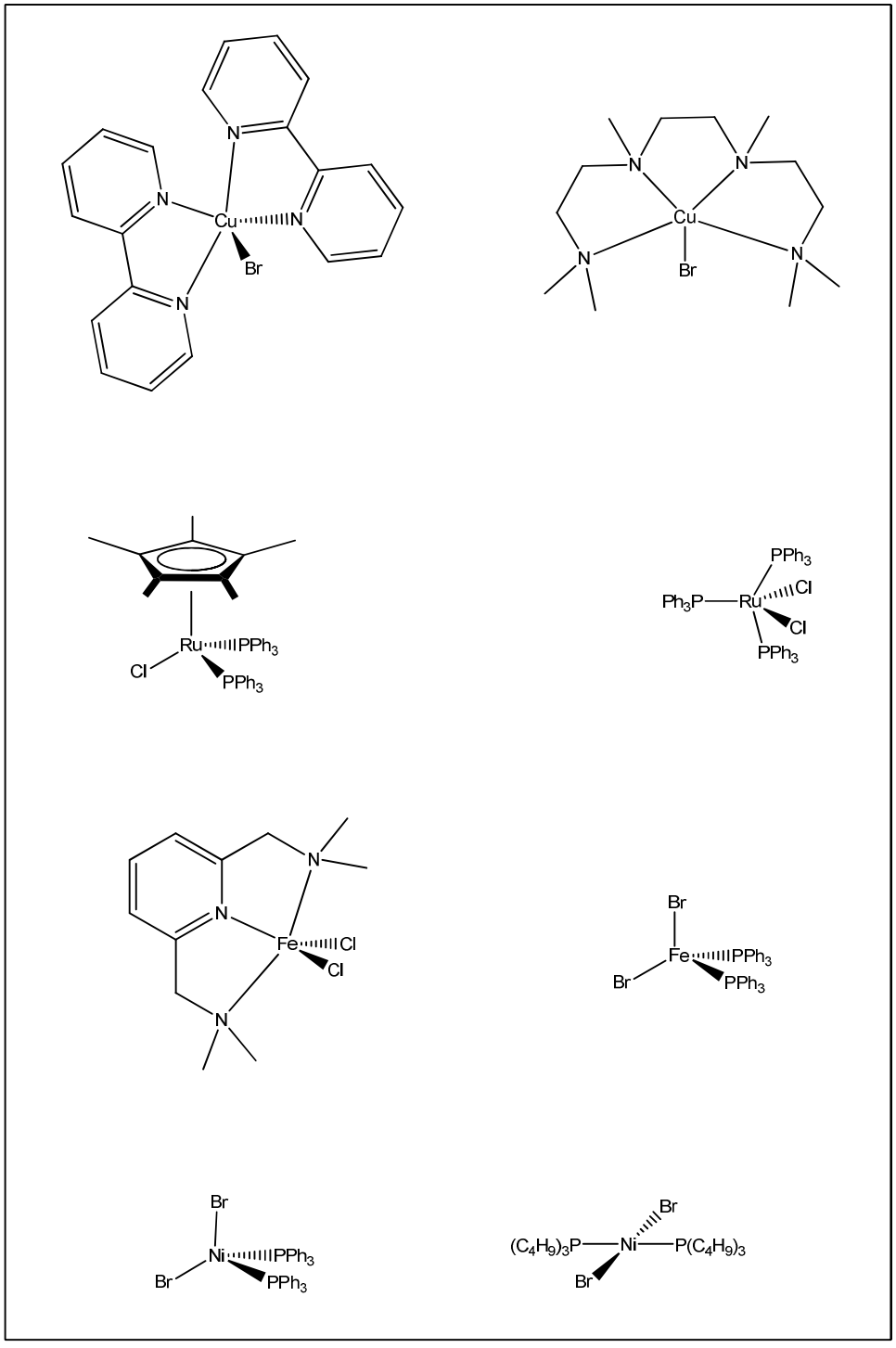

Figure 1. 2 - Examples of ATRP Catalysts

application of ATRP to many monomer systems since the stability of the active species can be tuned to match the stability of the propagating species.

1.3.2 ATRP Mechanism

The main feature of ATRP is the formation of dormant and active transition metal complexes through one electron inner sphere transfers at the metal center. In these reactions, an alkyl halide is chosen as the initiator[12]. Ideally, an initiator similar in structure to the monomer being used is chosen as shown in steps A and B of Scheme 1. 9[14, 47]. This structural similarity ensures that the R-X bond is of similar strength in the dormant species as in the initiator so that the rates of radical formation are similar and the radical is not trapped in the dormant species permanently[7, 18]. The first step of the initiation, step A of Scheme 1. 9, is the one electron transfer from the activated organo halide through halogenation of the metal complex, at this point the complex is considered to be activated and the initial radical is formed[7, 12, 14, 18, 47]. Formation of the propagating radical occurs through the addition of the initiator radical to a monomer unit, step B in Scheme 1. 9.

At this point, the propagating radical can progress through several pathways, the first is continued propagation resulting in the formation of a polymer chain as shown in Scheme 1. 9 C. The propagating radical can also enter the dormant complex through the deactivation process show in step D in Scheme 1. 9[14, 46]. This deactivation cannot be permanent if the polymerization is considered living, rather, an equilibrium is formed where the propagating radical is reformed along with the activated form of the transition metal catalyst[14, 46]. Ideally, the equilibrium will lie to the left resulting in the radicals spending more time in the dormant form than propagating[18, 46]. However, the exchange should be facile and in consequence the radical should be formed often but only for short periods[7]. In this manner, all of the chains, the number of which is determined by the number of organohalides initially used and any side reaction which may occur, grow at an equal rate producing a polymer product with a low PDI. If instead, the equilibrium were more to the right, each radical chain would have an extended time in the propagation stage. When this is the case, the product becomes more similar to uncontrolled free radical polymerization where

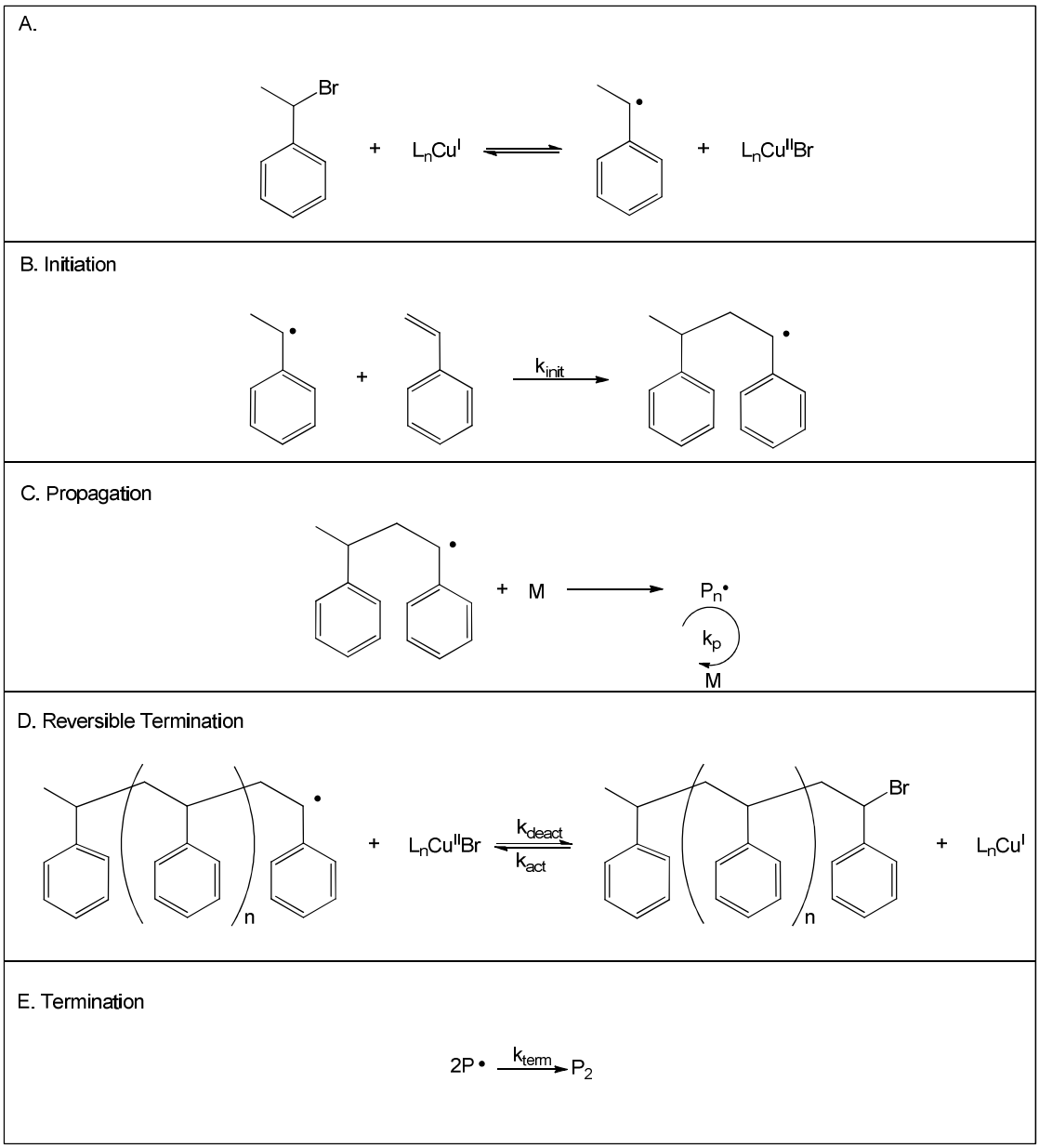

Scheme 1. 9 - ATRP Mechanism

lack of control leads to a poorly defined high PDI product. Conversely, if the equilibrium lies to much towards the dormant complex, exchange is drastically decreased and the polymerization is either dramatically slowed or halted. The final mechanistic fate of the propagating radicals is termination, step E of Scheme 1. 9. Generally in ATRP, the main termination route is through combination of two propagating radical chains[18]. Most often termination occurs early in the polymerization resulting in a higher molecular weight than expected because the termination of these chains lowers the number of growing radicals throughout the rest of the synthesis.

1.3.3 Benefits of ATRP

ATRP is an extremely versatile LRP system and can be used for almost all monomers that can be polymerized through free radical polymerization if the appropriate conditions are chosen[7, 48]. There are classes of monomers that ATRP is not well suited for, monomers with low reactivity and acrylics[18, 48]. The latter monomers prove difficult to polymerize with transition metal catalysts because of the reactivity with the metal centers forming metal carboxylates[18]. This complex will inhibit the formation of the active ATRP catalyst and remove the metal complex from the polymerization. One major benefit of ATRP is the formation of the halogenated polymer chains at the conclusion of the polymerization, this activated end group allows for easy synthesis of graft and block copolymers[12, 14]. The largest concern with use of ATRP is the removal of the metal catalyst. In many applications, even very small quantities of metal are not tolerated, therefore, removal methods are essential. Some complexes, especially those utilizing iron, are removed fairly easily however, for most catalysts this proves difficult and can make the method unsuitable[49]. ATRP is extremely useful due to the ease of changing conditions for use with different monomers, ease of reaction procedure, and availability catalysts and initiators.

1.4 Reversible Addition-fragementation Chain Transfer (RAFT)

In 1998 Charmot at Rhodia Chimie developed the macro-molecular design via interchange of xanthates (MADIX) technique[52] while Rizzardo at the CSIRO Institute proposed the RAFT process[21]. Both of these techniques are based on identical transfer processes[53, 54] and since RAFT is a more general term and applies to a variety of chain transfer agents it has become the general term for this type of transfer[54, 55]. The wide range of agents available in

RAFT allows for the control of a broader range of monomers than MADIX; for example, MADIX chain transfer agents are not able to control acrylate or styrene type monomers[55-57] but narrow molecular weight distribution products can be synthesized with RAFT[21, 55].

1.4.1 Importance of Chain Transfer Agent Structure

RAFT is a DT process and therefore, relies entirely on the initiator for the injection of primary radicals[10, 47, 54, 58]. The chain transfer agents (CTA) utilized in RAFT polymerizations are typically thiocarbonylthio complexes[8, 10, 11, 14, 21, 53, 54, 58-63] or xanthates in the case of the MADIX class polymerizations[14, 53]. The general formula for these molecules, Figure 1. 3, indicates Z as the activating group and R as the leaving group. Activation of the C-S double bond is strongly impacted by the Z group which will greatly influence k_{add}[10, 53]. An increase in k_{add} can be achieved by utilizing Z substituents with π orbitals, which stabilize the radical through resonance, or electron withdrawing groups, since radical attacks are typically nucleophilic[58]. Alternately, groups with high steric bulk can increase the k_{add}, however, this can also lower the transfer activity of the CTA[54]. Increased activation of the C-S double bond will increase the k_{add} to the point where it is competitive with k_p[54]. With increasing k_{add} the intermediate radical will become stabilized lowering the rate of fragmentation (k_β)[10]. Stabilization of the intermediate radical can occur to the extent where radical lifetimes become significant and cause retardation of the k_p[12, 59].

The R substituent of the CTA has little impact on the k_{add}[54, 59, 64], but plays a crucial role in k_β, since a weak S-R bond will favor fragmentation of the intermediate radical as well as the ability to reinitiate the polymerization[53, 58]. Leaving group ability can be improved in several ways: increased steric hindrance, inclusion of electron withdrawing groups, and radical stabilization of the R substituent[53, 54]. Direct weakening of the S-R bond will occur with the first two conditions and for the third condition, fragmentation to a stabilized radical will be favorable. Therefore, R substituents which form stable radicals after fragmentation will have an increased k_β so the

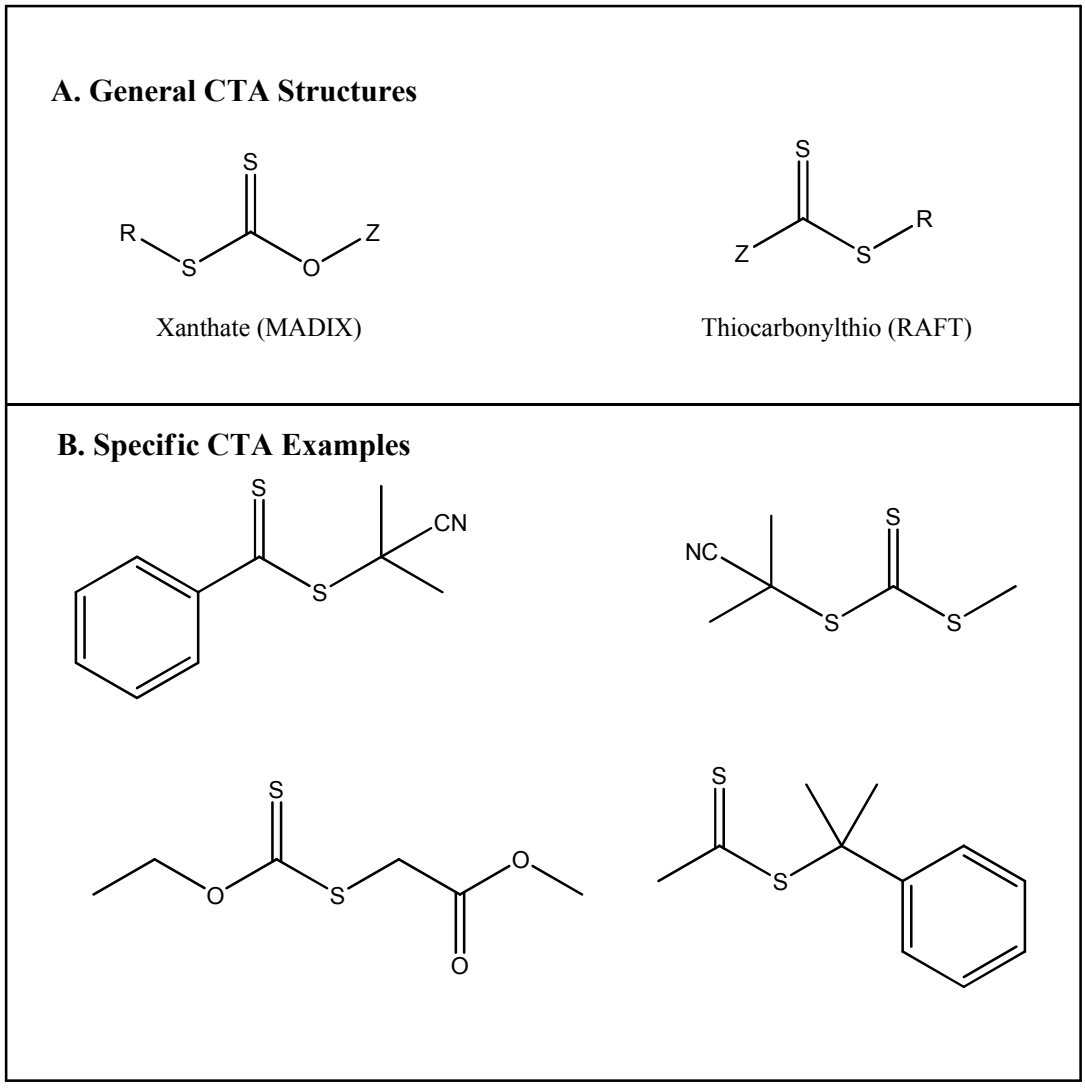

Figure 1. 3 - Chain Transfer Agent Structures

ordering for preferred fragmentation will be tertiary>secondary>primary radical formation[54, 64]. Once the R substituent has fragmented from the CTA, it is necessary for the radical to reinitiate the polymerization[8, 10, 64, 65], therefore, some groups which are excellent stable radicals will not be suitable R groups, eg. triphenylmethyl[53, 59].

The ability to tune the R and Z substituents of the CTA gives the RAFT polymerization mechanism its incredible flexibility and ability to mediate an extensive variety of monomers[8, 55, 59, 63]. Monomers which form extremely stable radicals can be countered by increasing the activation of the C-S double bond through tuning use of a stabilizing Z substituent, whereas monomers which form less stable radicals can be mediated with a less activated C-S double bond that will prevent the intermediated radical from being overly stabilized[8]. Tuning the C-R bond confers the ability to create a bond that will be more easily fragmented than the P_n-S bond formed through the addition of the propagating radical to the thiocarbonyl bond in the CTA. This ensures fragmentation of the appropriate unit during the chain transfer. Through appropriate tuning of the R and Z substituents in this manner the RAFT CTA can be tuned to be used with an extremely wide variety of monomers.

1.4.2 RAFT Mechanism

Mechanistically the RAFT process is identical to conventional free radical polymerization in both the initiation and termination steps[8, 10, 14, 54], Scheme 1. 10 A and E, and is considered a DT process dues to the use of external radicals[12, 47, 66], however, the propagation route is modified by the addition of the CTA, Scheme 1. 10 B, C, and D. Addition of the propagating radical (P_n •) to the activated C-S double bond of the CTA is the first step of the mediation of the polymerization, Scheme 1. 10 A[8, 60, 64]. This process results in the formation of an intermediate radial (IR) that is stabilized by the Z substituent on the CTA[54, 58, 64]. Assuming that the IR is not overly stabilized and the S-R bond is weaker than the S-P_n bond, the IR will proceed through the fragmentation step resulting in the polymeric CTA dormant species and a radical (R •) being released into the bulk[8, 12, 53, 60]. Stabilization of R • will promote the fragmentation step of the chain transfer, however, R • must still be able to reinitiate the polymerization step[10, 58, 64].

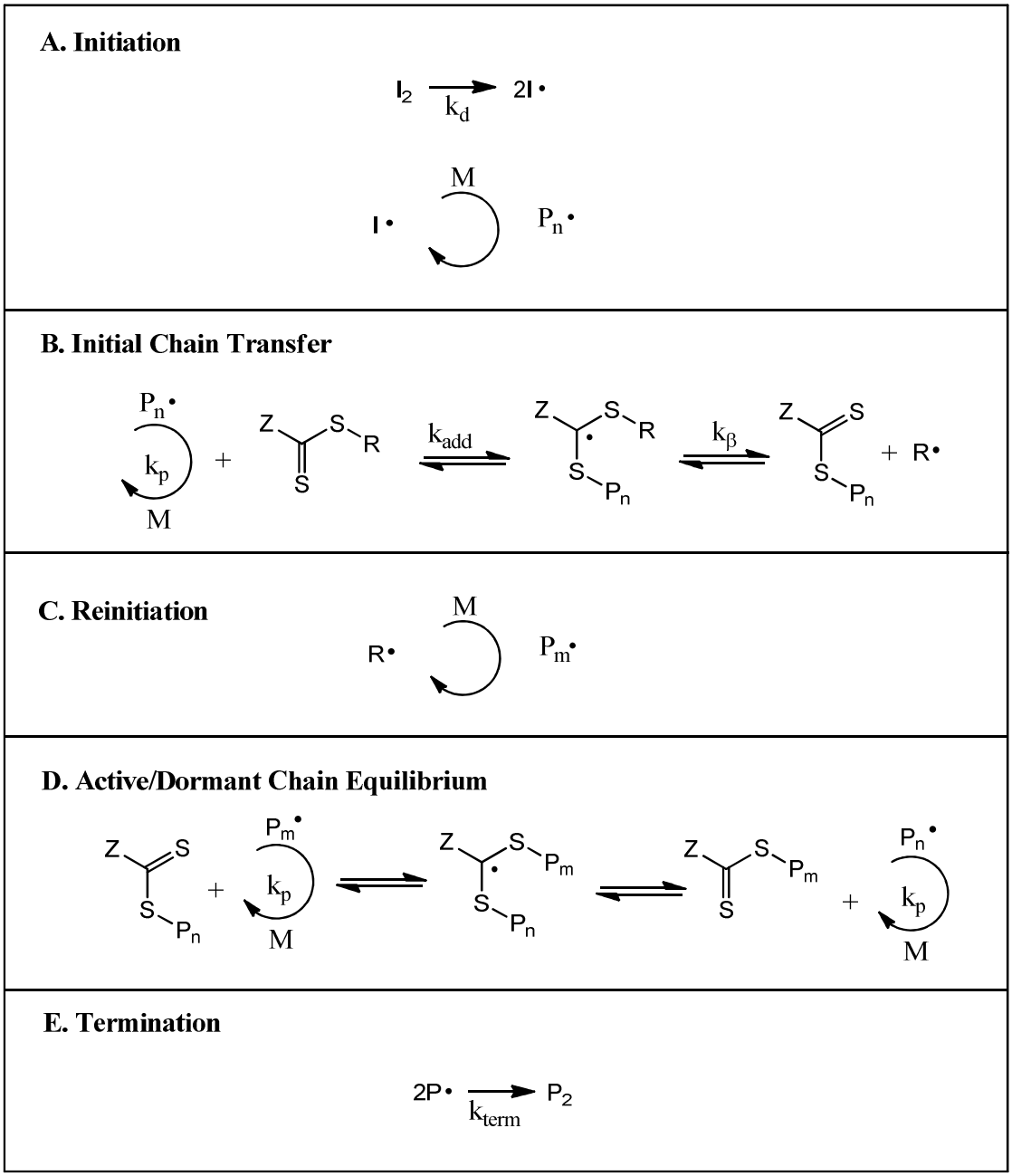

Scheme 1. 10 - RAFT Polymerization Mechanism

Reinitiation, Scheme 1. 10 C, occurs when the R• interacts with the monomer to produce polymeric propagating radicals (P_m•); the P_m• then adds to the activated C-S double bond of the polymeric CTA, Scheme 1. 10 D[64]. Formation of the intermediate with the two polymeric groups then results in the active/dormant chain equilibrium process[8, 53, 64]. Fragmentation of the intermediate radical into the dormant species and the active propagating polymer chain is approximately equally likely for both P_n and P_m resulting in equal probability of growth and creating a linear relationship between molecular weight and percent conversion[8, 11, 58]. Minimization of propagating radical termination is necessary to maintain the living character of the system. If for instance, the active/dormant chain transfer constant (k_{tr}) is slow, them some propagating radical will spend a significant amount of time in the bulk increasing the likelihood of interactions with other radicals in a termination process while others maintain their bond to the CTA in the dormant species. Therefore, the equilibrium rate must approach or exceed that of propagation in order to ensure that only a few monomers are added to the propagating radical in each cycle providing each chain with a similar rate of growth[53, 54]. Further reduction of the termination mechanism can be obtained by lowering the concentration of the initiator species relative to the CTA[10, 54]. This diminishes the concentration of active radicals since the initiator is the solitary free radical source. By lowering the amount of free radical available the termination mechanism is further suppressed. Equal growth of the propagating chain combined with lowered termination rates and the ability of the CTA to maintain the radical in the dormant complex lend RAFT its living character

1.4.3 Advantages of RAFT

While all LRP mechanisms provide improvements over conventional free radical polymerization in areas such as low molecular weight distributions, the ability to predict molecular weights and the ability to restart the polymerization through the dormant species, RAFT has several unique advantages[14, 59]. Tunability of the CTA, through the R and Z substituents, allows for an increased tolerance to a variety of monomers, solvents, and conditions increasing the versatility of the process to well beyond typical LRP techniques[21, 53, 55, 59]. RAFT polymerizations also are performed in a manner very similar to conventional free radical polymerizations.

Typically, the only change is the addition of the CTA which improves the commercial viability of the technique since it can be implemented fairly easily where polymers are already being synthesized[53]. Additionally, RAFT can be used to create polymers with complex molecular structures as well as synthesizing the polymers for use in the creation of complex superstructures, eg. brushes, stars, etc[8, 10, 53, 63]. These benefits of the RAFT technique provide a system that fills several niches where other LRP processes have proven inappropriate.

1.5 Cobalt-mediated Radical Polymerization (CMRP)

Use of cobalt complexes as LRP catalysts was first reported by two groups, Wayland[67] and Harwood[68], in 1994. Interest in organocobalt(II) complexes arose from their use as sources of carbon-centered radicals[25] in organic synthesis such as in equilibrium of the thermal isomerization of the B12 coenzyme[23, 69] as reported by Finke and Daikh. In these reactions, the critical features is the facile homolytic cleavage of the Co-C bond under relatively mild thermal or photolytic reaction conditions[69]. This behavior results in the persistent radical effect (PRE)[20, 22] which allows the cobalt complexes to act as radical sources for radical addition reactions[25, 69-71]. Modification of the catalysts used in typical organic reactions, cobalt porphyrin derivatives for Wayland's group[19, 24, 26, 67, 70, 72] and cobaloxime for Harwood's group[68], allows the systems to be used in polymerizations which can be considered successive radical addition reactions resulting in chain growth. Initiially, both groups focused on the polymerization of acrylates but further work has expanded to include acrylic acid[24], vinyl esters, and vinyl acetate[25, 71, 73], which has proven extremely difficult through other LRP methods. While this method is not extremely versatile[25], it is useful for monomers which are difficult to polymerize through other methods, proceeds at very low temperatures (0˚C to 60˚C)[24, 67, 71, 74], and provides excellent control even at high molecular weights.

1.5.1 Importance of Cobalt Complex Structure

In comparison to the other LRP methods described within this text, CMRP utilizes a very small number of metal complexes as possible catalysts. While Harwood's group employed

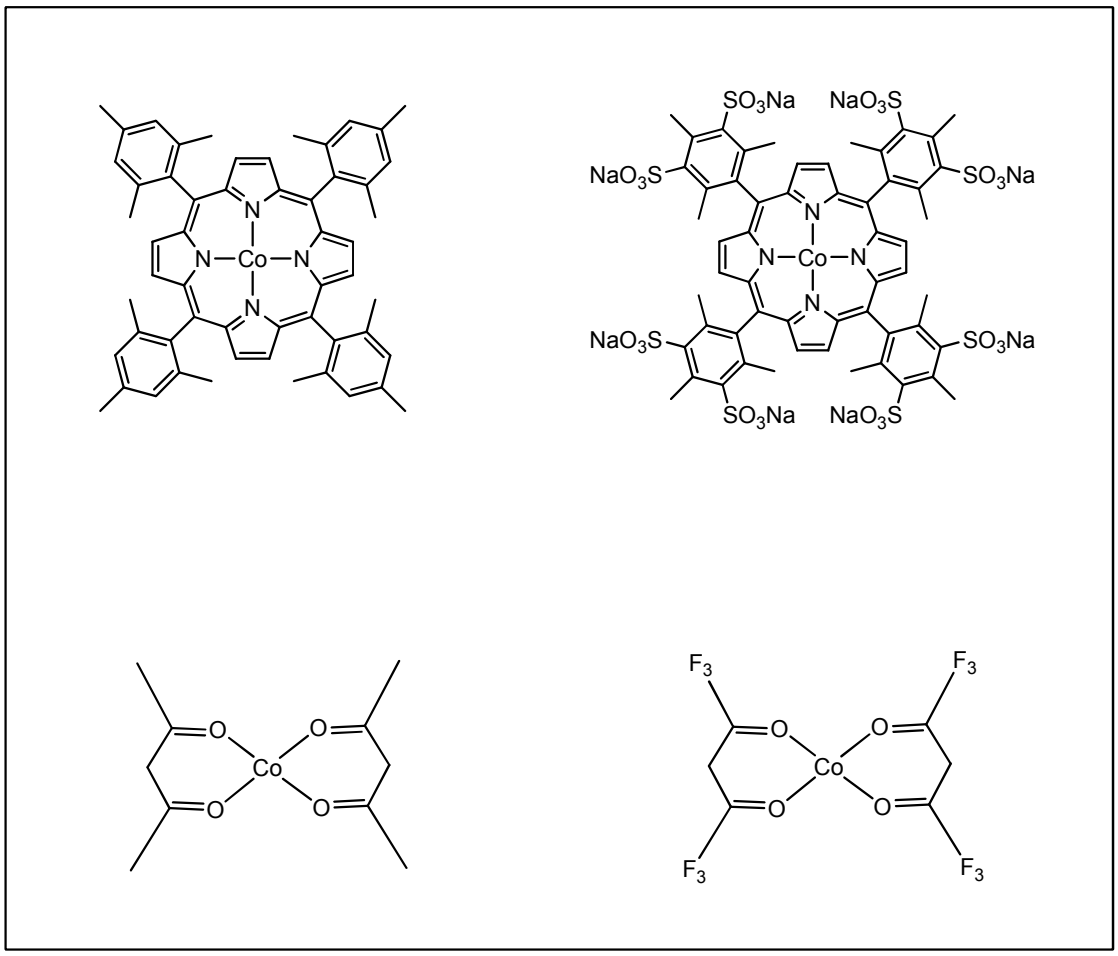

Figure 1. 4 - CMRP Catalyst Examples

cobaloximes[68] in their initial CMRP techniques the two major groups of catalysts were developed using porphyrin[19, 24, 26, 67, 70, 72] or acetylacetonate, by the Jérôme group[71], derivatives as shown in Figure 1. 4. One of the most important considerations for the development of appropriate catalysts for CMRP, is minimizing the incidence of catalytic chain transfer polymerization (CCTP)[25]. Cobalt (II) complexes within these families have proven effect as chain transfer catalysts due to their propensity to have dehaydrocobaltation during vinylation[25]. Structural changes to the ligands are the most efficient means to tip the balance to CMRP and away from CCTP.[69] Increasing the steric bulk of the ligand is shown to increase the tendency of CMRP since the H-abstraction pathway is blocked.

Another feature of these complexes is the ability to tune the ligands in order to modify the solubility of the complex . Two extremes of this functionality are shown in the porphyrin derivative complexes presented in Figure 1. 4. In the first example, Co(TMP) , the ligand is highly nonpolar and useful for reactions performed in nonpolar solvents, commonly benzene[19, 26, 70, 75]. The second molecule, Co(TMPS), is sulfonated in order to increase the polarity of the ligand this allows it to be used in polymerizations of monomers like acrylic acid which is performed in aqueous solution[24]. As well as tuning the ligand in order to alter the solubility of the species, the ligand may also be tuned to change the Co-C bond strength of the organoradical complexed to the catalyst. In order for the polymerization to be controlled, the propagating radical needs to spend a majority of its time in the dormant complex. However, if the bond Co-C bond is too strong facile homolytic cleavage is not observed and the radical is trapped in the dormant state[71, 74]. If this is the case, after all of the cobalt molecules have formed dormant complexes, the polymerization will continue uncontrolled since the catalyst is no longer active within the reaction[74]. Given the fact that different monomers form radicals of different strengths and stabilize the reduced cobalt compound differently ligands are chosen for the cobalt complex in order to provide bond dissociation energy in a range suitable for LRP to result.

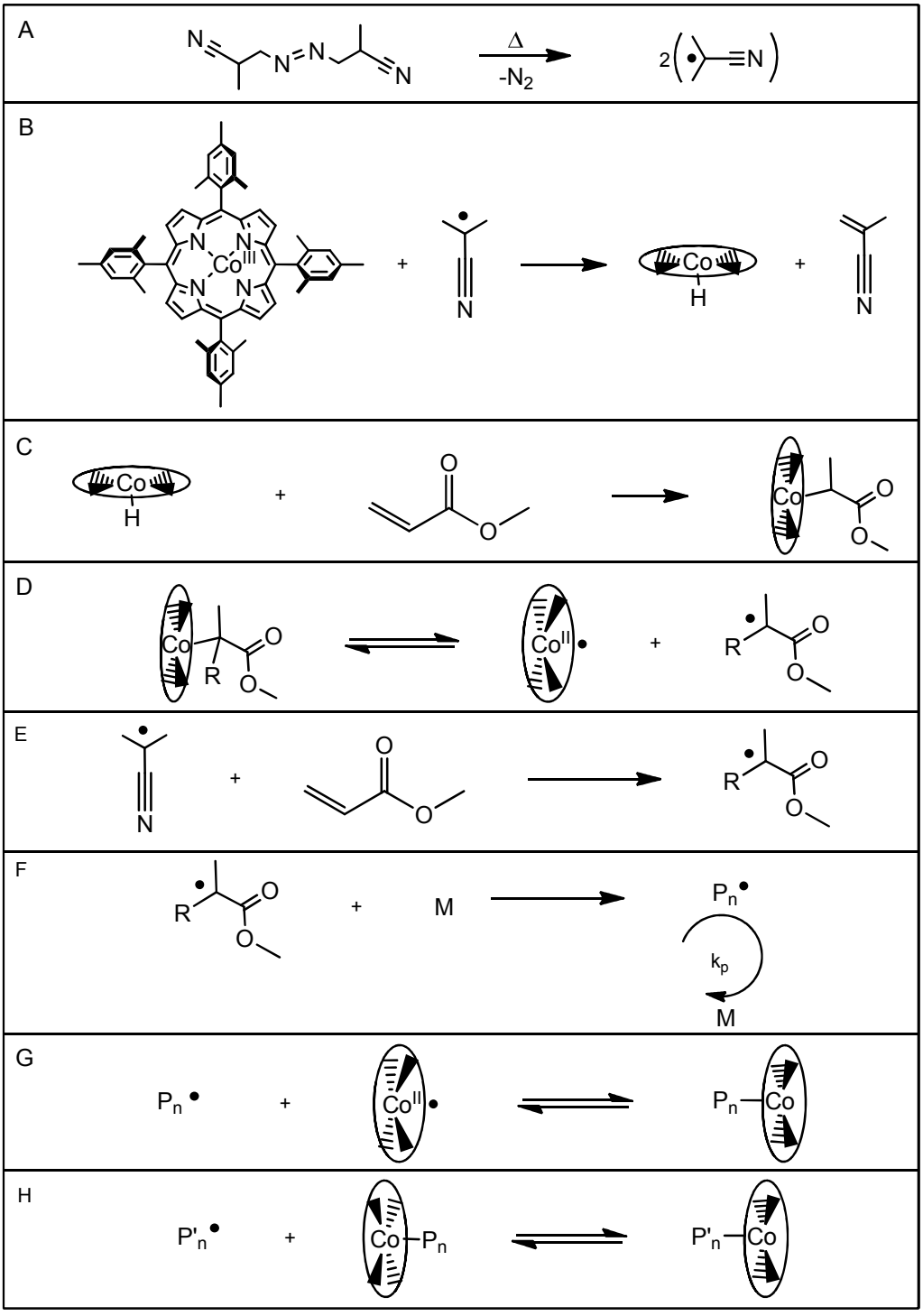

Scheme 1. 11 - CMRP Mechanism

1.5.2 CMRP Mechanism

While most LRP techniques are classified as either RT or DT processes, mechanistic studies of CMRP indicate that both pathways occur in these polymerizations[19, 24, 25, 74]. Most CMRP reactions utilize azo compounds[24], such as AIBN, as an external source of radicals, as show in Scheme 1. 11, however, some studies have utilized preformed L_nCo-R complexes rather than generating this species in situ. When the synthesis is initiated using an L_nCo-R species only the RT pathway is possible if no outside radicals are added to the reaction[25]. In the sample mechanism presented, AIBN is used the external radical source. Upon the application of heat thermal decomposition results in the formation of two identical organo radical and the loss of one N_2 molecule, indicated in Scheme 1. 11 A[19]. When these initiating radicals interact with the cobalt catalyst, Co^{III}(TMP) in this case show in reaction B of Scheme 1. 11, a Co(II) hydride is formed and the cyanoisopropyl radical is terminated and becomes unsaturated[19, 75]. The organo Co(II) complex is then formed through a reaction with the monomer, methyl acrylate is used in this example, as shown in the reaction in Scheme 1. 11 C.

Another route to the formation of the organo-cobalt radical in situ also occurs in conjunction with the mechanism previously discussed and is shown in the reactions presented in steps E and D in Scheme 1. 11. In this reaction series, the cyanoisopropyl radical from AIBN, step A, directly through addition to the monomer molecule resulting in a monomer based organo radical, step E Scheme 1. 11[19, 25]. Once this radical is formed interaction with the Co(TMP) occurs as indicated by the equilibrium in step D of Scheme 1. 11. In the case of the formation of the organo-cobalt complex, the reaction of interest is shown as the equilibrium proceeds from right to left[25, 71]. The R group shown in the organometallic complex formed in step D is hydrogen if the route to the complex is via the first mechanism. If instead, the complex is formed through the second mechanism described, the R represents a cyanoisopropyl group from the external initiator.

Steps A – E are shown to be the major reactions occurring until a large majority, in most cases almost the entirety, of the Co^{III}(TMP) complex is converted to the organo-cobalt (II) complex[26, 75]. This characteristic of the mechanism results in an observable induction period

where no polymerization occurs because all of the radicals being produced early in the process are being utilized for the formation of the Co(II) compound[19, 24, 26, 71, 75, 76]. After full conversion of the cobalt catalyst, polymerization begins to progress following steps D and F – H in Scheme 1. 11[19]. Step D is important for the propagation because the homolytic cleavage of the Co-C bond, when the reaction progress from left to right, result in formation and release of the propagating radical[24, 75]. Once the radical is formed, addition of monomer radicals occurs, step E of Scheme 1. 11, resulting in a propagating polymer radical chain.

Formation of the propagating radical then leads to two possible routes for control of the polymerization: reversible termination and degenerative transfer. As noted previously, unlike many of the other LRP models, CMRP progresses using both mechanisms. The reversible termination method is presented as step G of Scheme 1. 11 where the dormant complex is the internal source of radicals[19, 24, 26, 75]. Step H in Scheme 1. 11 represents the degenerative transfer mechanism where a radical formed in the reaction bulk through the use of an external radical source displaces the radical chain in the dormant complex[19, 24, 75]. Both mechanisms have been proven to occur in CMRP reactions. The biggest difference between the two is that a reaction which progresses mainly through the RT pathway, very low concentrations of azo initiators, has a low rate of polymerization in comparison to the DT path[19, 25]. In either case, the reaction rate is also highly dependent on temperature since the homolytic cleavage of the Co-C bond is much more facile with added thermal energy.

Ideally, the mechanism presented in Scheme 1. 11 is the only route for the polymerization resulting in a fully living system. However, in all synthesis some amount of termination is observed following one of the pathways presented in Scheme 1. 12[75]. Reactions A and B shown in Scheme 1. 12 are typical termination routes seen in a variety of free radical polymerization mechanisms. Both of these reactions are bimolecular terminations, the first results from hydrogen abstraction and the second is combination, which result in the termination of two radicals with each reaction[67]. Reaction C of Scheme 1. 12 presents a termination step in

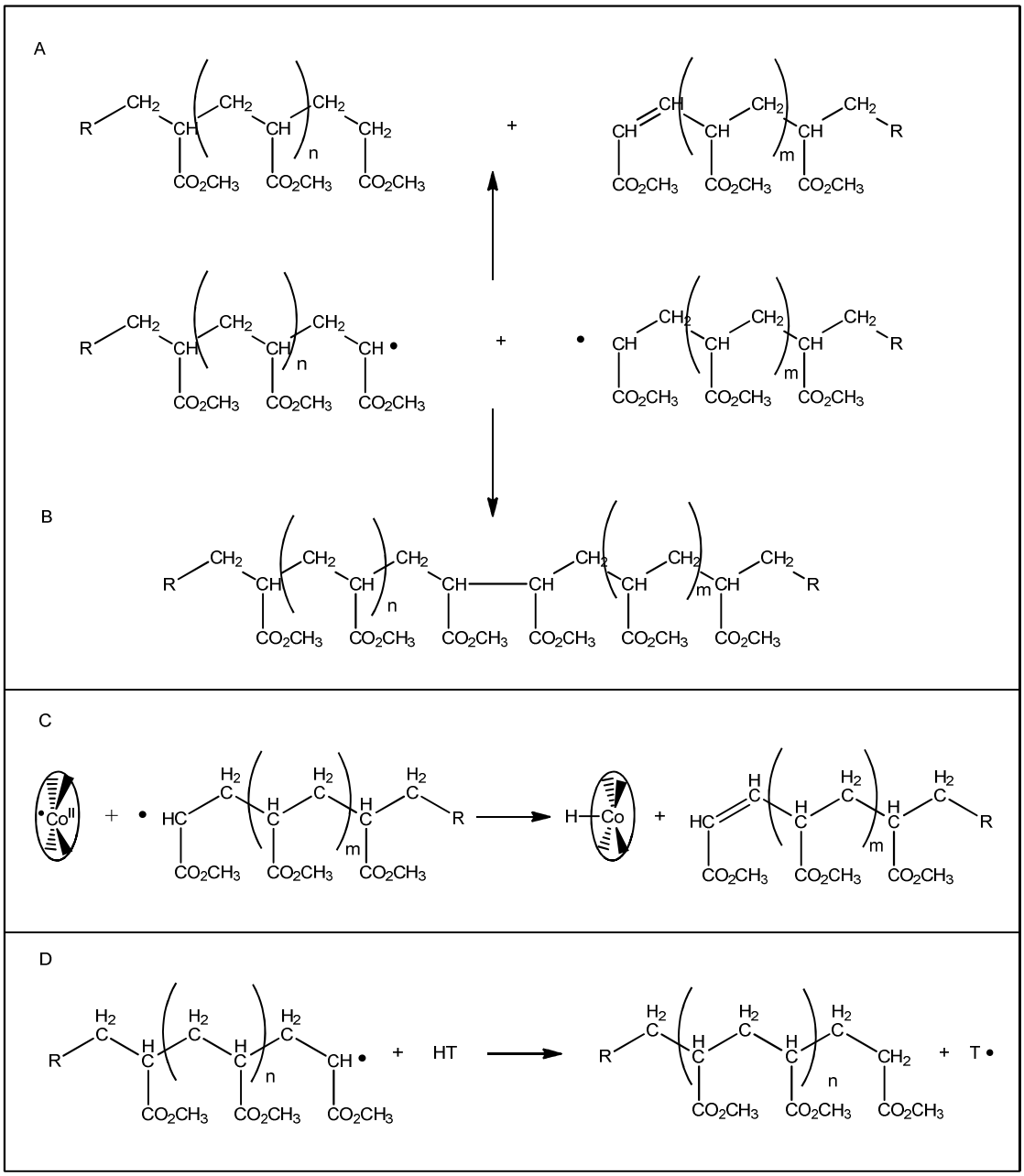

Scheme 1. 12 - CMRP Termination Mechanisms

which the cobalt radical is involved. Instead of forming a dormant species with the propagating radical, a hydrogen is abstracted resulting in a unsaturated polymer chain and a cobalt hydride complex[24, 67, 70]. In the last termination mechanism, Scheme 1. 12 D, a hydrogen radical is transferred from the monomer, polymer, or solvent resulting in a terminated propagating chain and an undesirable radical , T•[67]. If the reactions presented in Scheme 1. 12 are minimized in comparison with those shown in Scheme 1. 11, a well defined polymer with a low PDI is synthesized[25, 70]. The rate of this polymerization is dependent on the reaction temperature and the identities of the monomer and initiator species.

1.5.3 Advantages of CMRP

The most important benefit of the use of CMRP for synthesizing well-defined polymers is its ability to control the polymerization of difficult polymers such as vinyl acetate,[69, 73, 76] only very recently has RAFT proven to be another option. In fact, CMRP is promising partially due to its ability to control polymerizations of monomers with very different functionalities and solubilities[73]. However, in comparison with some of the previously discussed methods, CMRP remains fairly limited in versatility and continued research into appropriate cobalt complexes for mediation is necessary to continue growth in the field. Another feature that is important in CMRP is its ability to continue control even at very high molecular weights and high conversion. Finally the temperature required for polymerization is very low compared to other techniques[76]. Both the ability to control polymerization at high conversions and low temperatures for synthesis are important because it allows for more efficient production of polymers as long as the cobalt complexes can be reused. Therefore, recovery of the catalyst is also an important area of interest of research for this method. Use of this method has proved important because of its ability to polymerize hard to control monomers as well as interesting block copolymers[70]. Continued research is however necessary to make CMRP a widely used method and an important industrial syntheses.

1.6 Nanoparticle Synthesis Applications of Polymers Synthesized Using LRP Methods

Development of LRP techniques has progressed in order to meet the demands of the materials fields. Polymers with very specific properties or architectures are required for many

current applications, highlighting the importance of LRP as a synthetic technique[77, 78]. Nanotechnology is one major field where polymers synthesized using LRP methods are proving to be extremely useful. One area that is especially important is the synthesis of metal nanoparticles. Interest in nanoparticles lies in their unique properties[79-83] as well as the ability to create catalysts with large active surface area and low metal quantity[84-87]. While there are many methods currently available little is known about the synthetic mechanism and many of the techniques utilize very harsh reaction conditions[79, 80, 84]. There are two techniques that are most commonly used: application of amphiphilic copolymers to create nanoreactor micelles[83, 88-91] and high temperature reflux of metal precursors in the presence of polymers and reducing agents, polyol synthesis[80, 87, 92].

1.6.1 Nanoparticle Synthesis Utilizing Polymer Micelles

Synthesis of metal nanoparticles using polymer micelles requires the use of block copolymers where the blocks differ have different properties, polarity or acidity are the most common. In current research, the metal species are isolated in the core of the micelles by creating a more favorable environment for the polar complexes[79]. Use of amphiphilic block copolymers in a fairly nonpolar solvent will create a core where the metal complexes will migrate to the polar core[77, 89]. Another system where solvents with higher polarity are used require a polymers with a polar-polar coordinating formation. In this case, both blocks are polar so the formation of the micelle is entirely dependent on the polar coordinating block's ability to coordinate to the metal species[90]. The important feature of this type of system is that the reactions can be performed in water[90, 93] which is important for the development of more environmentally friendly techniques. Control in particle size and shape are determined by the micelles ability to separate the metal species from the bulk eliminating the possibility of metal reduction outside of the micelles.

In some reactions, typically those using polymers with block of different polarities, the micelle is first created and then a polar solution of the metal species is added and allowed to equilibrate until all of the metal complexes have migrated to the polar core[89]. While in syntheses where both blocks are the same polarity, the addition of the solution containing the metal species

allows for the formation of the micelles since the coordination to the metal is what provides the linkages between the different polymer chains[90]. In either case, once the micelles are formed with the metal complexes in the core, polar reducing agents such as sodium borohydride[88, 90, 91, 93] are added to the reaction mixture. Upon the introduction of the reducing agent, nanoparticle formation will begin within the micellar core. By restricting the mobility, especially in cases where the micelle has been crosslinked[88], of the metal complexes, the size and shape of the particle formed is determined by the micelle[90]. If all of the metal is incorporated within the micelles, a narrow distribution of particle size should be observed. When the synthesis results in a wide size distribution, the metal complex was not sufficiently isolated in the micelle cores and reduction is occurring both in the core and in the reaction bulk.[91, 93]

This type of synthetic technique has proven extremely useful for formation of nanoparticles of various metals in different size ranges[94]. Increasing the concentration of metals, changing the identity of the polymer, and different reduction speed account for the versatility found in this method. Micelles prove to be ideal nanoreactors for nanoparticles since they are immediately stabilized through the steric bulk of the polymer surrounding the particles preventing agglomeration[93]. The introduction of polar-polar micelles creates a unique opportunity in the field of medicine for the metal particles synthesized in this manner. If the micelles are produced in an aqueous solution, they can be used as delivery agents[53, 88] where once the micelle reaches an area of differing polarity the contents are released due to destruction of the micellar structure.

1.6.2 Polyol Particle Synthesis

Metal particle synthesis using homopolymers as stabilizers is considered a self-assembly method where the various components are added to a solution and give the desired results[80, 95]. Alcohols are most commonly used as the reducing agent in these techniques and are used in large quantities to increase the solubility of the polymer as well. In these reactions, a metal precursor complex is added to a water-alcohol solution with the desired polymer[82, 92]. This solution is then refluxed for an hour or more until the reaction is seen to go to completion. Uv-vis spectroscopy is the most common method[92, 95, 96] utilized to monitor the progress of the reaction since a majority of the metal complexes are active in this region[92]. As the particles form, the

polymers self-assemble around the particles through interaction with the surface. This self assembly is responsible for the control of the particle size since the particle ceases growth when they are completely encapsulated by the polymer.

After the reaction mixture is cooled the stabilized particles are separated and redispersed[96]. Ultimately the polymer plays several roles in these preparations: they influence the size and shape of the particles, act as stabilizers, and affect the catalytic behavior. Size and shape are influenced by the polymer identity due to differing interaction strengths given the different functional groups on the polymer chains[83]. The stronger the polymer-metal interaction the more quickly the capping occurs resulting in smaller particles. These interactions can also inhibit the growth of different faces of the metal crystal while allowing growth of other faces changing the shape of the particle that is ultimately formed.

One of the most important functions, and what is typically considered the primary function of the polymer, is the stabilization of the particles[94]. As in 1.6.1, the polymers are utilized as stabilizers because of the steric bulk[82, 83, 87] that they add to the particle inhibiting the ability of the metal centers to combine with each other. If the polymer is chosen properly agglomeration is prohibited and the nanoparticles remain small with a narrow size distribution for an extended period[87]. This is an important property since the desired behavior of the particles is often exclusively due to their size. Therefore, in order for the particles to be useful industrially the properties must remain consistent for long periods so the stabilization is essential.

Lastly, the catalyst behavior of the metal nanoparticles can be strongly influenced by the chosen polymer. In order for the particles to remain catalytically active, the substrates must be able to reach the particle within the protective polymer coating. This means that the environment created by the polymer must be designed so that the desired compounds are able to migrate to the particle[87]. Changing the identity of the polymer can alter the polarity, electrostatic properties, or structural formation around the nanoparticle creating particles with catalytic specificity[87]. The metal-polymer surface interaction can also affect the catalytic properties of the nanoparticle. When polymers coordinate or interact with the surface of the particle the behavior of the metal is changed since this will change the metal characteristics from those of a pure metal surface[87].

This method has been utilized in order to synthesize metal nanoparticle of various metals[80, 85, 87] in a wide variety of sizes[87, 92, 96], however, very little is known about the mechanism which drives the nanoparticle assembly.

1.7 References

1. Szwarc, M., *Angewandte Chemie-International Edition* **1958,** *70* (20), 632-632.

2. Szwarc, M., *Journal of Polymer Science* **1954,** *13* (69), 317-318.

3. Szwarc, M.; Levy, M.; Milkovich, R., *Journal of the American Chemical Society* **1956,** *78* (11), 2656-2657.

4. Szwarc, M.; Rembaum, A., *Journal of Polymer Science* **1956,** *22* (100), 189-191.

5. Levy, M., *Polymers for Advanced Technologies* **2007,** *18* (9), 681-684.

6. Chen, X. J.; Sanchez-Gaytan, B. L.; Hayik, S. E. N.; Fryd, M.; Wayland, B. B.; Park, S. J., *Small* **2010,** *6* (20), 2256-2260.

7. Ayres, N., *Polym. Rev.* **2011,** *51* (2), 138-162.

8. Moad, G.; Rizzardo, E.; Thang, S. H., *Australian Journal of Chemistry* **2006,** *59* (10), 669-692.

9. Colombani, D., *Prog. Polym. Sci.* **1997,** *22* (8), 1649-1720.

10. Moad, G.; Rizzardo, E.; Thang, S. H., *Australian Journal of Chemistry* **2005,** *58* (6), 379-410.

11. Moad, G.; Rizzardo, E.; Thang, S. H., *Accounts Chem. Res.* **2008,** *41* (9), 1133-1142.

12. Braunecker, W. A.; Matyjaszewski, K., *Prog. Polym. Sci.* **2007,** *32* (1), 93-146.

13. Gridnev, A. A.; Ittel, S. D.; Fryd, M.; Wayland, B. B., *Organometallics* **1996,** *15* (1), 222-235.

14. Moad, G.; Soloman, D. H., *The Chemistry of Radical Polymerization* 2nd ed.; Elsevier: New York, 2006.

15. Greszta, D.; Mardare, D.; Matyjaszewski, K., *Macromolecules* **1994,** *27* (3), 638-644.

16. Porter, N. A.; Allen, T. R.; Breyer, R. A., *Journal of the American Chemical Society* **1992,** *114* (20), 7676-7683.

17. North, A. M.; Reed, G. A., *Transactions of the Faraday Society* **1961,** *57*, 859-870.

18. Patten, T. E.; Matyjaszewski, K., *Advanced Materials* **1998,** *10* (12), 901-+.

19. Wayland, B. B.; Peng, C. H.; Fu, X. F.; Lu, Z.; Fryd, M., *Macromolecules* **2006,** *39* (24), 8219-8222.

20. Fischer, H., *Macromolecules* **1997,** *30* (19), 5666-5672.

21. Chiefari, J.; Chong, Y. K.; Ercole, F.; Krstina, J.; Jeffery, J.; Le, T. P. T.; Mayadunne, R. T. A.; Meijs, G. F.; Moad, C. L.; Moad, G.; Rizzardo, E.; Thang, S. H., *Macromolecules* **1998,** *31* (16), 5559-5562.

22. Johnson, C. H. J.; Moad, G.; Solomon, D. H.; Spurling, T. H.; Vearing, D. J., *Australian Journal of Chemistry* **1990,** *43* (7), 1215-1230.

23. Daikh, B. E.; Finke, R. G., *Journal of the American Chemical Society* **1992,** *114* (8), 2938-2943.

24. Peng, C. H.; Fryd, M.; Wayland, B. B., *Macromolecules* **2007,** *40*, 6814-6819.

25. Debuigne, A.; Poli, R.; Jerome, C.; Jerome, R.; Detrembleur, C., *Prog. Polym. Sci.* **2009,** *34* (3), 211-239.

26. Lu, Z.; Fryd, M.; Wayland, B. B., *Macromolecules* **2004,** *37* (8), 2686-2687.

27. Moad, G.; Rizzardo, E.; Solomon, D. H., *Polymer Bulletin* **1982,** *6* (11-1), 589-593.

28. Solomon, D. H.; Rizzardo, E.; Cacioli, P. Substd. alkyl-amine cpds. - useful as controlled growth free radical polymerisation initiators for unsaturated monomers. AU8430378-A, 1985.

29. Georges, M. K.; Veregin, R. P. N.; Kazmaier, P. M.; Hamer, G. K., *Macromolecules* **1993,** *26* (11), 2987-2988.

30. Moad, G.; Rizzardo, E., *Macromolecules* **1995,** *28* (26), 8722-8728.

31. Chong, Y. K.; Ercole, F.; Moad, G.; Rizzardo, E.; Thang, S. H.; Anderson, A. G., *Macromolecules* **1999,** *32* (21), 6895-6903.

32. Bertin, D.; Gigmes, D.; Marque, S. R. A.; Tordo, P., *Macromolecules* **2005,** *38* (7), 2638-2650.

33. Hawker, C. J.; Bosman, A. W.; Harth, E., *Chemical Reviews* **2001,** *101* (12), 3661-3688.

34. Grubbs, R. B., *Polym. Rev.* **2011,** *51* (2), 104-137.

35. Gossage, R. A.; Van De Kuil, L. A.; Van Koten, G., *Accounts Chem. Res.* **1998,** *31* (7), 423-431.

36. Minisci, F., *Accounts Chem. Res.* **1975,** *8* (5), 165-171.

37. Abraham, M. H.; Hogarth, M. J., *Journal of Organometallic Chemistry* **1968,** *12* (3), 497-&.

38. Szmant, H. H., *Science* **1967,** *158* (3798), 250-&.

39. Kato, M.; Kamigaito, M.; Sawamoto, M.; Higashimura, T., *Macromolecules* **1995,** *28* (5), 1721-1723.

40. Wang, J. S.; Matyjaszewski, K., *Journal of the American Chemical Society* **1995,** *117* (20), 5614-5615.

41. Wang, J. S.; Matyjaszewski, K., *Macromolecules* **1995,** *28* (23), 7901-7910.

42. Brandts, J. A. M.; van de Geijn, P.; van Faassen, E. E.; Boersma, J.; van Koten, G., *Journal of Organometallic Chemistry* **1999,** *584* (2), 246-253.

43. Braunecker, W. A.; Itami, Y.; Matyjaszewski, K., *Macromolecules* **2005,** *38* (23), 9402-9404.

44. Kotani, Y.; Kamigaito, M.; Sawamoto, M., *Macromolecules* **1999,** *32* (8), 2420-2424.

45. Uegaki, H.; Kotani, Y.; Kamigaito, M.; Sawamoto, M., *Macromolecules* **1998,** *31* (20), 6756-6761.

46. Wang, B. Q.; Zhuang, Y.; Luo, X. X.; Xu, S. S.; Zhou, X. Z., *Macromolecules* **2003,** *36* (26), 9684-9686.

47. Kwak, Y.; Nicolay, R.; Matyjaszewski, K., *Australian Journal of Chemistry* **2009,** *62* (11), 1384-1401.

48. Tsarevsky, N. V.; Braunecker, W. A.; Matyjaszewski, K., *Journal of Organometallic Chemistry* **2007,** *692* (15), 3212-3222.

49. Ouchi, M.; Terashima, T.; Sawamoto, M., *Accounts Chem. Res.* **2008,** *41* (9), 1120-1132.

50. Takahashi, H.; Ando, T.; Kamigaito, M.; Sawamoto, M., *Macromolecules* **1999,** *32* (20), 6461-6465.

51. Takahashi, H.; Ando, T.; Kamigaito, M.; Sawamoto, M., *Macromolecules* **1999,** *32* (11), 3820-3823.

52. Corpart, P.; Charmot, D.; Biadatti, T.; Zard, S.; Michelet, D.; Zard, S. Z.; Copart, P. Block polymer synthesis - by controlled radical polymerisation. WO9858974-A, 30 Dec, 1998.

53. Boyer, C.; Bulmus, V.; Davis, T. P.; Ladmiral, V.; Liu, J. Q.; Perrier, S., *Chemical Reviews* **2009,** *109* (11), 5402-5436.

54. Favier, A.; Charreyre, M. T., *Macromolecular Rapid Communications* **2006,** *27* (9), 653-692.

55. Monteiro, M. J., *Journal of Polymer Science Part a-Polymer Chemistry* **2005,** *43* (15), 3189-3204.

56. Adamy, M.; van Herk, A. M.; Destarac, M.; Monteiro, M. J., *Macromolecules* **2003,** *36* (7), 2293-2301.

57. Monteiro, M. J.; Sjoberg, M.; van der Vlist, J.; Gottgens, C. M., *Journal of Polymer Science Part a-Polymer Chemistry* **2000,** *38* (23), 4206-4217.

58. Moad, G.; Rizzardo, E.; Thang, S. H., *Polymer* **2008,** *49* (5), 1079-1131.

59. Moad, G.; Chiefari, J.; Chong, Y. K.; Krstina, J.; Mayadunne, R. T. A.; Postma, A.; Rizzardo, E.; Thang, S. H., *Polymer International* **2000,** *49* (9), 993-1001.

60. Monteiro, M. J.; de Brouwer, H., *Macromolecules* **2001,** *34* (3), 349-352.

61. Chiefari, J.; Mayadunne, R. T. A.; Moad, C. L.; Moad, G.; Rizzardo, E.; Postma, A.; Skidmore, M. A.; Thang, S. H., *Macromolecules* **2003,** *36* (7), 2273-2283.

62. Chong, Y. K.; Krstina, J.; Le, T. P. T.; Moad, G.; Postma, A.; Rizzardo, E.; Thang, S. H., *Macromolecules* **2003,** *36* (7), 2256-2272.

63. Moad, G.; Rizzardo, E.; Thang, S. H., *Australian Journal of Chemistry* **2009,** *62* (11), 1402-1472.

64. Goto, A.; Sato, K.; Tsujii, Y.; Fukuda, T.; Moad, G.; Rizzardo, E.; Thang, S. H., *Macromolecules* **2001,** *34* (3), 402-408.

65. Mayadunne, R. T. A.; Rizzardo, E.; Chiefari, J.; Chong, Y. K.; Moad, G.; Thang, S. H., *Macromolecules* **1999,** *32* (21), 6977-6980.

66. Zetterlund, P. B.; Kagawa, Y.; Okubo, M., *Chemical Reviews* **2008,** *108* (9), 3747-3794.

67. Wayland, B. B.; Poszmik, G.; Mukerjee, S. L.; Fryd, M., *Journal of the American Chemical Society* **1994,** *116* (17), 7943-7944.

68. Harwood, H. J.; Arvanitopoulos, L. D.; Greuel, M. P., *Polym. Prep. (Am Chem Soc Div Polym Chem)* **1994,** *43* (2), 287-288.

69. Hurtgen, M.; Detrembleur, C.; Jerome, C.; Debuigne, A., *Polym. Rev.* **2011,** *51* (2), 188-213.

70. Wayland, B. B.; Basickes, L.; Mukerjee, S.; Wei, M. L.; Fryd, M., *Macromolecules* **1997,** *30* (26), 8109-8112.

71. Debuigne, A.; Caille, J. R.; Jerome, R., *Angewandte Chemie-International Edition* **2005,** *44* (7), 1101-1104.

72. Peng, C. H.; Scricco, J.; Li, S.; Fryd, M.; Wayland, B. B., *Macromolecules* **2008,** *41* (7), 2368-2373.

73. Debuigne, A.; Poli, R.; De Winter, J.; Laurent, P.; Gerbaux, P.; Wathelet, J. P.; Jerome, C.; Detrembleur, C., *Macromolecules* **2010,** *43* (6), 2801-2813.

74. Hurtgen, M.; Debuigne, A.; Jerome, C.; Detrembleur, C., *Macromolecules* **2009,** *43* (2), 886-894.

75. Li, S.; de Bruin, B.; Peng, C. H.; Fryd, M.; Wayland, B. B., *Journal of the American Chemical Society* **2008,** *130* (40), 13373-13381.

76. Debuigne, A.; Champouret, Y.; Jerome, R.; Poli, R.; Detrembleur, C., *Chemistry-a European Journal* **2008,** *14* (13), 4046-4059.

77. Sanchez-Gaytan, B. L.; Cui, W. H.; Kim, Y. J.; Mendez-Polanco, M. A.; Duncan, T. V.; Fryd, M.; Wayland, B. B.; Park, S. J., *Angewandte Chemie-International Edition* **2007,** *46* (48), 9235-9238.

78. Lowe, A. B.; Sumerlin, B. S.; Donovan, M. S.; McCormick, C. L., *Journal of the American Chemical Society* **2002,** *124* (39), 11562-11563.

79. Murray, C. B.; Kagan, C. R.; Bawendi, M. G., *Annu. Rev. Mater. Sci.* **2000,** *30*, 545-610.

80. Wiley, B.; Sun, Y. G.; Xia, Y., *Accounts Chem. Res.* **2007,** *40* (10), 1067-1076.

81. Wang, Y.; Herron, N., *J. Phys. Chem.* **1991,** *95* (2), 525-532.

82. Duff, D. G.; Edwards, P. P.; Johnson, B. F. G., *J. Phys. Chem.* **1995,** *99* (43), 15934-15944.

83. Mayer, A. B. R., *Polymers for Advanced Technologies* **2001,** *12* (1-2), 96-106.

84. Antolini, E.; Perez, J., *Journal of Materials Science* **2011,** *46* (13), 4435-4457.

85. Zhong, C. J.; Luo, J.; Fang, B.; Wanjala, B. N.; Njoki, P. N.; Loukrakpam, R.; Yin, J., *Nanotechnology* **2010,** *21* (6).

86. Mukerjee, S.; McBreen, J., *Journal of Electroanalytical Chemistry* **1998,** *448* (2), 163-171.

87. Mayer, A. B. R.; Mark, J. E.; Hausner, S. H., *Journal of Applied Polymer Science* **1998,** *70* (6), 1209-1219.

88. Oishi, M.; Miyagawa, N.; Sakura, T.; Nagasaki, Y., *Reactive & Functional Polymers* **2007,** *67* (7), 662-668.

89. Egorova, E. M.; Revina, A. A., *Colloids and Surfaces a-Physicochemical and Engineering Aspects* **2000,** *168* (1), 87-96.

90. Sidorov, S. N.; Bronstein, L. M.; Valetsky, P. M.; Hartmann, J.; Colfen, H.; Schnablegger, H.; Antonietti, M., *Journal of Colloid and Interface Science* **1999,** *212* (2), 197-211.

91. Vamvakaki, M.; Papoutsakis, L.; Katsamanis, V.; Afchoudia, T.; Fragouli, P. G.; Iatrou, H.; Hadjichristidis, N.; Armes, S. P.; Sidorov, S.; Zhirov, D.; Zhirov, V.; Kostylev, M.; Bronstein, L. M.; Anastasiadis, S. H. In *Micellization in pH-sensitive amphiphilic block copolymers in aqueous media and the formation of metal nanoparticles*, 2005; pp 129-147.

92. Chen, C. W.; Tano, D.; Akashi, M., *Colloid and Polymer Science* **1999,** *277* (5), 488-493.

93. Bronstein, L. H.; Sidorov, S. N.; Valetsky, P. M.; Hartmann, J.; Colfen, H.; Antonietti, M., *Langmuir* **1999,** *15* (19), 6256-6262.

94. Pachón, L. D.; Rothenberg, G., *Applied Organometallic Chemistry* **2008,** *22* (6), 288-299.

95. Jiang, S. P.; Liu, Z.; Tang, H. L.; Pan, M., *Electrochimica Acta* **2006,** *51* (26), 5721-5730.

96. Yan, X. P.; Liu, H. F.; Liew, K. Y., *Journal of Materials Chemistry* **2001,** *11* (12), 3387-3391.

Chapter 2 – Development of Vanadate Complexes for Use as RAFT Chain Transfer Agents

2.1 Introduction

Conventional RAFT chain transfer agents (CTAs) have been based off of xanthate[1, 2] or thiocarbonylthio complexes[1-13] where the activating and leaving groups, Z and R respectively can be tuned for better performance with particular monomers. CTA's have proven extremely versatile due to the high tunability of the species and provide control to the widest range[1, 6, 7, 9, 13, 14] of monomers of any LRP method. The aim of this project was to develop CTAs using vanadium analogues of the traditional compounds. Vanadium was chosen as the desired metal center for several reasons. Complexes with high oxidation states are common for vanadium and it is believed that this characteristic will stabilize the intermediate radical that is formed during the RAFT mechanism[15-18]. By using vanadium complexes several leaving groups are possible allowing for several sites for the chain transfer to occur increasing the rate of polymerization. Scheme 2. 1 provides the chain transfer mechanisms that are expected with the use of vanadyl complexes. It is apparent that for this mechanism to be the preferred route, the O-R bond must be weaker than the bond formed through addition of the polymer chain. This will then cause coordination of the polymer radical and loss of R• to be the main route allowing for the formation of three oxy-polymer sites on the vanadyl complex. Following the initial chain transfer steps, the dormant-active complex equilibrium will progress through the exchange of any of the polymer chains on the vanadium complex with equal probability for any of the sites since the bond energies will be approximately equal. Use of a metal center may also provide a route to monomers which are traditionally polymerized using ATRP or CMRP. Polymerization using the RAFT method is advantageous over these other LRP techniques since the conditions are similar to those used in conventional free radical polymerization and are not as sensitive as ATRP and CMRP.

2.2 Tris(1-propyl) Orthovanadate

The first candidate chosen for study as a RAFT CTA was tris(1-propyl) orthovanadate (Compound 1), shown in Figure 2. 1. This compound was obtained commercially from Gelest (>95% purity) and used as received. A stability study of solutions containing methyl acrylate (MA),

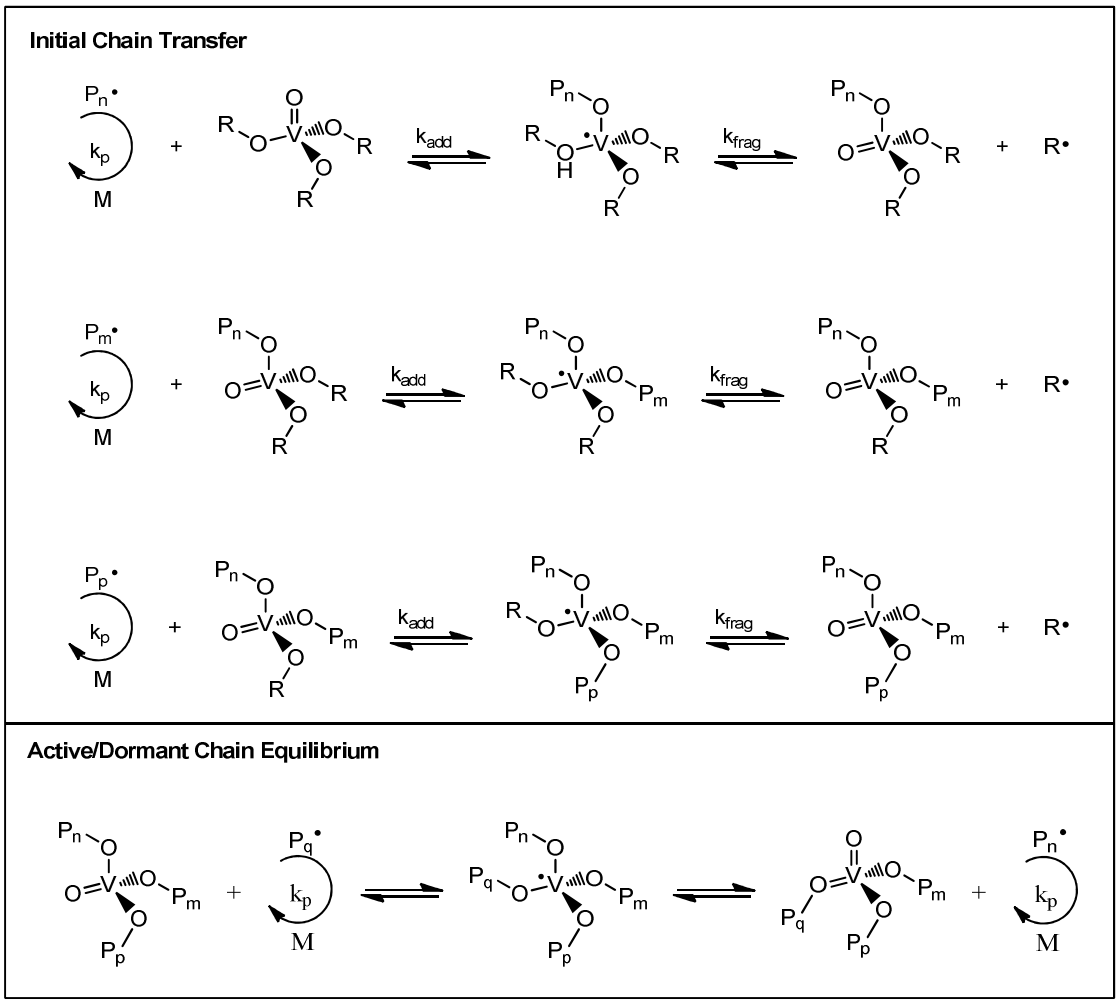

Scheme 2. 1 - RAFT Chain Transfer Mechanisms Using a Vanadyl Complex

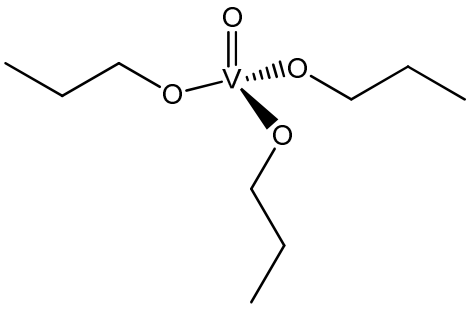

Figure 2. 1 - Tris(1-propyl) Orthovanadate Structure, Compound 1

2,2'-azobisisobutyronitrile (AIBN), and Compound 1 in vacuum adapted NMR placed in a 60˚C water bath following three freeze-pump-thaw cycles was performed in order to choose an appropriate solvent for the polymerization reactions. Benzene, pyridine, chloroform, and dichloromethane were used as the experimental solvents. Slow precipitation of a light yellow solid was observed for the benzene solution, while the solution containing pyridine had immediate precipitation of a brown solid. All of the components remained in solution for the chloroform and dichloromethane solutions, however, a large portion of the dichloromethane vaporizes to fill the NMR tube lowering the amount of solvent available during the reaction. Although chloroform is not an ideal choice of solvent for systems utilizing free radicals due to its donating capabilities, these studies suggest it is the most appropriate solvent for this particular system.

Methyl acrylate was the monomer chosen for the polymerization study using Compound 1 with conditions similar to those reported using tradition carbon centered CTAs[3]. Every experiment was prepared in deuterated chloroform and contained 1 x 10^{-3} M total possible initiator radicals, assuming two radicals per AIBN molecule and 65 percent efficiency, and 2.75 M MA and were run at 60˚C. The concentration of Compound 1 was varied from 3.0 x 10^{-3} M to 1.3 x 10^{-2} M. All polymerizations were performed in vacuum adapted NMR tubes after freeze-pump-thawing the solution a minimum of three cycles. Initial observation of the reaction was performed via ^{1}H-NMR, where during the analysis all of the NMR tubes being used were cooled with a dry-ice acetone bath in order to halt the reaction and maintain the timing. After the reaction progressed the desired amount the NMR tubes were opened and the solution was dried using the high vacuum line to remove the excess monomer and solvent prior to GPC analysis. The solid polymer was then dissolved in tetrahydrofuran and run through a 0.45μm PTFE filter. Gel permeation chromatography, GPC, analysis of each sample was then performed on a Shimadzu modular system using a Polymer Laboratories 5.0 μm PLgel guard column(50 x 7.5 mm) and three linear PLgel columns (1 x 10^{6}, 1x 10^{4}, and 5 x 10^{2} Å). The columns were in a 40˚C oven (CTO-10A) and the spectra were obtained with a UV-vis detector (SPD-10AV) and a differential refractometer (RID-10A). Each run employed THF as the eluent and was run at a flow rate of 1

ml min^{-1}. The GPC was calibrated using narrow peak width polystyrene standards (Easical from Polymer Laboratories) ranging from 580 to 7.5 x 10^6 g mol^{-1}.

The kinetic rate plots of three MA polymerization runs with varying concentrations of compound 1 are shown in Figure 2. 2. Each run shows a distinct induction period which is inconsistent with the RAFT mechanism[8, 11, 19]. For a typical RAFT polymerization, polymerization begins immediately and a linear first order rate plots is seen. Also, a decrease in the PDI of the products is observed, since initially the polymer chain growth is proceeding through a conventional free radical route until the initial chain transfer is completed for each CTA molecule. The data from the runs with Compound 1 shows fairly linear behavior following the induction period, the induction time for each run is provided in Table 2. 1. All three experiments have a similar rate after the onset of polymerization, suggesting that at this point of the run the rate is independent of Compound 1 concentration. This rate is significantly lower than the rate for standard polymerizations which have the same conditions without the addition of Compound 1. GPC data obtained for these experiments show that all of the products have PDIs over 2.0 which suggest that there is no control of the polymerization.

All of the data suggests that Compound 1 is not a suitable CTA for the polymerization of MA. However, the induction periods at the beginning of each run do imply that Compound 1 is removing the external radicals formed during this time in some manner. The low rate of polymerization, which is consistent with inappropriate CTA choice[3], may be due to the loss of radicals to Compound 1 during the induction period limiting the number available after Compound 1 is no longer inhibiting the polymerization. These results indicate that monomer, small oligomers, or solvent radicals may be transferring to Compound 1 as was expected for the polymer chain as shown in the initial chain transfer steps of Scheme 2. 1. Once this transfer has taken place, the n-propyl radical does not leave the molecule and the vanadium complex no longer interacts with any of the newly produced radicals. An overly strong O-R bond could be responsible for this behavior, and since the n-propyl radical is poorly stabilized given it will be a primary radical on an

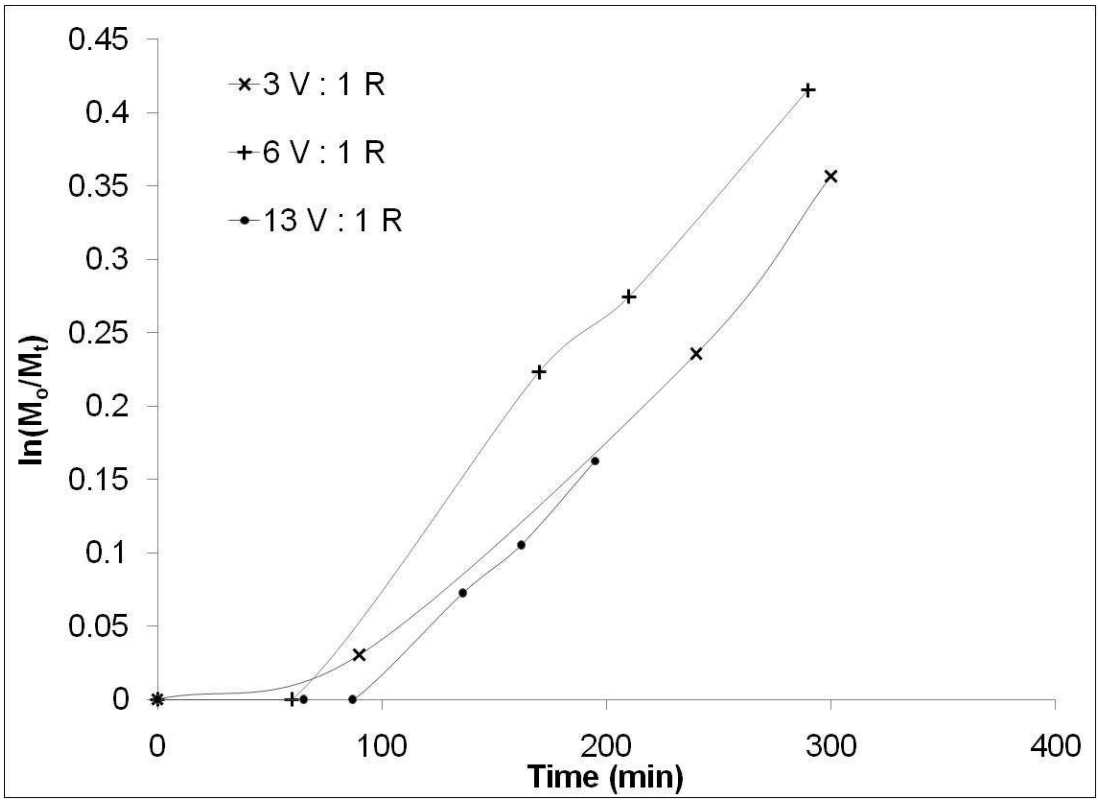

Figure 2. 2 - Kinetic Rate Plot of the Polymerization of MA with Compound 1 with Various Ratios of Vanadium to AIBN initiator Radicals

Experiment	Obs. Ind Time (min)
3 V : 1 R•	74
6 V : 1 R•	39
13 V : 1 R•	92

Table 2. 1 - Observed Induction Time for the Runs Presented in Figure 2. 2

unbranched hydrocarbon chain this is a reasonable assumption. After all of the Compound 1 molecules in the solution have been deactivated, polymerization will progress but at a slower rate since some of the propagating radicals have been trapped by Compound 1. The mechanism of deactivation described appears to fit all of the experimental evidence and indicates that Compound 1 is not suitable as a RAFT CTA.

2.3 Tris(2-propyl) Orthovanadate

The second RAFT CTA candidate, tris(2-propyl) orthovanadate (Compound 2) shown in Figure 2. 3, was chosen since the leaving group will be a tertiary radical greatly increasing its stability in comparison to that formed from Compound 1. Tris(2-propyl) orthovanadate was obtained commercially from Gelest (> 95% purity). For these experiments, the concentration of Compound 1 was maintained at 1×10^{-2} M and the concentration of MA was 0.5 M. AIBN was used as the external radical source and the concentration was varied to change the vanadium to radical ratios for the experiment. The solutions were prepared in deuterated chloroform and after preparation as described in Section 2.2 and placed in a 60°C water bath. Polymerization was monitored by ^{1}H-NMR and GPC was performed on the products using the instrumentation described previously.

Kinetic rate plots of the polymerization of MA with Compound 2 are provided in Figure 2. 4. Unlike Compound 1, there is no distinct induction period for either of these experiments as expected for a RAFT polymerization and linear behavior suggests a first order rate for the system. A decrease in the rate with a decrease in the concentration of external radicals is observed through the lower slope of the run using a 1.16 R• to vanadium center ratio. All of this data suggests that the polymerization may be progressing through the RAFT mechanism. However, GPC analysis of the polymers synthesized during these experiments suggest that there is little control of the polymerization given that the PDIs are extraordinarily high, between 2.2 and 2.4. In this case, it appears as though Compound 2 is more than likely completely bypassed during the polymerization. Unlike Compound 1, there are no indications that Compound 2 is interacting with the initiator radicals so trapping is unlikely. Given this data it was concluded that Compound 2 is not a viable CTA for RAFT polymerization.

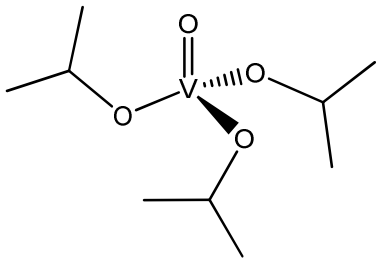

Figure 2. 3 - Tris(2-propyl) Orthovanadate Structure, Compound 2

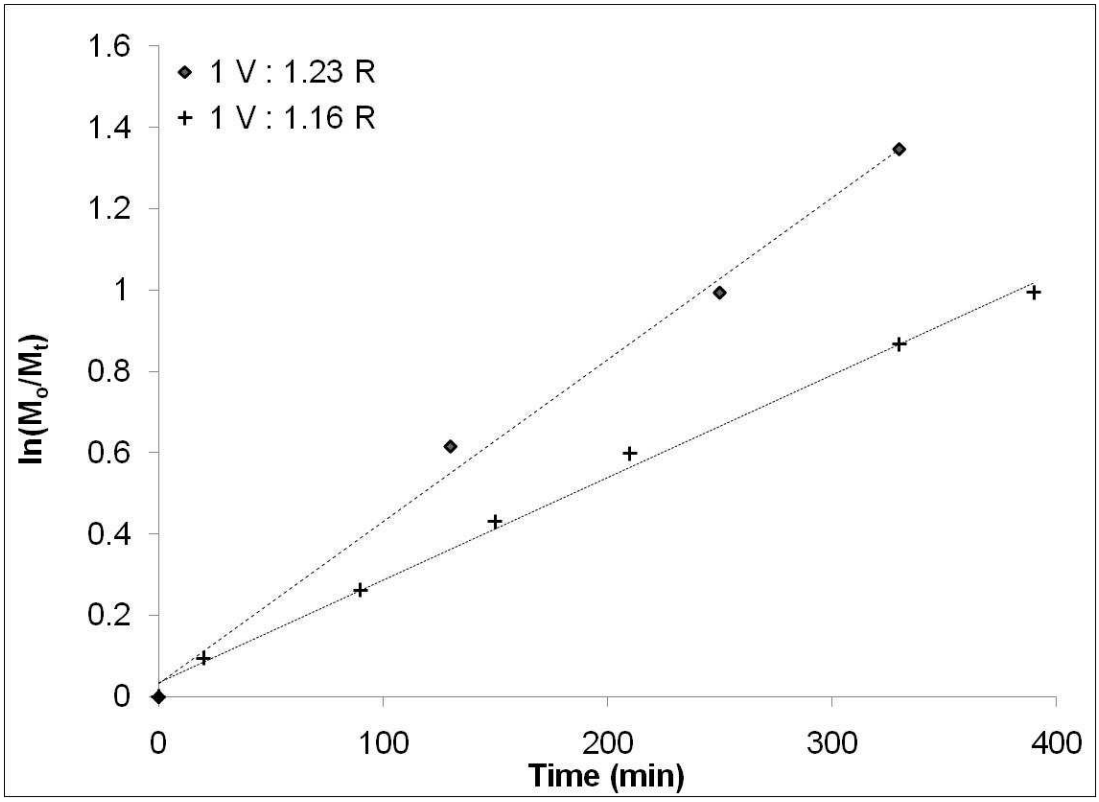

Figure 2. 4 - Kinetic Rate Plot of the Polymerization of MA with Compound 2 with AIBN as the External Radical Source

2.4 Other Vanadium Complexes

Two other vanadium complexes were tested as RAFT polymerization CTAs, shown in Figure 2. 5 and Figure 2. 6. These compounds were synthesized using a modified literature method[20]. The appropriate ligand, 2,6-diisopropylphenol for Compound 3 and 1-phenylethanol for Compound 4, was mixed in a 3:1 ratio with tris(2-propyl) orthovanadate under nitrogen in n-hexane for Compound 3 or toluene for Compound 4. The solutions were refluxed for approximately four hours. Following the reaction completion the excess solvent was removed through rotaevaporation. The solid products were then kept under vacuum in the refrigerator to inhibit exposure to water. Characterization of the products was performed using ^{1}H-NMR.

Compound 3 and Compound 4 were tested as CTA for RAFT polymerization. Since the R• expected to be released by Compound 4 if the desired mechanism is followed is the same as that formed by the styrene monomer, styrene was chosen as the monomer for this system. Unfortunately, polymerizations using Compound 4 and styrene produced no polymer. Compound 3, 5 x 10^{-3} M, was used in the polymerization of MA, 2.2 M. AIBN, 3 x 10^{-3} M, was used as the external radical source and the solutions were prepared in deuterated chloroform and run at 60˚C after the preparation described in Section 2.2. The polymerization was tracked by ^{1}H-NMR and GPC analysis was performed using the instrumentation described previously.

The kinetic rate plot for the polymerization is provided in Figure 2. 7. A linear relationship with no induction period is seen as expected in a polymerization processing through the RAFT mechanism. A major decrease in polymerization rate occurs in comparison to standard solutions which do not contain Compound 3. This suggests that if the polymerization is following the RAFT mechanism the BDE of the O-R and O-P_n are not sufficiently labile, decreasing the rate at which the radicals reenter the solution. In addition to this information GPC analysis shows all of the samples analyzed have PDIs over 1.7 which is high for a RAFT polymerization. Also, throughout the reaction, the formation of a precipitate is observed in each NMR tube. Therefore, the data suggests that Compound 3 is not acting as a CTA in this polymerization.

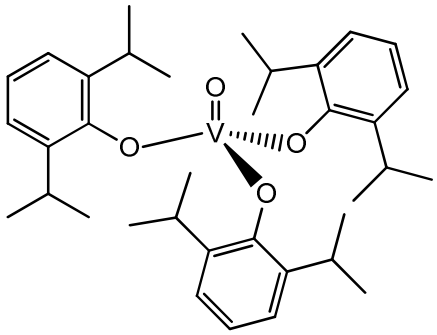

Figure 2. 5 - Tris(2,6-diisopropylphenyl) Orthovanadate Structure, Compound 3

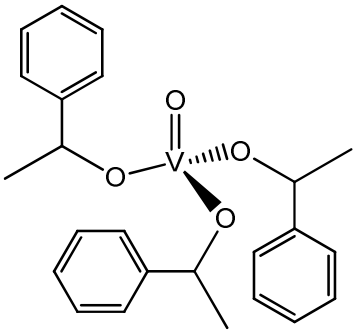

Figure 2. 6 - Tris(1-phenylethyl) Orthovanadate Structure, Compund 4

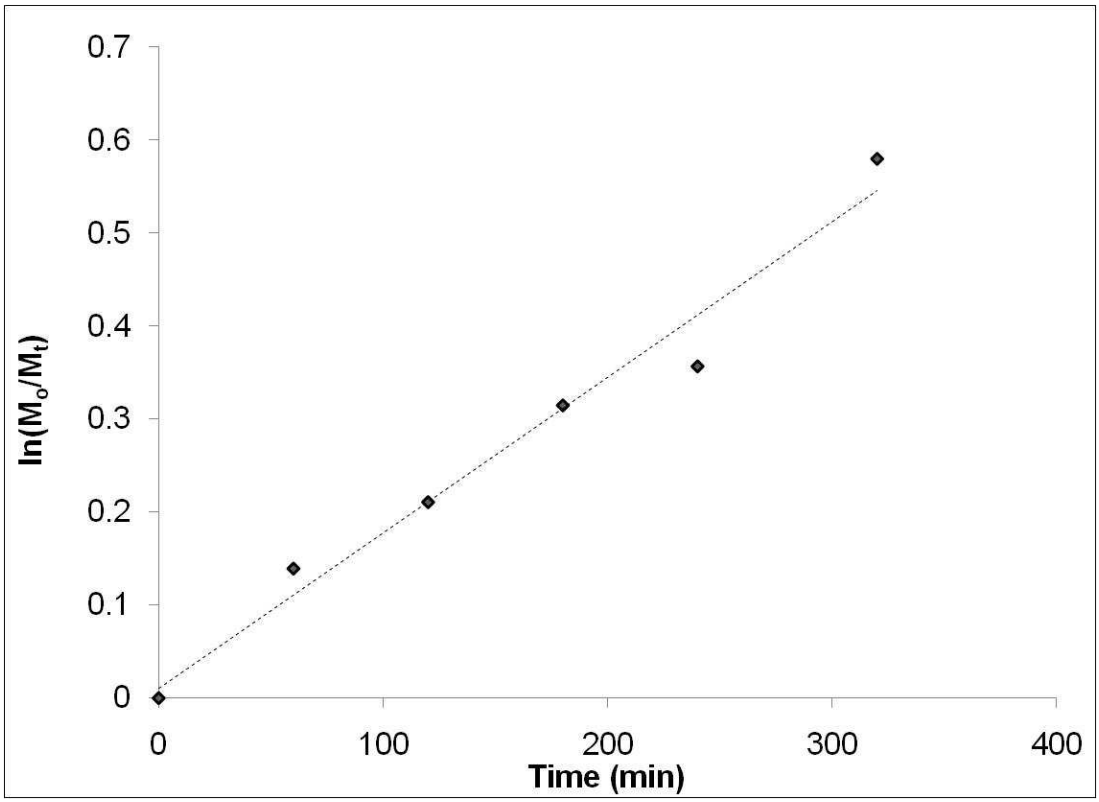

Figure 2. 7 - Kinetic Rate Plot of the Polymerization of MA with Compound 3 Using AIBN as the External Radical Source

2.5 Summary

Four vanadium complexes were tested as CTA for RAFT polymerization, Compounds 1, 2 , and 3 with MA and Compound 4 with styrene. Compound 1 appears to react with the radicals formed in the external radicals given the induction time observed in the kinetic rate plot. However, it appears as though this reaction serves to trap the radicals and form strong O-R bonds which do not interchange with radicals in the solution. Polymerization progresses uncontrolled following the isolation of the Compound 1 through radical trapping. Compound 2 was then used since the isopropyl groups will form more stable radicals which should decrease the O-R bond strength. In these experiments, no induction period was observed and a linear kinetic rate plot is observed, but extremely high PDIs were found though GPC analysis. This implies that the polymerization progresses through a mechanism which does not utilize Compound 2 since there is no apparent change in behavior from a conventional free radical polymerization. Compound 3 also produces a linear rate plot with no induction period, but has significantly lower PDIs than those found for Compound 2. However, the formation of a precipitate throughout the reaction suggests that the addition of radicals to the vanadium complex lowers its solubility resulting in isolation from the polymerization mixture. Finally, the addition of Compound 4 results in an inhibition in styrene polymerization. Given all of this data it is apparent that these vanadium compounds are not good RAFT polymerization CTAs. If use of vanadium complexes as CTAs is possible it appears significant changes to the structure must be made.

2.6 References

1. Boyer, C.; Bulmus, V.; Davis, T. P.; Ladmiral, V.; Liu, J. Q.; Perrier, S., *Chemical Reviews* **2009,** *109* (11), 5402-5436.

2. Moad, G.; Soloman, D. H., *The Chemistry of Radical Polymerization* 2nd ed.; Elsevier: New York, 2006.

3. Moad, G.; Rizzardo, E.; Thang, S. H., *Australian Journal of Chemistry* **2005,** *58* (6), 379-410.

4. Favier, A.; Charreyre, M. T., *Macromolecular Rapid Communications* **2006,** *27* (9), 653-692.

5. Moad, G.; Rizzardo, E.; Thang, S. H., *Polymer* **2008,** *49* (5), 1079-1131.

6. Moad, G.; Chiefari, J.; Chong, Y. K.; Krstina, J.; Mayadunne, R. T. A.; Postma, A.; Rizzardo, E.; Thang, S. H., *Polymer International* **2000,** *49* (9), 993-1001.

7. Chiefari, J.; Chong, Y. K.; Ercole, F.; Krstina, J.; Jeffery, J.; Le, T. P. T.; Mayadunne, R. T. A.; Meijs, G. F.; Moad, C. L.; Moad, G.; Rizzardo, E.; Thang, S. H., *Macromolecules* **1998,** *31* (16), 5559-5562.

8. Monteiro, M. J.; de Brouwer, H., *Macromolecules* **2001,** *34* (3), 349-352.

9. Moad, G.; Rizzardo, E.; Thang, S. H., *Australian Journal of Chemistry* **2006,** *59* (10), 669-692.

10. Chiefari, J.; Mayadunne, R. T. A.; Moad, C. L.; Moad, G.; Rizzardo, E.; Postma, A.; Skidmore, M. A.; Thang, S. H., *Macromolecules* **2003,** *36* (7), 2273-2283.

11. Chong, Y. K.; Krstina, J.; Le, T. P. T.; Moad, G.; Postma, A.; Rizzardo, E.; Thang, S. H., *Macromolecules* **2003,** *36* (7), 2256-2272.

12. Moad, G.; Rizzardo, E.; Thang, S. H., *Accounts Chem. Res.* **2008,** *41* (9), 1133-1142.

13. Moad, G.; Rizzardo, E.; Thang, S. H., *Australian Journal of Chemistry* **2009,** *62* (11), 1402-1472.

14. Monteiro, M. J., *Journal of Polymer Science Part a-Polymer Chemistry* **2005,** *43* (15), 3189-3204.

15. Crans, D. C., *Pure and Applied Chemistry* **2005,** *77* (9), 1497-1527.

16. Hillerns, F.; Rehder, D., *Chemische Berichte* **1991,** *124* (10), 2249-2254.

17. Priebsch, W.; Rehder, D., *Inorganic Chemistry* **1990,** *29* (16), 3013-3019.

18. Joseph, K.; Deshpande, S. S.; Gopinathan, S.; Gopinathan, C., *Indian Journal of Chemistry Section a-Inorganic Bio-Inorganic Physical Theoretical & Analytical Chemistry* **1983,** *22* (2), 159-160.

19. Goto, A.; Sato, K.; Tsujii, Y.; Fukuda, T.; Moad, G.; Rizzardo, E.; Thang, S. H., *Macromolecules* **2001,** *34* (3), 402-408.

20. Henderson, R. A.; Hughes, D. L.; Janas, Z.; Richards, R. L.; Sobota, P.; Szafert, S., *Journal of Organometallic Chemistry* **1998,** *554* (2), 195-201.

Chapter 3 – Development of Catalysts for Use as CMRP Catalysts

3.1 Introduction

Constant development of catalysts and conditions suitable to cobalt mediated polymerization (CMRP) has occurred since the discovery of the process[1, 2] in 1994 by the Wayland and Harwood groups. The largest area of interest is the expansion of monomers to which CMRP is applicable. Complexes initially used for this method were cobalt complexes with open bonding sites where the ligand provides a large amount of steric bulk. This is especially obvious in the complexes containing porphyrin derived ligands. With these complexes the great importance of steric hindrance is directly observed by looking functionality of different compounds containing ligands with different sterics[3]. Two ideal molecules for study are cobalt tetramesitylporphyrin, Co(TMP), and cobalt tetraphenylporphyrin, Co(TPP)[3-5]. Structurally the only difference between these two complexes is the addition of mesityl groups to the phenyl groups of the TPP ligand. This addition adds significant bulk to the ligand partially blocking the open sites found on the cobalt center.

Both of these compounds have been studied for their use for controlling polymerizations, but have led to very different results. Co(TPP) is very useful in catalytic chain transfer polymerization where hydrogen abstraction is necessary for the mechanism[4]. This type of polymerization results in polymers with a high polydispersity index (PDI), but allow for a fast reaction rate and can be used to form lower molecular weight polymer, from hundreds to tens of thousands of units[3]. On the other hand, Co(TMP) has increased congestion around the open sites on the cobalt center forcing the substrates to conform to a specific geometry for approach. Restriction of the Co-C bond formation inhibits the rate of hydride abstraction effectively eliminating the ability of cobalt compound to catalyze catalytic chain transfer. Instead, homolysis of the Co-C bond is favored and as long as this is a facile process with a rate close to that of the rate of polymerization control of the polymerization is observed.

Controlled radical polymerizations using the CMRP technique were first performed on acrylate systems using cobalt complexes with ligands derived from porphyrin compounds and also with cobaloximes, both of which must have high sterics in order for CMRP to be the preferred mechanism[4]. Early research focused on the use of systems where the dormant cobalt

species was prepared prior to introduction into the polymerization synthesis. With this method the polymerization is controlled through the reversible termination (RT) pathway. Reliance on the persistent radical effect (PRE) results in an extremely slow polymerization rate where the rate determining step will be the homolysis of the Co-C bond and the release of the only radicals available to the system[4]. As CMRP research progressed, it was found that with the injection of excess radicals the reaction could progress at a much faster rate since the degenerative transfer (DT) pathway is also available[4, 6]. With the use of external radicals, the rate is no longer determined by the rate of homolysis, rather the polymerization rate approaches that of traditional free radical polymerization and is determined by the concentration and identity of the external radical source[6]. In systems employing an external radical source the RT pathway is far too slow to compete with the DT path. However, if the polymerization is run past the point where the external radicals are fully exhausted, the reaction is seen to continue but at a much slower rate. This indicates that the RT mechanism is now in control of the reaction[4-6]. This increase in polymerization rate increased the usefulness of the CMRP technique.

Unfortunately, the monomers which can be controlled using these complexes are extremely limited restricting the perceived usefulness of the process. However, in 2005 Jérôme reported the polymerization of vinyl acetate (VAc) using the CMRP technique with a bis(acetylacetonato) cobalt (II) compound[7]. This progress was extremely important for the field since CMRP had been proven able to control polymerizations of highly active monomers, while this had proved impossible with any other technique at the time, opening the technique to new applications. Prior to this development, block copolymers incorporating VAc had proven extremely difficult to synthesize. Utilizing CMRP, Jérôme reported the synthesis of poly(vinyl acetate)-b-polystyrene[8] demonstrating the process' profound ability to control monomers with extremely different properties. Incorporation of VAc into block copolymers proves particularly useful since conversion to polyvinyl alcohol can be achieved simply through hydrolysis of the vinyl acetate units[8-10] adding to the utility of the technique. Following the discovery of the ability of $Co(acac)_2$ to control the polymerization of VAc by Jérôme, Wayland's group reported similar findings employing Co(TMP) as the cobalt catalyst in 2008[10, 11]. Through the use of either

Co(TMP) or $Co(acac)_2$ various copolymers of VAc have been synthesized[8, 10, 12] using monomers such as butyl acrylate, methyl acrylate, and styrene. It is important to note, in every copolymer preparation VAc forms the second block and will end with the Co-C bond. VAc must be polymerized last since the radical is extremely unstable due to lack of stabilizing groups[12]. Therefore, when the Co-VAc bond forms a high bond dissociation energy (BDE) is observed and the presence of more stable radicals, such as methyl acrylate, will not result in exchange. However, if CMRP is first performed on the other monomer of interest, a weaker Co-polymer bond is formed which then will facilely exchange with the VAc monomer adding the second block.

Another important aspect of the use of $Co(acac)_2$ in successful CMRP LRP is the significant change in structure from the porphyrin and cobaloxime derivatives used initially. One obvious feature is the complexation of the ligand oxygen atoms rather than nitrogen[9, 12-14]. This change is important because the presence of four nitrogens about the cobalt coordination center has proven crucial for activity as a catalytic chain transfer polymerization catalyst[15]. Incorporation of oxygen into the coordination sphere[16, 17] inhibits hydrogen abstraction preventing the CCTP route and minimizing a mechanism which is detrimental to LRP. $Co(acac)_2$ is also interesting because the sterics around the cobalt center are much lower than what is observed in Co(TMP). This indicates that it is possible to control LRP employing the CMRP technique with lower sterics than was initially believed. In fact, these complexes appear to be able to polymerize a wider range of monomers than Co(TMP). Given this information, research into developing cobalt catalysts with similar structures continues in order to continue to tune the ligands for continued increases in the versatility of the CMRP technique. In most cases, the organocobalt dormant complex is synthesized in situ and an external radical source is employed which will result in the mechanism mainly being driven by the DT pathway. These conditions allow for the CMRP reaction to proceed at a rate similar to a traditional free radical polymerization making the process more serviceable for possible industrial use in the future.

3.2 Co(Salen)

The first compound chosen for testing as a CMRP catalyst was Co^{II}(salen), Compound 1 in Figure 3. 1. Structurally there are several reason that Co^{II}(salen) was determined to be a potentially promising candidate. First, as with other CMRP catalysts, Compound 1 has two open sites around the cobalt center[2, 4-7, 10]. These open sites allow for coordination of the radicals produced in the polymerization to complex from either side. Since there are two open sites, both the RT and DT pathways should be viable since a new radical can approach the back of the organometallic for the DT mechanism. If the DT path is possible for using this catalyst duringfor the polymerization, a significant increase in rate will be observed when compared with complexes that only employ an RT mechanism[6] making the process more interesting for future applications. Another area of interest in this molecule is around the coordination sphere, for the Co^{II}(salen) the ligand is coordinated to the cobalt center through two oxygen and two nitrogen. The coordination of the ligand to the cobalt center is important for minimizing the opportunity for CCTP, which is an undesirable mechanism in CMRP. Previous work has indicated that the likelihood of the CCTP route is severely decreased if there are not four nitrogen atoms in the coordination sphere of the catalyst[15].

Another design method used to minimize the CCTP pathway in development of CMRP is to increase the steric bulk of the ligand. The initial complexes utilized in CMRP have cobalt coordinated to its ligands through four nitrogen atoms, Co(TMP)[2] and cobaloximes[1] in particular, for these complexes the CCTP pathway was avoided through the high steric bulk found in the ligands coordinated to the cobalt center. Increasing the sterics of the ligand minimizes the β hydrogen abstractions necessary for CCTP by restricting access to the metal center. While this restriction has proven extremely important with ligands coordinated by four nitrogen atoms, in 2005 Jerome's use of $Co(acac)_2$ demonstrated the use of a cobalt catalyst with lower sterics[7]. The critical change with the use of $Co(acac)_2$ is the coordination of the acac ligand through four oxygen centers. This replacement minimizes the CCTP pathway without the use of a high steric bulk ligand. With the use of Co^{II}(salen), the ligand sterics are between those seen in Co(TMP)

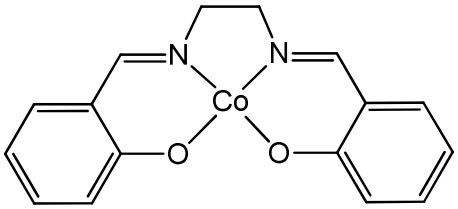

Figure 3. 1 - Co^{II}(salen) Structure, Compound 1

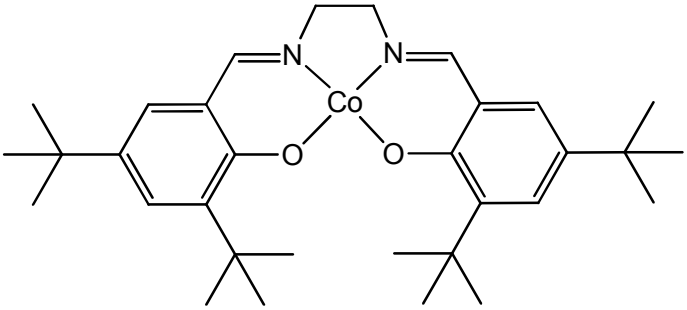

Figure 3. 2 - N,N'-Bis(3,5-di-*tert*-butylsalicylidene)-1,2-ethanediamino Cobalt (II) Structure, Compound 2

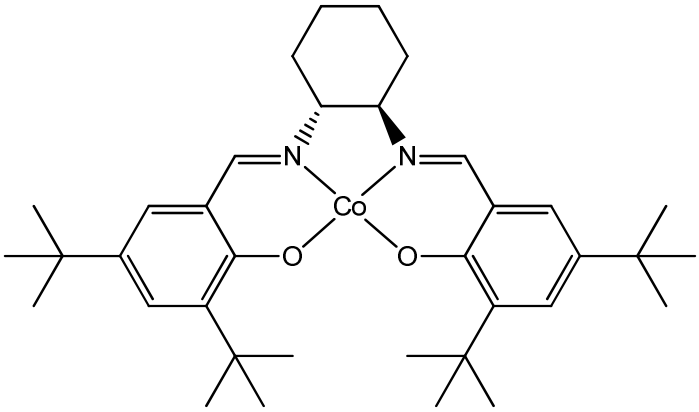

Figure 3. 3 - (R,R)-N,N'-Bis(3,5-di-*tert*-butylsalicylidene)-1,2-cyclohexanediamino Cobalt (II), Compound 3

and $Co(acac)_2$ which combined with the ligation of the ligand through two nitrogen and two oxygen atom is expected to combine both properties to minimize the CCTP mechanism sufficiently while promoting the LRP CMRP pathway. The structure of the Co^{II}(salen) was believed to be ideal for a CMRP catalyst combining properties seen in previous models.

3.2.1 Synthesis and Standardization

Preparation of Co^{II}(salen) was performed through insertion of Co^{ii} into N,N'-ethylenebis(salicylimine). Previous group members performed the condensations of ethylenediamine and salicylaldehyde to synthesize yellow, crystallized N,N'-ethylenebis(salicylimine), salen. Insertion of the cobalt center into the salen ligand was performed according to the following using a method reported by Jacobsen[18]. Cobalt (II) acetate tetrahydrate was used as received to prepare a 25mmol solution in methanol and a 20mmol solution of salen was prepared in dichloromethane. The cobalt and salen solutions were then mixed together under nitrogen and allowed to stir at room temperature for 15 minutes. Using a water-ice bath the solution was cooled to 0˚C and the solution was allowed to stir for another 30minutes. During this time, the formation of an orange-red precipitate was observed. The solid was then collected via vacuum filtration and rinsed with cold methanol in order to remove the excess cobalt acetate. The solid was then fully dried on the high vacuum line.

^{1}H-NMR of the Co^{II}(salen) complex was used to confirm that the complex was correctly synthesized through comparison with known peak values[19, 20]. Very low concentrations of Co^{II}(salen) are necessary for CMRP runs. Since mass measurements in this range prove very inaccurate, a solution is prepared and standardized for later use. For this system a solution of Co^{II}(salen) is prepared in chloroform at approximately 1×10^{-3}M and the salen ligand is used as the standard compound. A small aliquot is then place in a vacuum adapted NMR tube and dried. An aliquot of salen in deuterated chloroform is added to the NMR tube to resolubilize the cobalt solid. ^{1}H-NMR of the solution is then taken and using an the ratio of integrated peaks the concentration of Co^{II}(salen) in the stock solution was calculated using the known salen standard concentration.

3.2.2 Radical Polymerization of Methyl Acrylate in the Presence of Co^{II}(salen)

Initial testing of Co^{II}(salen) as a CMRP catalyst was performed using the radical polymerization of MA in a similar manner to the conditions used for Co(TMP)[2, 6, 10, 11, 21, 22]. AIBN was utilized as an external radical source in all trials utilizing Co^{II}(salen) so the DT and RT mechanisms are both possible for this system. Unlike Co(TMP), the polymerization runs were performed in deuterated chloroform since the compound was found to be insoluble in benzene. Halogenated solvents are atypical choices of solvent for free radical polymerization due to the high tendency of halogen abstraction, however, Co^{II}(salen) was found to only be soluble in these types of solvents.

In every run, the concentration of Co^{II}(salen) was 1 x 10^{-3} M and the concentration of MA was held at 2.5 M. For these studies 2,2'-azobisisobutyronitrile, AIBN shown in Figure 3. 4, was used as the external radical source. Various concentrations of AIBN were utilized in order to obtain information on the effect of changing the radical to cobalt ratio. Each run was performed at 60˚C where the half-life of the thermal initiator is calculated to be 16.5 hours from information provided by the Wako[23]. All polymerizations were performed in vacuum adapted NMR tubes after freeze-pump-thawing the solution a minimum of three cycles. Initial observation of the reaction was performed via ^{1}H-NMR, where during the analysis all of the NMR tubes being used were cooled with a dry-ice acetone bath in order to halt the reaction and maintain the timing. After the reaction progressed the desired amount, the NMR tubes were opened and the solution was dried using the high vacuum line to remove the excess monomer and solvent prior to GPC analysis. The solid polymer was then dissolved in tetrahydrofuran and run through a 0.45μm PTFE filter. Gel permeation chromatography, GPC, analysis of each sample was then performed on a Shimadzu modular system using a Polymer Laboratories 5.0 μm PLgel guard column(50 x 7.5 mm) and three linear PLgel columns (1 x 10^6, 1x 10^4, and 5 x 10^2 Å). The columns were in a 40˚C oven (CTO-10A) and the spectra were obtained with a UV-vis detector (SPD-10AV) and a differential refractometer (RID-10A). Each run employed THF as the eluent and was run at a flow

AIBN

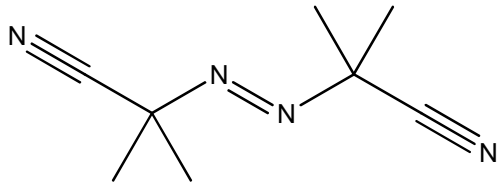

□-70

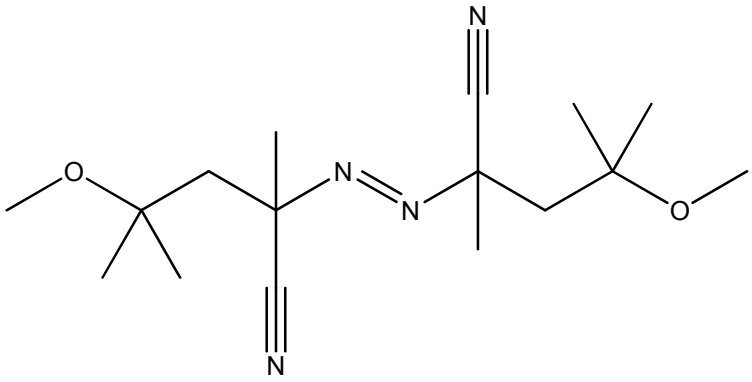

Figure 3. 4 – Azo Initiator Structures

rate of 1 ml min^{-1}. The GPC was calibrated using narrow peak width polystyrene standards (Easical from Polymer Laboratories) ranging from 580 to 7.5 x 10^6 g mol^{-1}.

First order kinetic rate plots are shown in Figure 3. 5 of three MA polymerization runs with Co^{II}(salen). In these experiments, the AIBN concentration was varied while all of components were held constant at the conditions stated previously. Assuming that each AIBN molecule thermally decomposes to two initiator radicals and the efficiency of these radicals is 65 percent, the ratio of cobalt centers to radicals for these runs were 1:30, 1:10, and 1:6, concentrations of AIBN were 2.20 x 10^{-2}, 7.31 x 10^{-3}, and 4.48 x 10^{-3} M respectively. Decreasing the concentration was accompanied by a decrease in the rate of polymerization as was expected since the reaction is AIBN rate dependent. While the general trend is followed a much more linear behavior is expected for LRP since the external radical source is not expended in the range of time the reactions were observed.

Another important feature of these experiments is the observed induction periods. While this is much less apparent for the high concentration run, 1:30, a linear best fit line can be drawn for each set of conditions utilizing the points where polymerization has been observed. When this analysis was performed, the x axis intercept is calculated to find the induction period for each run. These values are found in Table 3. 1 and are seen to increase with a decrease in radical concentration as expected. The theoretical times for the concentration of radicals that have entered the reaction solution to equal that of Co^{II}(salen) give the assumptions given previously were calculated and are shown in Table 3. 1. This concentration is critical if the reaction is progressing according to CMRP since the cobalt (II) must be converted to the organometallic cobalt (III) compound in order to act as a mediator. By comparing the observed and theoretical induction periods for the polymerization, it is obvious that while the observed time does increase with decreasing radical concentration, the time becomes increasingly shorter than what is expected.

The final analysis performed on the polymers produced during these experiments is GPC in order to determine the polydispersity index, PDI, which is a good indicator of the even growth

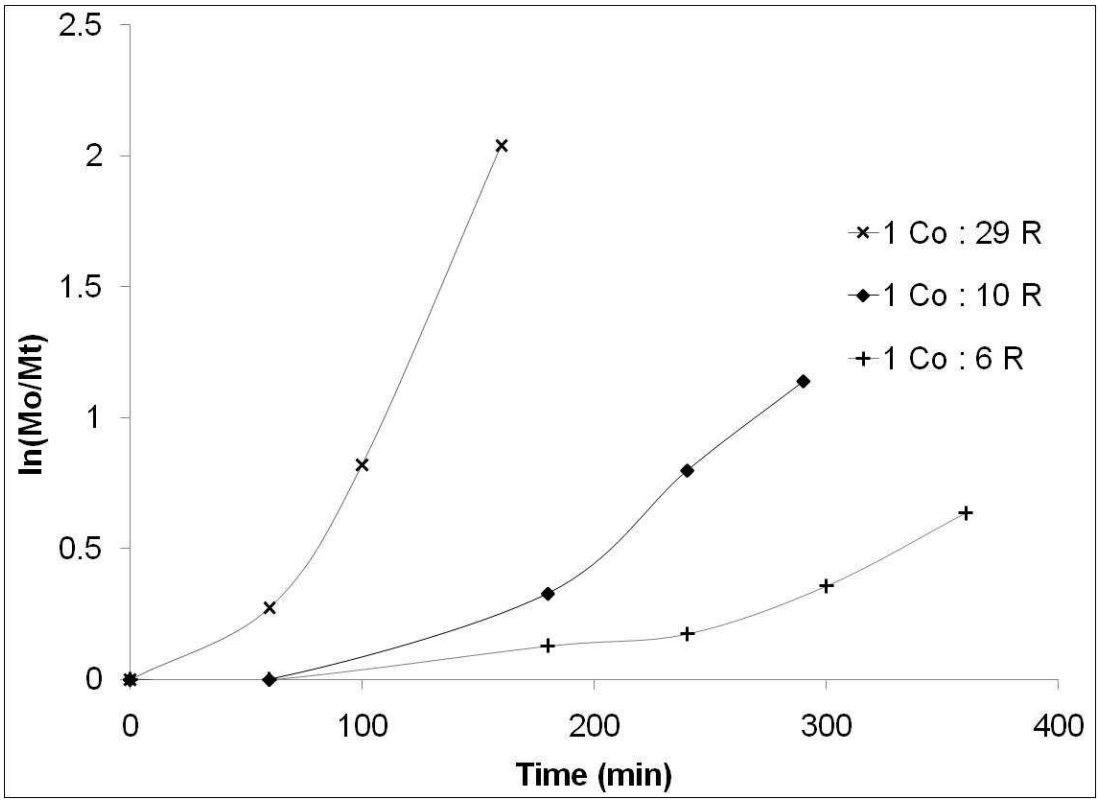

Figure 3. 5 - Kinetic Rate Plot for the Polymerization of MA with Co(salen) Using Various Concentrations of AIBN

Experiment	Theo. Ind Time (min)	Obs. Ind Time (min)
1 Co : 29 R•	50	50
1 Co : 10 R•	160	125
1 Co : 5 R•	260	160

Table 3. 1 - Theoretical and Observed Induction Times for the Polymerization of MA with Co(salen)

which is necessary for Co^{II}(salen) to be acting as a LRP mediator. For these runs the PDIs were typically around 2.0 with the 1.6 being the lowest value. The PDIs for these polymers are extremely high, some polymers produced through traditional free radical polymerization have been observed with lower PDIs, and indicate a complete lack of control during the polymerization process. Unfortunately, these non-ideal behaviors (non-linear behavior, short induction periods and extremely high PDIs suggest that Co^{II}(salen) is not an appropriate choice of CMRP catalyst.

Several observations seem to indicate why Co^{II}(salen) was not able to mediate the MA polymerization. During the reactions the color of the solutions were observed changing from a dark red-orange to a more brown-green. This is a significant change and indicates that there has been a major change at the cobalt center. This color change is also seen in the stock solution after extensive storage. The shortened induction period also suggests that a 1:1 ratio of cobalt to initiator radicals is not necessary in order for the polymerization to progress. However, the addition of Co^{II}(salen) to the reaction mixture does inhibit chain growth in the beginning of synthesis giving evidence to the trapping of at least a portion of the radicals formed through thermolysis. After the induction period, the rate of reaction is seen to be nearly identical to that of the standard solutions which contain only AIBN and MA. From these rates it appears as though the polymerization proceeds without employing the cobalt complex as a mediator. Examination of this information gives an idea of what may be occurring in this system. Given the similarity of the observation, both long term and short term, with the addition of heat and free radicals to the system, it appears as though use of chloroform as the solvent is unacceptable. Abstraction of the chlorine atom from the solvent could result in irreversible coordination to the cobalt center blocking the formation of the desired organometallic species. Once all of the cobalt complexes have been blocked all of the radicals entering the solution will result in propagation of the polymer, as in conventional free radical polymerization. This explanation therefore would account for the induction period as well as the rate of polymerization observed following the induction period. Given the issues observed with the use of halogenated solvents in this system and the lack of solubility in other non-donating solvents no further testing was performed using this compound.

3.3 N,N'-Bis(3,5-di-*tert*-butylsalicylidene)-1,2-ethanediamino Cobalt (II)

Based on the results from the study of Co^{II}(salen) as a CMRP catalyst, Compound 2, Figure 3. 2, was chosen as the next CMRP catalyst candidate with the belief that the addition of the *tert*-butyl groups would improve solubility in non-coordinating solvents. The salen derivative was synthesized using a procedure adapted from Jain[24], shown in Scheme 3. 1. While the reported condensation reaction was performed in water, 3,5-di-tert-butyl-2-hydroxybenzaldehyde is insoluble in aqueous solutions. Instead, the reaction was carried out in methanol so that a homogenous mixture was obtained. For this synthesis 40 mmol of 3,5-di-tert-butyl-2-hydroxybenzaldehyde was dissolved in methanol and the solution was purged with nitrogen. 24 mmol of ethylenediamine was injected into the solution and the mixture was stirred at 308K overnight. The mixture was then cooled, and cold water was added to cause the solid product to crash out of solution. Vacuum filtration followed by a cold water rinse was used to collect the bright yellow product and the solid was placed on the high vacuum line for drying. ^{1}H-NMR was used to verify formation of the desired product.

Following the synthesis of the 3,5,-di-*tert*-butyl salen ligand, cobalt was inserted using the method described in Section 3.2.1 resulting in a dark red solid. Confirmation of the formation of Compound 2 was observed through the significant shift of peaks in the ^{1}H-NMR, in deuterated pyridine, due to the formation of the paramagnetic complex. Solubility of the Compound 2 complex was then tested in several solvents in order to determine it viability as a CMRP catalyst given the results observed for Co^{II}(salen) . Compound 2 was found to be nearly insoluble in benzene, acetone, toluene, and methanol and soluble in a several halogenated solvents as well as pyridine. Unfortunately, all of the solvents in which there is good solubility are donating solvents and will coordinate to the cobalt center during storage or polymerization runs. In fact, color changes were observed with these solvents over the course of a few days. No further studies were performed on Compound 2, due to its limited solubility in non-coordinating solvents.

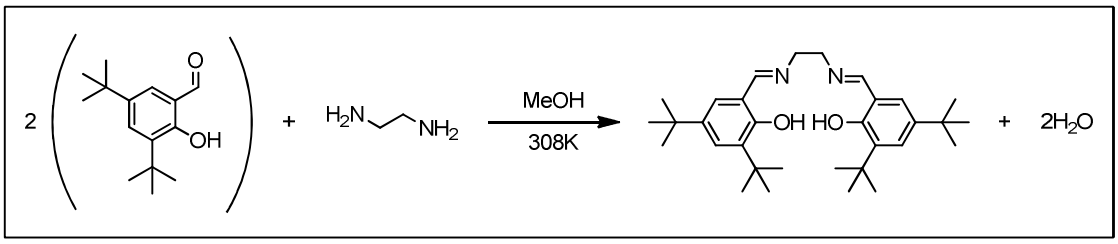

Scheme 3. 1 - Condensation Reaction for the Synthesis of N,N'-Bis(3,5-di-*tert*-butylsalicylidene)-1,2-ethanediamine

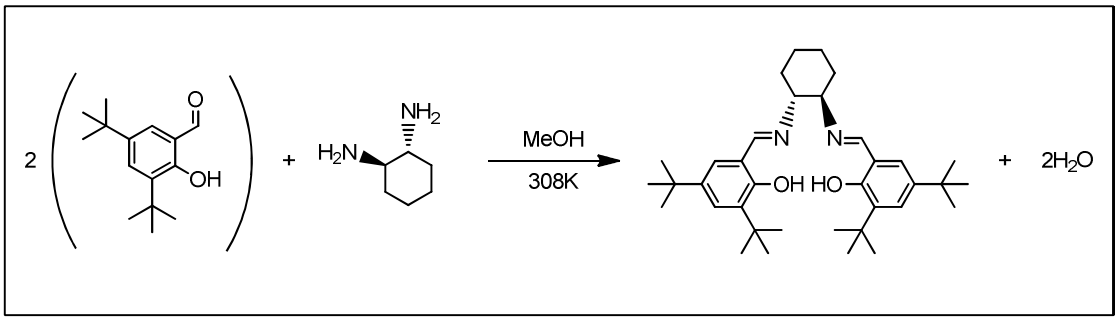

Scheme 3. 2 - Condensation Reaction for the Synthesis of (R,R)-N,N'-Bis(3,5-di-tert-butylsalicylidene)-1,2-cyclohexanediamine.

3.4 (R,R)-N,N'-Bis(3,5-di-*tert*-butylsalicylidene)-1,2-cyclohexanediamino Cobalt (II)

With the intention of increasing the solubility while maintaining structural similarities to Compounds 1 and 2, Compound 3, Figure 3. 3, was chosen as a candidate for studies as a CMRP catalyst. The ligand used in this complex has previously been used coordinated to a manganese metal center and is commonly known as Jacobsen's catalyst and used as an epoxidation catalyst [25-29]. This compound has also been used in its cobalt (III) form as a epoxidiation catalysts to produce enatioenriched products[18]. During the synthesis of Jacobsen's catalysts the compound is dissolved in both toluene and heptanes while the cobalt (III) derivative is used for epoxidation in tetrahydrofuran suggesting that Compound 3 may have greater solubility in a wider variety of solvents that Compounds 1 or 2.

3.4.1 Synthesis and Standardization

Prior to synthesis of the (R,R)-N,N'-Bis(3,5-di-tert-butylsalicylidene)-1,2-cyclohexanediamine ligand, the R,R form of 1,2–diamino cyclohexane was isolated from a racemic mixture. A sample of the racemic mixture was added to a solution of l-glutamate in an aqueous solution. When l-glutamate is added to the compound it will bond with the R, R form causing it to precipitate out of the solution while the S,S form remains unbound and soluble allowing for the separation of the two racemates. Separation of R,R-1,2–diamino cyclohexane from the l-glutamate was then accomplished by adding the solid to equal volumes of dichloromethane and a 2M aqueous NaOH solution followed by vigorous agitation. After the layers are allowed to separate R,R-1,2–diamino cyclohexane is found in the organic layer. Once this layer is isolated, the production is dried using rotary evaporation to remove the dichloromethane.

One equivalent of R,R-1,2–diamino cyclohexane and two equivalents of 3,5-di-tert-butyl-2-hydroxybenzaldehyde are then mixed as described in Section 3.2.1 according to a modified version of the procedure reported by Jain[24], Scheme 3. 2. Two syntheses were run, one as an aqueous solution with the addition of a small amount of acetone to increase the aldehyde solubility and the other was run in a methanol solution as described in Section 3.3. A much

higher yield and conversion was achieved using the methanol solution likely due to incomplete dissolution in the aqueous solution. After isolating the yellow (R,R)-N,N'-Bis(3,5-di-tert-butylsalicylidene)-1,2-cyclohexanediamine product and confirming its identity and purity through comparison of the 1H-NMR to the literature values[27], insertion of the cobalt into the ligand was performed as described in Section 3.2.1. A brick red solid was formed and confirmed to be (R,R)-N,N'-Bis(3,5-di-tert-butylsalicylidene)-1,2-cyclohexanediamino Cobalt (II) through comparison of the ^{1}H-NMR spectrum to literature values of similar complexes[19, 20, 27].

Compound 3 was found to be soluble in benzene and the stock solution was prepared using benzene since it is non-coordinating. For the standardization, the solutions are prepared with dichloromethane and deuterated dichloromethane. While this is not appropriate for long term storage or as the solvent for the polymerization reaction, it provides better peak separation for the standardization and does not cause adverse effects at the low temperature and short time required to obtain the ^{1}H-NMR spectra necessary for standardization. Vanillin was used as the internal standard and the integration of the *tert*-butyl peaks of the complex were used in order to calculate the concentration of the stock solution.

3.4.2 Radical Polymerization of Methyl Acrylate in the Presence of Compound 3

Initial studies on Compound 3's ability to mediate polymerizations via the CMRP mechanism were performed on MA. The reactions all employed 2,2'-azobis(4-methoxy-2,4-dimethylvaleronitrile), V-70 shown in Figure 3. 4, as the external radical source which should create an environment where DT will be the favored reaction mechanism. Compound 3 and the MA were held at constant concentrations, 1 x 10^{-3} and 2.5 M respectively, throughout the trials. Various concentrations of V-70 were employed to monitor the change in behavior in accordance with changing initiator to cobalt ratios. The polymerization temperature was maintained at 50˚C where calculations using the information supplied by Wako give a half-life for the thermal decomposition of V-70 as 36 minutes. The setup and analysis of each trial was performed in the manner described in Section 3.2.2 using the same instrumentation.

The kinetic rate plots for methyl acrylate polymerization using Compound 3 with V-70 as the external radical source and from 0.68 to 1.4 radicals to 1 cobalt centers are shown in Figure 3. 6. As with the data shown in Section 3.2.2 and reports of polymerizations using Co(TMP), a defined induction period is observed in every experiment. The ratios of radical to cobalt given for these runs provides the number of radicals that will enter solution assuming a 60 percent efficiency for V-70 and full decomposition. Using this information, examination of the plots provide several useful pieces of information. The run with the lowest concentration of radicals proves extremely important since polymerization occurs in a system where the "required" number of radicals will never be injected into the polymerization mixture. The importance of this observation lies in the fact that previous studies have shown that for the CMRP mechanism full conversion from Co^{II} to Co^{III} was required before polymerization would progress.

Using a linear best fit line for the data where polymerization is progressing, the induction period for each experiment was determined through calculation of the y-intercept, these values, as well as the theoretical induction times, are provided in Table 3. 2. In every experiment, the number of radicals injected is far less than required to result in a 1:1 ratio with cobalt, shown in the final column of Table 3. 2. By performing polymerization runs with significantly lowered concentrations of MA, 0.612M, and a 1:1.1 ratio of cobalt centers to radicals, it is possible to monitor the conversion of Co^{II} to Co^{III} with ^{1}H-NMR. Converting the complex from a paramagnetic to a diamagnetic species results in a dramatic change in the position and resolution of the peaks resulting from the hydrogen atoms on the ligand. Monitoring the decrease in size of the *tert*-butyl peak found at -0.48 ppm in comparison to the TMS peak within the sample provides a method for determining the oxidation of Compound 3. In these studies, the peak decreases but never fully disappears, at minimum 20 percent of the Co^{II} species still remains, which indicates that polymerization must begin without full conversion to the Co^{III} complex. Since far fewer radicals are necessary than expected for progression of the polymerization, when calculating the theoretical induction period the observed time is significantly shorter than the calculated values. Increasing the concentration of radicals in the polymerizations should result in shorter induction

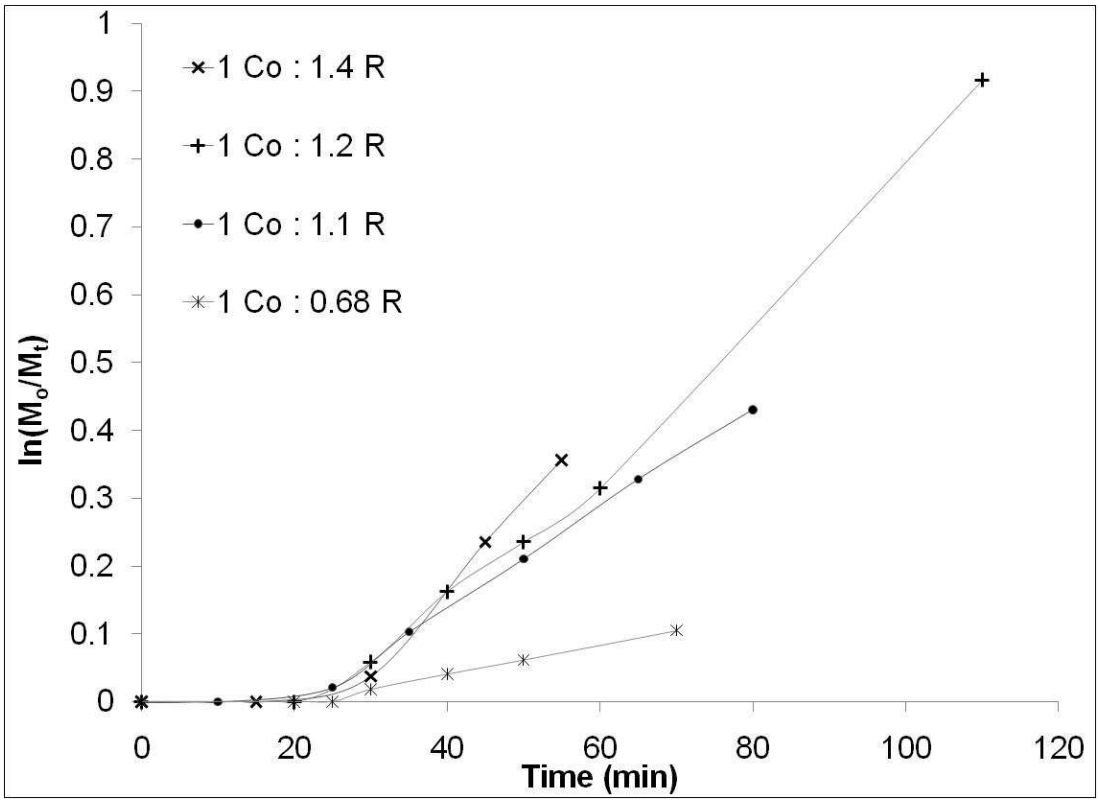

Figure 3. 6 - Kinetic Rate Plot for the Polymerization of MA with Compound 3 Using Various Concentrations of V-70

Experiment	Theo. Ind Time (min)	Obs. Ind Time (min)	Co : R• by Obs. Ind Time
1 Co : 1.4 R•	68	26	1.8 : 1
1 Co : 1.2 R•	91	26	2.1 : 1
1 Co : 1.1 R•	144	22	2.9 : 1
1 Co : 0.68 R•	N/A	22	4.4 : 1

Table 3. 2 - Observed and Theoretical Induction Times and Injected R for the Radical Polymerization of MA with Compound 3

times, this is shown by the increasing values of the theoretical induction time in Table 3. 2, however, these experiments suggest there is no real connection between radical concentration and induction time for these reactions.

Following the induction period, the kinetic rate plot shows a linear relationship which is anticipated for a CMRP reaction. All of the data for these experiments is collected well before the V-70 is exhausted so the linear behavior shown in Figure 3. 6 is not expected to level off since the DT mechanism will be fully in control throughout the trials. When the polymerization operates the DT mechanism, the rate of polymerization is determined exclusively by the initiator concentration. Comparing the post induction period portion of the kinetic rate plots of the four runs with varying concentrations of V-70, shows a reduction of the slope with the decrease in injected radicals thereby verifying that the polymerization rate is dependent on the V-70 concentration as expected. Standard polymerizations were run under the same conditions as those described, excluding Compound 3. Linear regression lines were added to the kinetic rate plots of this data. The slopes of these lines demonstrate that the polymerization rate without Compound 3 in the solution is approximately triple that found for the runs containing Compound 3. LRP generally progress at lower rates than standard free radical polymerizations since the radicals spend a portion of their time in the dormant complex. The observed decrease in rate therefore is a positive sign that Compound 3 is acting as a mediator throughout the polymerization.

Data from GPC analysis of the runs described previously is summarized in Figure 3. 7 and Table 3. 3. The molecular weight of the polymer is found to increase non-linearly with a decrease in slope at higher conversions. Early in the reaction, the polymers are significantly larger than the theoretical mass, assuming the growth of one polymer chain for each cobalt center, but as the conversion increases the molecular mass approaches and the crosses the expected value ending in a mass significantly lower than the theoretical mass. Coupled with the earlier results, this observation is likely due to the polymerization beginning prior to the conversion of all of Compound 3. When polymerization begins with only a small portion of

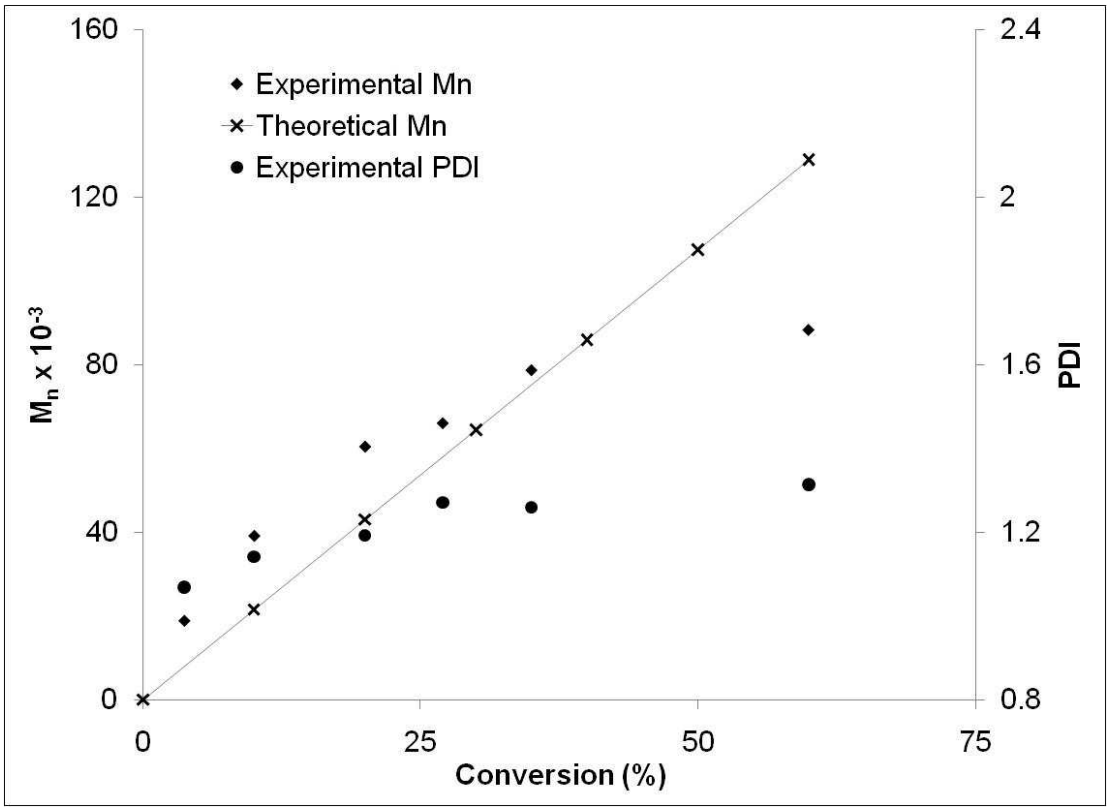

Figure 3. 7 - Molecular Weight Dependence on Conversion, Experimental and Theoretical, and PDI of MA Polymerized in the Presence of Compound 3

Conversion (%)	Mn (g/mol)	PDI
3.7	18813	1.069
10	39103	1.141
20	60410	1.192
27	66029	1.271
35	78684	1.259
60	88303	1.314

Table 3. 3 - Conversion, Molecular Weight, and PDI of MA Polymers Synthesized Using Compound 3

Compound 3 oxidized to the +3 state, if mediating is occurring through the cobalt center, very few chains will be initiated. If fewer chains are initiated than was assumed for the calculation of the theoretical molecular mass, the observed mass will be higher than the theoretical since the polymerization is occurring through fewer chains. If this is the case, the PDI should remain relatively low especially at lower conversions since the polymerization is proceeding through the CMRP mechanism. Throughout the polymerization Compound 3 continues to be converted, initiating more chains. This behavior will slightly increase the PDI until equilibrium is achieved between the Co^{II} and Co^{III} species since the new chains will have polymerized over a shorter time period. The PDI for the polymers does in fact show this relationship, shown in the last column of Table 3. 3, there is a slight increase as the percent conversion increases but overall the values are close enough to unity to suggest a control of the polymerization.

All of the evidence provided for the free radical polymerization of MA with Compound 3 suggests that polymerization begins prior to full oxidation of the cobalt complex. While this is not consistent with previous reported CMRP systems, the decrease in linear kinetic rate plot, induction period, polymerization rate and low PDI suggest that the polymer is in fact being mediated by Compound 3. This is further supported by experiments performed with the addition of pyridine to the polymerization mixture. Pyridine is a strong coordinating molecule and was added to the solutions in a 1:1 ratio with Compound 3 in order to block one open site of each metal center. In these experiments, complete loss of control was observed by: fast polymerization rate, no observable induction period, high PDI, and extremely large molecules. From this information, it is apparent that the loss of the open site in Compound 3 prevents mediation of the polymerization leading to results consistent with conventional free radical polymerization. However, the short induction periods, non-linear conversion versus molecular weight relationship, and polymerization in systems which the external radical source is not present in high enough concentration to ever reach 1:1 ratio with Compound 3 are all observations inconsistent with previously reported CMRP systems. What all of the data suggests is that a significant alteration to the initiation step of the CMRP mechanism takes place. For this

system, equilibrium between the dormant complex and propagating radicals begins prior to full oxidation of Compound 3. In fact, the complete conversion to the Co^{III} was not observed but once the polymerization begins to progress the propagation steps of the CMRP mechanism appear to be followed resulting in a well defined polymer product. While Compound 3 does not precisely follow the CMRP mechanism described previously, Section 1.5.2, the complex does appear able to mediate the polymerization of MA.

3.4.3 Radical Polymerization of Vinyl Acetate in the Presence of Compound 3

Vinyl acetate, VAc, was chosen as the second monomer of interest since CMRP has proven extremely useful as a LRP when compared to other techniques. If Compound 3 has the ability to control the polymerization of VAc , this is a large increase in system versatility due to the large difference in properties when compared to MA. Unlike MA, CMRP requires the injection of a higher ratio of radicals, typically significantly higher than 1:1 ratio with the metal centers[9, 10]. For these experiments AIBN was used as the thermal initiator under the same conditions described in Section 3.2.2. For each of the polymerization runs, the concentration of Compound 3 was maintained at 1×10^{-3} and solutions were kept at 60˚C throughout the run. The concentrations of AIBN and monomer were varied as described. Polymerization was monitored via ^{1}H-NMR and the polymer products were analyzed using the instrumentation described in Section 3.2.2.

At low AIBN concentrations, no polymerization was observed when Compound 3 was present in the solution, large increases in radical concentration were necessary for polymerization to progress. Kinetic rate plots of several runs are provided in Figure 3. 8. As with the previous examples using Compound 1 and Compound 3 for the polymerization of MA, a distinct induction period is observed in each experiment. Using the method described in Section 3.4.2 the observed induction times were calculated and compared to the theoretical values, Table 3. 4. Unlike the MA polymerizations, the induction period is significantly longer than expected and between 1.7 and 2.2 radicals have entered the solution before polymerization is observed. These results are similar to those seen in the polymerization of VAc using Co(TMP) as the CMRP mediator, in these studies 1.7:1 ratio of radical to cobalt centers were necessary prior to the onset

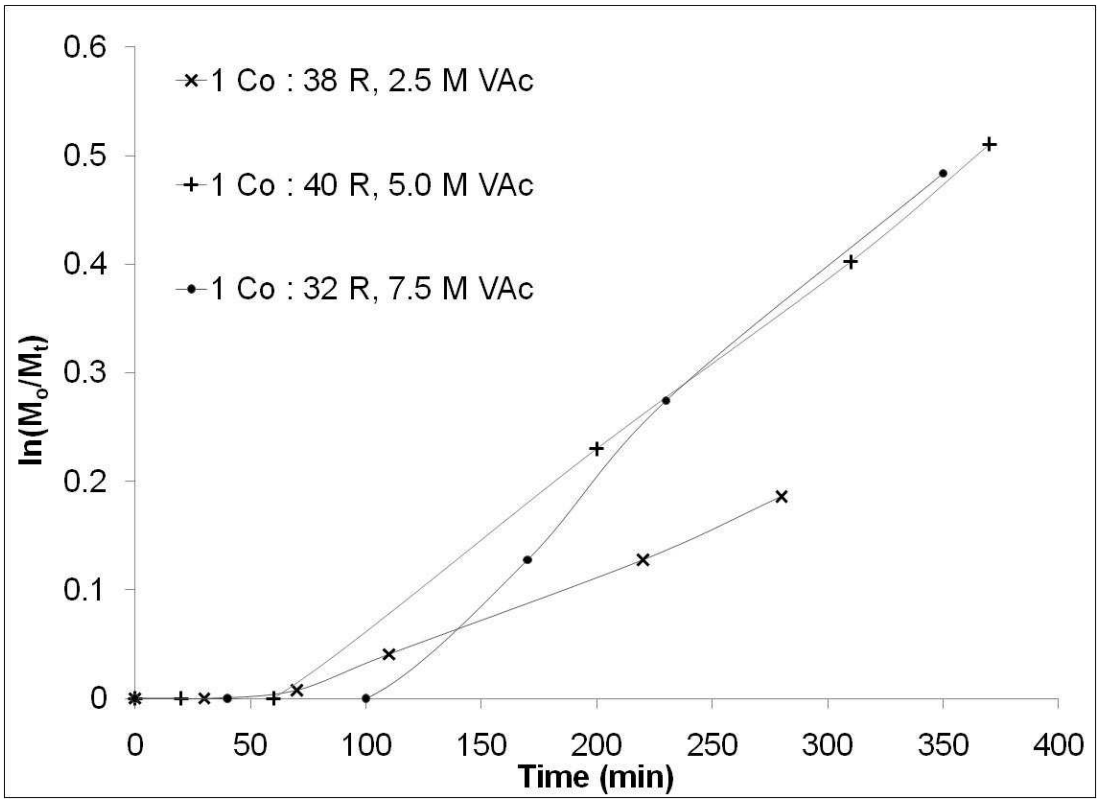

Figure 3. 8 - Kinetic Rate Plot for the Polymerization of VAc with Compound 3 Using Various Concentrations of AIBN

Experiment	Theo. Ind Time (min)	Obs. Ind Time (min)	Co : R• by Obs Ind Time
1 Co : 40 R• 5.0 M VAc	36	63	1 : 1.72
1 Co : 38 R• 2.5 M VAc	37	65	1 : 1.70
1 Co : 32 R• 7.5 M VAc	45	100	1 : 2.16

Table 3. 4 - Observed and Theoretical Induction Times and Injected R for the Radical Polymerization of VAc with Compound 3

of polymerization[10]. This behavior appears to be due to the decreased stability of the VAc radicals when compared to MA causing inefficiency in the conversion of the cyanoisopropyl radicals to VAc radicals. A decrease in the polymerization rate compared to that observed with MA can be attributed to the increased Co-C bond strength when formed with the VAc radical. Figure 3. 9 provides data showing the significant rate decrease for the VAc polymerization when compared to MA. In this plot, the MA experiment was run with half of the radical concentration of the VAc experiment, but had both a shorter induction period and larger slope which indicate a higher polymerization rate. The last three points of the MA run provided in this figure were also analyzed by GPC, and the PDI's were found to be between 1.29 and 1.49 suggesting that the CMRP mechanism described for Compound 3 previously was still being followed even at high radical concentrations since the PDI of the standard solution, no Compound 3 but same conditions, was 2.0.

Following the induction period, the linear behavior of the kinetic rate plot of the VAc polymerization, Figure 3. 8, indicates a first order mechanism which is expected for the CMRP mechanism. The increasing slopes mainly correspond to the increase in monomer concentration, since there is very little change in radical concentrations between the three experiments. GPC analysis was performed on samples of the polymers produced during these runs, shown in Figure 3. 10 and summarized in Table 3. 5. All the PDI are in the 1.4 to 1.5 range which is not ideal and slightly higher than those reported using Co(TMP)[10], but is still significantly lower than the standards which did not contain Compound 3, PDI's were all around 2.0. Ideally, a linear relationship should be observed between molecular weight and percent conversion for a system that is truly living. Figure 3. 10 clearly shows that this is not the case for the current system, however, precedence is found in the literature[10, 11] for non-linear behavior similar to that seen for the polymerization using Compound 3. Deviations toward lower molecular weights than the theoretical values increase with increasing conversion indicating non-deal behavior. These deviations likely cause the increase in PDI due to dead chains which are no longer able to propagate.

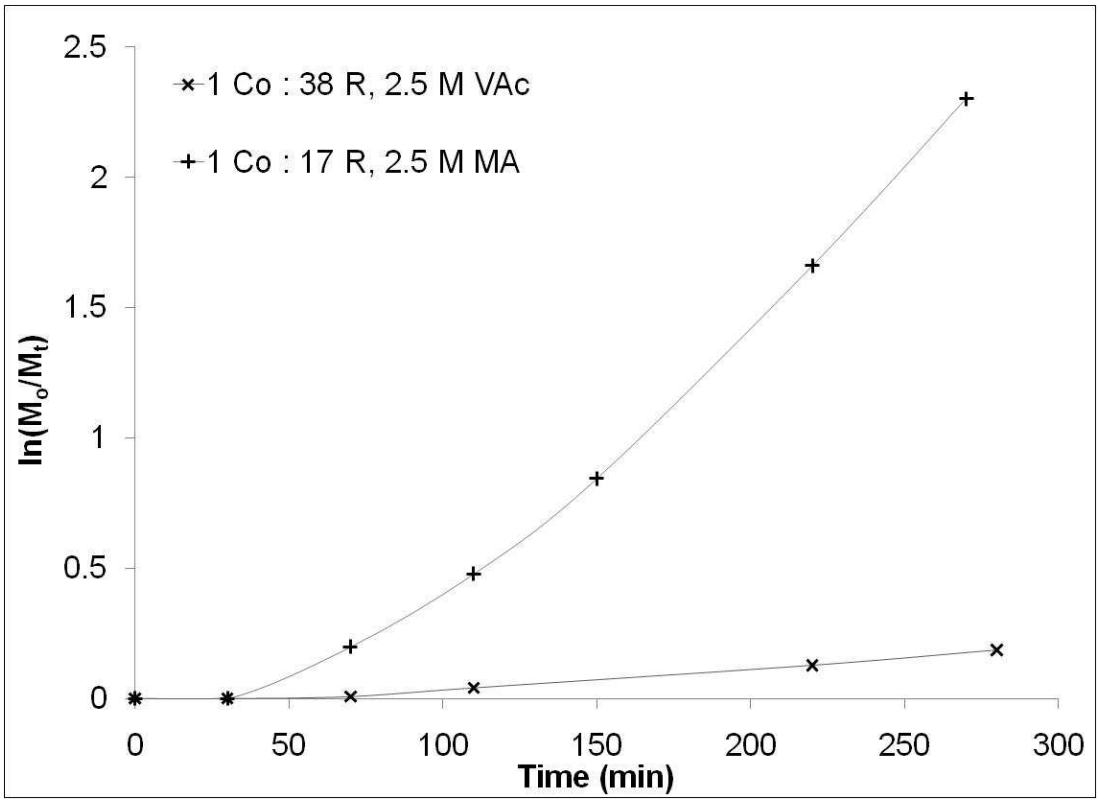

Figure 3. 9 - Kinetic Rate Plot Comparing the Rate of Polymerization of VAc and MA in the presence of Compound 3 at 60˚C with AIBN

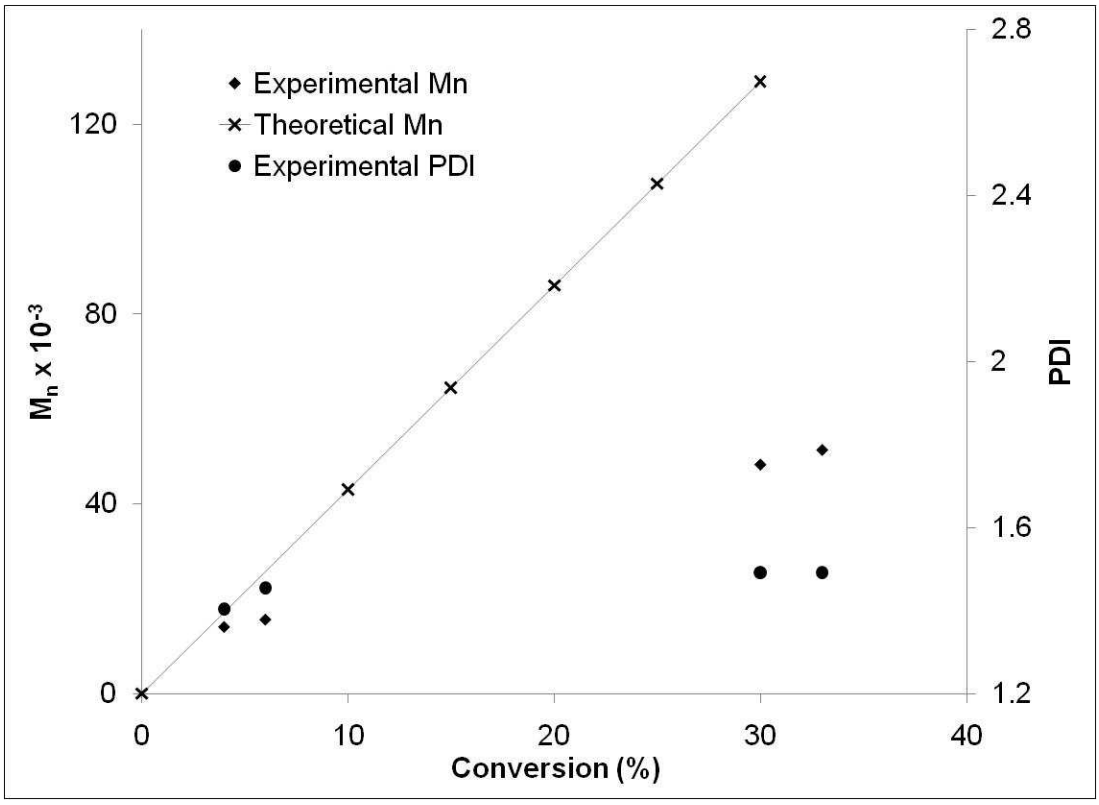

Figure 3. 10 - Molecular Weight Dependence on Conversion, Experimental and Theoretical, and PDI of VAc Polymerized in the Presence of Compound 3

Conversion (%)	Mn (g/mol)	PDI
4	14016	1.404
6	15559	1.454
30	48189	1.491
33	51278	1.492

Table 3. 5 - Conversion, Molecular Weight, and PDI of VAc Polymers Synthesized Using Compound 3

While some non-standard behavior is observed, Compound 3 does appear able to mediate the polymerization of VAc . In fact, many of the non-ideal observations for the system are similar to those previously seen in Co(TMP) polymerization of VAc[10, 11] including: extended induction period, high radical concentration, and non-linear molecular weight dependence on percent conversion. The linear kinetic rate plot after the onset of polymerization and low PDI's are all traditional indicators of the CMRP mechanism and indicate that Compound 3 is a promising catalyst for these systems.

3.5 Summary

Compound 3 appears to be the most promising candidate for use as a CMRP catalyst of those proposed and studied in this Chapter. Solubility is the major factor for these three compounds, and the ability to use Compound 3 in a non-donating solvent is an inherent advantage. Polymerization of MA and VAc are profoundly different due to the extreme difference in radical stability and the CMRP system is one of the few that has proven conducive to controlling both. While ideal results are not seen using Compound 3, observations mainly indicate that a living polymerization is occurring. The significant difference in BDE between Co-MA and Co-VAc is indirectly observed through the decrease in rate and increase in radicals necessary to promote polymerization in the VAc system. These behaviors are expected since there is such a large difference in properties between MA and VAc. While solubility for this class of molecules is undoubtedly a major issue for these compounds, the positive results seen for Compound 3 suggest promise for similar cobalt complexes as CMRP catalysts.

3.6 References

1. Harwood, H. J.; Arvanitopoulos, L. D.; Greuel, M. P., *Polym. Prep. (Am Chem Soc Div Polym Chem)* **1994,** *43* (2), 287-288.

2. Wayland, B. B.; Poszmik, G.; Mukerjee, S. L.; Fryd, M., *Journal of the American Chemical Society* **1994,** *116* (17), 7943-7944.

3. Gridnev, A. A.; Ittel, S. D.; Fryd, M.; Wayland, B. B., *Organometallics* **1996,** *15* (1), 222-235.

4. Debuigne, A.; Poli, R.; Jerome, C.; Jerome, R.; Detrembleur, C., *Prog. Polym. Sci.* **2009,** *34* (3), 211-239.

5. Peng, C. H.; Fryd, M.; Wayland, B. B., *Macromolecules* **2007,** *40*, 6814-6819.

6. Wayland, B. B.; Peng, C. H.; Fu, X. F.; Lu, Z.; Fryd, M., *Macromolecules* **2006,** *39* (24), 8219-8222.

7. Debuigne, A.; Caille, J. R.; Jerome, R., *Angewandte Chemie-International Edition* **2005,** *44* (7), 1101-1104.

8. Bryaskova, R.; Willet, N.; Debuigne, A.; Jerome, R.; Detrembleur, C., *Journal of Polymer Science Part a-Polymer Chemistry* **2007,** *45* (1), 81-89.

9. Debuigne, A.; Champouret, Y.; Jerome, R.; Poli, R.; Detrembleur, C., *Chemistry-a European Journal* **2008,** *14* (13), 4046-4059.

10. Peng, C. H.; Scricco, J.; Li, S.; Fryd, M.; Wayland, B. B., *Macromolecules* **2008,** *41* (7), 2368-2373.

11. Li, S.; de Bruin, B.; Peng, C. H.; Fryd, M.; Wayland, B. B., *Journal of the American Chemical Society* **2008,** *130* (40), 13373-13381.

12. Hurtgen, M.; Debuigne, A.; Jerome, C.; Detrembleur, C., *Macromolecules* **2010,** *43* (2), 886-894.

13. Debuigne, A.; Willet, N.; Jerome, R.; Detrembleur, C., *Macromolecules* **2007,** *40* (20), 7111-7118.

14. Wang, J. D.; Li, W.; Jiang, B. B.; Yang, Y. R., *Journal of Applied Polymer Science* **2009,** *113* (4), 2378-2391.

15. Gridnev, A. A.; Ittel, S. D., *Chemical Reviews* **2001,** *101* (12), 3611-3659.

16. Bandaranayake, W. M.; Pattenden, G., *Journal of the Chemical Society-Chemical Communications* **1988,** (17), 1179-1181.

17. Melby, L. R.; Janowicz, A. H.; Ittel, S. D. Polymerisation of acrylic and/or styrene monomers - using cobalt chelate chain transfer agent to control mol. wt. US4680352-A, 1987.

18. Schaus, S. E.; Brandes, B. D.; Larrow, J. F.; Tokunaga, M.; Hansen, K. B.; Gould, A. E.; Furrow, M. E.; Jacobsen, E. N., *Journal of the American Chemical Society* **2002,** *124* (7), 1307-1315.

19. Srivanavit, C.; Brown, D. G., *Inorganic Chemistry* **1975,** *14* (12), 2950-2955.

20. Migita, K.; Iwaizumi, M.; Isobe, T., *Journal of the American Chemical Society* **1975,** *97* (15), 4228-4232.

21. Lu, Z.; Fryd, M.; Wayland, B. B., *Macromolecules* **2004,** *37* (8), 2686-2687.

22. Wayland, B. B.; Basickes, L.; Mukerjee, S.; Wei, M. L.; Fryd, M., *Macromolecules* **1997,** *30* (26), 8109-8112.

23. Azo Polymerization Initiators. Wako, Ed.

24. Singh, M. S.; Singh, A. K.; Singh, P.; Jain, R. C., *Organic Preparations and Procedures International* **2005,** *37* (2), 173-177.

25. Santos, C. M. M.; Silva, A. M. S.; Cavaleiro, J. A. S.; Levai, A.; Patonay, T., *European Journal of Organic Chemistry* **2007,** (17), 2877-2887.

26. Santos, C. M. M.; Silva, A. M. S.; Cavaleiro, J. A. S.; Patonay, T.; Levai, A., *Journal of Heterocyclic Chemistry* **2006,** *43* (5), 1319-1326.

27. Larrow, J. F.; Jacobsen, E. N., (R,R)-N,N '-bis(3,5-di-tert-butylsalicylidene)-1,2-cyclohexanediaminomanganese(III) chloride, a highly enantioselective epoxidation catalyst. In *Organic Syntheses, Vol 75*, 1998; Vol. 75, pp 1-11.

28. Hanson, J., *Journal of Chemical Education* **2001,** *78* (9), 1266-1268.

29. Hughes, D. L.; Smith, G. B.; Liu, J.; Dezeny, G. C.; Senanayake, C. H.; Larsen, R. D.; Verhoeven, T. R.; Reider, P. J., *Journal of Organic Chemistry* **1997,** *62* (7), 2222-2229.

Chapter 4 – Synthesis of Platinum Nanoparticles Utilizing Polymers Synthesized via RAFT Polymerization

4.1 Introduction

Synthesis of nanoscale metal particles has become of intense interest over the past 20 years[1] due to the desire to harness their unique properties for use in applications as wide-ranging as from microelectronics to catalysis to medicine[2-6]. Materials sized in the nanometer regime have properties that differ greatly from those observed in either the bulk or molecular sizes and are highly size-dependent[2, 7]. Therefore, the ability to synthesize monodisperse particles on the nanometer scale has become increasingly important in order to study the importance of the novel properties of nanoscale materials. Currently the most commonly employed synthetic techniques can be placed into one of four classes[1]: transition metal precursor reduction[4, 8], electrochemical, reduction of organic ligands on organometallic precursors[9], and metal vapor deposition. This discussion will be limited to the transition metal precursor reduction technique.

Chiang and Turkevich at Princeton University first reported the synthesis of nanoparticles by reduction of transition metal precursors in the early 1960's.[10] These studies indicated that there the three necessary components for the synthesis of metal nanoparticles are a transition metal precursor, a reducing agent, and a stabilizer[2, 3]. Each of these components as well as the reaction conditions are factors which will determine the eventual particle size. While the metal precursor and reducing agent are important choices[8, 11, 12], the component with the most variability is the stabilizing agent[3, 12]. Most stabilizers will fall into one of three categories; polymer, ligand, or surfactant. Stabilization occurs through steric, electrosteric, electrostatic and/or depletion depending on the type of stabilizer[1]. Steric effects occur when large stabilizers such as polymers are used. Chains surrounding the particle create a reduction in the configurational freedom which reduces the entropy preventing particles from approaching each other close enough for irreversible agglomeration to occur. Polymers and surfactants typically stabilize through the steric route and the chain length of the molecule will affect the stabilization ability of the material[13]. Electrosteric effects occur when charged polymers, ionic surfactants, or blockcopolymers surround the particle[4, 12, 14, 15]. In this situation, the stabilization occurs through the entropy reduction caused by the long chains of the molecules as well as electrostatic

repulsions created by charges on the stabilizing agent. On the other hand, stabilization of nanoparticles with ions, ionic surfactants, and ionic polymers all have contributions from electrostatic repulsions. These charged protective agents coat the particles creating an unfavorable repulsion as they approach each other limiting contact between particles and therefore limiting agglomeration[14]. Finally, depletion is only viable for nonionic polymers. Stabilization in this case is achieved by unadsorbed polymer at high concentration limiting the ability of the nanoparticles to effectively travel through the medium and agglomerate[14]. The variety of stabilizing agents available allows for nanoparticle synthesis to be performed in a wide range of conditions while maintaining small monodisperse particles.

While the syntheses relying on polymer stabilizers utilizes a wide range of polymer types to tune the reaction for particular result or reaction conditions, there are generalities that apply to nearly every system; the reaction occurs at high temperatures[6, 11, 16], typically a reflux, and/or utilizes harsh reducing agents, such as $NaBH_4$[9, 12]. These methods have allowed for the formation of nanoparticles, however, it is often at the expense of gaining knowledge of mechanism driving the system. The research presented herein focuses on techniques utilizing special characteristics of the polymer to synthesize monodisperse nanoparticles under mild conditions. Utilization of mild reducing agents will extend the reduction time necessary to fully convert the metal cations to zero valent species. Traditionally, it is believed that length of reduction directly correlates to nanoparticle size and that production of very small monodisperse particles can only be obtained through faster reduction of the metal through high temperatures and/or stronger reducing agents.

4.2 Determination of Cation Effect

The first study presented herein focuses on the effect of the counter-ion of platinum complexes on the formation of nanoparticles. Platinic acid, $H_2[PtCl_6]$, potassium hexachloroplatinate (IV), $K_2[PtCl_6]$, and potassium tetrachloroplatinate (II), $K_2[PtCl_4]$, are the three complexes that were investigated. A 39,500 number average molecular weight M_n homopolymer

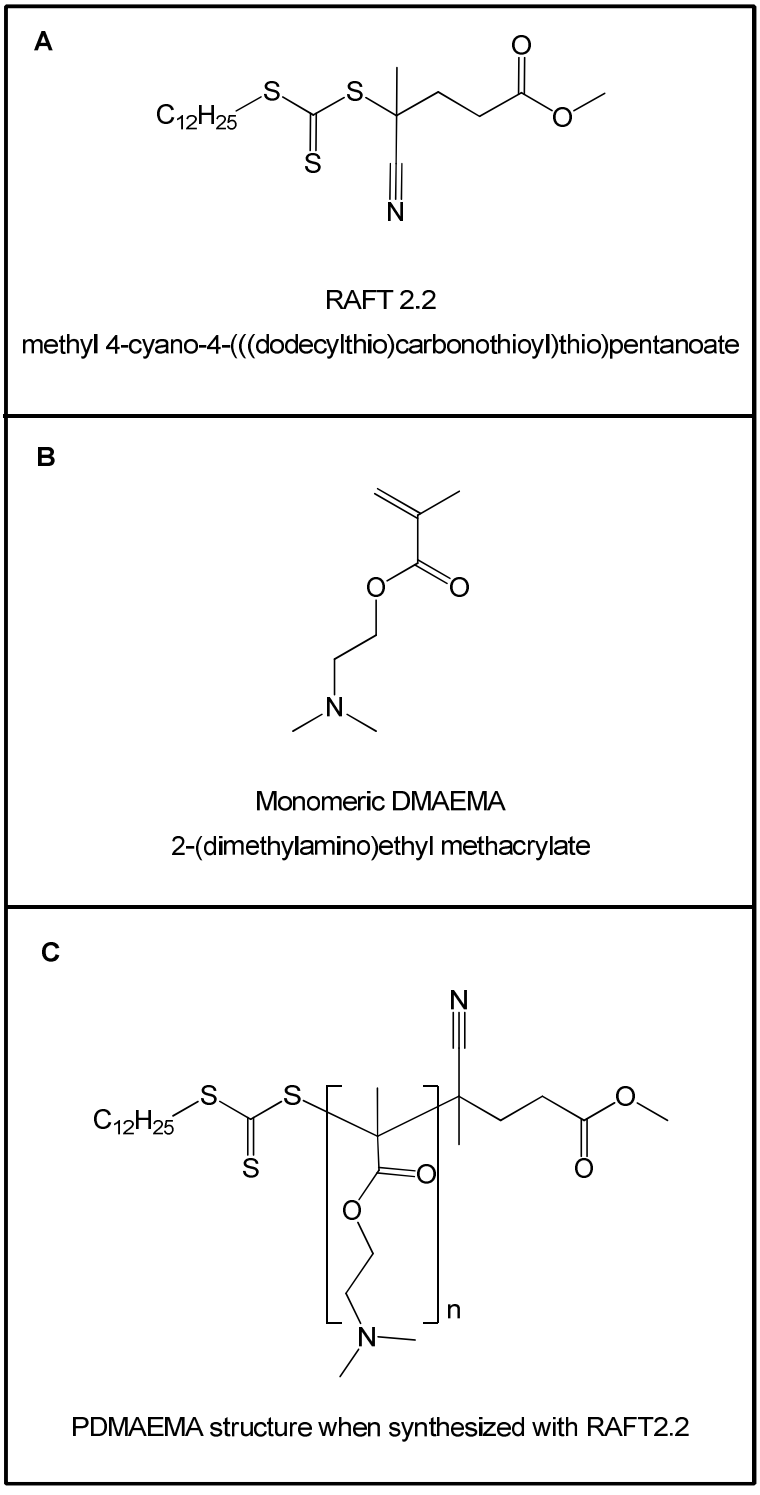

Figure 4. 1 - RAFT 2.2 Synthesis of PDMAEMA Molecules

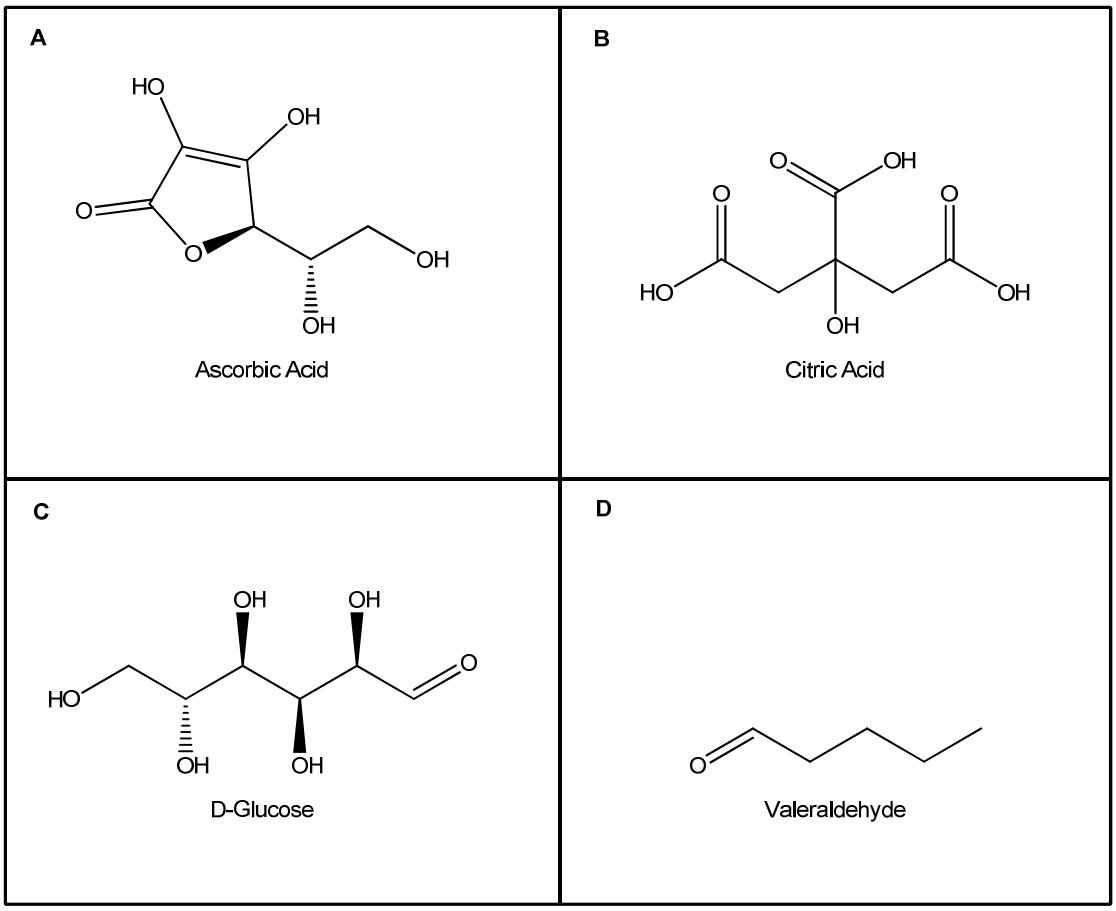

Figure 4. 2 - Structures of Reducing Agents Used in Nanoparticle Synthesis

of 2-(Dimethylamino)ethyl methacrylate (PDMAEMA), Figure 4. 1 C, is utilized as the stabilizing agent and ascorbic acid as the reducing agent, Figure 4. 2 A. This polymer has one amine group per unit which can interact with the transition metal or protons injected by the transition metal complex or the reducing agent.

4.2.1 UV-vis Study of Increasing Polymer to Platinum Ratios

In order to study the interactions between the PDMAEMA and platinum, titration studies were performed by varying the amount of polymer in solution in relation to a known amount of platinum. UV-vis spectra of the solutions were taken and show a strong relationship between ratio of platinum to PDMAEMA and the electronic spectra of platinum, Figure 4. 3 and Figure 4. 4. As reported by Swihart and Mason in 1970, two strong absorption bands are seen at ~202 and ~269nm for the $[PtCl_6]^{-2}$ species.[17] These bands both represent a $^1A_{1g} \rightarrow {}^1T_{1u}$ transition with the first being a $L_\sigma \rightarrow M$ transition and the second lower energy peak a $L_\pi \rightarrow M$ transition. Addition of PDMAEMA to solutions of Pt(IV) is marked by changes in the electronic spectra. As the number of donors available for each platinum complex increases from zero to seven, shown in Figure 4. 3 and Figure 4. 4, there is an increase in absorption of the 204nm peak as well as in the region between the two ligand-to-metal transfer bands. This indicates that there is an increase in the σ $L \rightarrow M$ charge transfer when an amine group donor group is present. A leveling off of this phenomenon is seen as the ratio approaches seven amine donors for every one platinum complex. It is important to note that this behavior is seen in both the $K_2[PtCl_6]$ and $H_2[PtCl_6]$ species, indicating that this interaction is independent of the counter-ion.

4.2.2 Reduction of Platinum Species with Ascorbic Acid

In order to study the effect of the cation on particle size control, reduction of the Pt(IV) and Pt(II) species was performed using ascorbic acid as the reducing agent. Each run was performed with a ratio of 7:1:10 of donor groups from PDMAEMA to platinum to reducing agent. Reduction of the platinum complexes was monitored by UV-vis resulting in the spectra show in Figure 4. 5, Figure 4. 6, and Figure 4. 7. It is important to note that the dramatic increase in absorbance of the peak at ~260nm results from the addition of a ten-fold excess of ascorbic acid,

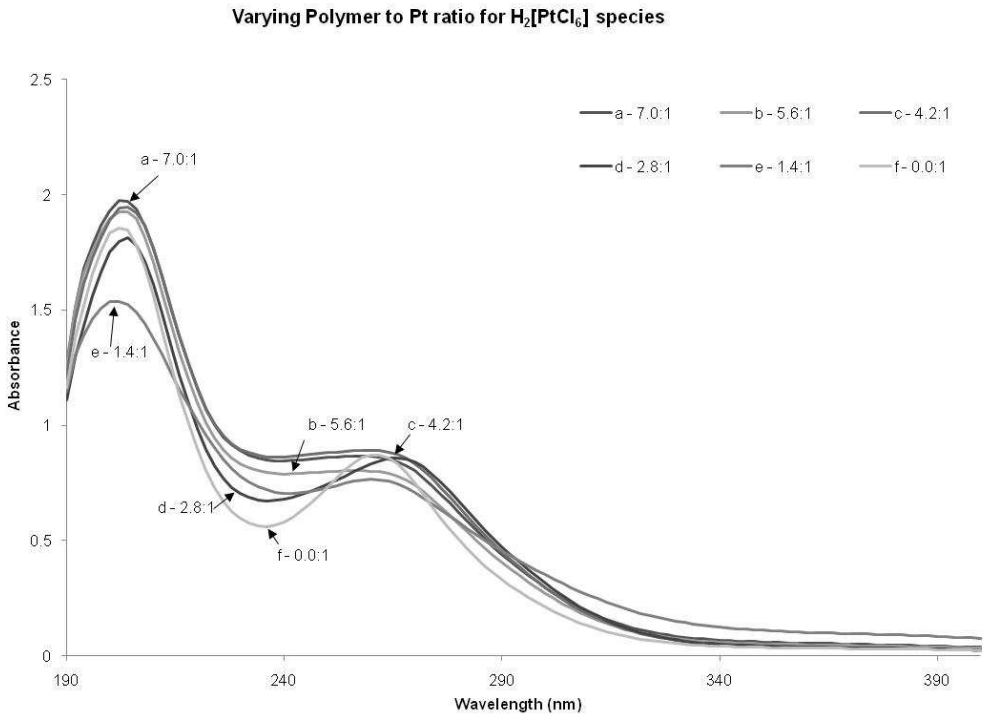

Figure 4. 3 - UV-vis Spectra of Varying Polymer to Pt Ratios for $H_2[PtCl_6]$

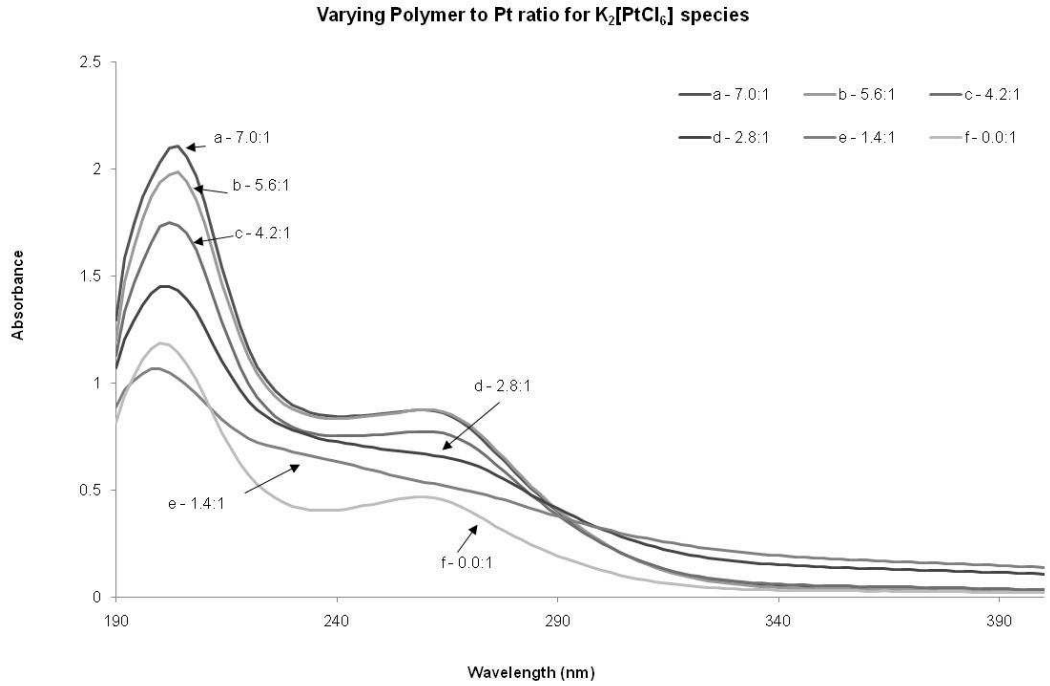

Figure 4. 4 - UV-vis Spectra of Varying Polymer to Pt Ratios for $K_2[PtCl_6]$

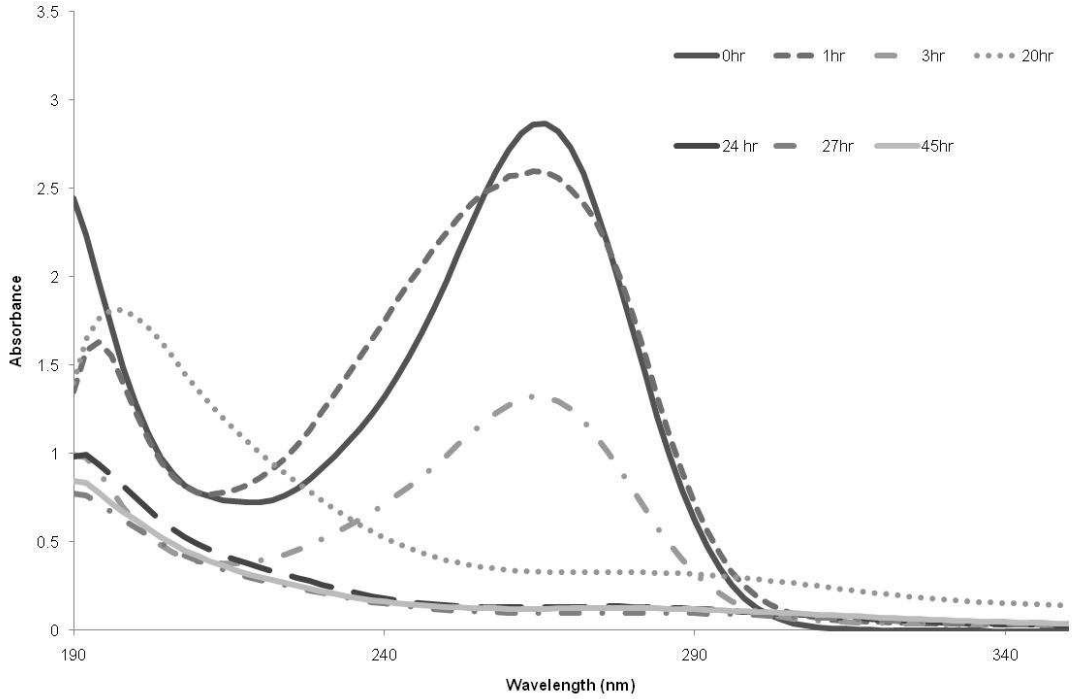

Figure 4. 5 - Reduction of $K_2[PtCl_4]$ in Solution with PDMAEMA by Ascorbic Acid

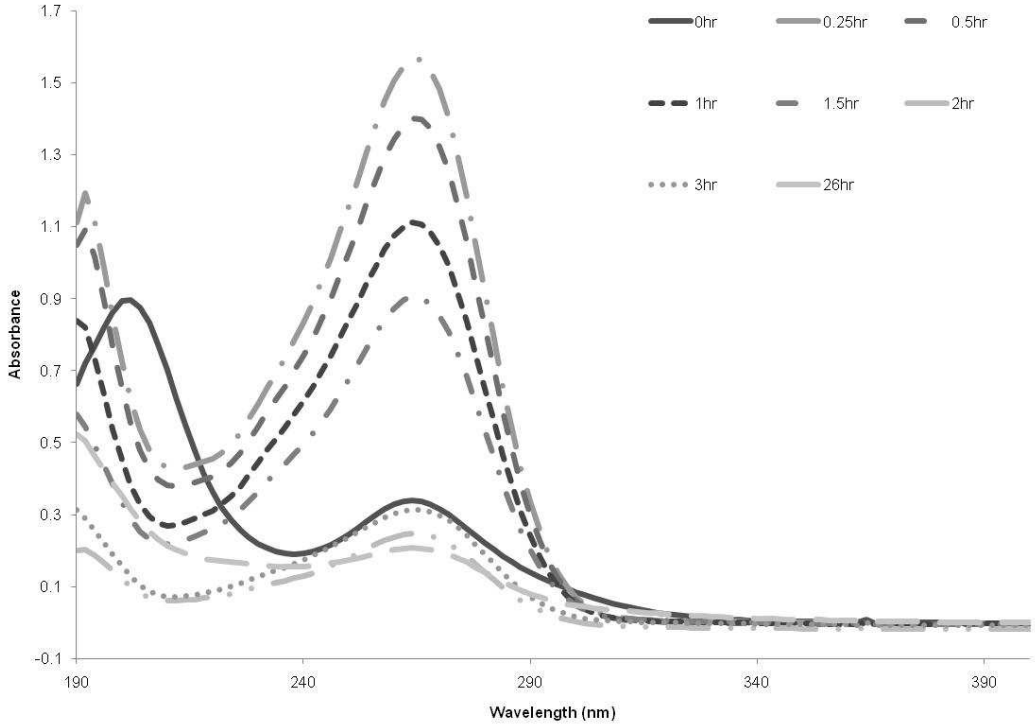

Figure 4. 6 - Reduction of $K_2[PtCl_6]$ in Solution with PDMAEMA by Ascorbic Acid

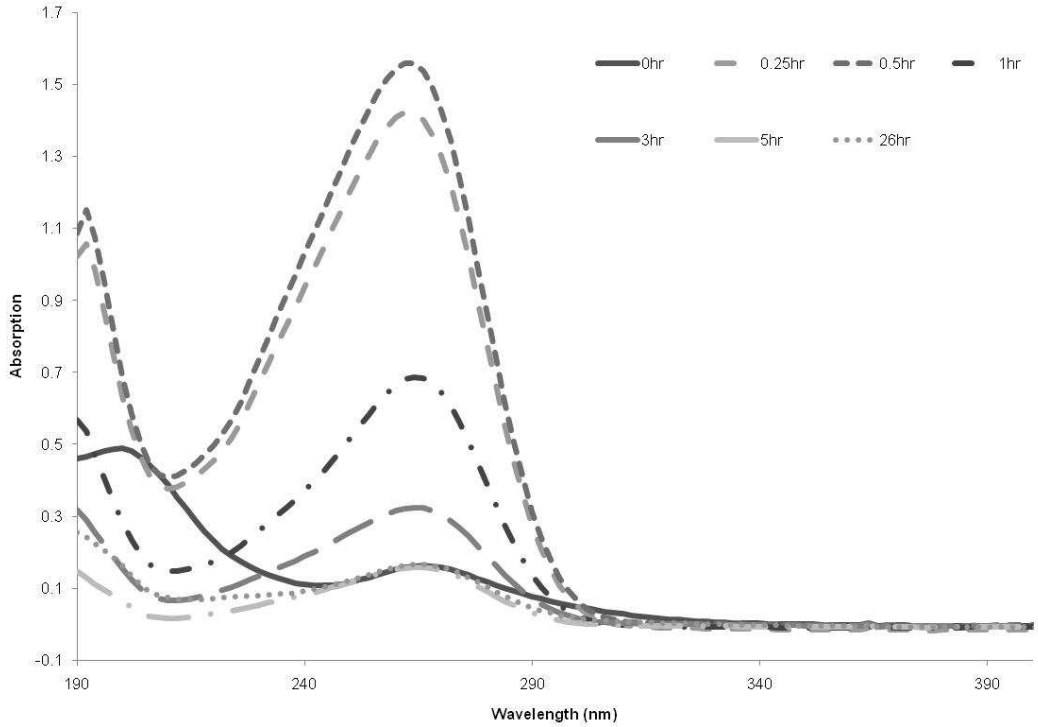

Figure 4. 7 - Reduction of $H_2[PtCl_6]$ in Solution with PDMAEMA by Ascorbic Acid

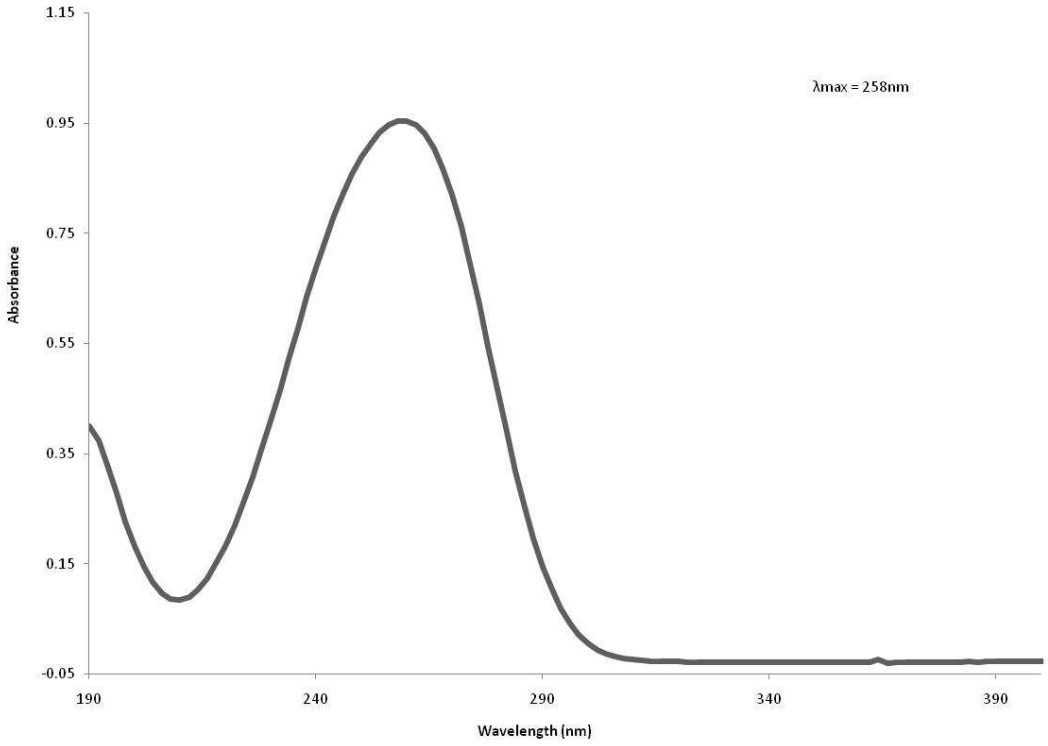

Figure 4. 8 - UV-vis Spectrum of Ascorbic Acid

Figure 4. 8, to the sample. After full reduction of the Pt (II) or (IV) to Pt (0) the concentration of ascorbic acid is observed to decrease in concentration as shown by the lowered absorbance over time of the peak at ~260nm. Since the reducing agent is present in a ten-fold excess, even after full reduction of the platinum molecules to platinum metal there should be a significant amount of ascorbic acid. However, it is observed in Figure 4. 6, Figure 4. 7, and Figure 4. 8 that the large excess of ascorbic is not seen when the reaction is allowed to continue after the platinum is judged to be fully reduced. This confirms the catalytic properties of the metal nanoparticles coated with a polymer system since it indicates continued oxidation of the excess of ascorbic acid by the platinum nanoparticles that have been synthesized and sterically stabilized by the polymer. Catalytic behavior by the particles even after the polymer has fully surrounded them is important for this synthetic technique to be useful for a majority of applications where particles with a large surface area per gram of platinum will be useful. If the polymer coating did not allow access by small molecules, this fabrication technique would not be applicable to systems where the platinum is to be used as a catalysts, such as fuel cell applications.

After confirming that the Pt had been fully reduced, TEM images were taken to determine the size of the particles synthesized. For each reaction, small aliquots were deposited onto carbon coated copper TEM grids and the liquid was allowed to evaporate. Each sample was prepared by repeating this process with five to fifteen drops of the solution. Representative images obtained from ascorbic acid reduction of $K_2[PtCl_4]$, $K_2[PtCl_6]$, and $H_2[PtCl_6]$ are shown in Figure 4. 9, Figure 4. 10, and Figure 4. 11 respectively. The results of the analysis of the images obtained is summarized in Table 4. 1. It was possible to get significantly larger sample size from the images of $H_2[PtCl_6]$ due to the large quantity of particles in each image due to the small particle size. Strikingly, the counter-ion is observed to have a great effect on the development of the particles as is seen by the large size and size distribution in the samples which resulted from the reduction of $K_2[PtCl_4]$ and $K_2[PtCl_6]$, 7.6 ± 3.1nm and 6.7 ± 3.4nm respectively, in comparison with the small relatively monodisperse particles synthesized from $H_2[PtCl_6]$, 1.12 ± 0.25nm. Histograms shown in Figure 4. 9, Figure 4. 10, and Figure 4. 11 show another interesting counter-

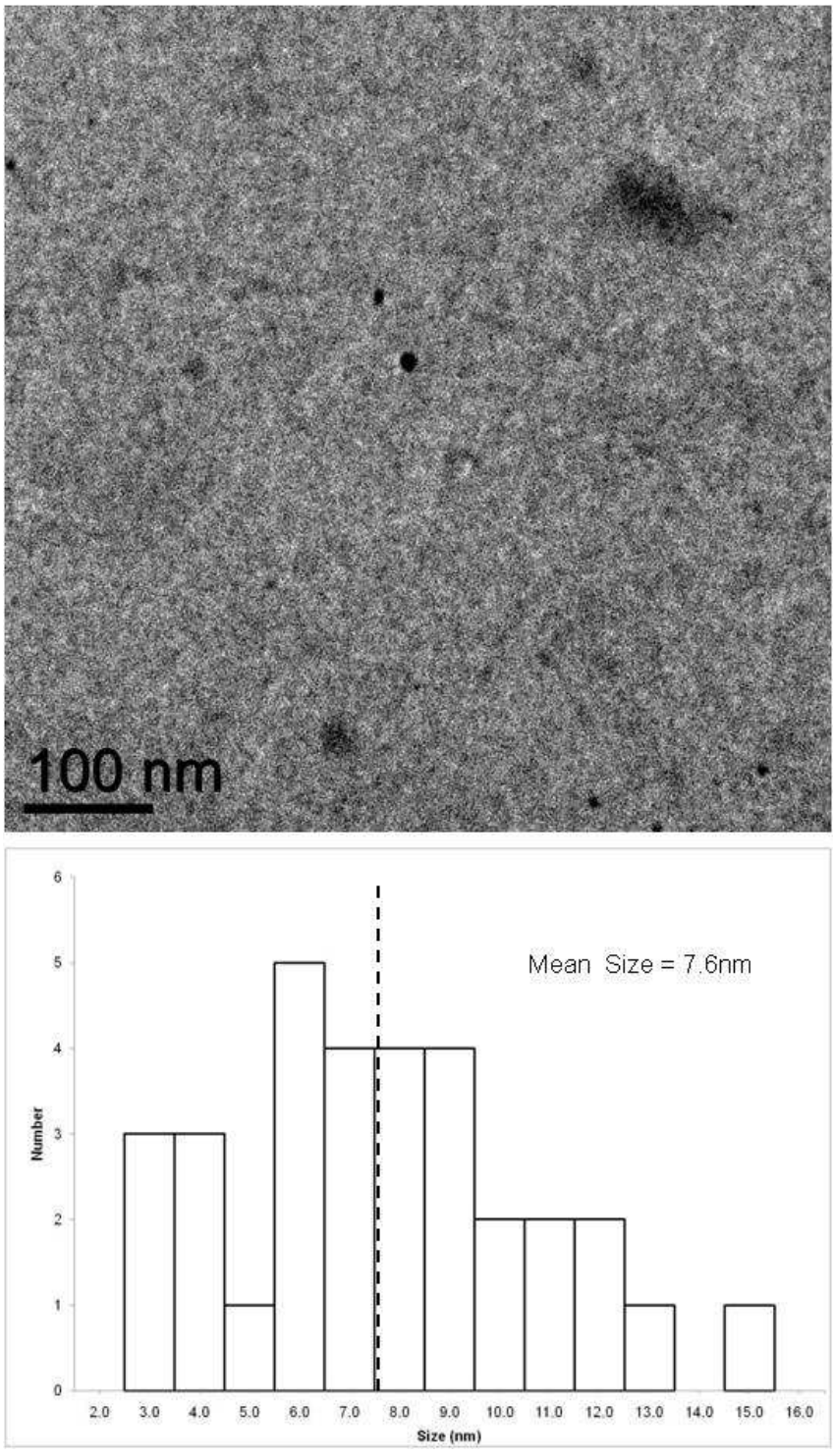

Figure 4. 9 - TEM Image and Analysis of Pt Particles Reduced from $K_2[PtCl_4]$ By Ascorbic Acid

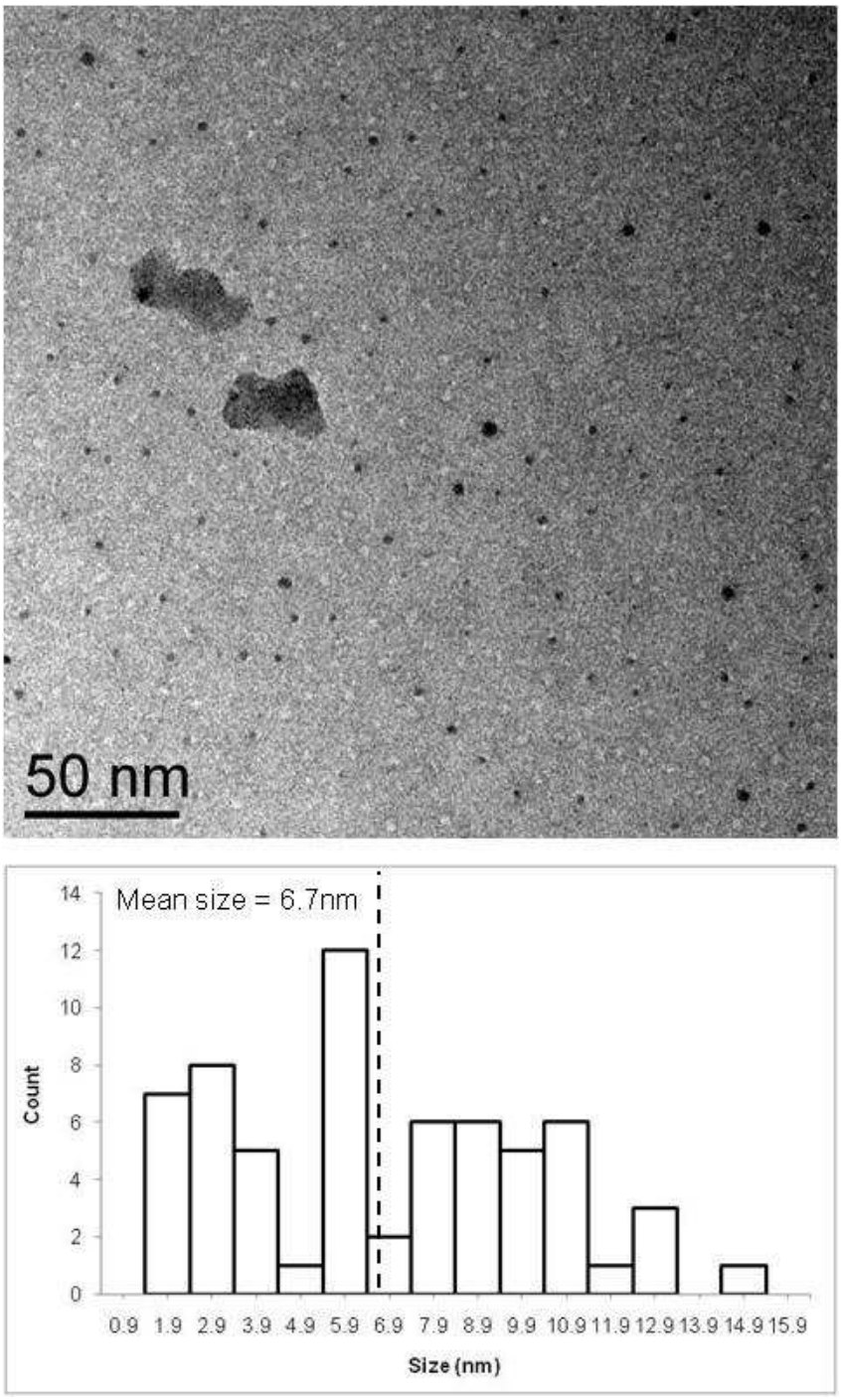

Figure 4. 10 - TEM Image and Analysis of Pt Particles Reduced from $K_2[PtCl_6]$ By Ascorbic Acid

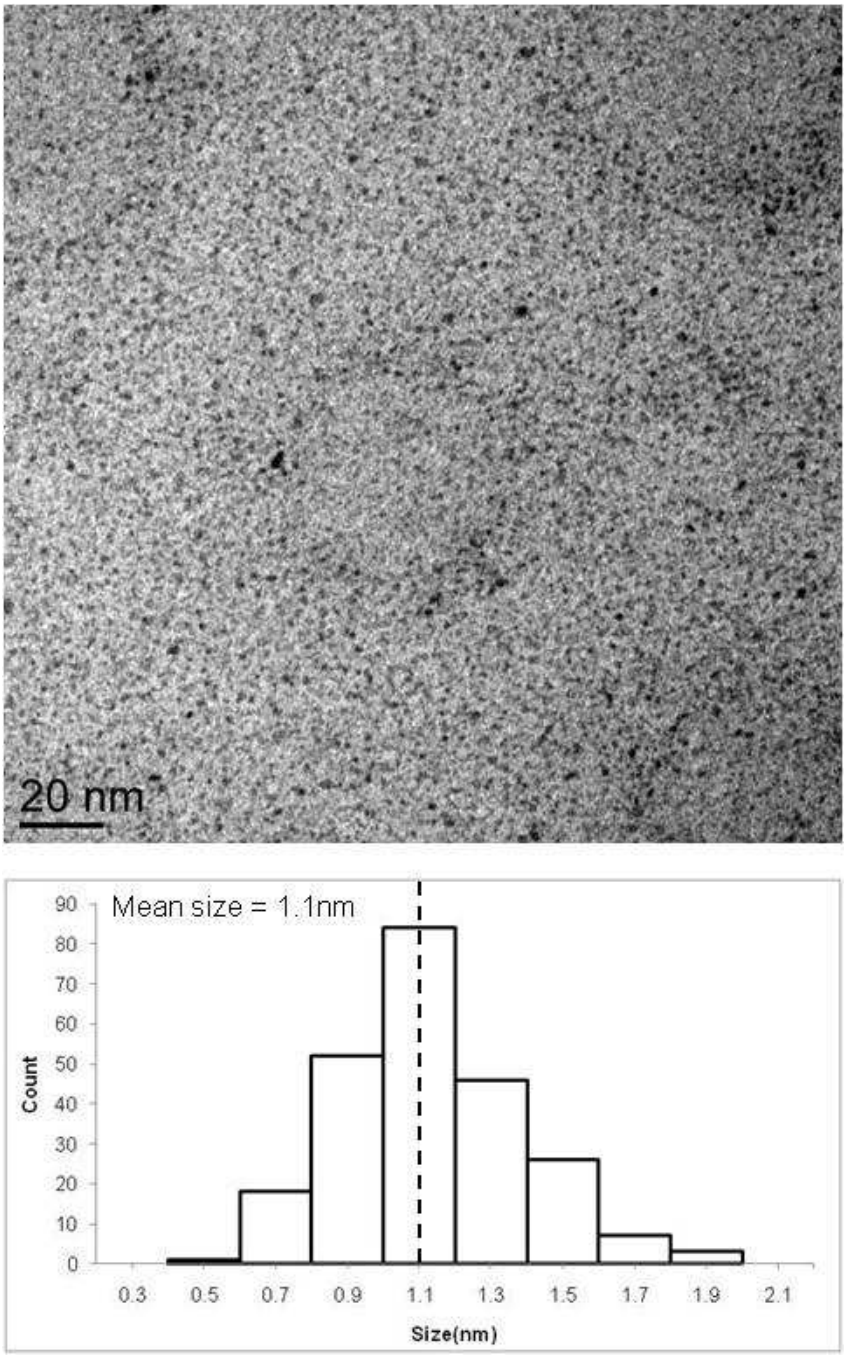

Figure 4. 11 - TEM Image and Analysis of Pt Particles Reduced from $H_2[PtCl_6]$ by Ascorbic Acid

Platinum Species	Average Particle Size (nm)	Sample Size
$K_2[PtCl_4]$	7.6 ± 3.1	32
$K_2[PtCl_6]$	6.7 ± 3.4	63
$H_2[PtCl_6]$	1.12 ± 0.25	237

Table 4. 1 - TEM Analysis Data for Pt(IV) and Pt(II) Species Reduced with Ascorbic Acid

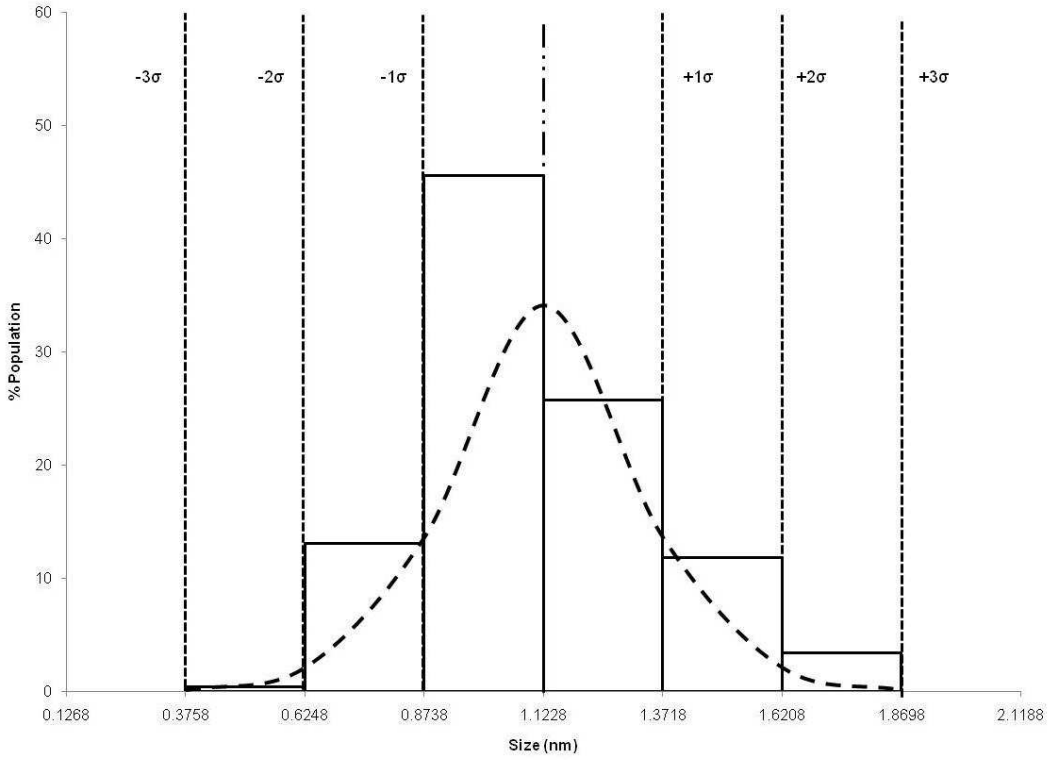

Figure 4. 12 - Gaussian Curve and $H_2[PtCl_6]$ Particle Size Distribution

ion effect; size distribution of the particles formed from $H_2[PtCl_6]$ very nearly follow a Gaussian distribution, Figure 4. 12, with some expected high-end tailing due to being at the small end of the resolution of the instrument. Particle size distributions for the $K_2[PtCl_4]$ and $K_2[PtCl_6]$ samples do not follow a normal distribution curve, instead there is approximately equal probability of finding particles at the minimum as at the maximum size. Since the particles reduced from the platinic acid follow a Gaussian distribution, this indicates that there is a convergence of the size to the mean. When potassium is the counter-ion, a normal distribution is not seen and the size of the particles is random. From these observations, it is clear that the counter-ion is critical for the development of regularly sized particles.

4.2.3 Conclusions

UV-vis data suggests that $K_2[PtCl_4]$, $K_2[PtCl_6]$, and $H_2[PtCl_6]$ all interact with PDMAEMA as observed by similar changes in the electronic spectra with the addition of polymer to platinum solutions. Reduction of Pt(IV) and Pt(II) species by ascorbic acid were observed via the electronic spectra. These experiments provide evidence that the reduced particles are able to act as catalysts since the large excess of reducing agent is oxidized after the platinum has been fully reduced. While there is evidence for Pt-polymer interaction in the electronic spectra, the results from the TEM analysis show a significant counter-ion effect on the particle size and distribution. Therefore, the Pt-polymer interaction seen in the electronic spectra is weaker than the driving force between the control of the particle size that is seen to occur in the TEM images of the reduced $H_2[PtCl_6]$.

4.3 Nanogel Formation and Control Studies

From the studies performed in section 4.2, it was determined that the counter-ion is significant factor for the synthesis of small mono-disperse platinum nanoparticles. The following studies focused on determining the particle synthesis control mechanism that is present in when platinic acid is utilized, while the control reactions were performed with potassium hexachloroplatinate. All of the work performed in this sections continues to use ~39,500K PDMAEMA from the original sample synthesized and utilized in the studies in section 4.2. The

following studies have allowed for a comprehensive theory for the mechanism of control during the synthesis of platinum nanoparticles from $H_2[PtCl_6]$ in the presence of PDMAEMA.

4.3.1 Pt-polymer Interaction

Determination of the Pt-polymer interactions began with analysis of solutions containing PDMAEMA and a platinum complex. As seen in the electronic spectra shown in Figure 4. 3 and Figure 4. 4, a perturbation of the platinum behavior is expected. For the initial study, solutions with a 7 to 1 ratio of polymer donor sites to platinum molecules are imaged by TEM, representative images from these runs are shown in Figure 4. 13 and Figure 4. 14. These images show interesting macrostructures formed by the polymer and Pt species. In the case of $H_2[PtCl_6]$ (Figure 4. 13), roughly spherical structures are formed while $K_2[PtCl_6]$ (Figure 4. 14) forms elongated ovals. In both of these cases, the Pt species influences the macrostructure of the polymer, which is expected given results seen in the electronic spectra of the platinum species combined with PDMAEMA. However, given the dramatically different shapes of the observed structures there are different driving forces depending on the counter-ion.

Preparation of the TEM grids requires that aliquots of the solution be dried onto the surface of the grid. This technique can create structures that are not present in solution by removing the solvent and dramatically changing the importance of certain intermolecular forces; presenting an erroneous view of what is occurring at standard reaction conditions. In order to probe the system at standard reaction conditions, dynamic light scattering (DLS) was utilized to analyze the reaction in solution at room temperature. Figure 4. 15 shows representative DLS spectra of $K_2[PtCl_6]$ and $H_2[PtCl_6]$; the average hydrodynamic diameter of the samples are 10.9nm and 93.1nm respectively and DLS measurements of neat polymer solution have a hydrodynamic diameter of 6.7nm. These measurements indicate that platinic acid mixed with PDMAEMA results in the formation of particles in solution as well as those observed in the TEM images obtained of the same solution. On the other hand, $K_2[PtCl_6]$-PDMAEMA solutions present nothing significantly larger than the size of the polymer without the addition of platinum. From these observations, it is apparent that the intermolecular forces driving the formation of the

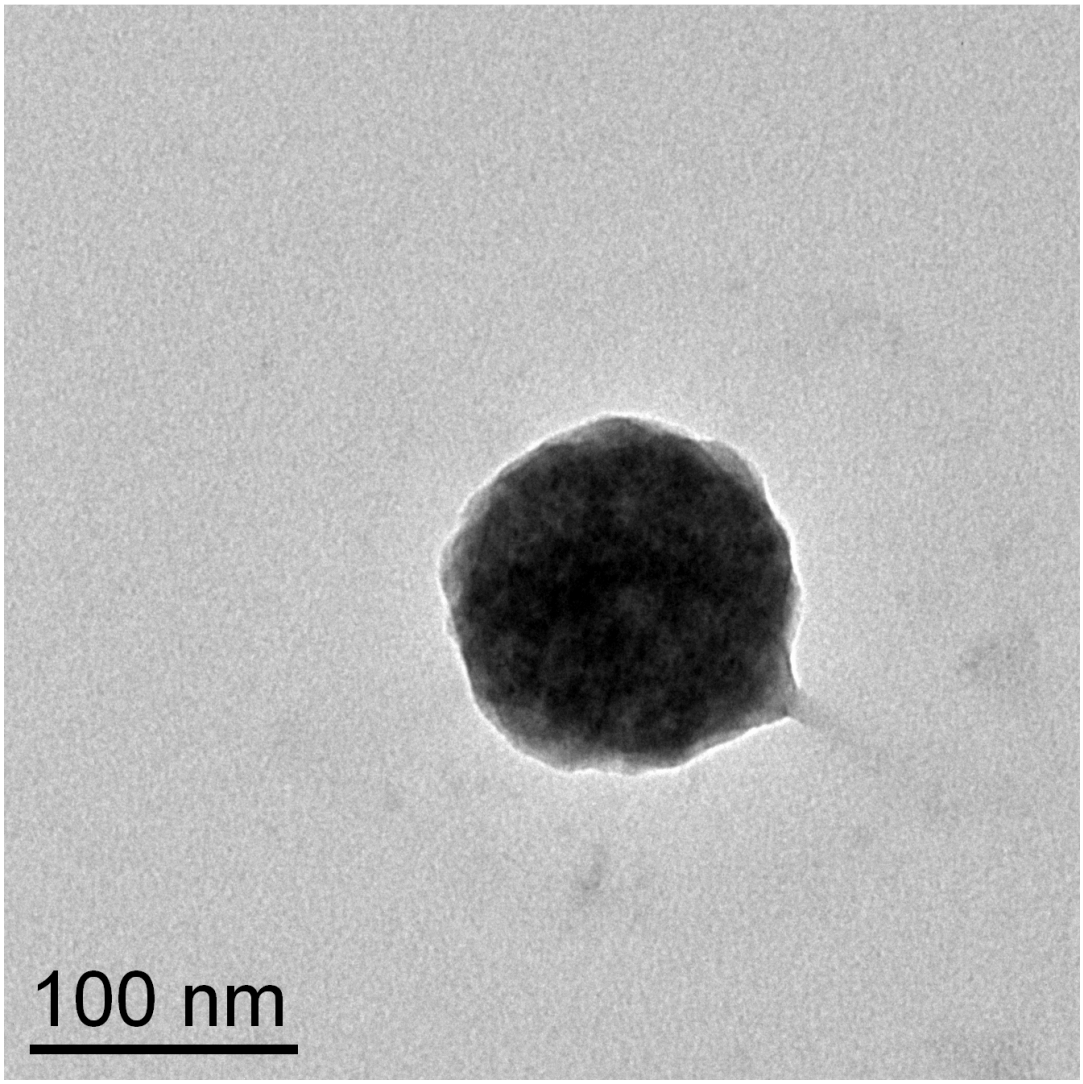

Figure 4. 13 - TEM Image of $H_2[PtCl_6]$ Mixed with PDMAEMA

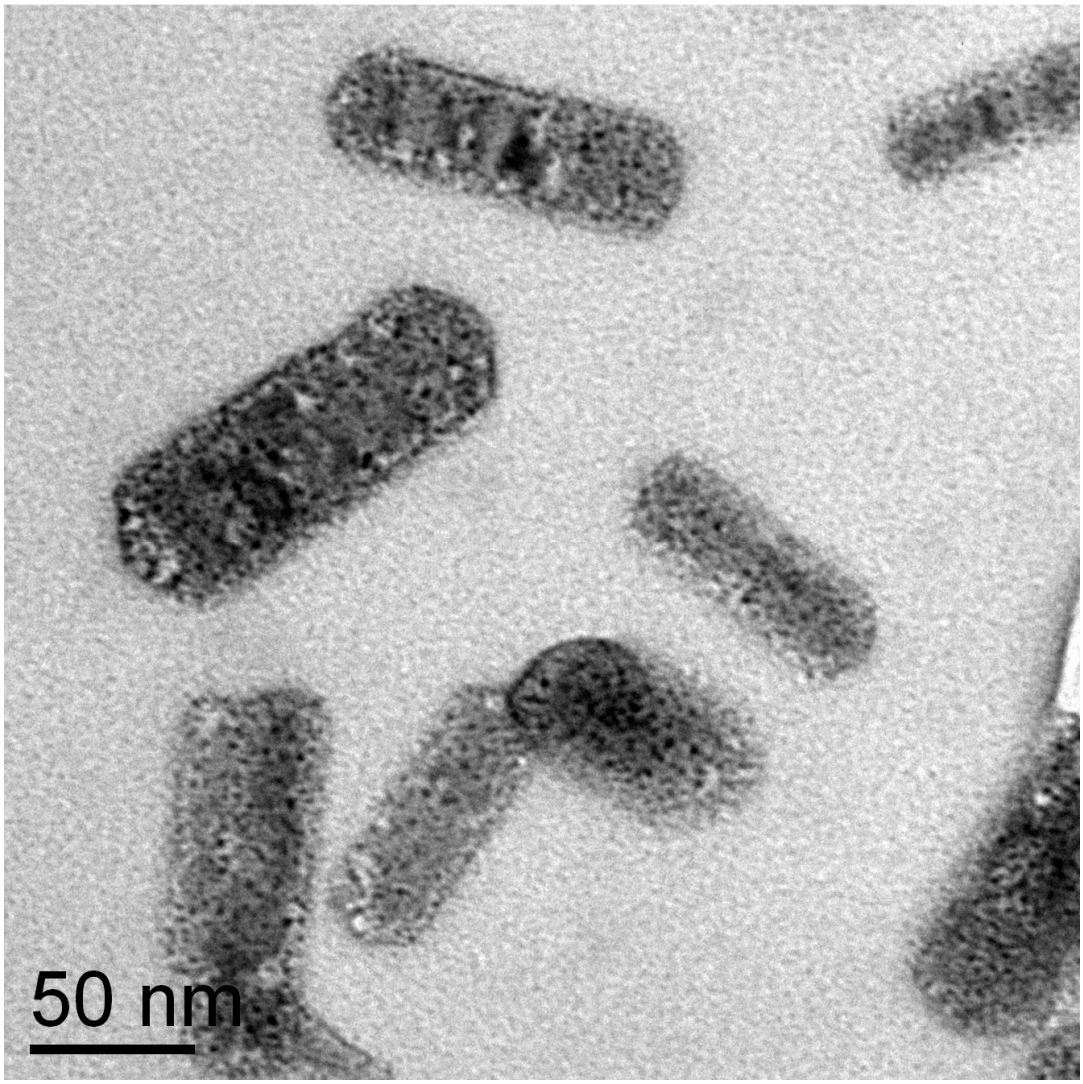

Figure 4. 14 - TEM Image of $K_2[PtCl_6]$ Mixed with PDMAEMA

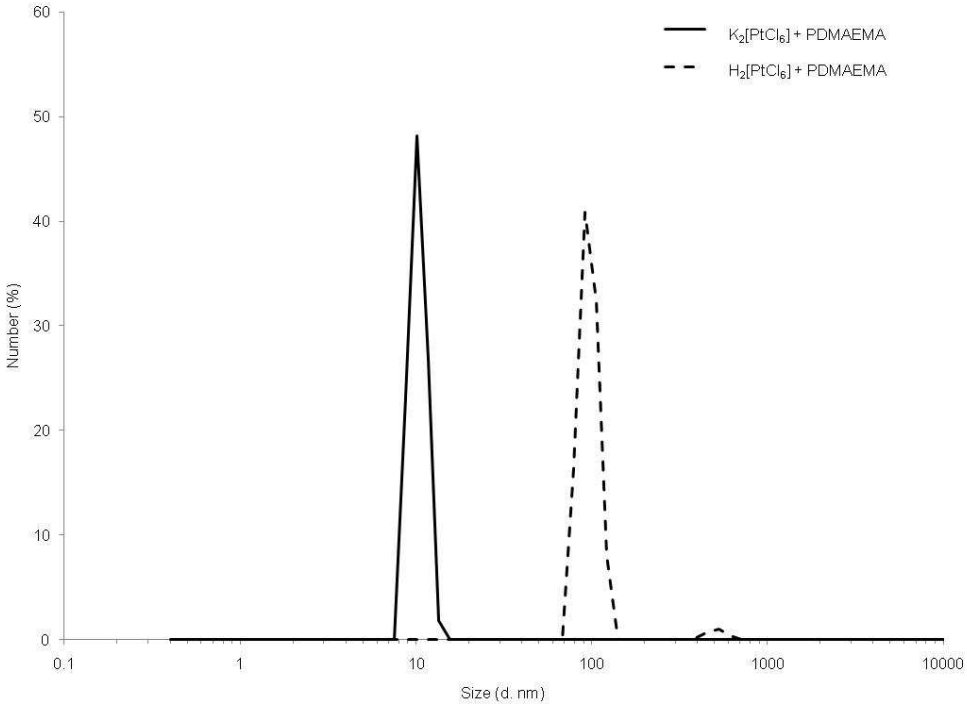

Figure 4. 15 - DLS Spectra of Pt Species with PDMAEMA

macrostructures seen in TEM images taken of $K_2[PtCl_6]$-PDMAEMA solutions are not the same as those observed in $H_2[PtCl_6]$-PDMAEMA solutions.

Lack of formation of particles in $K_2[PtCl_6]$-PDMAEMA solutions, Figure 4. 15, coupled with the macrostructures seen in the TEM and observations of changes in the electronic structure via UV-vis reveal an important feature of this system. While a Pt-polymer interaction is seen for both platinum species, in the case of $K_2[PtCl_6]$ the forces driving the formation of large polymer-Pt particles becomes dominant only through the evaporation of the solvent. At this point, the Pt will migrate into the polymer since the swollen polymer chains are the last are to fully dehydrate. Once the water has been removed, the $[PtCl_6]^{-2}$ anion no longer has strong ion-dipole intermolecular forces available however, the amine group on each unit in the PDMAEMA chain is still available and donor-metal intermolecular forces become the dominant interaction.

Macrostructures are able to form as the Pt begins to associate with the polymer chains because each chain has several hundred amine groups available. Each of these chains can, therefore, associate with many platinum molecules and, since this species is a divalent anion, each platinum has the possibility of interacting with two separate chains. In this manner, the platinum anion can act as a molecular cross-linker for the polymer creating large Pt-polymer particles as seen in Figure 4. 13 and Figure 4. 14. This intermolecular force is shown to not be strong enough while in solution to create large Pt-polymer particles but becomes the driving force for the macrostructures, seen in Figure 4. 14, after the solvent is evaporated off for deposition of the sample onto the TEM grid. However, the donor-metal intermolecular forces are present in solution in both the $K_2[PtCl_6]$ and $H_2[PtCl_6]$ systems as shown by the change in the $L_\pi \rightarrow M$ transfer band at ~260, Figure 4. 3 and Figure 4. 4. These observations demonstrate that the donor-metal intermolecular forces are the dominant force for the formation of the macrostructures, seen in TEM images, for $K_2[PtCl_6]$ but are not for $H_2[PtCl_6]$.

The acidic character of $H_2[PtCl_6]$ is significant in this system due to PDMAEMA's ability to accept a proton on the amine group and form a cationic polymer chain since two protons will be available from each platinum molecule injected. In the runs analyzed by TEM and shown in

Figure 4. 13, the ratio of amine donor groups in the PDMAEMA to protons from $H_2[PtCl_6]$ to platinum is 7:2:1. At this ratio, particles with a hydrodynamic diameter of ~93.1nm, dotted line in Figure 4. 15, and a spherical shape, Figure 4. 13, are observed. These observations differ from those seen for $K_2[PtCl_6]$ in size and shape respectively suggesting that some other mechanism is responsible for the formation of the macrostructure seen in the TEM images. Platinic acids ability to donate two protons allows for a cationic polymer to form, shown in Scheme 4. 1 A, through the addition of the protons to the amine groups on each unit of PDMAEMA. $[PtCl_6]^{-2}$ is then available to form ionic bonds with the cationic polymer; since this species is a dianion, it will effectively act as a cross-linking agent for the polymer chains, Scheme 4. 1 A.

The strength of the ionic intermolecular forces is substantially greater than the dipole-ion interaction between $[PtCl_6]^{-2}$ and water so it will be the dominant force driving the mechanism. DLS measurements confirm this hypothesis since in large particles are observed in solutions of PDMAEMA and $H_2[PtCl_6]$. The significant difference in shape by TEM analysis of $K_2[PtCl_6]$ and $H_2[PtCl_6]$ further validates the premise since the particle shape will be driven by ionic interactions the shape formation of linked polymer will not depend on evaporation of the solvent. Rather, the observed macrostructure should be directly related to structure the cross-linked polymer takes while in solution. In this case, a sphere of polymer cross-linked through platinum is logical since this type of shape will them minimize surface area between the polymer and water.

4.3.2 Acid-Polymer Control Studies

In order to further investigate the mechanism of the formation of the macroparticles seen in section 4.3.1, several acids were employed to mimic the behavior of the platinic acid when mixed with PDMAEMA. By utilized organic acids, the Pt-polymer intermolecular forces are eliminated allowing a clear representation of the role of polymer protonation and multivalent anions in macroparticle formation. Succinic acid, sulfuric acid, acetic acid, and hydrochloric acid were used in these studies; this provides information about the effect of mono- versus di- acids as well as weak versus strong acids. Each acid was mixed with PDMAEMA to obtain a donor, amine group on each unit, to proton ratio of 7:2 to replicate the conditions of the Pt experiments.

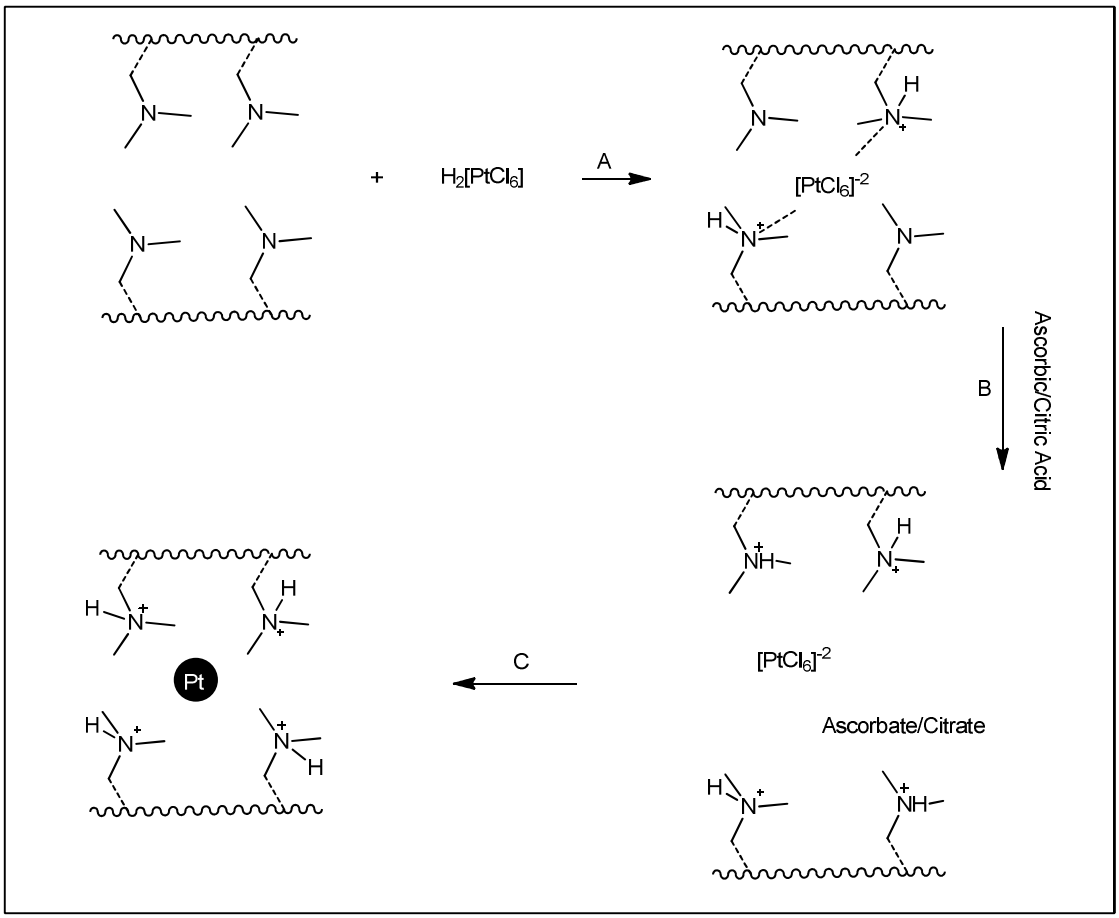

Scheme 4. 1 - General Mechanism for Formation of Pt Nanoparticles with PDMAEMA Reduced by Ascorbic or Citric Acid

DLS analysis was performed on the solutions; representative spectra are shown in Figure 4. 16 and the data is summarized in Table 4. 2. Hydrochloric acid, acetic acid, and neat PDMAEMA all have a hydrodynamic diameter of ~10nm; this evidence suggests that there is no particle formation for the mono-acids. Logically, this is expected since the conjugate base will only be able to create an ionic bond with one PDMAEMA site; therefore, no cross-linking should be possible. On the other hand, data from analysis of succinic acid and sulfuric acid both show the formation of large particles in solution, ~200 and ~300 d.nm respectively. Conjugate bases of these acids will be dianions and should be able to associate with two PDMAEMA sites. This will allow for some amount of cross-linking between PDMAEMA chains resulting in the formation of macrostructures as seen in the DLS spectra. These studies confirm the hypothesized mechanism shown in Scheme 4. 1 A that through formation of a cationic polymer by protonation of the amine groups in each unit, multivalent anions are able to create ionic bonds with the polymer. Cross-linking then occurs since the anion can bond with more than one polymer chain resulting in the formation of large anion-PDMAEMA particles.

TEM analysis of the $H_2[PtCl_6]$-PDMAEMA mixture resulted in images of large spherical macrostructures, Figure 4. 13, in which there is ambiguity with what the lighter areas represent. It appears that the gray area of the structures should represent the polymer portions of the particle, while the darker areas are where the Pt resides. However, it is unclear whether PDMAEMA is electron dense enough to create an image as seen in Figure 4. 13. If polymer is not being shown in these images as the lighter gray portions of the particle the only other assumption is that the whole image is being created by varying densities of Pt. In order to elucidate the meaning of the images seen by TEM analysis of $H_2[PtCl_6]$-PDMAEMA, TEM images of succinic acid-PDMAEMA solutions were obtained. By imaging a solution, which was seen to be cross-linked (see above) like the $H_2[PtCl_6]$-PDMAEMA solutions, without Pt, any particle that is imaged is guaranteed to be solely PDMAEMA resolving the question of whether TEM analysis will be able to show PDMAEMA as well as Pt in the macrostructures. Succinic acid and PDMAEMA were combined to create a donor from each PDMAEMA unit to proton ration of 7:2, as in the DLS studies.

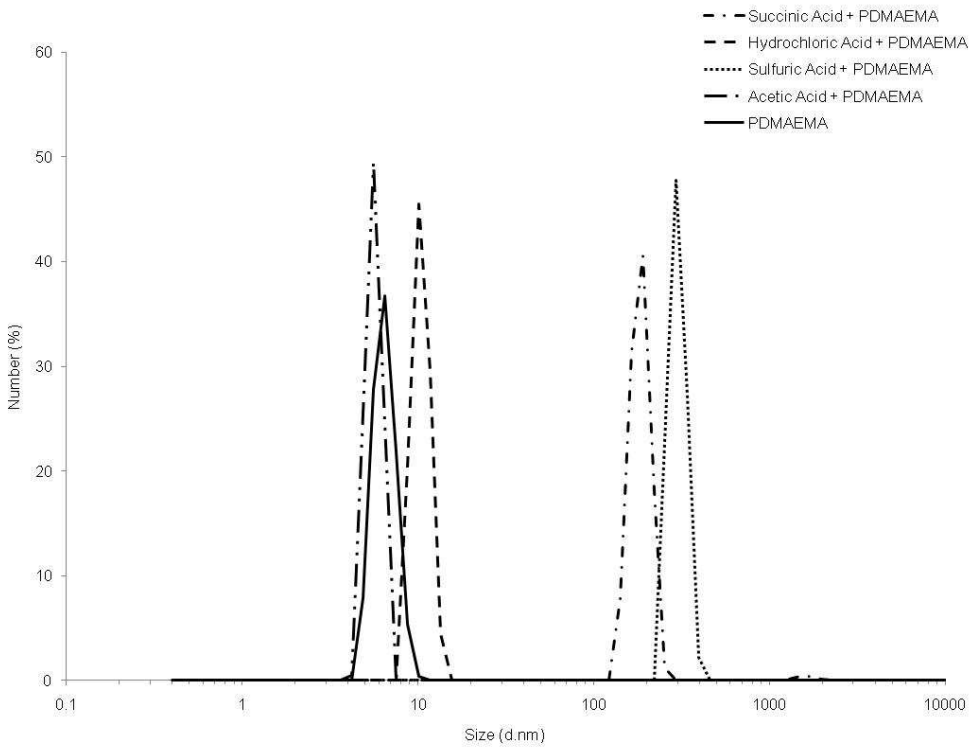

Figure 4. 16 - DLS Spectra of PDMAEMA and Various Acids

System	Avg (d.nm)
Sulfuric Acid	319
Succinic Acid	185
Acetic Acid	11.0
Hydrochloric Acid	10.4
Polymer	6.7

Table 4. 2 - DLS Data Summary of PDMAEMA and Various Acids

Figure 4. 17 is a representatitve image of those obtained by TEM of the succinic acid-PDMAEMA solution. In Figure 4. 17, a particle very similar to what is seen in the TEM image of $H_2[PtCl_6]$-PDMAEMA, Figure 4. 13, is observed. This provides clear evidence that, when cross-linked, PDMAEMA is sufficiently electron dense to be observed by TEM. Also, these images confirm that the structure seen in Figure 4. 13 are characteristic of structures formed via PDMAEMA cross-linking and that the lighter areas should correspond to polymer areas. Therefore, the darker areas where there is higher electron density will be regions where Pt has collected. From the TEM analysis of the succinic acid-PDMAEMA solutions, there is further evidence that mechanism put forward in Scheme 4. 1 A is appropriate for this system.

4.3.3 Analysis of Pt-PDMAEMA TEM Images

Comparisons of Figure 4. 13 to Figure 4. 17 shows that there is one significant difference between the two images; the uneven electron density across the sphere in Figure 4. 13 compared to the even density of the sphere in Figure 4. 17. Although it appears as though the dark spots in the image produced from the $H_2[PtCl_6]$-PDMAEMA solution are area of reduced Pt nanoparticles, the electronic spectra of the solution taken immediately prior to deposition onto the TEM grid confirms that the Pt is still in its Pt(IV) state. These dark areas are also seen in images of $K_2[PtCl_6]$-PDMAEMA solution, Figure 4. 14, where the Pt is also observed to be Pt(IV) by UV-vis spectroscopy. One explanation for this phenomenon is that the molecular Pt is acting as an electron stain for the PDMAEMA structures.

Pt complexes have previously been utilized as staining agents in biological systems to allow for the use of TEM to obtain images at the subcellular level.[18-20] In these systems, the Pt complexes, are substituted for the traditional Gram stain, iodine-potassium iodide, as the complexing anion for crystal violet(CV)[18, 20, 21] or the organism is washed with Pt, or another metal complex such as uranium or gallium, supplemented buffers[19]. For the Gram stain systems, CV and the Pt complex migrate into the cell and the CV^+ carbocation forms a precipitate through the complexation with the Pt anion[18]. The samples are then washed to remove any excess CV and Pt from outside of the cells[18, 20, 21]. What remains is electron opaque Pt-CV precipitates within

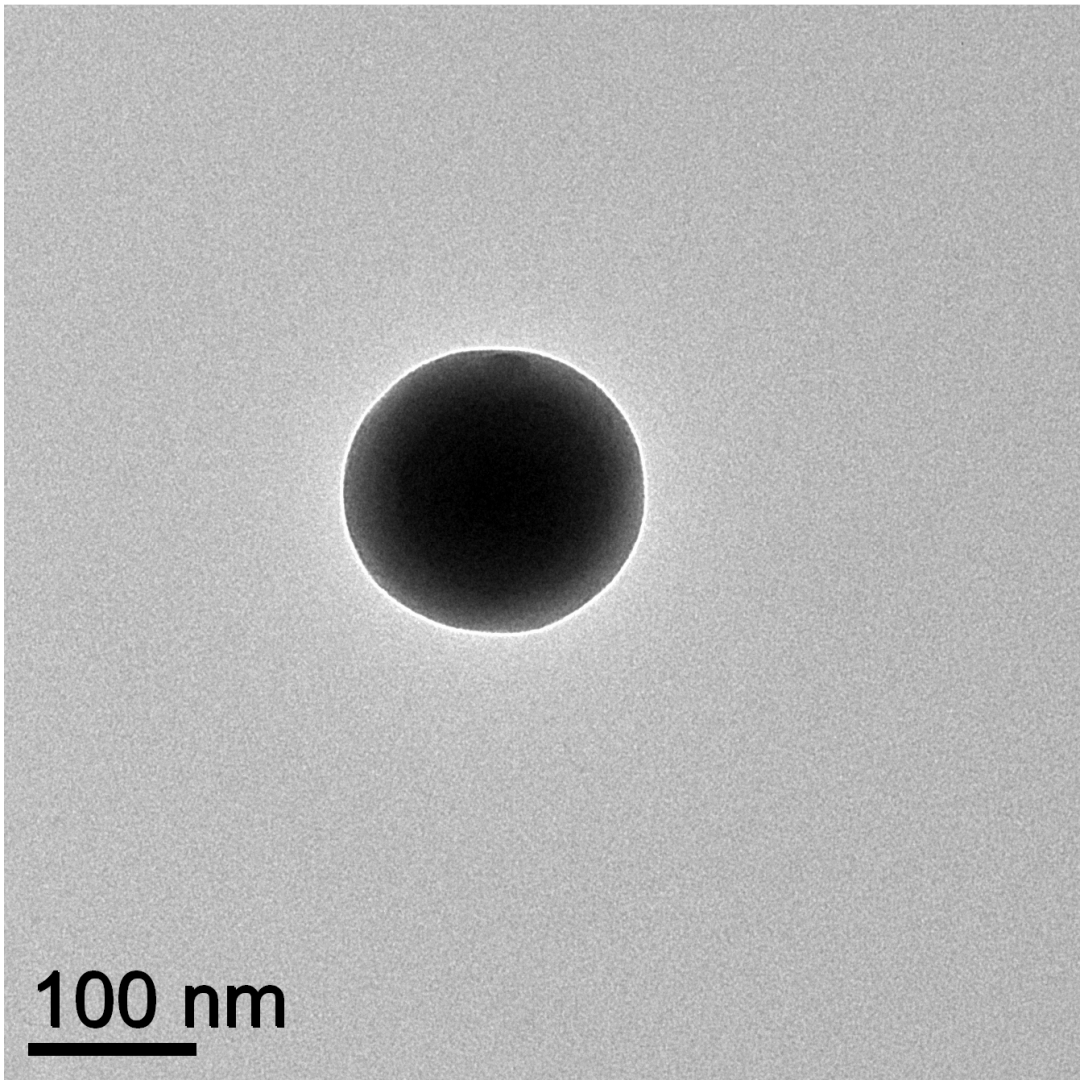

Figure 4. 17 - TEM Image of PDMAEMA and Succinic Acid

the cellular structure which allow for TEM; providing images of the subcellular structures[21]. In the traditional stain experiments, cells were washed with metal supplemented PIPES buffer and incubated for several hours and finally washed with PIPES buffer to remove excess metal ions[19]. TEM images of these organisms reveal detailed structural features due to metal associated with the membranes of the cells compared with a barely discernable structure when an unstained cell is imaged[19].

Both staining techniques result in systems strikingly similar to the Pt-PDMAEMA system being studied. While the biological applications are used to image cellular structure, these are analogous to the polymer structures in the inorganic system. Cell walls and other cellular structures are composed of biological polymers such as polysaccharides[19] and peptidoglycan[20], therefore, the present a similar system to our organic polymers. As with the biological stains, it is believed that in the Pt-polymer process the Pt molecules are aggregating within the polymer structure and acting as an electron opaque stain. While the polymer is electron dense enough to be imaged via TEM, the addition of the Pt aggregates creates darker areas within the large structures seen in the images much like the metals in the biological stains provide more electron dense areas within the cells structures with which they have associated[18-21]. In the case of $K_2[PtCl_6]$-PDMAEMA, the Pt is seen in higher contrast since less polymer will be present in each oblong structur. Because the Pt-polymer structure is much weaker so fewer strands will be interlinked with each other which creates less electron dense polymer areas.

4.3.4 Conclusions

The observations presented within this section provide insight into the early portion of the mechanism by which PDMAEMA is able to direct the formation of Pt nanoparticles. Scheme 4. 1 A outlines the formation of large Pt-PDMAEMA particles formed through ionic interactions between the cationic protonated PDMAEMA polymer chain and the di-anion Pt unit. DLS data confirms the presence of large particles when $H_2[PtCl_6]$ is used and lack thereof for $K_2[PtCl_6]$, Figure 4. 15, providing evidence of the importance of an available proton and therefore of the creation of cationic polymer chains. The use of organic acids provide a means to investigate the

importance of the di-anion by removing any Pt intermolecular forces that may have been influencing the formation of the structures seen in Figure 4. 13 and Figure 4. 14. From the DLS data, it is shown that the diacids, succinic and sulfuric, result in the formation of large particles, >200nm, while the monoacids, hydrochloric and acetic, show nothing significantly larger in size than the neat polymer. This study confirms the role of the dianion as a cross-linker of the protonated PDMAEMA since the diacids were able to create particles with the polymer and the monoacids did not show this ability.

TEM analysis of the succinic acid-PDMAEMA resulted in images very closely resembling those seen in images of $H_2[PtCl_6]$-PDMAEMA providing evidence that the shape of the large macrostructure is driven by the Pt-polymer ionic bonds rather than ion-dipole intermolecular forces responsible for the shapes seen in images of $K_2[PtCl_6]$-PDMAEMA. The only substantial difference seen between the succinic acid-PDMAEMA and $H_2[PtCl_6]$-PDMAEMA images is the variation in contrast across the large particles with the succinic acid images having almost no variation and the presence of many small dark areas in the images of the particles containing platinum. This can be rationalized by examining techniques found in biological imaging where metals are used as electron opaque stains to allow TEM to be utilized to image at the subcellular level. These methods utilize metals as Gram or traditional staining agents adding them to organisms where the Pt-CV complex or metal complex associate with cellular structures, which can are biological polymer, allowing for TEM imaging. From these experiments a direct correlation can be seen with Pt acting as a electron opaque stain for PDMAEMA even as Pt(IV). All of these studies present ample verification of the formation of the structure seen in Scheme 4. 1 A which will be termed the nanogel from this point forward.

4.4 Reducing Agent Effects

Initial studies were performed utilizing ascorbic acid as the reducing agent for the synthesis of platinum nanoparticles. These studies focus on the impact of ascorbic acid as well as several other reducing agents on the mechanism of control of synthesis of metallic

nanoparticles. Unless otherwise noted, reactions were performed with a large excess of reducing agent a 10:1 ratio to platinum.

4.4.1 Ascorbic and Citric Acid

Initial results, section 4.2, confirmed that utilization of ascorbic acid in the Pt-PDMAEMA system will result in the formation of small monodisperse nanoparticles if protons are the counter-ion of the platinum complex and the platinum ion is a dianion. However, due to the large peak in the electronic spectra, Figure 4. 8, which overlaps the region of the Pt(IV) $L_{\pi} \rightarrow M$ transition, it can be used only for certain studies. DLS and TEM analyses were performed on Pt-PDMAEMA reactions reduced with ascorbic acid. From these observations, the mechanism seen in Scheme 4. 1 B was determined. This process is characterized by the destruction of the nanogel due to the protonation of every amine site in the PDMAEMA chains, releasing the platinum anions from their tight association with the polymer.

The acidic character of ascorbic acid is not immediately apparent as there is no carboxylic unit within the molecule. Ascorbic acid's acidic character results from the conjugated system formed from the double bond, carbonyl group, and hydroxyl group. Conjugation within the molecule stabilizes the conjugate base by providing a route to two resonance structures, Figure 4. 18, greatly increasing the acidity of the hydroxyl group. Therefore, the use of ascorbic acid as a reducing agent will result in the proton injection and considering the large quantity of reducing agent utilized for the reduction of platinum in the Pt-PDMAEMA system this will create a large excess of protons in the reaction. Protonation of every unit within the PDMAEMA chains greatly increases solubility in aqueous solution creating interactions with water and the conjugate base that compete with the ionic bond formed with the platinum dianions breaking apart the nanogel.

The effect of the addition of ascorbic acid was monitored by performing DLS immediately after adding ascorbic acid to the reaction solutions. Spectra shown in Figure 4. 19 show the analysis of the Pt-PDMAEMA system at three different stages: prior to, immediately following, and three days after the addition of ascorbic acid to the reaction solution. Prior to the addition of ascorbic acid the average hydrodynamic diameter is 93.1nm representing the nanogel formation

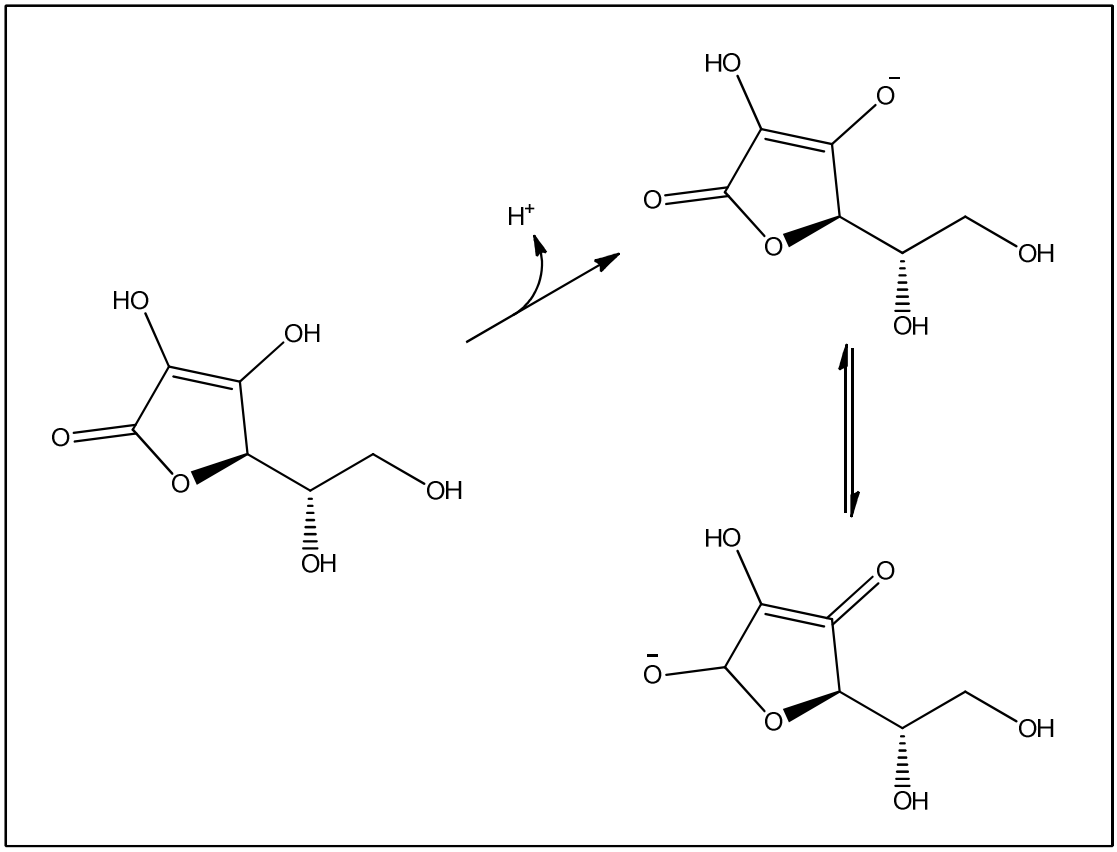

Figure 4. 18 - Ascorbic Acid and Ascorbate

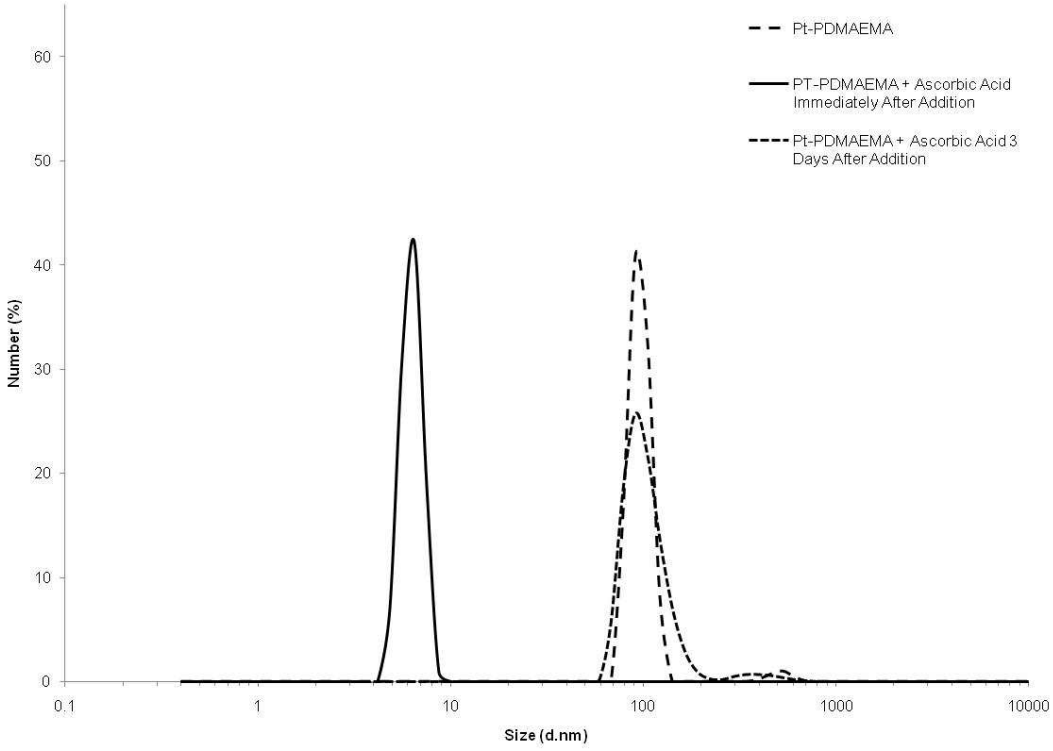

Figure 4. 19 - DLS Spectra of Ascorbic Acid Reduction of Pt-PDMAEMA

which is expected with the addition of $H_2[PtCl_6]$ to PDMAEMA as seen in the previous studies. Immediately following the addition of ascorbic acid to the reaction mixture, the average hydrodynamic diameter dramatically decreases to 5.5nm. The large decrease in particle size approximately to that of neat PDMAEMA solution confirms the destruction of the nanoparticles as hypothesized in the mechanism proposed in Scheme 4. 1 B.

By analyzing the reaction after complete reduction of the platinum, DLS data corresponding to the point where aliquots are removed for TEM analysis is obtained. Particles with average hydrodynamic diameters of 103nm are seen via DLS measurements of fully reduced solutions. These observations coincide with part C of Scheme 4. 1. During this stage of the synthesis, the platinum particles are formed as the polymer chains adsorb to the surface fully wrapping around the particle. At this point, 1.12 ± 0.25nm are observed in TEM images of the same solution. The ten-fold increase in size disparity between data reported in TEM and DLS measurements is directly related to the PDMAEMA coating the platinum particles. This coating will not be electron dense enough to be observed by TEM but will effect DLS measurements. Swelling of the PDMAEMA chains coating the platinum resulting from particles being analyzed while in a dilute aqueous solution will coincide with the larger particle size seen in DLS analysis.

Citric Acid, shown in Figure 4. 2 B, was utilized for several experiments since it does not have a intense peak in the same region as ascorbic acid and the Pt(IV) $L_\pi \rightarrow M$ transfer band. However, there is a less intense peak in the electronic spectra, Figure 4. 20, at ~205nm which overlaps the $L_\sigma \rightarrow M$ transfer band of Pt(IV). Therefore, while it is useful for observation of the decline of the $L_\pi \rightarrow M$ transfer peak, Figure 4. 21, interference from the electronic spectrum of citric acid will make it unsuitable for analysis concerning the change in the $L_\sigma \rightarrow M$ throughout reduction of the Pt(IV) species. Since this is also an acidic reducing agent, similar DLS spectra are expected. As in the experiments performed with ascorbic acid, the citric acid is in a 10:1 ratio with platinum, so there will be a large quantity of protons injected into the solution with the addition of citric acid.

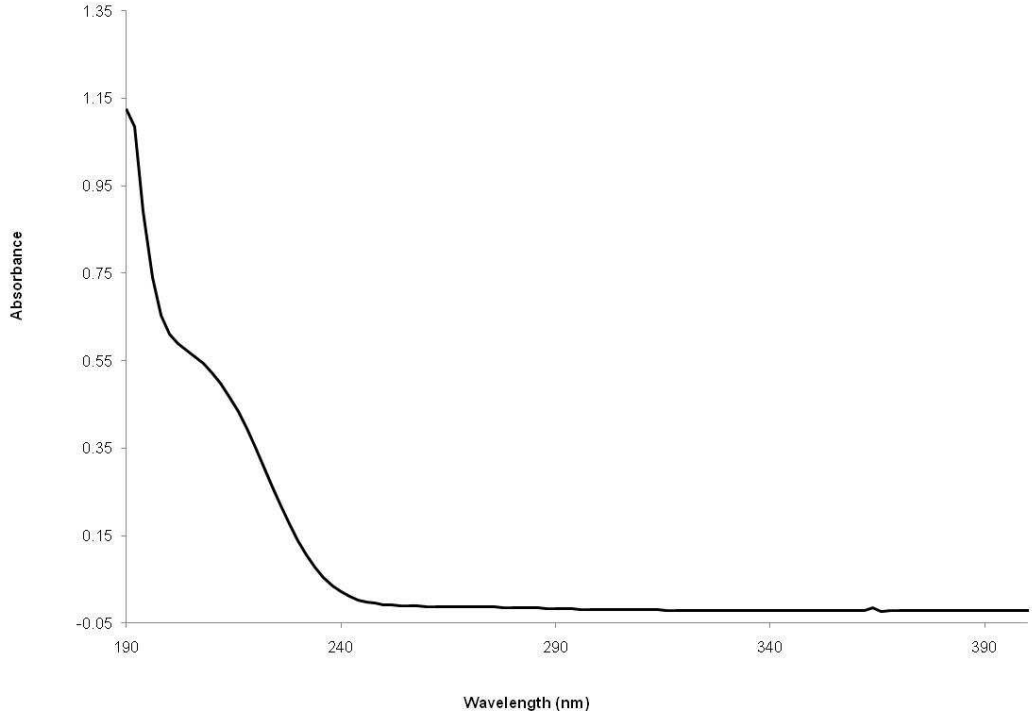

Figure 4. 20 - Citric Acid UV-vis Spectrum

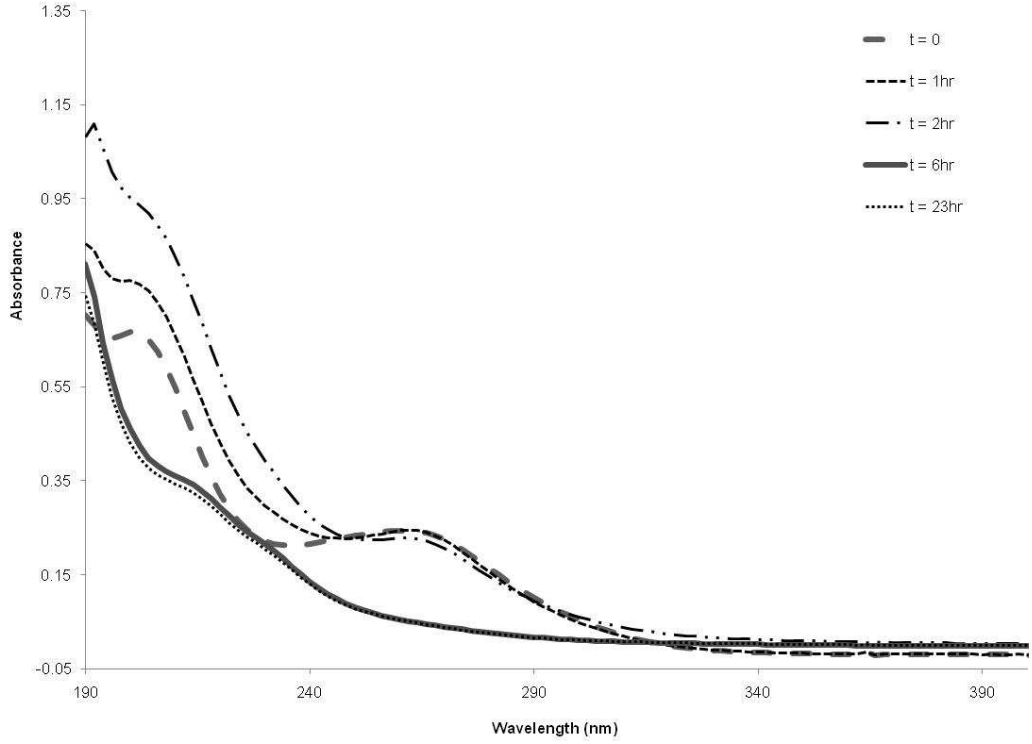

Figure 4. 21 - Citric Acid Reduction Spectra of $H_2[PtCl_6]$

DLS analysis was performed at three separate points throughout the experiment, shown in Figure 4. 22: prior to, immediately following, and three days after the addition of citric acid to the reaction solution. In these spectra similar results are seen to those of ascorbic acid; initially, prior to the addition of citric acid large particles are seen with an average hydrodynamic diameter of 90.1nm, followed by destruction of the nanogel seen in the spectra of the solution immediately following the addition of citric acid where the average hydrodynamic diameter of the particle is reduced to 15.5nm, and finally after several days of reduction a return of large particles with an average hydrodynamic diameter of 71.8nm. These results further confirm the mechanism proposed in Scheme 4. 1 and broadens the applicability to any acidic reducing agent.

Determination of the platinum nanoparticle size was achieved by obtaining TEM images of the reaction solution; a representative image and size analysis is shown in Figure 4. 23. Analysis of 150 platinum nanoparticles resulted in an average size of 0.92 ± 0.26nm. These particles are slightly smaller and have a higher relative standard deviation compared with those produced using ascorbic acid as the reducing agent, Figure 4. 11 and Table 4. 1. Inspection of the histogram, Figure 4. 23, for the platinum nanoparticles reduced with citric acid reveal a much less normal size distribution than in the ascorbic acid reaction with significant high-end tailing. This indicates that there is wider variability in the speed at which the nanoparticles become fully stabilized by the PDMAEMA with the larger particles being produced when reduction of the platinum complexes occur further from the polymer chains while the very small particles were reduced while still in a close proximity to the polymer.

Adherence to the mechanism proposed in Scheme 4. 1 provides an adequate rationale for these observations. Once the nanogel is destroyed, dispersion of the platinum anions into the bulk will occur irregularly and reduction of some platinum will occur in vicinity of the polymer chains while some will begin reducing farther from the PDMAEMA chains. This behavior results in some particles taking an extended time to be fully enveloped and stabilized by the PDMAEMA chains forming larger particles. On the other hand, other particles reduce in a close vicinity to the PDMAEMA chains and are quickly stabilized forming very small particles. When these two

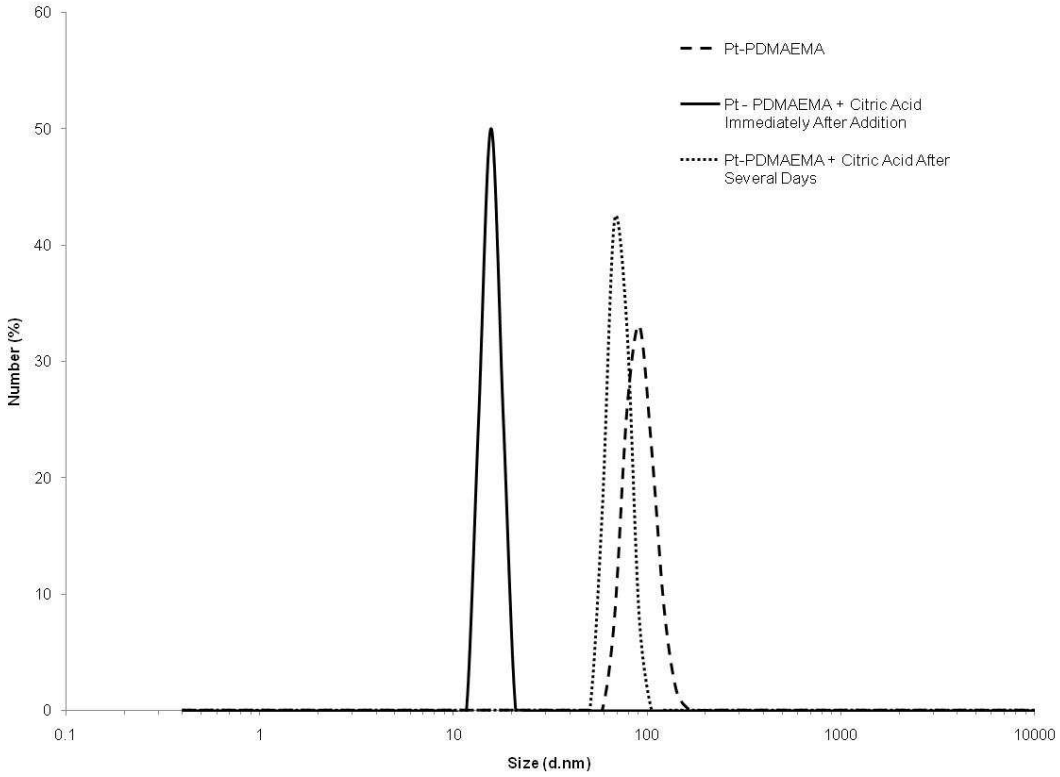

Figure 4. 22 - DLS Spectra of Citric Acid Reduction of Pt-PDMAEMA

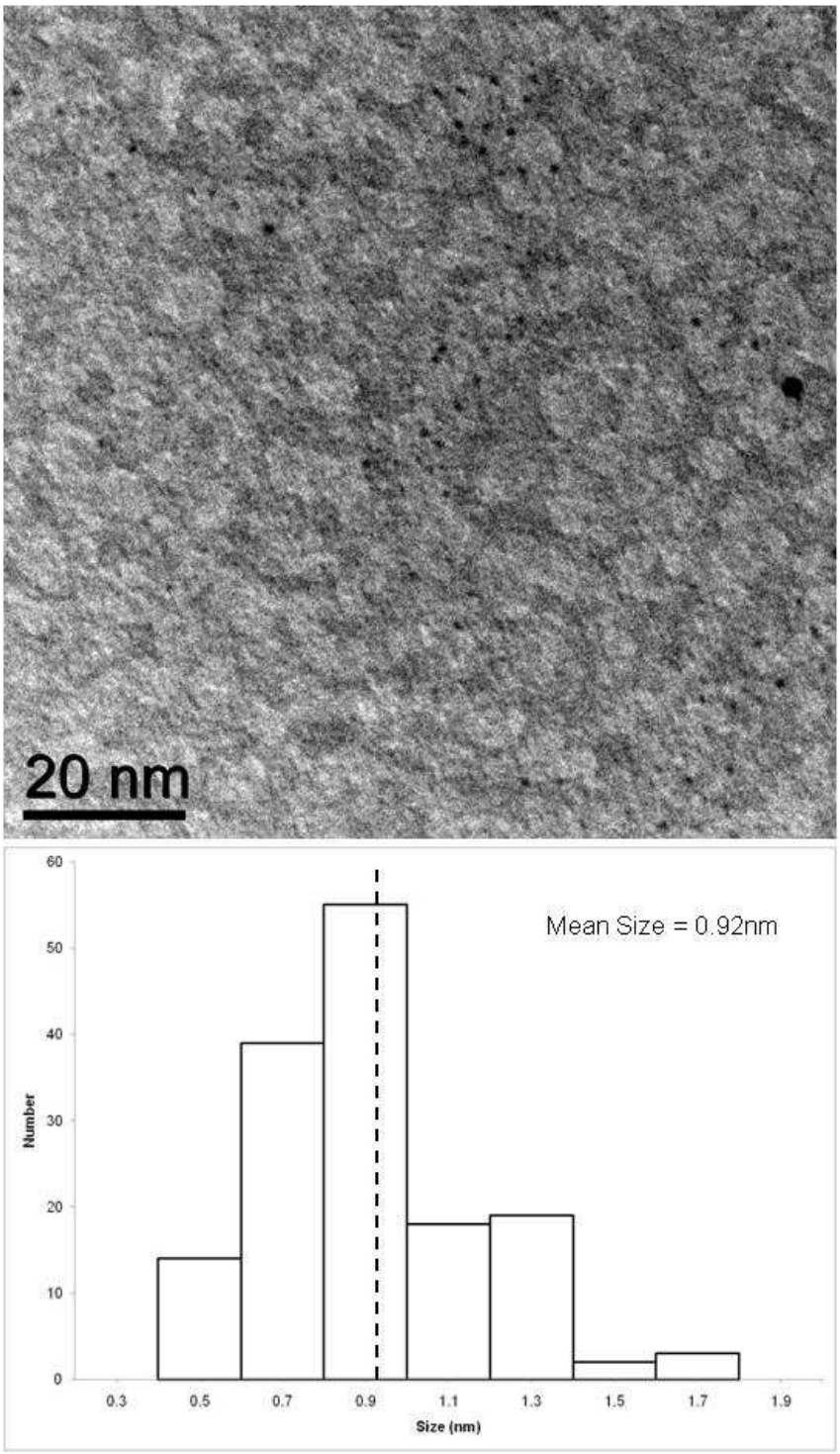

Figure 4. 23 – TEM Image and Analysis of $H_2[PtCl_6]$ Reduced By Citric Acid

processes are combined a larger size distribution will be observed. Previous studies shown in section 4.2, illustrate the importance of the nanogel in the ability of PDMAEMA to control the formation of small monodisperse platinum particles. In the work presented within this section it is apparent that during the reduction by acidic reducing agents of the Pt(IV) species to Pt(0) the nanogel is disrupted through the injection of a large number of protons, which results in the protonation of every DMAEMA unit of the polymer. Considering the impact of the nanogel on the control as seen in the cation studies, it appears beneficial to attempt to maintain the Pt-PDMAEMA particles throughout the reduction. For this reason utilization of a neutral reducing agent was pursued.

4.4.2 D- Glucose

In order to maintain the nanogel throughout the formation of the nanoparticles and avoid step B in Scheme 4. 1, D-glucose, Figure 4. 2 C, was chosen as a reducing agent for continued studies on the impact of the nanogel on the control mechanism during particle formation. D-glucose is a neutral water-soluble reducing sugar and was chosen because the initial addition of glucose to the Pt-PDMAEMA reactions will not result in the injection of excess protons that was seen in the experiments utilizing acidic reducing agents in section 4.4.1. Further, D-glucose is transparent throughout the region of the electronic spectra which is monitored for the reduction of Pt(IV) to Pt(0). These features are a large improvement over the previous reducing agents ascorbic and citric acid.

Figure 4. 24 is an image of reaction solutions utilizing the three different reducing agents mentioned so far in this work: citric acid, d-glucose, and ascorbic acid. Reducing agent was added to vials, containing PDMAEMA and $H_2[PtCl_6]$ in a 7:1 donor to Pt ration, at the same time effectiviely starting the reaciton at the same moment. These solutions were allowed to stir for several weeks after full reduction of the platinum complex before this picture was taken. The important feature in Figure 4. 24 is the difference in the color development of the three solutions. Vials 14 and 16 are significantly darker in color than Vial 15 which is resultant from the ascorbic acid and citric acid reducing agents oxidation products spectrum, while, D-glucose remains the

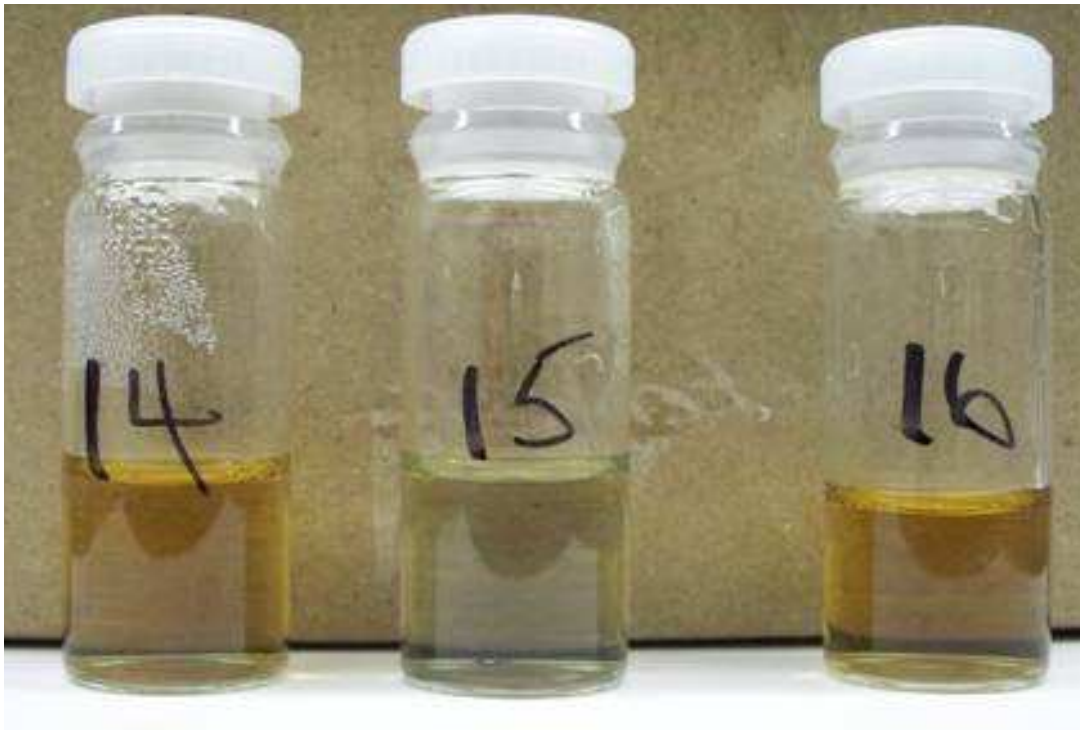

Figure 4. 24 - Reaction Solutions After Several Weeks of Stirring Using Citric Acid (Vial 14), D-glucose (Vial 15), and Ascorbic Acid (Vial 16)

color of the initial solution. This provides visual evidence of the benefit of the UV-vis transparency of D-glucose compared to the strong color development of ascorbic and citric acid.

Observation of the reaction throughout the reduction of the platinum by D-glucose via UV-vis, Figure 4. 25, provides a much clearer picture of the changes to the electronic spectra as Pt(IV) is reduced to Pt(0) compared to what results from the citric acid or ascorbic acid reactions. As expected prior to addition of D-glucose, the $^1A_{1g} \rightarrow {}^1T_{1u}$ bands representing the $L_\sigma \rightarrow M$ and $L_\pi \rightarrow M$ transitions are slightly altered through the addition of PDMAEMA from the neat solution spectra as seen in the experiments described in Section 4.2.1 in the spectra in Figure 4. 4 and Figure 4. 3. After the introduction of D-glucose to the reaction mixture, the intensity of the two major bands is seen to decrease slowly. At approximately 5.5 hours the absorption is seen to hit a minimum where there isno longer an observable peak but there is a significant amount of absorption from 190nm to approximately 250nm. Following this minimum, the absorption between 190nm and 230nm increases and a shoulder at approximately 225nm becomes apparent by the time full reduction is observed at 24 hours. D-glucose allows for a full investigation of the reduction spectra of Pt (IV) since it has proven to be inactive in the region of interest for the platinum reduction. The shape of the UV-vis spectrum of the nanoparticles was obscured by a large peak at approximately 260nm and in the region between 190nm and 240nm for the ascorbic acid and citric acid reductions respectively. Without the presence of these peaks, the shoulder at approximately 225nm becomes apparent while in the reactions utilizing the other reducing agents it cannot be detected. Retention of the nanogel upon addition of a neutral reducing agent is expected since this will not result in the injection of a large surplus of protons in the system. In order to test this hypothesis, DLS measurements were taken of the reaction solution when utilizing D-glucose as the reducing agent, Figure 4. 26. Initial measurements of the Pt-PDMAEMA solution have an average hydrodynamic diameter of 93.2nm. Immediately following the introduction of D-glucose, a slight decrease in particles size is seen as the average diameter is 42.5nm while following several days of reduction the average size of the reduced platinum nanoparticles surrounded by PDMAEMA is 96.6nm. The initial and final particle size are

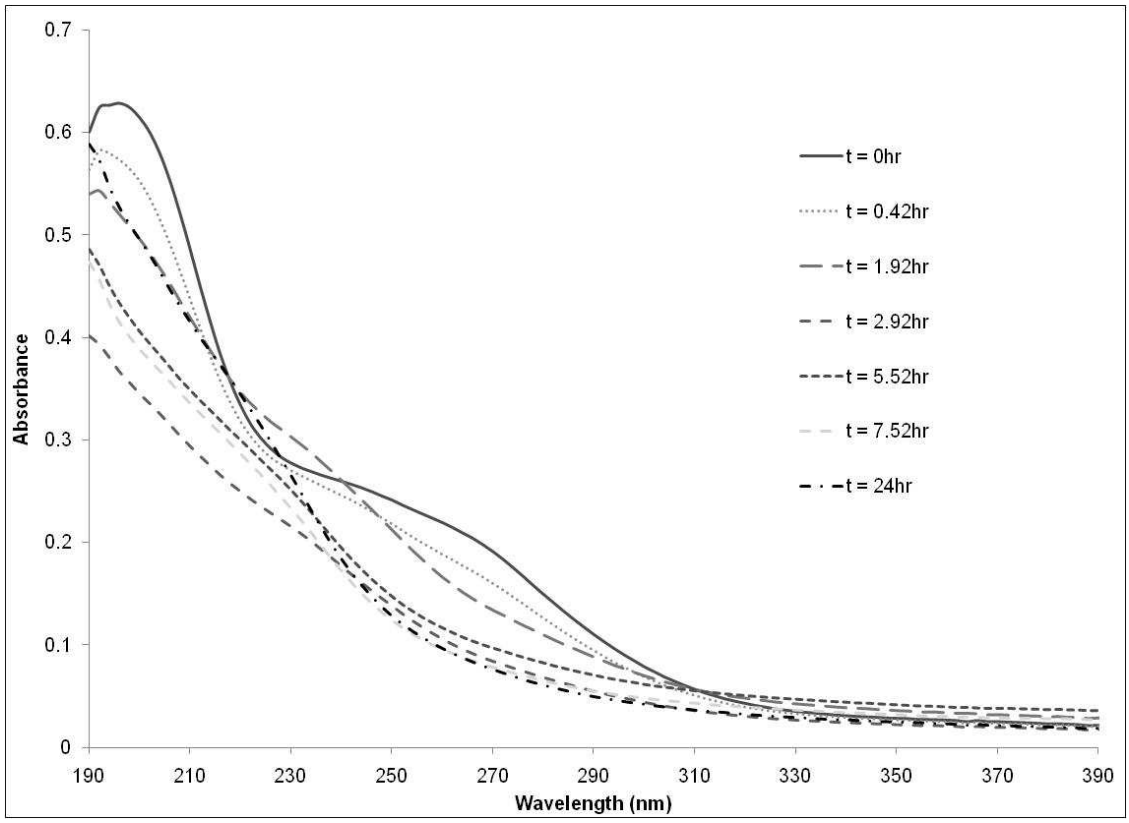

Figure 4. 25 - UV-Vis of Reduction of Pt(IV) by D-Glucose

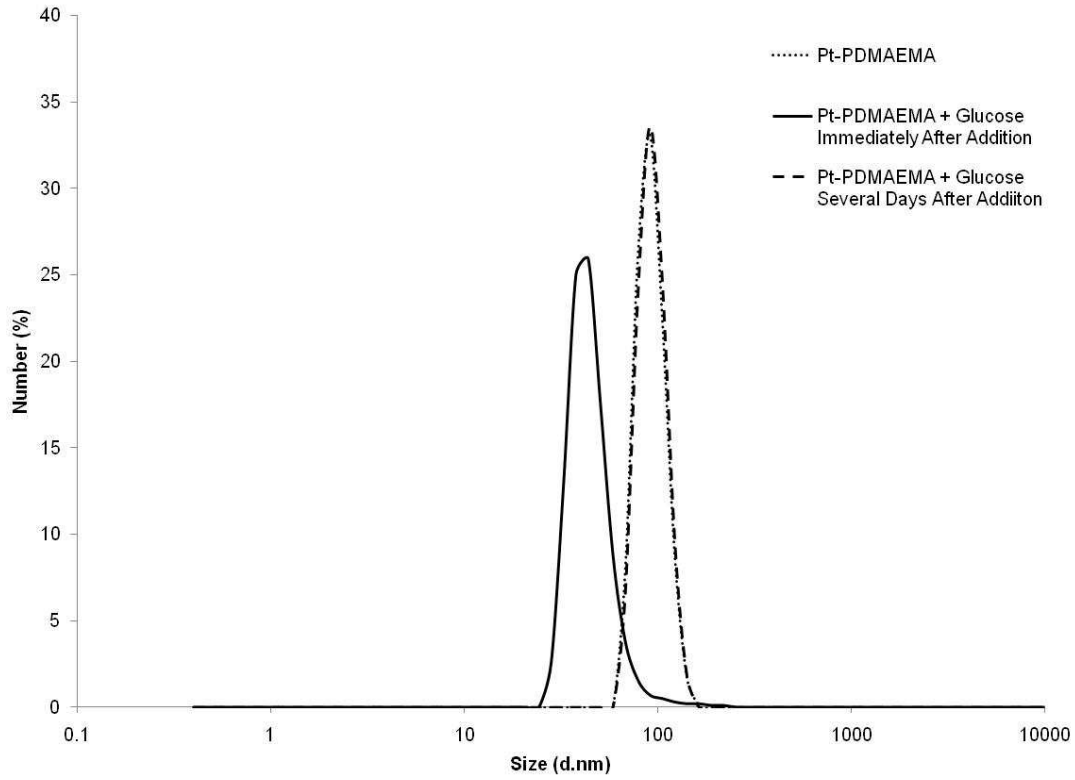

Figure 4. 26 - DLS Spectra of Glucose Reduction of Pt-PDMAEMA

consistent with those seen in the Pt-PDMAEMA systems where ascorbic or citric acid are utilized as the reducing agent. However, immediately following the addition of D-glucose the particle remains significantly larger than that of the samples following the addition of ascorbic or citric acid as well as that of the neat PDMEAMA solution spectrum. These observations confirm that the use of a neutral reducing agent has a significant impact on the mechanism of control. While a contraction of the Pt-PDMAEMA particles is seen, the nanogel is not destroyed with the introduction of D-glucose as is seen in the ascorbic and citric acid systems.

By maintaining the nanogel structure, the mechanism is altered from that seen in Scheme 4. 1 to the mechanism illustrated in Scheme 4. 2. The key difference between these two routes is observed in step B. In Scheme 4. 1, the nanogel is shown to break apart due to the introduction of protons from the acidic reducing agents, while in Scheme 4. 2 B the nanogel is maintained until the platinum is reduced breaking the ionic bond with the cationic polymer. Reactions following the mechanism proposed Scheme 4. 1 result in the reduction of the platinum within the bulk since the destruction of the nanogel frees the anionic platinum species. While the $K_2[PtCl_6]$ reduction is shown to be uncontrolled, Section 4.2, due to the reduction in the bulk caused by the weak Pt-PDMAEMA interactions with the neutral DMAEMA units, the initial formation of the Pt-PDMAEMA nanogel with $H_2[PtCl_6]$ increases the proximity of the platinum anions to the polymer chains.

This nearness of the reducing platinum to the PDMAEMA chains decrease the time necessary for the encapsulation of the particles with polymer to occur when compared to $K_2[PtCl_6]$. Therefore, control of the particle formation occurs since all of the platinum is reducing in the vicinity of the polymer where they can immediately be stabilized by encapsulation with PDMAEMA. On the other hand, in the $K_2[PtCl_6]$ system, the polymer and platinum complexes are further separated so the time required for the PDMAEMA chains to diffuse close enough to the reducing platinum to adsorb to the particles is much greater and more unpredictable. Consequently, some particles will stop growing while they are small while others continue growing, resulting in particles several times larger. This behavior is noted in the analysis, histogram show in Figure 4. 6, of the TEM image of particles reduced from $K_2[PtCl_6]$. While small

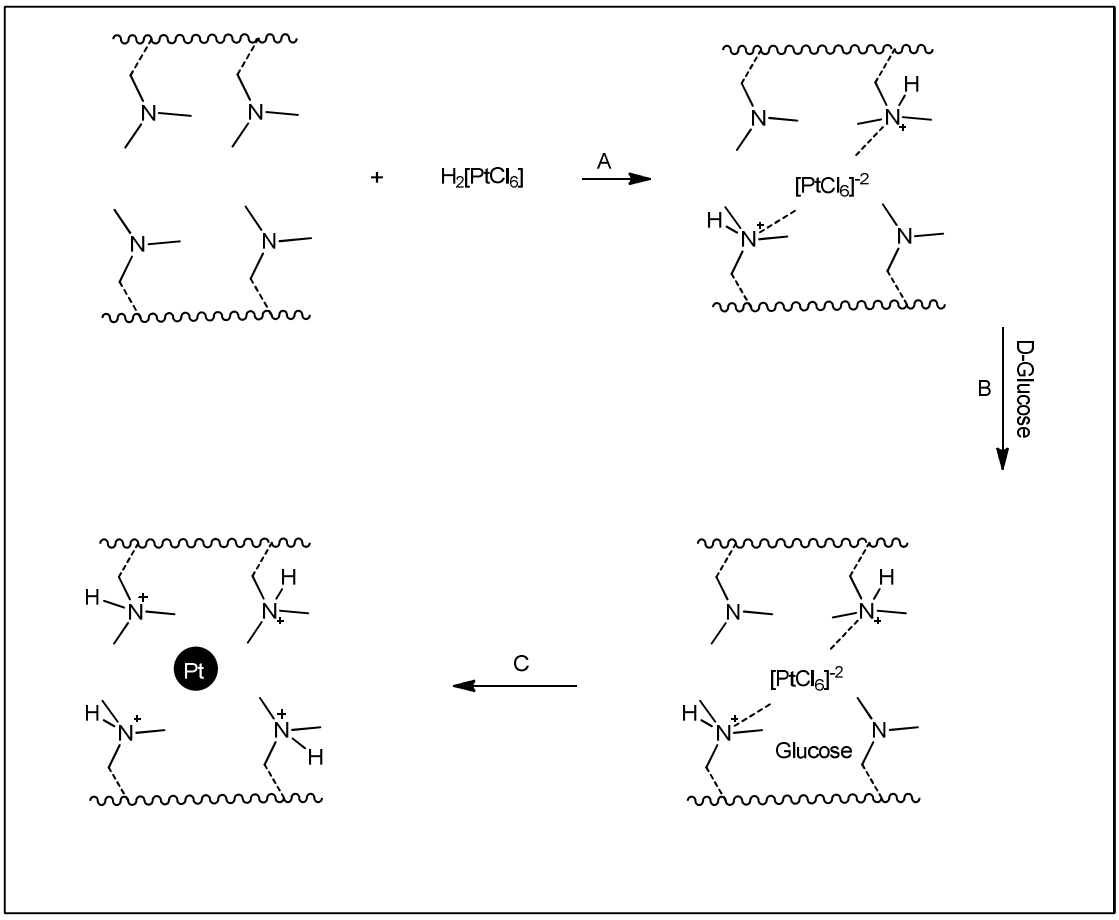

Scheme 4. 2 - General Mechanism for Formation of Pt Nanoparticles with PDMAEMA Reduced by Glucose

particles are observed in these images, less than 3nm, there is also a great number of larger particle, from 5 to 15nm.

Reactions following the mechanism shown in Scheme 4. 2 will not occur in the bulk since the nanogel remains intact throughout the addition of the reducing agent. Reduction then takes place within the gel and the platinum is only released from the ionic bonds with the cationic polymer after being reduced. Maintenance of the Pt-PDMAEMA structure ensures that the platinum is in immediate contact with the polymer chains throughout reduction. This enables immediate adsorption onto the nanoparticles as they form stabilizing the particles after a very short growth time. Therefore, particles formed via the mechanism shown in Scheme 4. 2 should be small and monodisperse.

TEM analysis was performed on reactions with a donor to platinum to reducing agent ratio of 7:1:10 where PDMAEMA was the donor source, $H_2[PtCl_6]$ provides the platinum, and D-glucose is the reducing agent. A representative image is shown in Figure 4. 27 with a histogram showing the size analysis. The average size of the 158 particles analyzed in the TEM images taken of the platinum reduced by D-glucose in the presence of PDMAEMA is 0.74 ± 0.13nm. A fairly normal distribution curve is seen in the histogram indicating a convergence to the mean as seen in the $H_2[PtCl_6]$ system that is reduced with ascorbic acid. Particles reduced with D-glucose are shown to be significantly smaller and more monodisperse than those produced utilizing ascorbic acid as the reducing agent. These observations confirm the mechanism proposed in Scheme 4. 2 since the smaller particles indicate more rapid encapsulation of the nanoparticles by the PDMAEMA. Faster adsorption of the polymer onto the surface of the platinum particles is indicative of continued Pt-PDMAEMA interactions as proposed in step B of Scheme 4. 2. Therefore smaller, more monodisperse particle formation can be attributed to a change in step B from Scheme 4. 1 compared to Scheme 4. 2.

Given the transparency of D-glucose in the UV-vis region, proven ability to maintain the nanogel, and its ability to control the formation of small monodisperse particles it is an ideal candidate for continued use as the reducing agent in the Pt-PDMAEMA system. D-glucose was

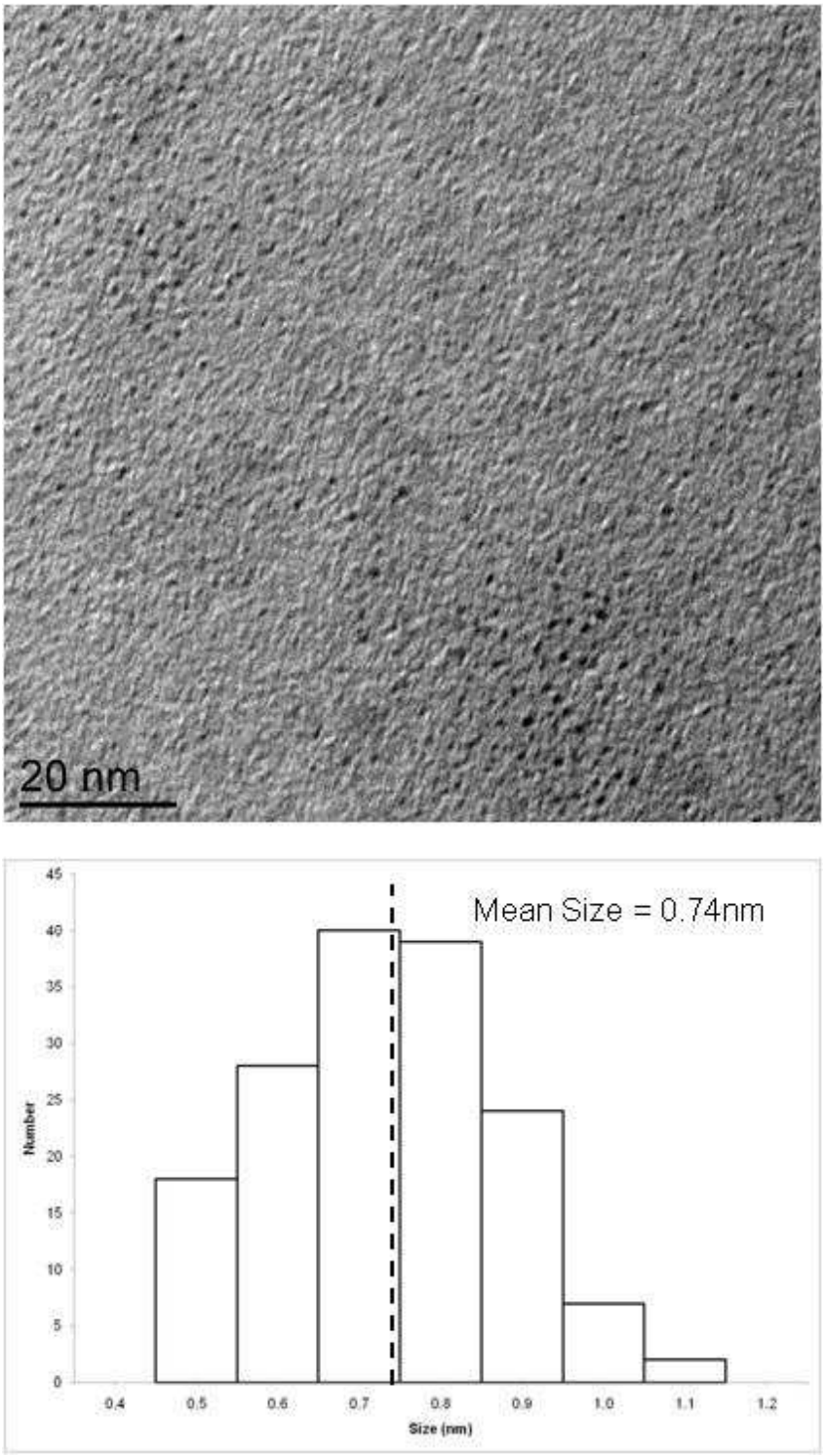

Figure 4. 27 - TEM Image and Analysis of Pt Particles Reduced from $H_2[PtCl_6]$ by Glucose

utilized for many of the following studies, however, its solubility in water allows for it to be in an equilibrium where it is present both in the bulk solution and within the nanogel. Further investigations included increasing the concentration of platinum in the reaction solutions. Dialysis of these solutions reveal that in these reactions a significant portion of the platinum is found outside of the nanogel. Therefore, since a significant portion of the D-glucose in the system will also be found in the bulk, a portion of the platinum will be reduced outside of the nanogel circumventing the control mechanism.

4.4.3 Valeraldehyde

D-glucose's hydrophilicity creates an equilibrium where reducing agent is likely to be found both within the nanogel and in the bulk solution. This provides a route for reduction of the platinum complexes outside of the macroparticles which have been shown to provide growth control for the metal nanoparticles. In order to minimize the reduction of the platinum from occuring outside of the nanogel, valeraldehyde, Figure 4. 2 D, was chosen as the reducing agent for the system. Valeraldehyde's five carbon tail lowers the solubility in water sufficiently to shift the equilibrium constant to a majority of the reducing agent residing within the nanogel. The electronic spectra of valeraldehyde is also transparent within the UV-vis region providing an unambiguous method for observing the reduction of Pt(IV).

Another advantage of valeraldehyde as a reducing agent is the clear oxidation reaction, Scheme 4. 3, it undergoes. One site is available for oxidation in this molecule opposed to the multiple sites in ascorbic acid, citric acid, and glucose. This allows for the number of electrons released via the oxidation of the reducing agent to be precisely known and controlled. The reduction mechanisms of ascorbic acid, citric acid, and glucose are well known in biological systems where they are oxidized via enzyme catalyzed chemical reactions. However, mechanisms for uncatalyzed reactions are unknown, making it difficult to predict the quantity of electrons released through oxidation of the reducing agents. Therefore, the use of valeraldehyde is advantageous since the number of electrons available for reduction of the platinum species can

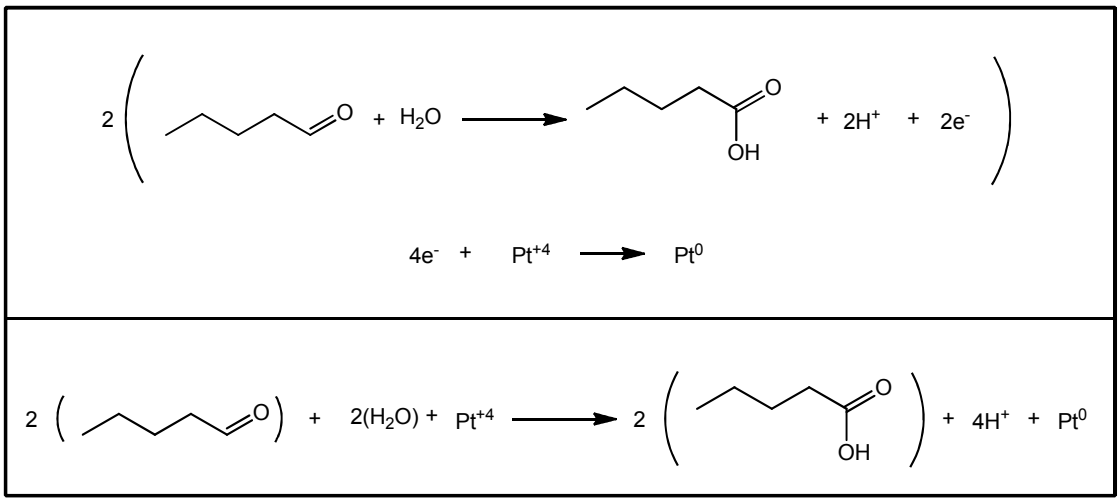

Scheme 4. 3 - Mechanism of the Reduction of Platinum by Valeraldehyde

be easily quantified providing a significant benefit for reactions where changes to the rate of reduction are required.

Initial runs with valeraldehyde were performed in a similar manner to the reactions in the previous sections with $H_2[PtCl_6]$ as the cross-linker in a 7:1 donor to platinum ratio and a 10:1 reducing agent to platinum ratio. TEM grids were prepared in the same manner as described previously and a representative image is shown in Figure 4. 28. Sizing of 74 particles seen in the images obtained via TEM resulted in an average size of 1.18 ± 0.23nm. The histogram of the data shown in Figure 4. 28 shows a fairly normal distribution curve indicating that the average size of the particles is, in fact, trending towards the mean. These results are consistent with those seen for the reduction of $H_2[PtCl_6]$ by the previous choices of reducing agent. This indicates that reduction of Pt(IV) utilizing valeraldehyde remains controlled as in the systems employing D-glucose.

4.4.4 Conclusions

Ascorbic acid, citric acid, D-glucose, and valeraldehyde were assessed for their ability to produce well defined platinum particles when used as the reducing agent for the platinum-PDMAEMA system. In all cases, $H_2[PtCl_6]$ was necessary as the complex provides both the desired metal as well as the proton necessary to form the cross-linked nanogel. Initial results were obtained exploiting ascorbic acid as the reducing agent. While good results of the particles being synthesized were obtained, an intense peak in the UV-vis spectrum at approximately 260nm made ascorbic acid unsuitable for studying the reduction spectra of the Pt (IV) to Pt(0) process. However, this peak did provide evidence that the particles' surface remains active since they are able to process the large excess of ascorbic acid. Citric acid was employed next since it the less absorption is seen in the region of interest for the platinum complexes. Once again, control of the particle synthesis is observed, however, a peak is observed in the UV-vis spectra in an important region of the platinum spectrum. For both of the previous reducing agents, destruction of the nanogel after their introduction is observed in the DLS analysis.

Given the importance of the nanogel to the proposed mechanism it was determined that

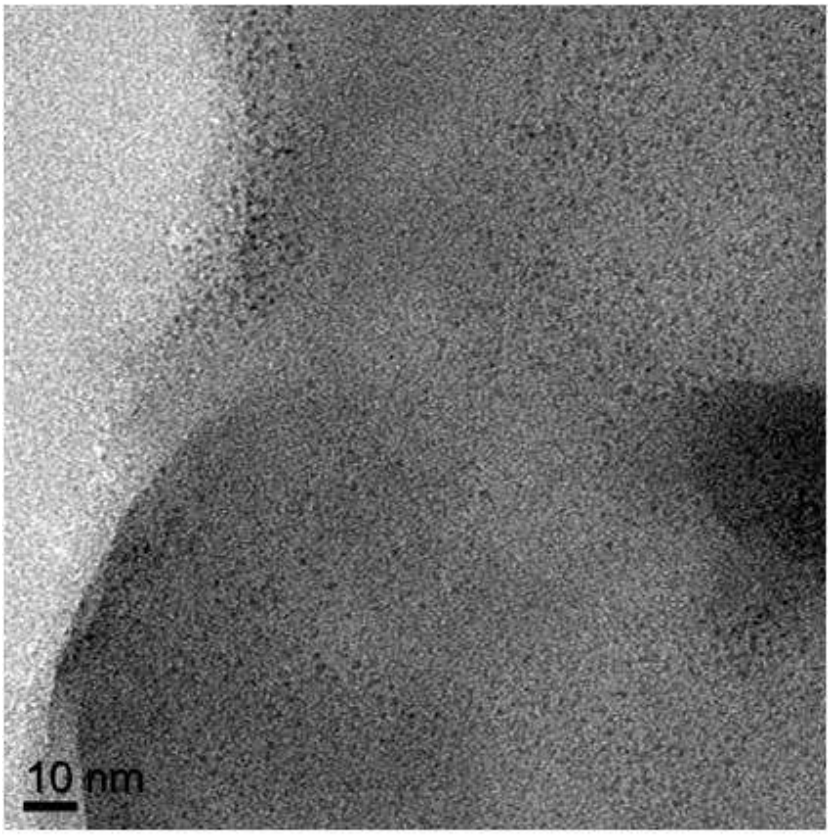

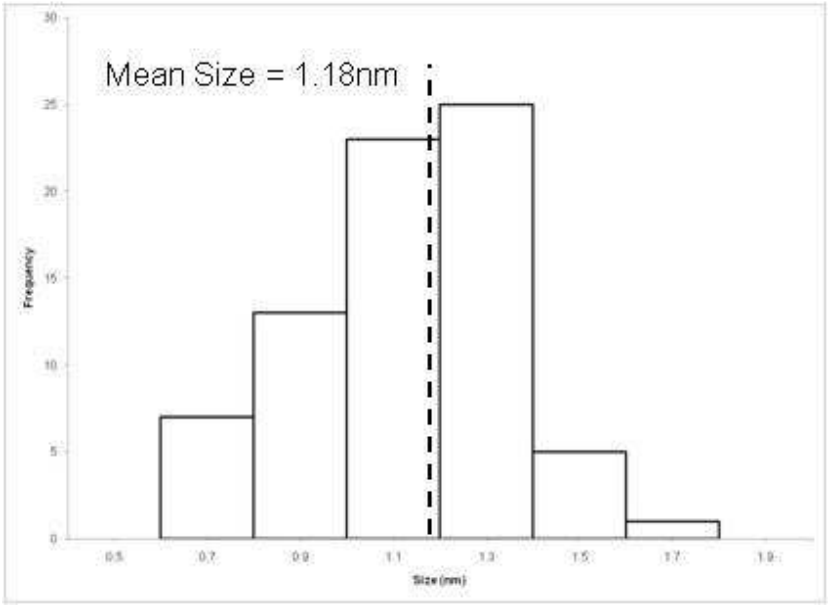

Figure 4. 28 - TEM Image and Analysis of Pt Particles Reduced from $H_2[PtCl_6]$ by Valeraldehyde

a neutral reducing agent should provide a route to a mechanism that results in more control of the formation since the nanogel is never destroyed. D-glucose was chosen as the reducing agent for several reasons: it is highly soluble in water, will not release protons that will destroy the nanogel superstructure, and lack of absorption in the UV-vis region of importance for reduction of Pt(IV). Use of D-glucose resulted in the continued presence of the nanogel superstructure after the introduction of the reducing agent as shown in the DLS results. Particles of significantly smaller sizes were produced with this mechanism demonstrating the importance of maintaining the nanogel.

D-glucose as well as the platinum complex are highly soluble in water and while the desired reaction occurs in the nanogel an equilibrium will occur between the aqueous bulk and the less polar nanogel superstructure. Consequently, the reduction could be occurring in the bulk as well as in the controlled nanogel environment. In an effort to diminish the effect of the reaction occurring outside of the nanogel, valeraldehyde was chosen as a possible candidate for a lower solubility reducing agent. Small reasonably monodisperse particles were synthesized utilizing valeraldehyde as the reducing agent. This provides another reducing agent which is able to work with the PDMAEMA nanogel system to produce well defined nanoparticles. While all four compounds performed well for the platinum nanoparticle synthesis, ultimately the D-glucose and valeraldehyde proved most useful for these and further studies.

4.5 Nanoparticle Formation Using Succinic Acid as Nanogel Linkers

Common to all of the previous successful experiments is the composition of the metal complex. In every reaction, an acidic platinum complex which forms a dianion is utilized. The protons necessary for the formation of the cationic polymer is obtained solely from the platinum complex and the anion that forms following the dissociation of the protons then acts as the cross-linker forming the nanogel superstructure. While this system is particularly useful for the platinum species, it is extremely restrictive for applying this method to other metal complexes. If instead, the nanogel can be formed from a proton source outside of the metal complex the available metal is greatly increased. As seen in Section 4.3.2 PDMAEMA crosslinking can be achieved through

the use of diprotic acids. Given this precedence, succinic acid was studied as a proton source for the crosslinking. In these experiments, the donor to proton ratio was fixed at 7:2 as in the previous successful methods. Addition of succinic acid solution to the PDMAEMA solutions was always performed prior to the addition of any of the the other components. For each run the PDMAEM-succinic acid solution was allowed to stir for at least 15 minutes to ensure the incorporation of the protons and succinate anions as the crosslinkers. After this equilibrium was established, the other solutions were added in the desired order. Utilizing this method the mechanism of the reaction is altered slightly, Scheme 4. 4. The main alteration in this mechanism in steps B and C; after the addition of the metal complex the anion can exchange with the succiniate anion retaining the nanogel structure through its own interactions. It is important to note that in this system there is preferential use of potassium hexachloroplatinate. Introduction of excess protons is avoided in this manner, preventing increased solubility of PDMAEMA and destruction of the nanogel stability.

Initial runs were performed according to Scheme 4. 4 using a 7:2:1:10 donor to proton to platinum to D-glucose ratio in accordance with the concentrations utilized in the previous successful experiments. Figure 4. 29 shows a representative TEM image of the particles produced using this method. The size analysis of 78 particles resulted in an average platinum particle diameter of 1.23 ± 0.28nm. A fairly normal distribution of the particles is observed with some slight high end tailing, indicating that the results are trending to the mean. In comparison to the results seen using platinic acid as the proton source as well as the metal source in Section 4.4.2, the platinum particles synthesized are approximately double the size and have a similar amount of uncertainty associated with the measurements. The increase in particle size may be due to the decreased association of the platinum anions with the protonated DMAEMA units of the polymer complex. This allows the platinum to move more freely throughout the superstructure resulting in an increased level of interactions between the platinum anions and the growing particles. Most importantly these results have shown that crosslinking the nanogel prior to the addition of platinum to the reaction still provides a method of control for the nanoparticle

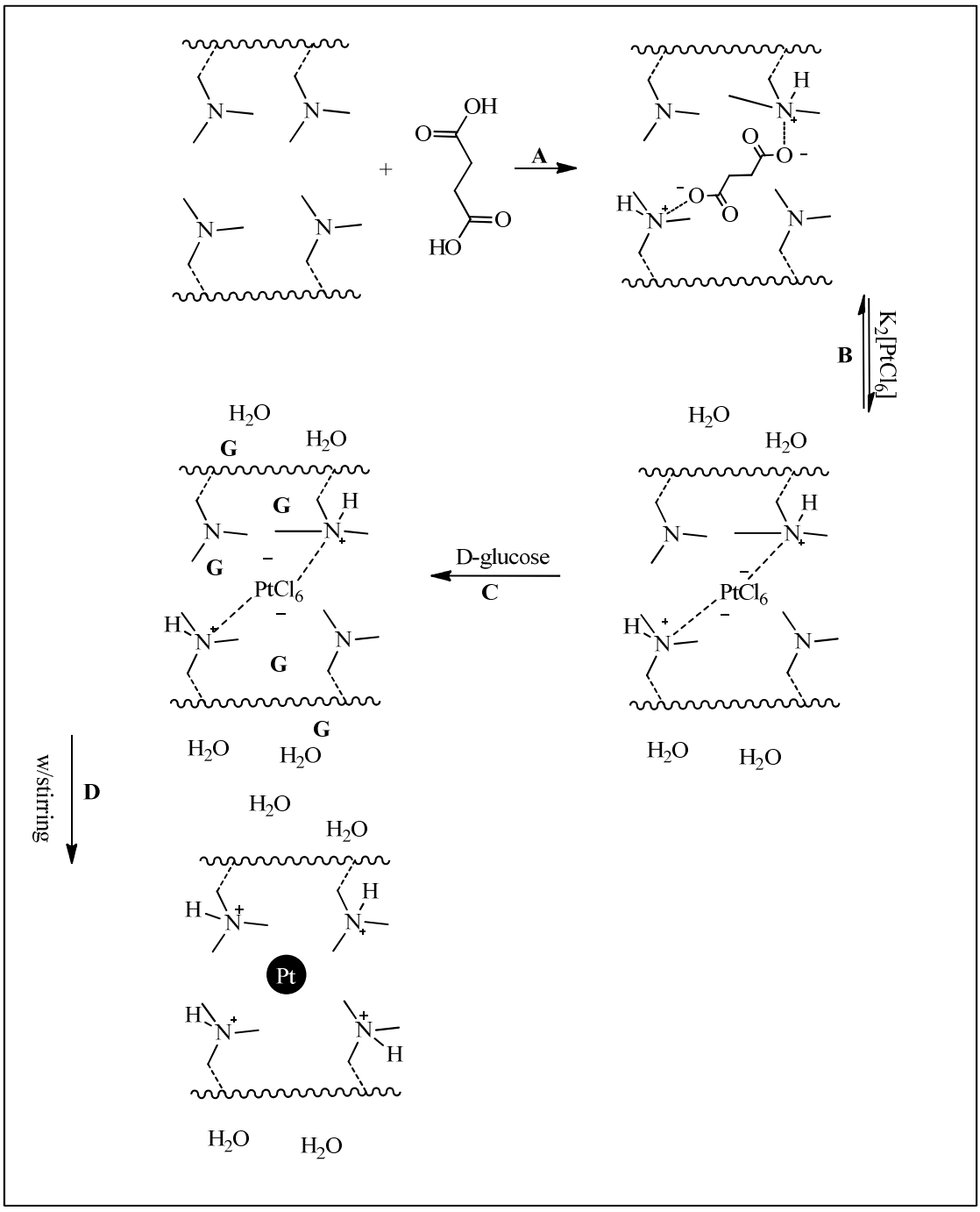

Scheme 4. 4 - Mechanism for the Formation of Platinum Nanoparticle Using Succinic Acid as a Crosslinker Using D-glucose

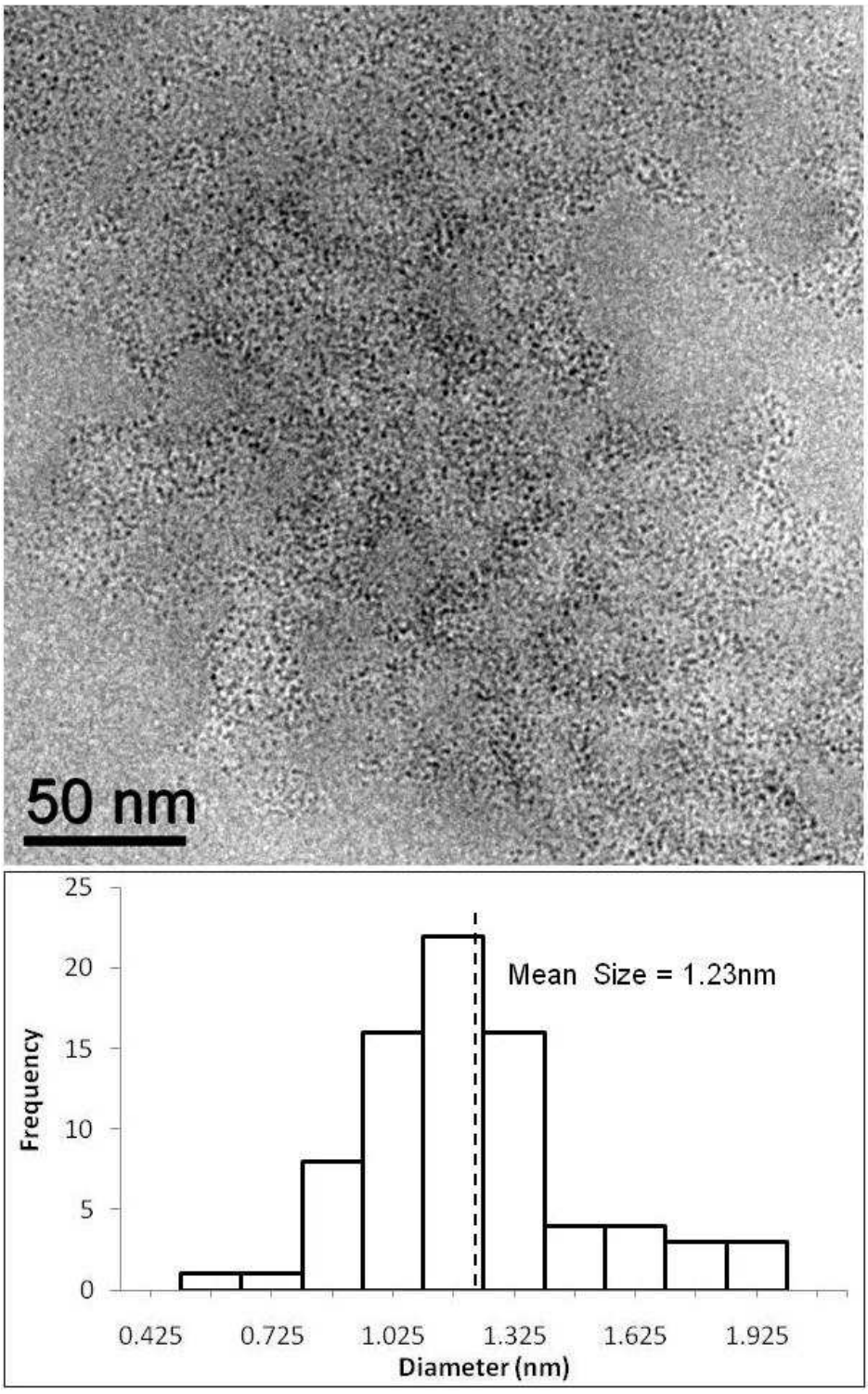

Figure 4. 29 - Pt Nanoparticles Synthesized Using Succinic Acid Cross-linked PDMAEMA With Reduction by D-glucose

formation proving the mechanism is viable for producing metal nanoparticles from nonacidic species. This is essential for expanding the control method to a variety of different metal systems.

Following successful nanoparticle production using succinic acid as the crosslinker and D-glucose as the reducing agent, valeraldehyde was substituted as the reducing agent to attempt to isolate the reduction inside the nanogel superstructure. The new mechanism is shown in Scheme 4. 5. Valeraldehyde is added to the reaction in step B and allowed to migrate into the nanogel before the addition of potassium palatinate, unlike in the previous reaction schemes. Migration into the nanogel is essential to prevent reduction from occurring in the aqueous bulk. By employing valeraldehyde, which is significantly less polar than the D-glucose, and adding it prior to the platinum species, reduction outside of the nanogel superstructure should be minimized.

TEM images of the platinum nanoparticles produced using the mechanism described in Scheme 4. 5 were obtained and analyzed. A representative image is provided in Figure 4. 30 as well as a histogram detailing the analysis of the platinum particle diameter size distribution. The average size of the 252 naoparticles which were sized is 0.99 ± 0.19nm which is significantly smaller and still well defined when compared to the particles produced using the method outlined in Scheme 4. 4. Looking at the histogram a reasonably normal distribution which trends towards the mean is seen with less of the high end tailing seen in the previous method. These results indicate that the formation of the particles is being controlled and since the particles are significantly smaller there is less time for particle growth prior to the full stabilization by the PDMAEMA polymer chains. Decreasing the likelihood of particle growth in the aqueous bulk is likely responsible for this reduction in size.

Two variations to the current system were performed to study the effects of concentration and reduction speed. The first experiment was performed with a considerably higher concentration of valeraldehyde. In this study, the ratio of donor to proton to platinum to valeraldehyde was altered to 7:2:1:100, a ten-fold increase in reducing agent concentration. This

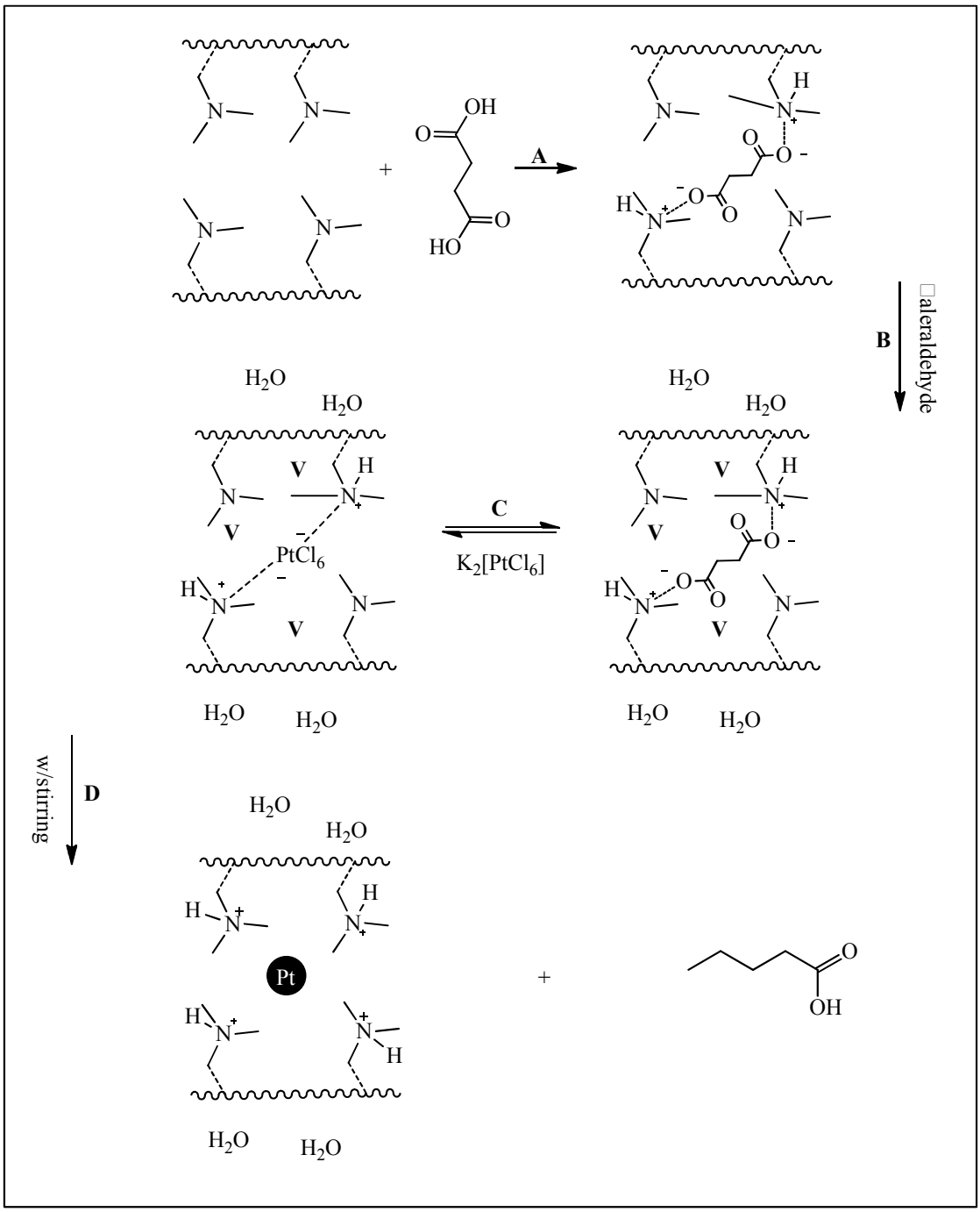

Scheme 4. 5 - Mechanism of Nanoparticle Synthesis via Valeraldehyde Reduction with Succinic Acid as the Cross-linker and the Addition of Valeraldehyde Prior to Pt

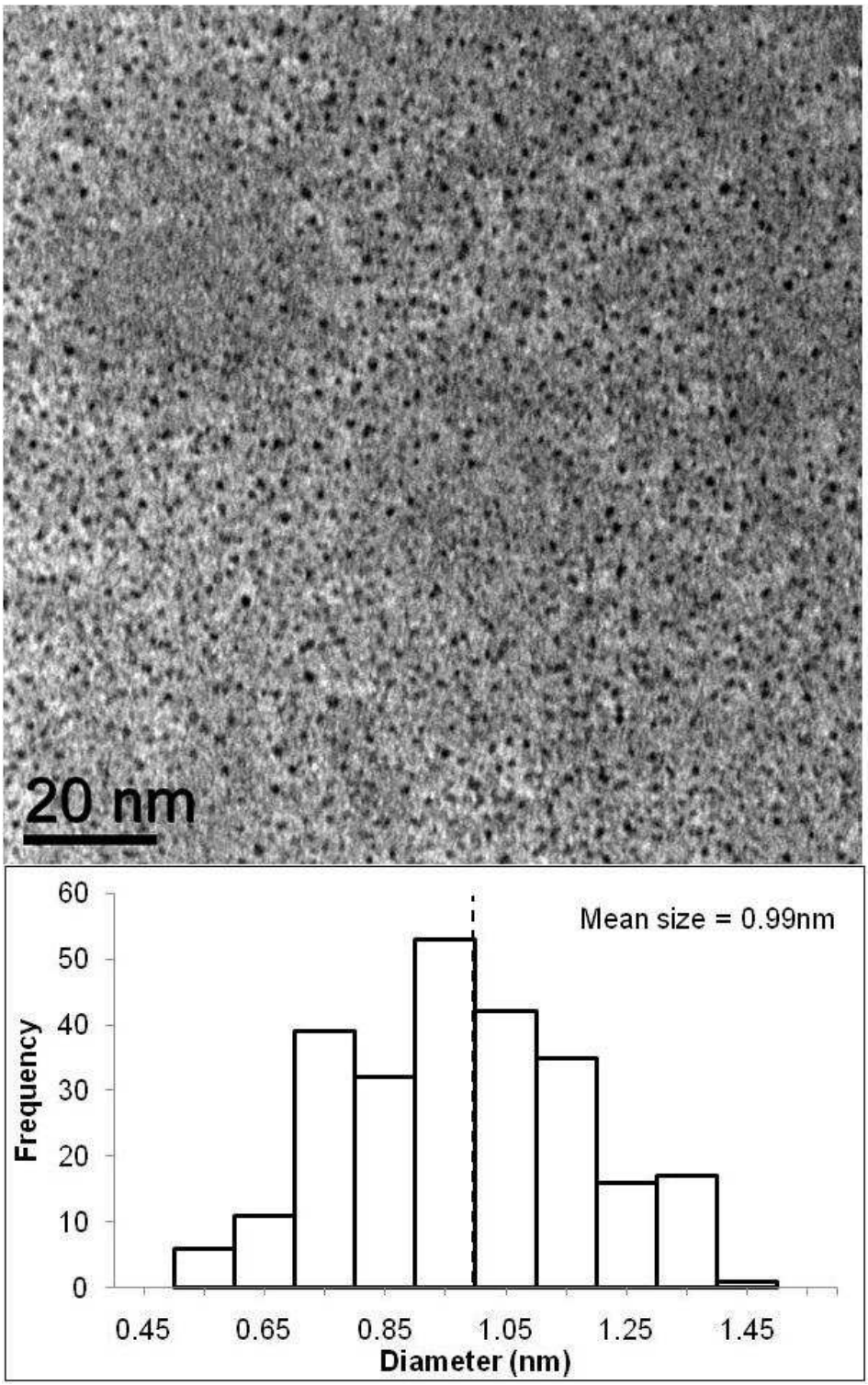

Figure 4. 30 - TEM Images and Histogram of Pt Particles Reduced by Valeraldehyde with a Nanogel Formed with Succinic Acid

alteration was accomplished by increasing the concentration of the stock solution ten-fold in order to maintain the overall concentrations by not adding addition water to the system. Using a highly concentrated aqueous solution of valeraldehyde, requires sonication prior to the addition of the desired amount of valeraldehyde to ensure a homogenous emulsion is formed. Particles produced with this high level of valeraldehyde were virtually identical in size to the particles formed with the normal valeraldehyde concentrations. The average particle diameter determined by analyzing 182 particles is 0.94 ± 0.23nm. A representative TEM image of these particles is shown in Figure 4. 31 along with a histogram detailing the size distribution. Distribution of the particles is seen to be fairly normal with only limited high end tailing. This study indicates that increasing the rate of the reaction does not cause any significant change in either particle size or dispersion.

Another study performed using the method described in Scheme 4. 5 was looking at the effect of increasing the platinum concentration in the system. In this study the platinum concentration, from potassium palatinate, was double to determine the effect this change would have on particle size and dispersity. For these reactions, a ratio of donor to proton to platinum to valeraldehyde of 7:2:2:20 was employed. The increase in the valeraldehyde in this case is to match the increase in concentration of the platinum (IV) anions maintaining the 1:10 ratio of metal centers to reducing agent that was used in numerous other successful systems for the studies previously presented in this manuscript. As in the previous two studies, the valeraldehyde was allowed to migrate into the nanogel superstructure prior to the addition of potassium palatinate; reducing the incidence of reduction in the aqueous bulk which the platinum anions can form an equilibrium between it and the nanogel. Doubling the concentration results in a significant increase in the size observed in the TEM images when compared to the previous two studies using succinic acid as the PDMAEMA crosslinker. The average diameter of the 322 particles analyzed was found to be 1.25 ± 0.25nm and the size distribution is shown in the histogram in Figure 4. 32. Similarly to the size distributions seen for these systems previously, a slight high end tailing is observed but the distribution is relatively normal with the size trending toward the

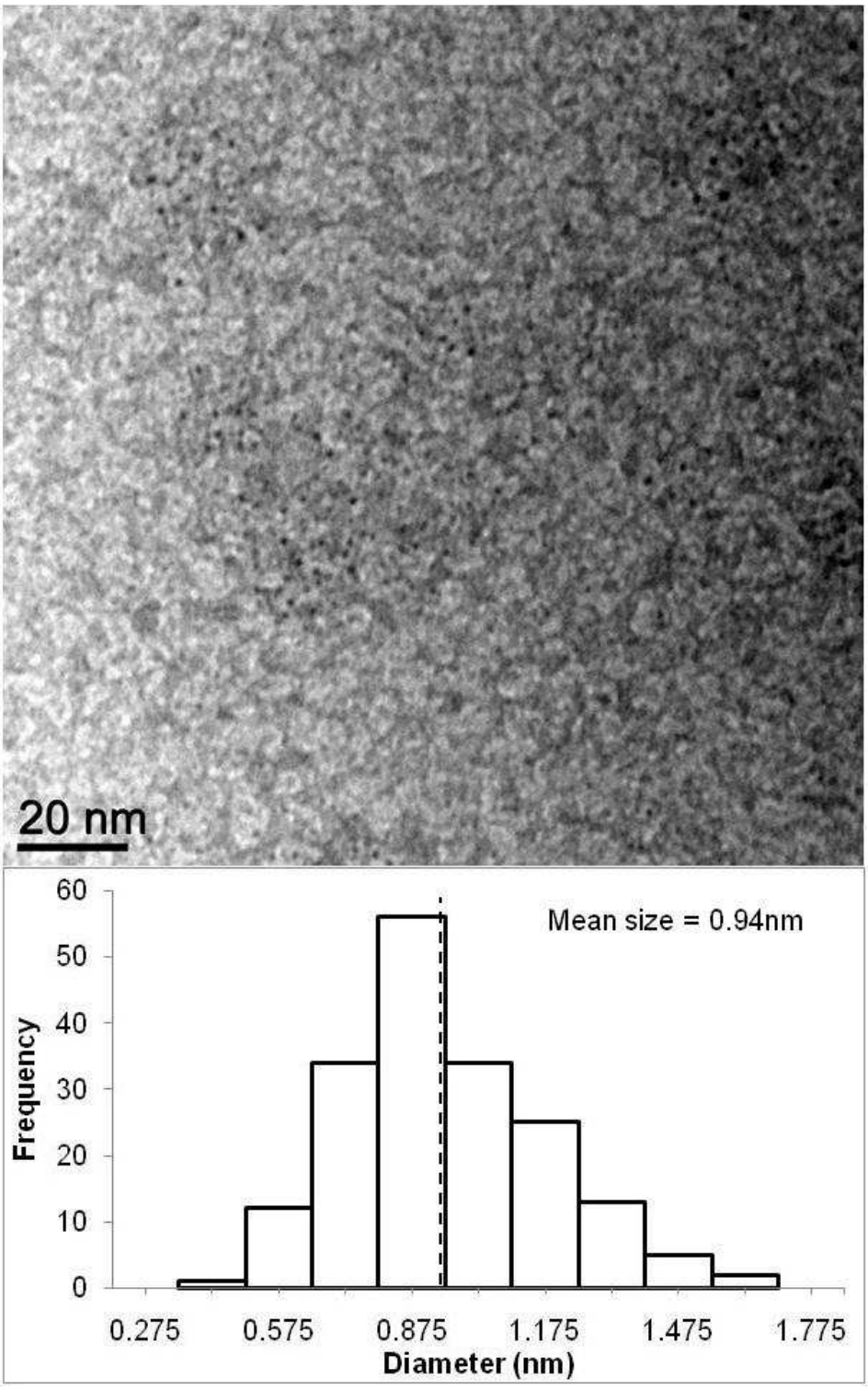

Figure 4. 31 - Pt Nanoparticles Produced with Succinic Acid Crosslinking and 10x the Valeraldehyde Concentration

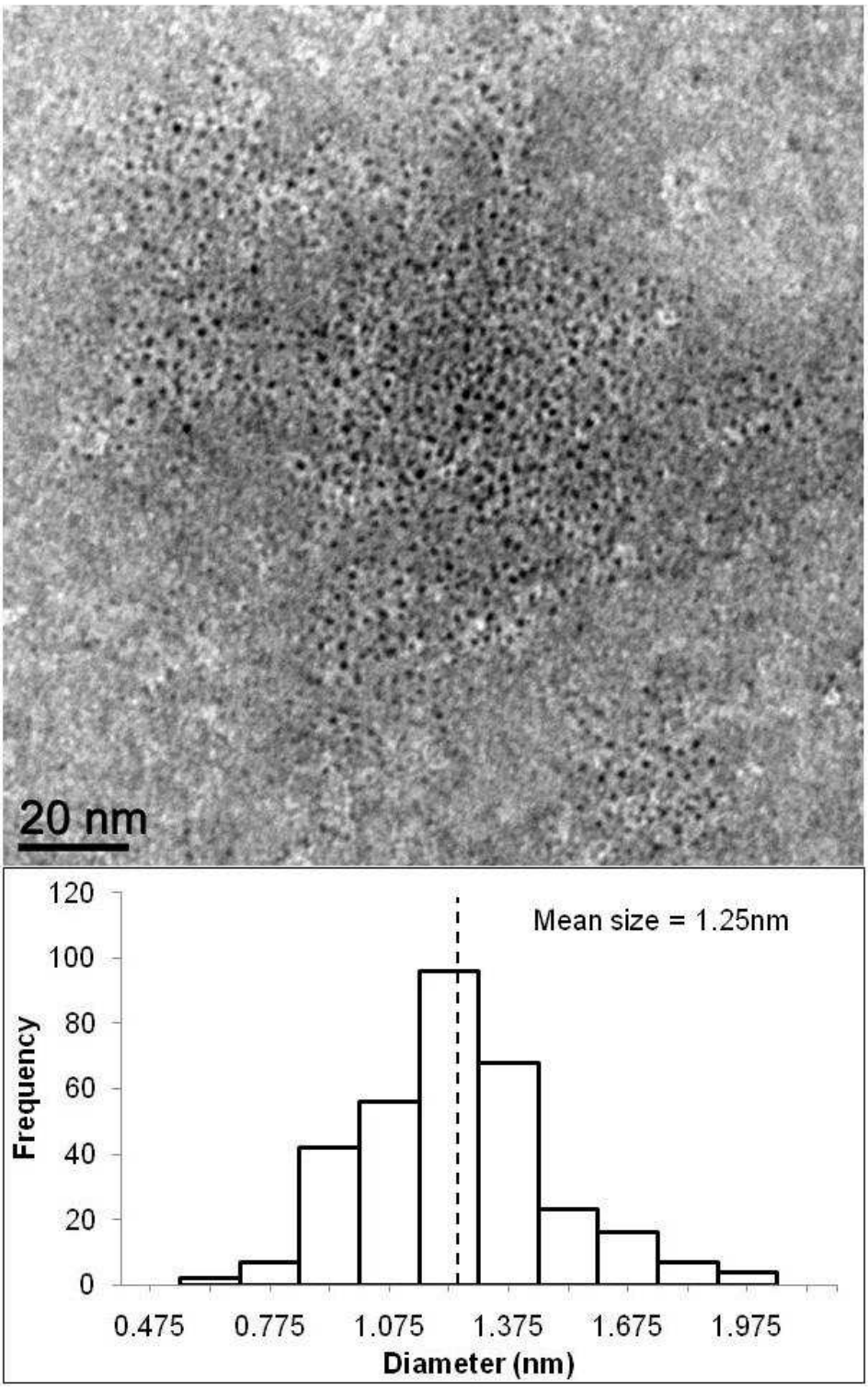

Figure 4. 32 - Pt Nanoparticles Produced with Succinic Acid Crosslinking and 2x the Platinum Concentration

calculated mean. The dispersity of these particles is the lowest, proportionally, of any of particles produced using succinic acid as the crosslinker indicating that the system is well controlled during the platinum particle formation. A representative image of these particles is shown in Figure 4. 32. From these results, it appears as though increasing the potassium platinate concentration results in a higher availability of platinum anions during the reduction process. Therefore, larger particles are produced prior to the complete stabilization of the particles by the PDMAEMA chains.

The studies in this section confirm that succinic acid can be used as the proton source and crosslinker for PDMAEMA nanogel formation. Non-acidic platinum species can then be utilized to form platinum nanoparticles. Both glucose and valeraldehyde can be used as the reducing agent, but valeraldehyde minimizes the amount of reduction that can take place in the aqueous bulk rather than within the nanogel where is will be controlled. Increasing the rate of reduction does not result in a change in the average platinum particle size, however, increasing the platinum concentration produces significantly larger particles. Most importantly, using this method a wide variety of metal particles should be able to be synthesized in a controlled manner.

4.6 Particle Size Control Studies

Synthesis of small monodisperse platinum nanoparticles is critical for the development of systems utilizing platinum as a catalysts since this minimizes the amount of material necessary by dramatically increasing the surface area. However, the ability to tune the size of the particles will expand the use of the particles to other applications. To achieve this goal, several variables were considered: platinum concentration, reducing agent concentration, and combination of $K_2[PtCl_6]$ and $H_2[PtCl_6]$ species. All of these studies were performed with the goal of increasing the size of the particles since 0.74 ± 0.13nm particles were synthesized with the current method and appear to be at the lower limit of the instrument resolution as well as what can be termed metallic platinum.

4.6.1 Platinum Concentration Studies

The most obvious route for tuning the platinum particle size is to increase the platinum concentration relative to the PDMEAMA. Theoretically the increased quantity of platinum should

create larger particles since each polymer chain is associated with more platinum anions. Increased platinum concentration should favor the growth of larger particles as reduction occurs since the platinum will be held in closer proximity to each other due to the Pt-PDMAEMA ionic interaction. This allows for increased particle size formation before the polymer adequately adsorbs to the surface of the particle, sterically inhibiting further growth or aggregation.

Platinum concentrations were increased while maintaining the PDMAEMA concentration used in the previous experiments. The ratio of reducing agent to platinum was also preserved at 10:1 resulting in an equivalent increase in overall reducing agent to that of the platinum complex. Doubling of the platinum concentration was performed resulting in the overall ratio of donor to platinum to reducing agent to become 7:2:20. In order to confirm that the mechanism was following that shown in Scheme 4. 2, since the only change to the system is the increase in platinum, the reaction was monitored by DLS to ensure formation and preservation of the nanogel after addition of the reducing agent to the reaction mixture. This data suggests, Figure 4. 33, that the reaction is not following the same pathway, Scheme 4. 2, as the previous reactions. Unlike the previous experiments, the addition of $H_2[PtCl_6]$ to PDMAEMA did not result in the formation of a larger particle instead the average hydrodynamic diameter was found to be 29.0nm. While this is somewhat larger than the size recorded of neat dilute PDMAEMA solution, there is a significant size difference when compared to that seen when the donor to platinum ratio was 7:1 rather than the 7:2 used in this reaction. It is important to note that through the doubling of $H_2[PtCl_6]$ the donor to proton ratio will also be doubled from 7:2 to 7:4. As seen in the work described in section 4.4.1, the injection of additional protons is detrimental to the existence of the Pt-PDMEAMA nanogel. Therefore, the observation of limited particle formation is not entirely unexpected. Immediately following the addition of D-glucose, the average hydrodynamic diameter is found to be 40.9nm and after full platinum reduction 41.7nm. The increase of size is likely due to encapsulation of the nanoparticles by the PDMAEMA chains as the Pt(IV) complex is reduced to Pt(0). Ultimately, the doubling of $H_2[PtCl_6]$ effects the mechanism proposed in

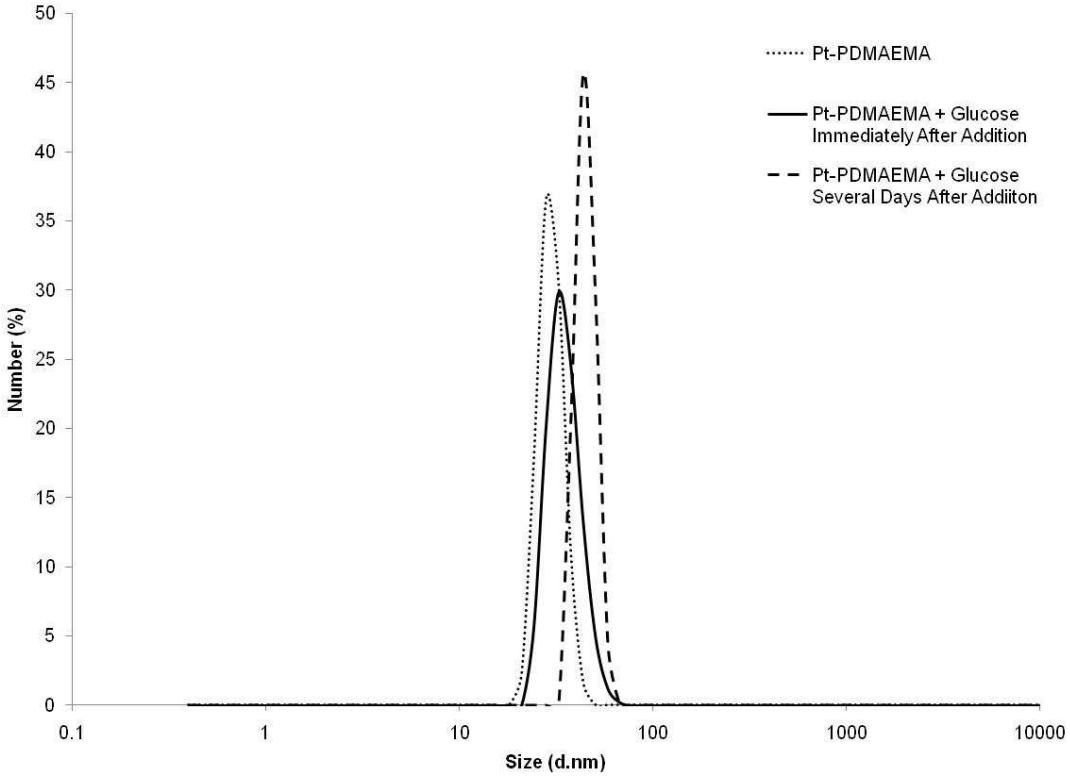

Figure 4. 33 - DLS Spectra of Glucose Reduction of Pt-PDMAEMA with a Doubling of the $H_2[PtCl_6]$ Concentration

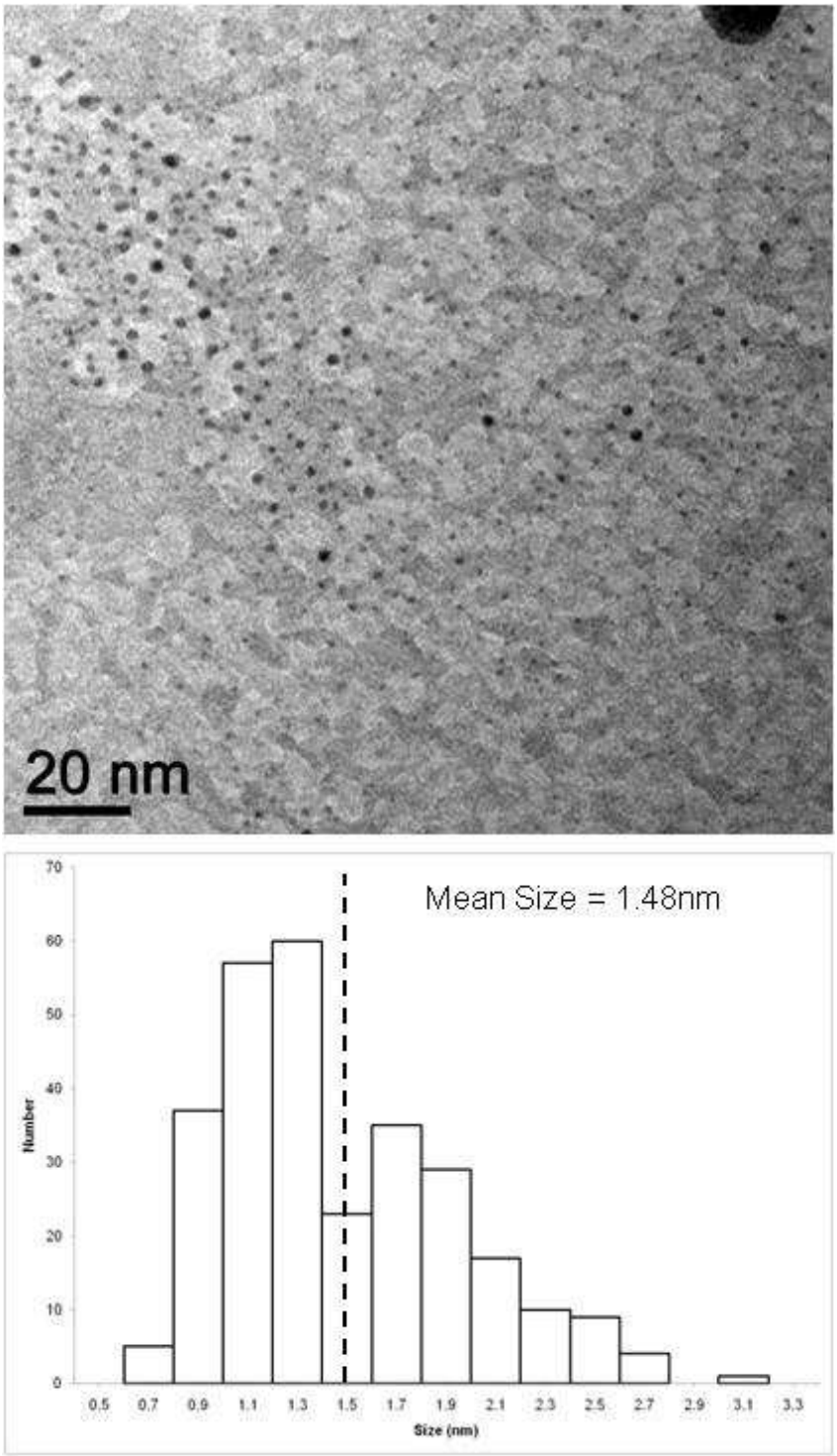

Figure 4. 34 - TEM Image and Analysis of Pt Particles Reduced from $H_2[PtCl_6]$ by Glucose with a Donor:Proton:Pt of 7:4:2

Scheme 4. 2 since the additional protons injected into the system result in a decrease of nanogel formation illustrated in step A.

An impact on the size and distribution of the nanoparticles formed is expected in relationship to the reaction run with a 7:2:1 ratio of donor to protons to platinum. TEM images were obtained from aliquots of the reaction solution. A representative image and analysis of 287 particles is shown in Figure 4. 34; the size of the particles in this sample were found to be 1.48 ± 0.47nm. From the histogram, it appears that there is a bimodal tendency in the size of the particles with a large number centered around 1.1nm and another group around 1.9nm; also, there is a significant amount of high-end tailing. These trends are significantly different than those observed in the samples containing a lower concentration of protons and are an indication that the data does not follow a normal distribution. This information confirms the hypothesis developed from the DLS observations; nanogel formation is inhibited by the increase in proton concentration from the doubling of $H_2[PtCl_6]$ altering the mechanism, Scheme 4. 2, from that seen in previous systems. Formation of the platinum nanoparticles becomes less controlled resulting in a larger dispersity since decreasing Pt-PDMAEMA nanogel presence diminishes the ability of the PDMAEMA to quickly adsorb to the nanoparticles halting their growth at similar stages.

From these studies it is clear that an increase in size of monodisperse platinum nanoparticles cannot be obtained by direct increase in the concentration of $H_2[PtCl_6]$. Particles synthesized in this manner do show a slight increase in average particle size however, there is also a large increase in dispersity. Changing the proportion of protons to donor sites alters the mechanism shown in Scheme 4. 2 dramatically decreasing the effect of the nanogel on nanoparticle formation. This emphasizes the importance of nanogel formation in the control mechanism as well as how the proton concentration in the system directly effects development of the nanogel. While an increase in platinum may be necessary to synthesize larger particles, the proton concentration will need to be constant to maintain control and produce monodisperse particles.

4.6.2 Combination of $K_2[PtCl_6]$ and $H_2[PtCl_6]$ Species in Particle Synthesis

One method of increasing the platinum concentration while maintaining the proton concentration is to use a mixture of $K_2[PtCl_6]$ and $H_2[PtCl_6]$. $H_2[PtCl_6]$ is used as the sole source of protons and maintained at a donor to platinum to proton ratio of 7:1:2 as in the studies in section 4.4.2. This will provide the protons necessary to act as a cross-linker with the platinum dianion species creating the Pt-PDMAEMA nanogel. Increasing the concentration of platinum is accomplished by adding additional $K_2[PtCl_6]$ which maintains the donor to proton ratio at 7:2. Additional $K_2[PtCl_6]$ should provide the platinum necessary to be able to produce larger particles since platinum is the limiting reagent in the system.

Studies utilizing PDMAEMA to platinum to proton ratios of 7:2:2, 7:4:2, and 7:6:2 were performed to investigate the effects of increasing the platinum ratio while maintaining the proton concentration. Throughout these experiments, the reducing agent is kept at a 10:1 with the platinum. Initial studies focused on doubling the platinum concentration while maintaining the proton ratio used in previous experiments. Addition of an equivalent of $K_2[PtCl_6]$ to the system used in section 4.4.2 is the first set of conditions utilized. DLS spectra were taken before, immediately after, and days after the addition of D-glucose as the reducing agent, Figure 4. 35, to probe the control mechanism of the synthesis of the nanoparticles. Unlike the results seen when $H_2[PtCl_6]$ is doubled, Figure 4. 33, particle formation is seen in the solution containing a donor to platinum to proton ratio of 7:2:2 where the additional equivalent of platinum is derived from the addition of $K_2[PtCl_6]$. The hydrodynamic diameter of the particles formed in this Pt-PDMAEMA solution before addition of a reducing agent is 103nm. This result is comparable to the data obtained in section 4.4 for the Pt-PDMAEMA solutions prior to reducing agent addition; confirming that maintaining the $H_2[PtCl_6]$ concentration will result in the formation of the nanogel even with the addition of $K_2[PtCl_6]$ to the reaction. Immediately following the addition of D-glucose to the reaction mixture, the average hydrodynamic diameter is 98.0nm indicating there no significant shrinkage of the particles as seen in section 4.4.2. Excess platinum is available in this set of conditions to replace the molecules that are immediately reduced. This allows the nanogel to

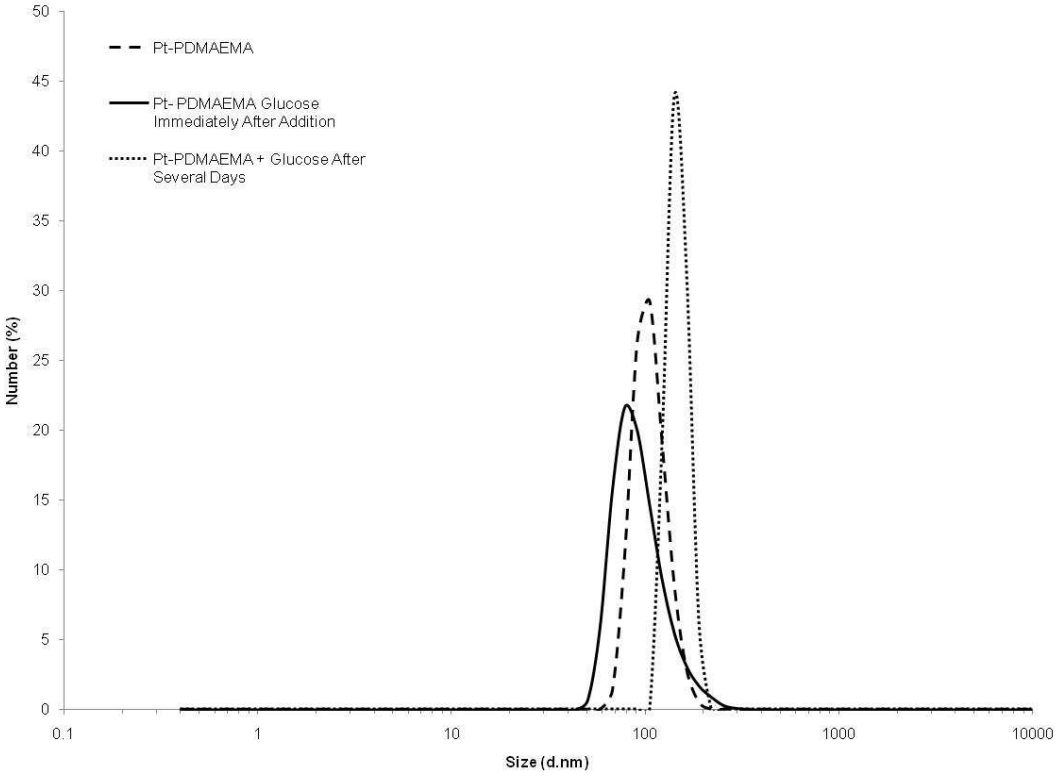

Figure 4. 35 - DLS Spectra of Reduction of Platinum by D-glucose where a Doubling of Platinum Concentration is Achieved by Adding an Equivalent of $K_2[PtCl_6]$ Creating a 7:2:2 Ratio of Donor:Platinum:Protons

retain all of the initial cross-links which will result in the particles showing no significant decrease in size unlike in the system in section 4.4.2 where each molecule reduced will result in the loss of one cross-link consequently triggering a shrinkage of the nanogel. Particles with an average hydrodynamic diameter of 152nm are observed in the final DLS spectra of the reaction after full reduction of the platinum complexes to Pt(0). These particles are significantly larger than those observed in 4.4.2 and may indicate the presence of larger platinum nanoparticles. The data obtained via DLS measurements indicates that the mechanism proposed in Scheme 4. 2 is suitable for this system since the nanogel is seen prior to and immediately following the addition of D-glucose.

TEM images of the system were obtained and a representative image and analysis are presented in Figure 4. 36. Analysis of 417 platinum nanoparticles resulted in a size of 1.34 ± 0.24nm. The resultant histogram of the size of the platinum nanoparticles has a relatively normal distribution which indicates the sample is trending towards the mean. A higher level of control is seen in this experiment than in section 4.6.1 where the excess protons caused the control mechanism to deviate from Scheme 4. 2. These results are significantly larger than those seen for the studies in section 4.4.2 where the only difference is the addition of one equivalent of $K_2[PtCl_6]$ indicating that increasing the concentration of platinum will result in larger particles if the proton concentration is maintained. Based on this experiment, it was determined that larger particles should be generated if the concentration of platinum is further increased through additional equivalents of $K_2[PtCl_6]$.

Platinum concentrations were increased to a 7:4:2 and 7:6:2 ratios of donor to platinum to protons while D-glucose was again maintained at a 10:1 ratio with the overall platinum concentration in order to increase the nanoparticle size. Initial runs were performed maintaining a similar overall polymer concentration, approximately 2×10^{-5} M, in the reaction mixture to those used in the runs examined in section 4.4.2. At this concentration of platinum to polymer, the solubility of the polymer was drastically lowered after the addition of the platinum solution. With extensive stirring it was possible to obtain a cloudy solution of the polymer, platinum, and

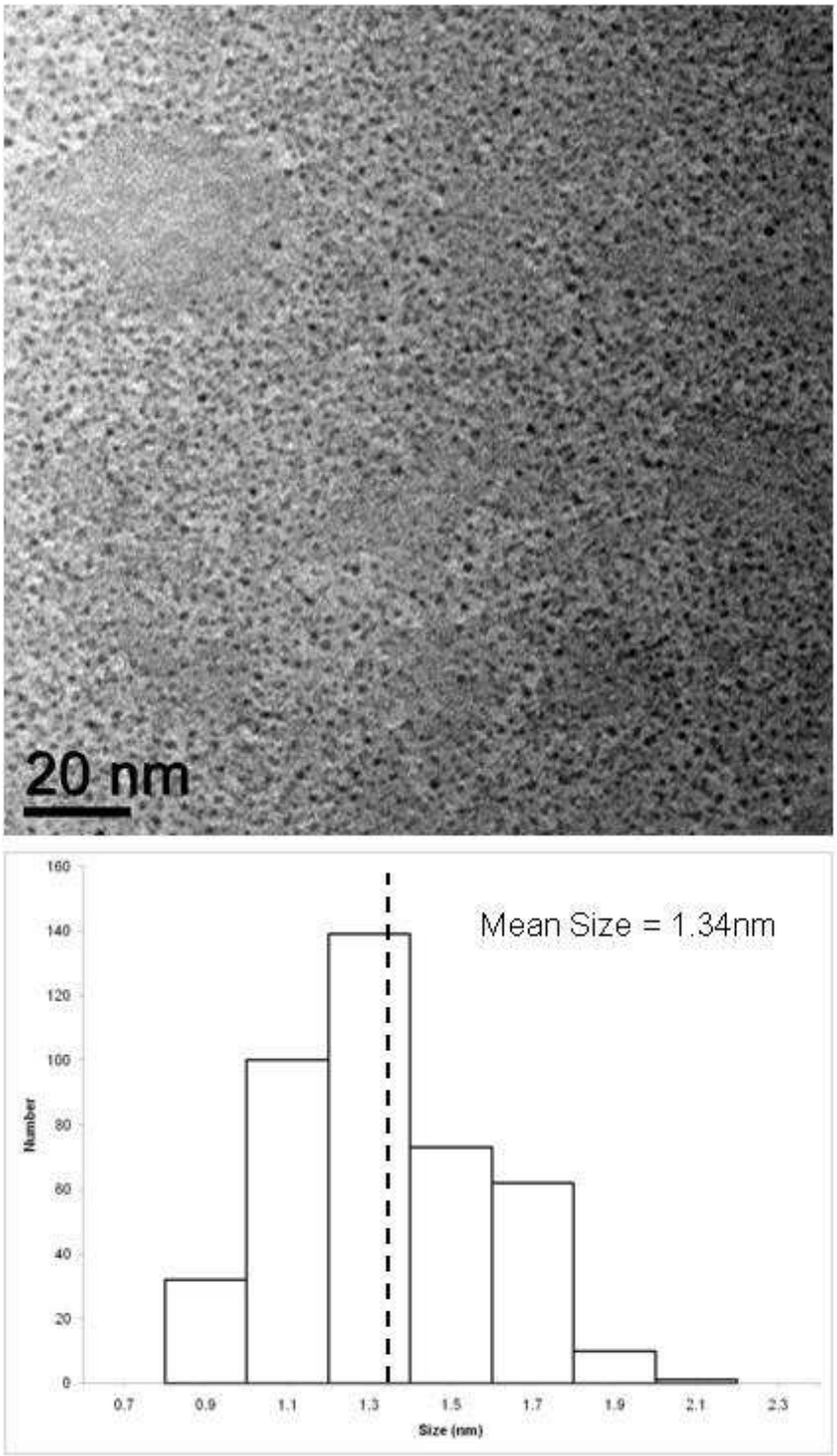

Figure 4. 36 – TEM Image and Analysis of Platinum Nanoparticles Synthesized by Reduction with D-glucose Where Donor:Platinum:Protons is 7:2:2

reducing agent however, upon standing the solution was seen to separate into a clear solution and yellow solid. Over the course of 8 days the platinum was not fully reduced and 10 additional equivalents of glucose were added to the solution. Following 5 more days of stirring to allow for full reduction to occur with no progress, the solution was diluted to encourage increased interaction between the water soluble glucose and the platinum bound within the PDMAEMA nanogel. Further reduction was obtained however, solubility issues still existed and full reduction of the platinum was not obtained.

Given the solubility issues of the Pt-PDMAEMA nanogel formation with increased concentrations of platinum, similar experiments performed were greatly diluted in comparison, one tenth the concentration. At this concentration, an emulsion is formed upon stirring of the components. An extremely decreased rate of reduction was still observed even at this lower concentration as is illustrated in Figure 4. 37. In these UV-spectra, a decrease in intensity and slight red shift of the peaks at ~190nm and ~260nm is seen after 24 hours. In previous runs with lower ratios of donor to platinum where increased solubility is observed, full reduction of the platinum complex is seen by ~24 hours. For these experiments, full reduction was seen much later as is shown by the curve at 194 hours in Figure 4. 37. This appears to be due to the decreased solubility of the nanogel decreasing the frequency of the platinum-glucose interactions. The images provided in Figure 4. 38 are representative for those seen in the samples from the 7:4 and 7:6 reactions. Images a) and b) are from experiments performed with four times the typical platinum concentration while c) and d) are from runs with six times the normal concentration. Both sets of experiments were performed using one equivalent of $H_2[PtCl_6]$ while the rest of the platinum is from $K_2[PtCl_6]$. Utilizing these ratios provides the increase in platinum while maintaining the donor to proton ratio at 7:2 providing the cross-linking necessary to form the nanogel and control the formation and stabilization of the platinum nanoparticles.

Figure 4. 39 provides another TEM image as well a size analysis of a 7:4 donor to platinum experiment. The average size of the 163 particles that were sized is 1.30 ± 0.27nm. From this data it is apparent that increasing the platinum ratio above the 7:2 ratio does not result

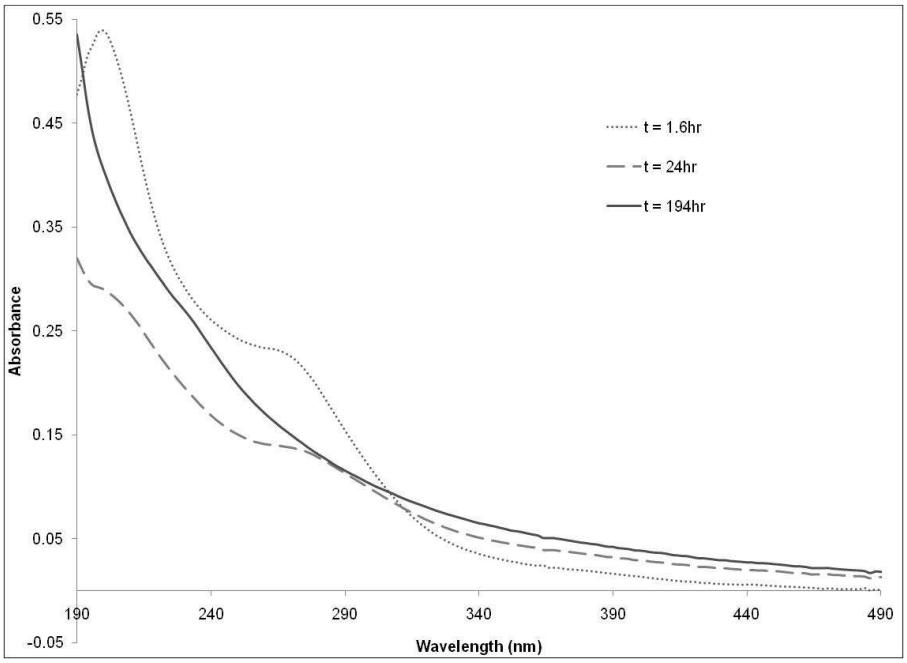

Figure 4. 37 - UV-vis Spectra of Reduction of Pt in a 7:4 Donor to Pt Ratio

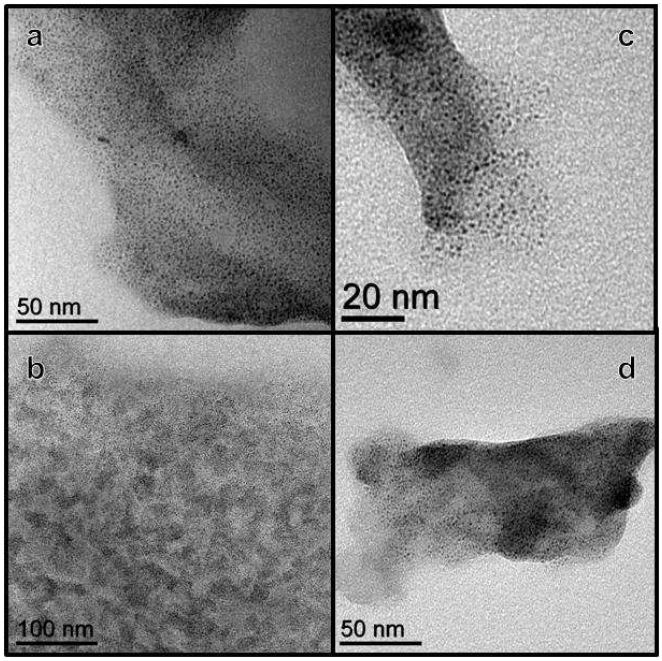

Figure 4. 38 - TEM Images of Pt Nanoparticles From a) and b) 7:4 and c) and d) 7:6 Donor to Pt Ratio Reactions

in an increase in particle size since the average sizes are virtually identical. What appears to be the most important difference between the 7:2 and the 7:4 and 7:6 ratio experiments is the density of the nanoparticles. For the high concentration runs, it appears as though the nanoparticles are denser especially considering the lowered density of these solutions in comparison to the 7:1 and 7:2 systems. The particles occur densely in what appears to be high concentrations of PDMAEMA indicating that instead of synthesizing larger particles an increased number of similar sized particles are formed. This would require the protonated donor sites on the PDMAEMA chains to be able to process more than one particle. After one particle has formed and is fully stabilized more platinum anions enter and interact with the nanogel structure until another particle is formed and stabilized.

4.6.3 Conclusions

Several methods were evaluated in an effort to synthesize platinum nanoparticles of various sizes. Initially increasing the concentration of platinic acid was employed. Unfortunately this results in the injection of excess protons effectively destroying the nanogel superstructure due to increasing the solubility of PDMAEMA through increased protonation. This decreases the control during the synthesis of the particles resulting in a much higher dispersity. In order to increase the platinum concentration while maintaining the proton ratio, a mixture of platinic acid and potassium palatinate were utilized. When the platinum concentration was doubled a significant increase in size was observed providing very promising results for using this route to create a large distribution of sizes that could be synthesized resulting in well defined particles. Unfortunately, further increases of the platinum concentration to four and six times the initial concentration did not result in larger particles. Instead particles similar in size to those observed in reactions with double the typical platinum concentration formed. While there is no significant change in particle size it does appear as though more particles are formed within the nanogel. This appears to indicate that when the concentration of the platinum species is increased to these higher concentrations, once a particle is formed the cationic sites on the PDMAEMA chains open back up and more platinum enters the nanogel structure and is controlled during reduction.

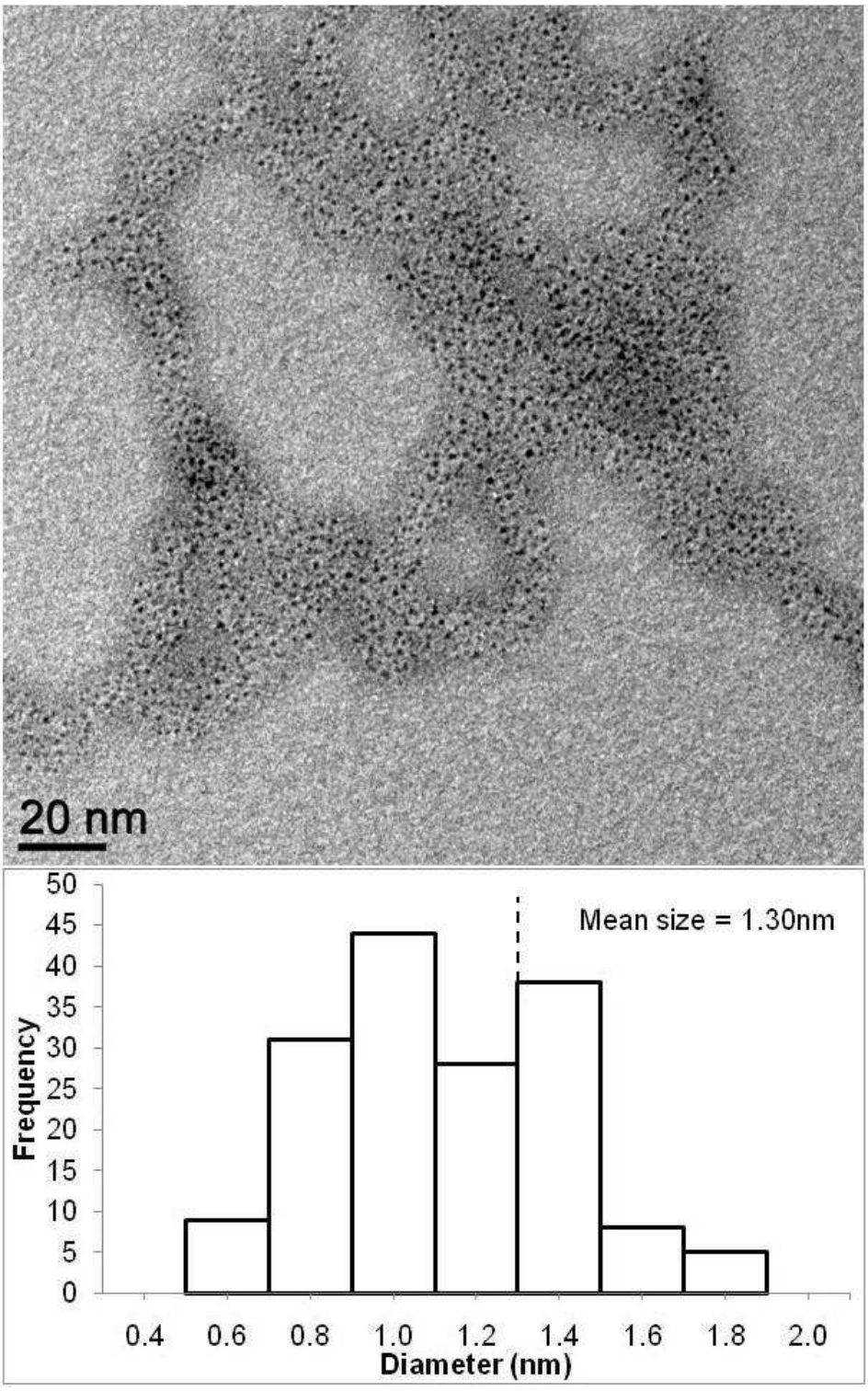

Figure 4. 39 - TEM Image and Histogram of Pt Nanoparticle From 7:4 Donor to Pt Solution

4.7 Expansion of Technique to Other Metals

While the ability to synthesize small mono-disperse platinum nanoparticles is extremely useful for applications in both commercial and academic fields as a lower cost catalyst than bulk platinum, use of this method in other metal systems greatly increases its overall versatility. The extremely volatile and high cost of platinum has contributed to continued research in development of non-platinum catalyst systems. Ultimately, use of iron, cobalt, nickel, and other low cost, widely available metals can decrease the cost of systems such as fuel cells. Gold and palladium were the two metals studied in this program, while these metals are still quite expensive extensive research into synthesis of nanoparticles via other pathways as well as their similar properties to platinum make them ideal candidates. Two gold, hydrogen tetrachloroaurate ($H[AuCl_4]$) and potassium tetrabromoaurate ($K[AuBr_4]$), and two palladium, potassium hexachloropalladate(IV) ($K_2[PdCl_6]$) and potassium tetrachloropalladate(II) ($K_2[PdCl_4]$) complexes were selected due to their similarity to the platinum complexes which were used previously.

4.7.1 Palladium Nanoparticle Synthesis

Palladium nanoparticles were synthesized using the method developed in Section 4.5. Initially, reactions with donor to proton to palladium to reducing agent ratios of 7:2:1:10 were prepared for the $K_2[PdCl_6]$ and $K_2[PdCl_4]$ complexes. Solutions of succinic acid and PDMAEMA were first mixed in order to prepare a linked nanogel. Next, the palladium solution is added and this mixture is allowed to stir providing time for the palladium cations to migrate into the nanogel structure before being exposed to the reducing agent. Finally, the valeraldehyde solution is added and the palladium is allowed to fully reduce. UV-vis spectra were taken throughout the reduction process, several DLS spectra were taken, and after full reduction TEM images were obtained.

Initially the Pd(II) and Pd(IV) species were studied, however, it was found that the Pd(IV) complex was unsuitable to the conditions required for the nanoparticle formation. Solutions of Pd(IV) auto-reduced resulting in the precipitation of Pd(0) species during storage and during the reduction process in competition with the desired reaction. TEM images taken of the resultant

solutions are shown in Figure 4. 40; in these images, a large size distribution is obvious. For these reasons, only work on $K_2[PdCl_4]$ was pursued after the initial studies.

Figure 4. 41 provides the UV-vis spectra for the reduction of $K_2[PdCl_4]$ with valeraldehyde. A red shift is initially seen as the λ_{max} shifts from 206nm to 218nm in the first 15min of the reduction. As the reaction continues over the course of several days, the peak increases and continues to shift slightly resulting in a final λ_{max} of 224nm; at this point the palladium is considered fully reduced. A representative TEM image of the palladium nanoparticles with a histogram showing the results of sizing of 123 particles from various images is shown in Figure 4. 42. The average size of the 123 palladium particles analyzed was found to be 1.04 ± 0.21nm. While a few aggregates are seen in the images overall the standard deviation indicates a relatively narrow polydispersity providing evidence that the particle formation is being controlled and stabilized by the nanogel.

4.7.2 Gold Nanoparticle Synthesis

Initially, gold nanoparticles were synthesized from $H[AuCl_4]$ and $K[AuBr_4]$ using the method developed in Section 0 where a solution of PDMAEMA is introduced to a solution of succinic acid first creating the nanogel framework prior to the addition to the metal complex. The gold was then added and stirred during which time the complex migrates into the nanogel. Valeraldehyde was added last to reduce the Au(III) species to Au(0) while UV-vis is used to track the reaction process the spectra for the reduction of the two species are shown in Figure 4. 43 and Figure 4. 44.

For the $K[AuBr_4]$ reduction, Figure 4. 43, there are initially a strong peaks in the spectrum of the complex in aqueous solution at 248nm and 368nm. Upon addition of PDMAEMA and valeraldehyde, the peak at 368 is fully suppressed while the 248nm peak is decreased to a small shoulder. Continued mixing of the solution first leads to the complete removal of the 248nm peak followed by the growth of a broad peak centered at 526nm that is typical of solutions containing gold nanoparticles. Slight differences are seen in the spectra for the reduction of the $H[AuCl_4]$ species. Most importantly, the peaks of the aqueous complex solution are both blue

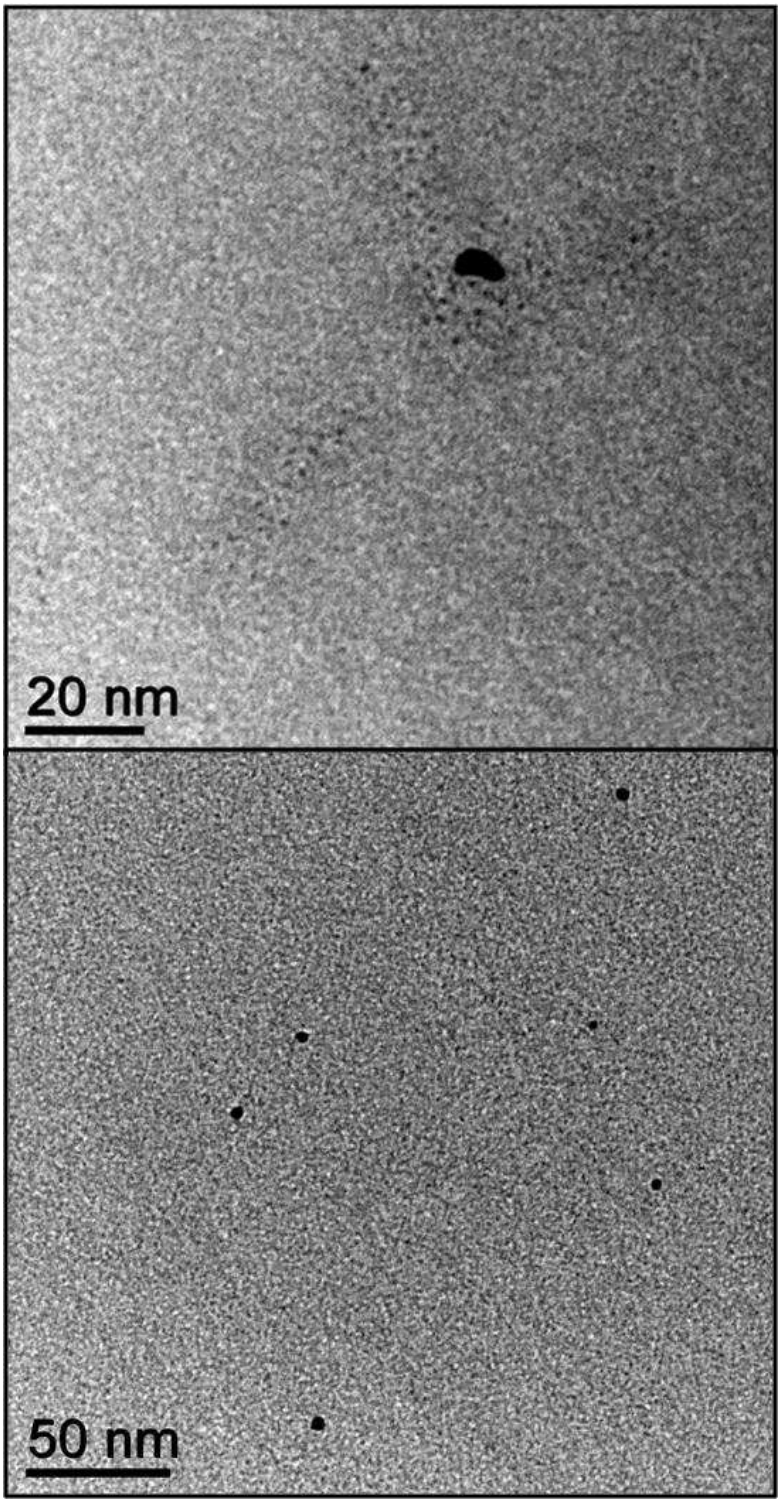

Figure 4. 40 - TEM Images of Reduced $K_2[PdCl_6]$

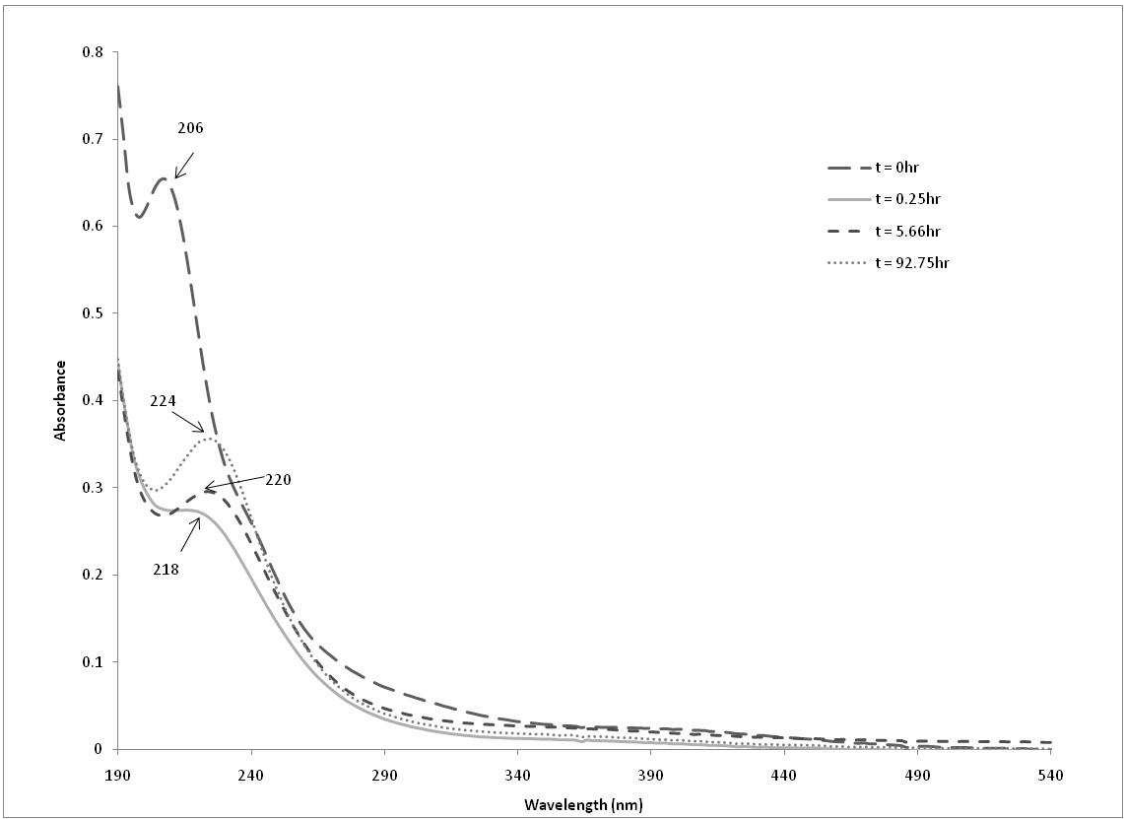

Figure 4. 41 - Reduction of $K_2[PdCl_4]$ with Valeraldehyde

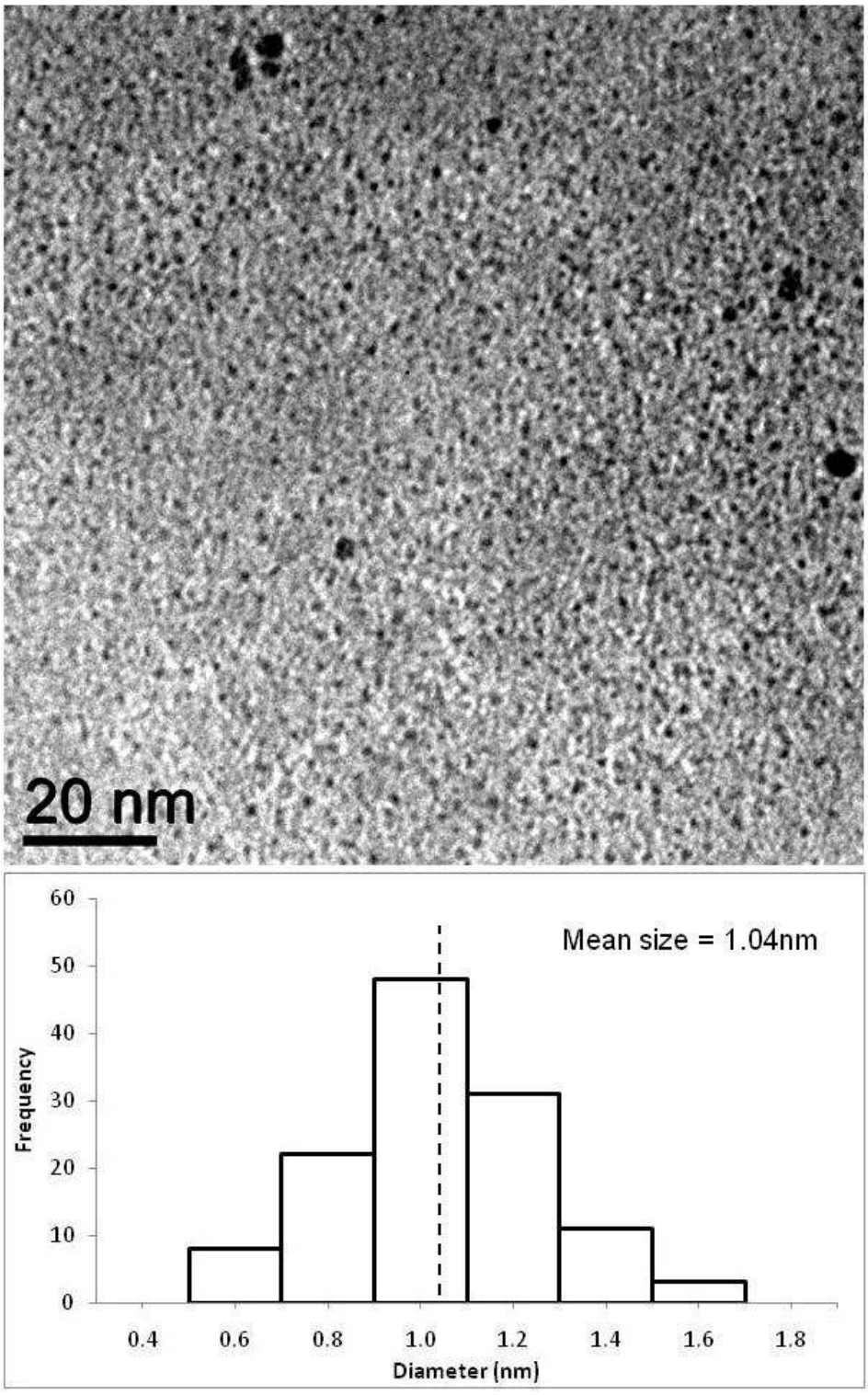

Figure 4. 42 - TEM Image and Histogram of Palladium Nanoparticles

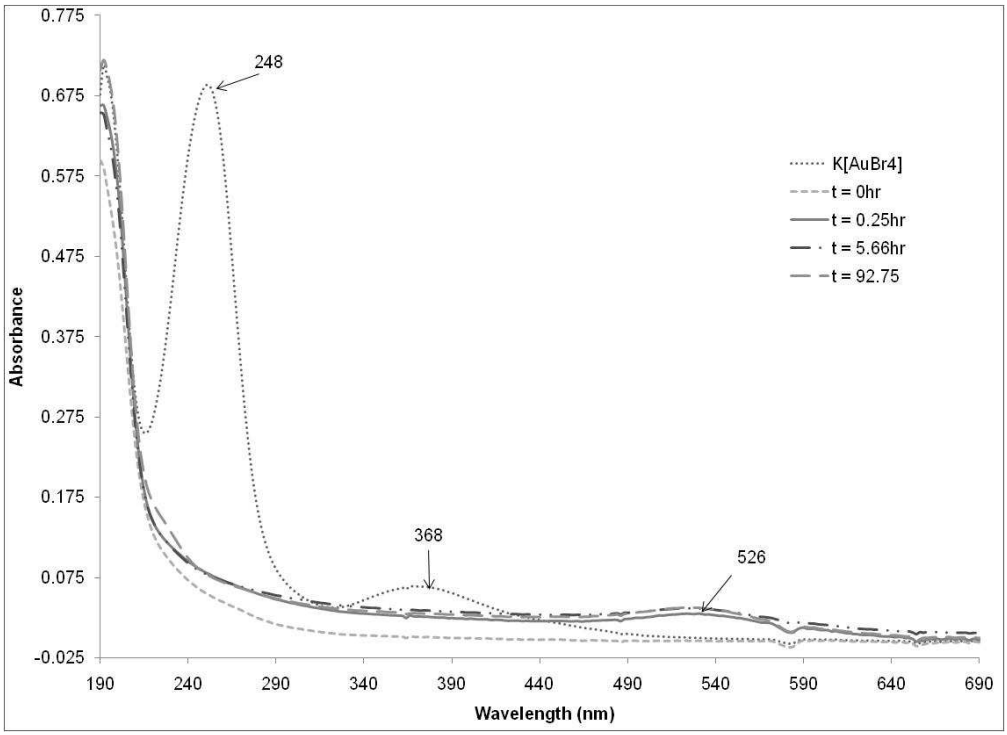

Figure 4. 43 - Reduction of $K[AuBr_4]$ with Valeraldehyde

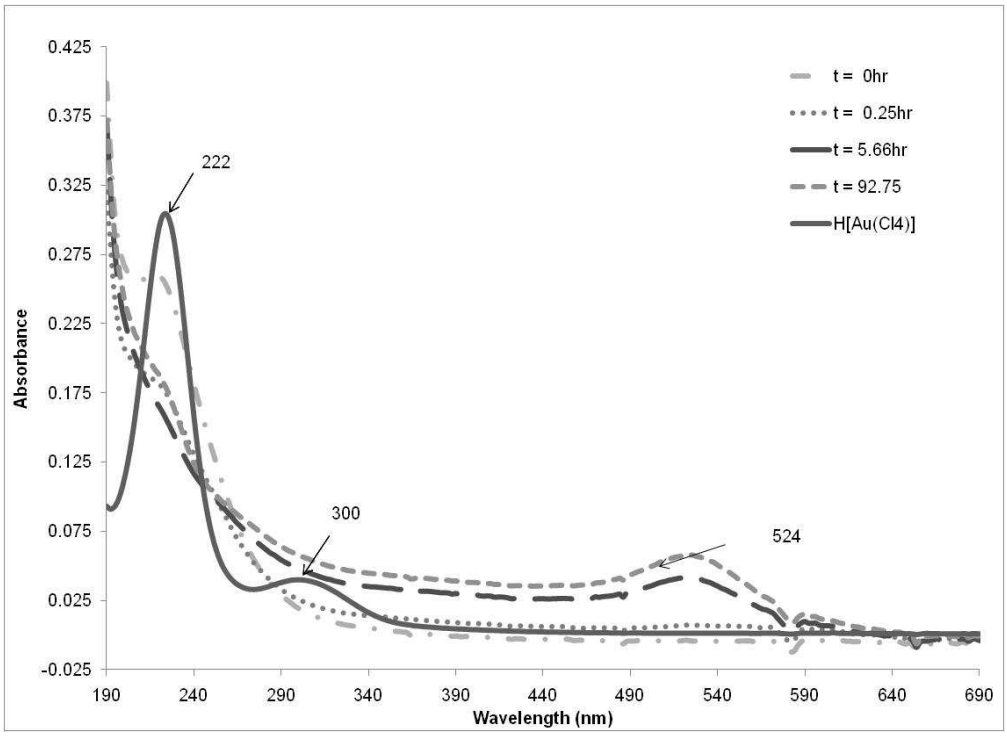

Figure 4. 44 - Reduction of $H[AuCl_4]$ with Valeraldehyde

shifted the 248nm peak is seen at 222nm and the 368nm peak is seen at 300nm. This shift is due to the increased strength and decreased size of the chlorine ligands compared to the bromine ligands seen in the first complex. As in the previous complex, the peaks at 222nm and 300nm are fully removed through the reduction while a broad peak has grown in centered at 524nm. The broad bands seen in the spectra of both complexes are the gold Plasmon bands which are seen when the gold particles are on the nanoscale. Previously it has been shown that the position of the Plasmon band is directly related to the size of the nanoparticles in the solution and that particles with large size difference will therefore have significantly different λ_{mas}'s for the band. Given this information it is important to note the similarity of Plasmon band positions in the spectra shown in Figure 4. 43 and Figure 4. 44 indicating the size of the particles being synthesized from the different complexes are relatively similar.

Synthesis of gold nanoparticle from the two different complexes were initially performed using the same ratio of donor to proton to metal to reducing agent, 7:2:1:10. Given that one species contains a proton as a counter-ion different ratios of the different solutions must be used in order to maintain the same ratios. Specifically, the initial concentration of succinic acid for the formation of the nanogel for the runs using $H[AuCl_4]$ as the metal species was halved in comparison to the concentration used in the $K[AuBr_4]$ runs. Unfortunately lowering the initial proton concentration for the nanogel formation will result in less cross-linking and a looser gel formation. This behavior appears to lead to larger less well defined gold particles. Looking at Figure 4. 45 and Figure 4. 46 syntheses utilizing the two different gold precursors can be compared. Analysis of the particles produced using $H[AuCl_4]$ as the precursor is seen in the histogram in Figure 4. 45; 80 gold particles were sized resulting in an average size of 14.1 ± 3.6nm. The distribution of the particles does not follow an ideal Gaussian curve but instead appears to have a broad range that is common for the particles rather than centering at the mean as seen in the platinum and palladium particle syntheses.

A representative TEM image and the analysis of the particles prepared from the $K[AuCl_4]$ precursor are seen in Figure 4. 46. Sizing of 118 particles resulted in an average size of

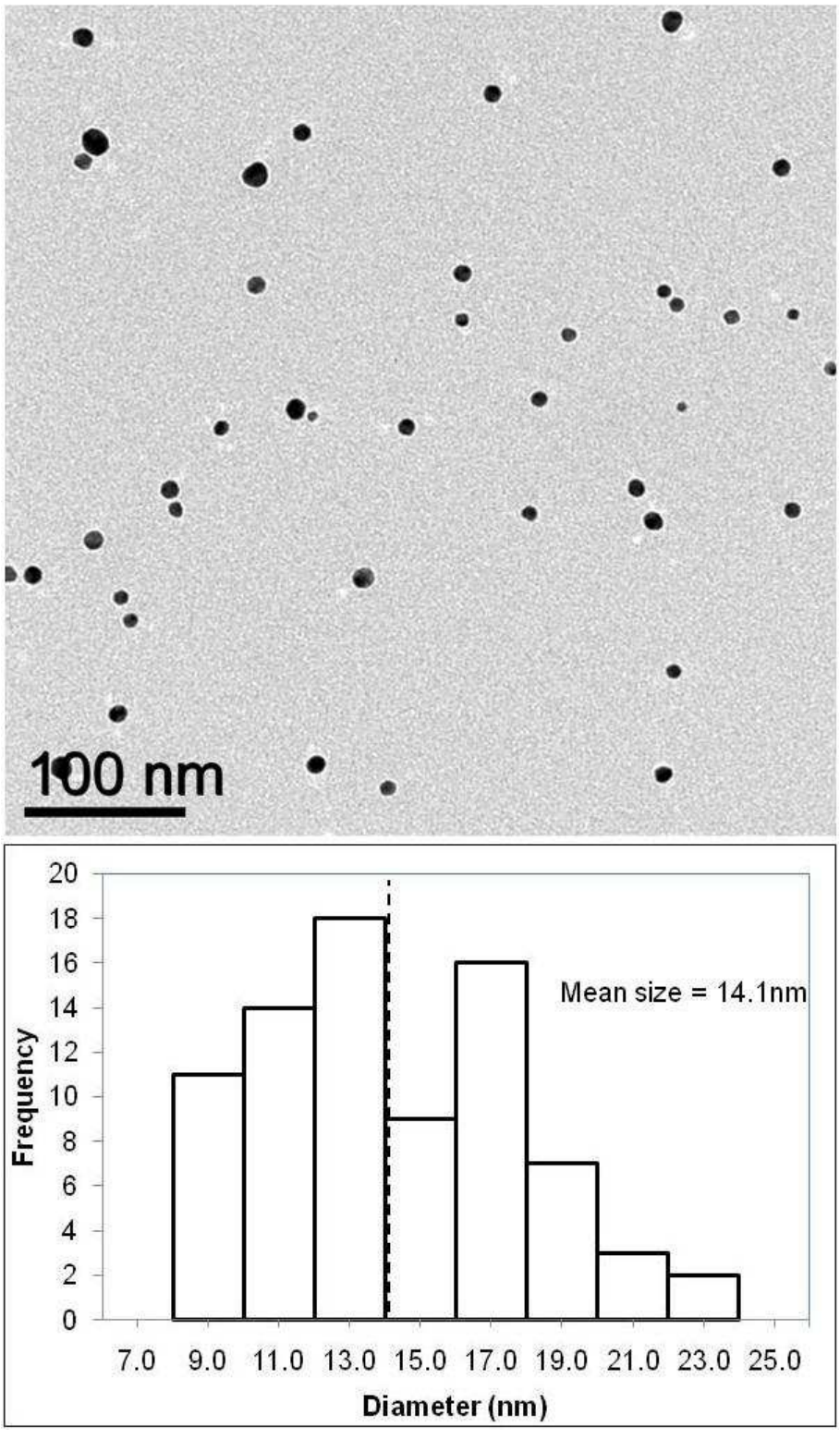

Figure 4. 45 – Valeraldehyde Reduced $H[AuCl_4]$

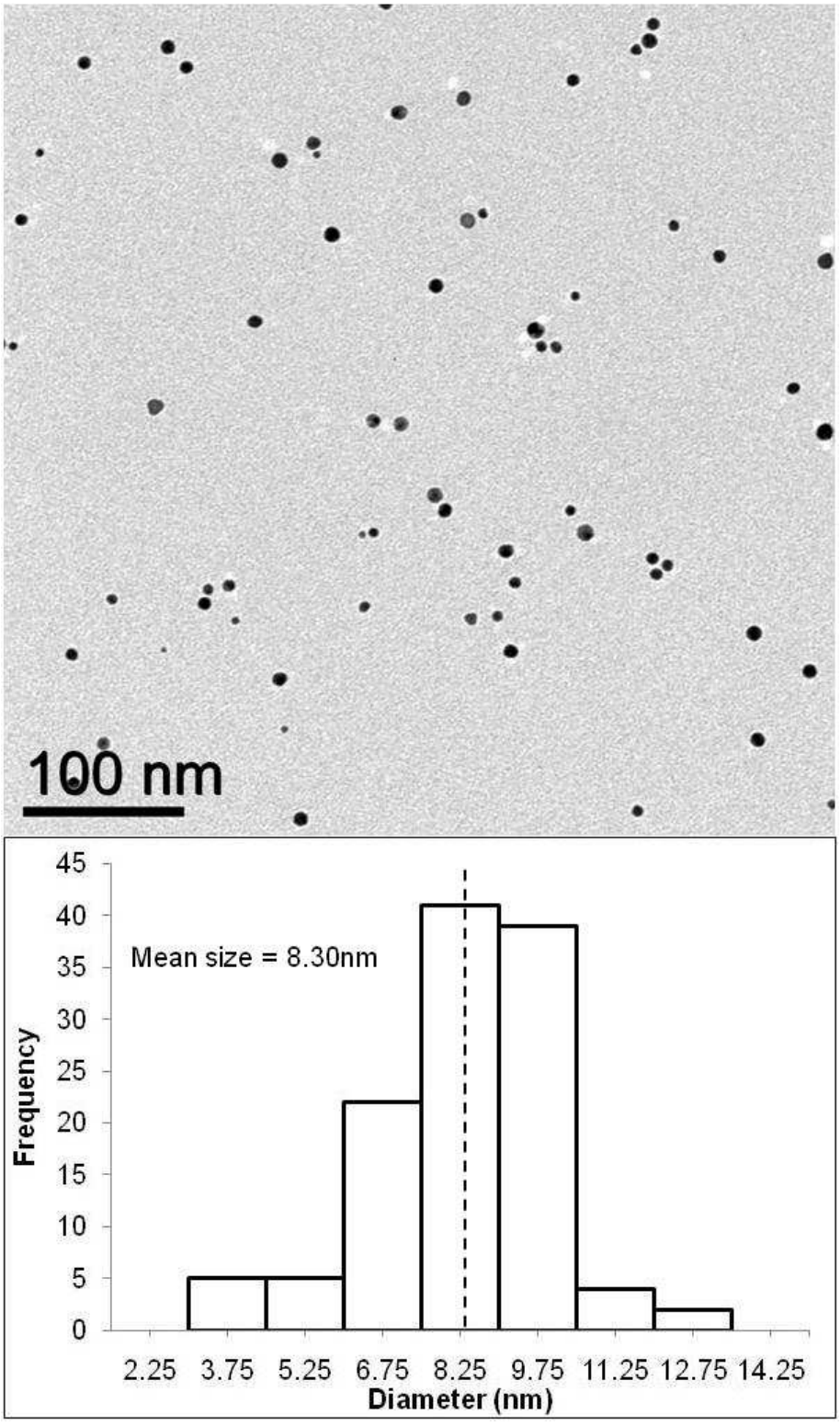

Figure 4. 46 – Valeraldehyde Reduced $K[AuBr_4]$

8.3 ± 1.7nm. The distribution of the particles, shown in the histogram, indicates a more normal distribution than in the H[AuBr4] distribution. For the preparation of these particles the protons were derived exclusively from the addition of succinic acid in the first step when the nanogel is created. Therefore, the nanogel that is produced should be the same composition as what is prepared for the platinum and palladium runs. Interestingly, one other major difference is seen between the two syntheses; the particles produced from the H[AuCl4] precursor are uniformly spherical. However, both pyramids and spheres are seen in the TEM images of the gold particles synthesized utilizing K[AuCl4]. This behavior indicates that the growth of the particles is progressing in two different paths during the synthesis. Comparison between the observed particle size and the location of the gold Plasmon band can be performed to confirm the behavior is as expected. Literature values[22] indicate that particles between 8 and 20nm should have a λ_{max} around 520nm. Comparing the data observed in the TEM images and UV-vis spectra for the synthesis of gold nanoparticles by the proposed method indicates that behavior seen in other methods is observed for this system as well.

Initial experiments synthesizing gold nanoparticles were performed following the mechanism shown in Scheme 4. 6: first creating the nanogel through the addition of succinic acid to PDMAEMA aqueous solution, adding the metal complex, and finally adding the reducing agent. Clearly for the gold complexes being utilized succinic acid is essential for creating the nanogel since both form monoanionic species which are incapable of creating a cross-linked species with PDMAEMA. Therefore, the succinic acid must first be added to the PDMAEMA solution and the addition of gold species will result an equilibrium where some of the succinate anions are displaced by gold anions as shown in the mechanism illustrated in Scheme 4. 6. Unfortunately, the metal complexs' high solubility in water makes migration between the nanogel and aqueous bulk solution highly likely. Therefore, upon addition of the reducing agent reduction can take place outside of the nanogel and consequently outside of the suggested mechanism of control. Unlike the metal anions, valeraldehyde is only very sparingly soluble in water and therefore highly prefers to be exclusively within the nanogel since this environment is much less polar.

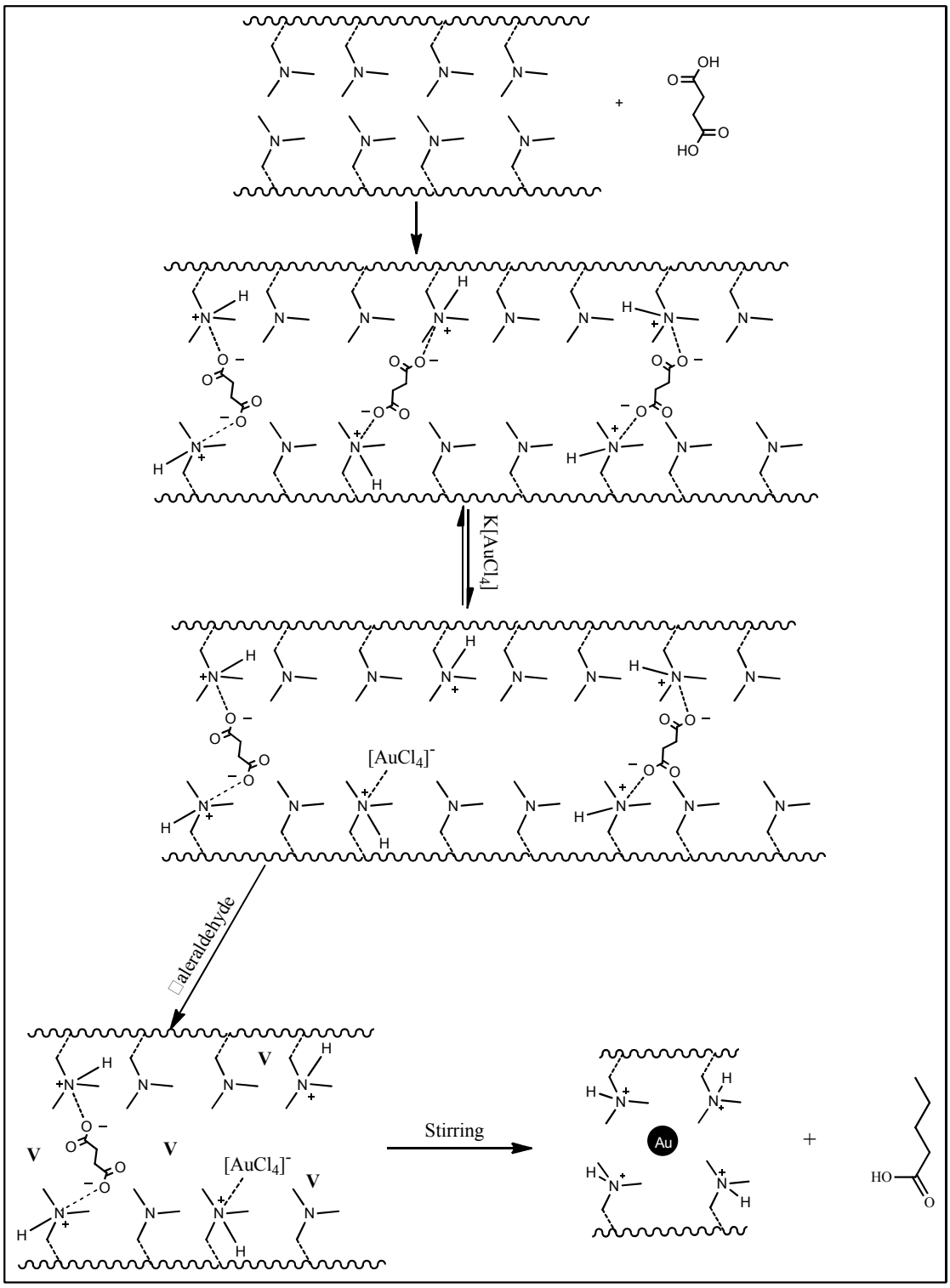

Scheme 4. 6 - Reaction Mechanism for Au Particle Synthesis

In response to these concerns, alterations to the synthesis were employed according to the mechanism described in Scheme 4. 7. Creation of the nanogel was performed first through the addition of succinic acid to PDMAEMA solution as in the previous experiments. Valeraldehyde was added next and allowed to stir for approximately 10 minutes to allow for full migration into the gel. This should fully remove the reducing agent from the bulk resulting in a more controlled reduction environment. Finally, the gold complexes were added and allowed to fully reduce. After the introduction of the gold complexes none of the reducing agent should be encountered until migration into the nanogel has occurred as in Scheme 4. 7. This will reduce the number of succinate anions being displaced. Also, the equilibrium created by the gold being able to migrate between the bulk aqueous solution and the less polar nanogel environments should greatly decreased since the complexes are immediately reduced upon entry. Solubility of the gold nanoparticles will be very low in the aqueous solution, decreasing the favorability of migration into the bulk. Also, as the gold reduces forming nanoparticles stabilization is achieved through coverage of the surface with PDMAEMA while simultaneously embedding it within the PDMAEMA nanogel.

For both $K[AuCl_4]$ and $H[AuBr_4]$, the nanogel was created by adding succinic acid to the PDMAEMA solutions creating a 7:2 ratio of the donor to proton. Therefore, in the case of $H[AuBr_4]$ when the metal complex was added the donor to proton ratio was increased to 7:3 while for $K[AuCl_4]$ there was no change. The initial runs of $K[AuCl_4]$ and $H[AuBr_4]$ using this method were performed with donor to proton to metal to reducing agent ratios of 7:2:1:10 and 7:3:1:10 respectively. UV-vis spectra of these experiments were the same as those seen previously, including the position of the Au Plasmon band. This indicates that the size of the particles have not changed significantly which was expected since the concentrations of the reducing agent and metal complexes has remained the same so the reduction should have occurred at the same rate with the same amount of gold to form into nanoparticles. TEM images were taken of nanoparticles formed in these experiments from $K[AuCl_4]$ and $H[AuBr_4]$ precursors.

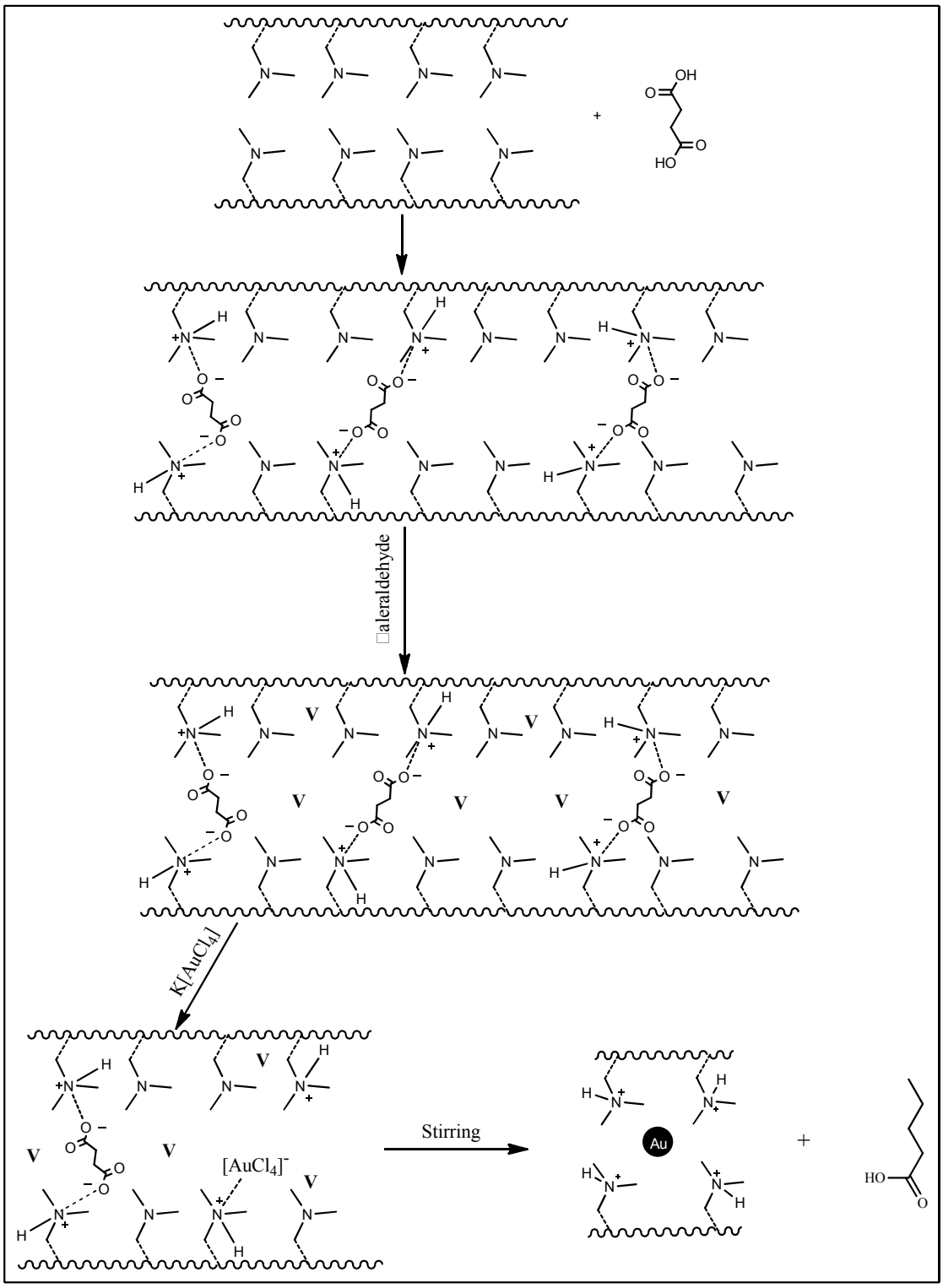

Scheme 4. 7 - Reaction Mechanism for Au Particle Synthesis Adding Metal After Valeraldehyde

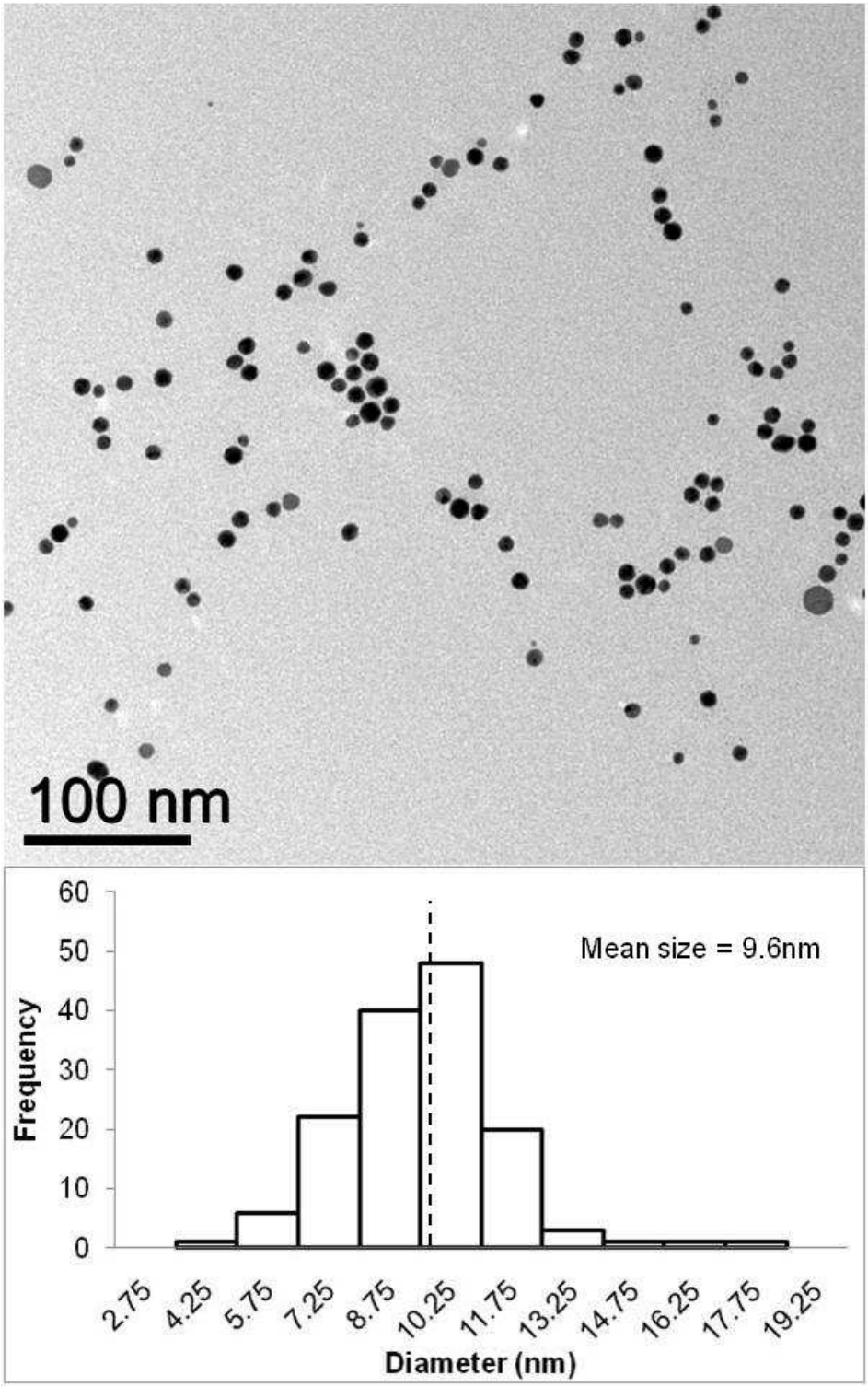

Figure 4. 47 - TEM Analysis of Au Particles Formed from the Reduction of $K[AuCl_4]$ with Valeraldehyde Added Prior to the Metal

Representative images from those obtained are shown in Figure 4. 47 and Figure 4. 48. The histograms of the particles produced from both precursors show a much more normalized curve than seen by the previous reaction method indicating that only one reaction pathway is present. Very little change in seen in the results for the $K[AuCl_4]$ nanoparticles the average size of the 143 particles analyzed is 9.6 ± 2.0nm which is slightly larger than seen by the previous reaction technique. However, a large change in seen in the results for the $H[AuBr_4]$ precursors particles. The average size of the 276 gold particles evaluated is 10.6 ± 2.1nm a significantly smaller, average diameter than was seen with the previous method. Distribution of the particles is also significantly more normal, even more so than the change seen in the results for the particles produced by the reduction of $K[AuCl_4]$. These results indicate a significant improvement of the method of synthesis of the gold nanoparticle from the $H[AuBr_4]$ precursor.

With the addition of 10 equivalents of valeraldehyde per metal complex the reduction was seen to progress at an extremely fast rate. The reaction was easily observed visually as the reaction begins a light golden color and when the gold has been reduced the solution is a deep intense purple color. In the previous reactions with the different gold complexes the transition from the golden solution to the violet solution occurs very quickly over the course of about 5 minutes. The gold reduction in these experiments is much more rapid than what is experienced in either the platinum or palladium experiments. Previously, increasing the reduction rate in the platinum experiments resulted in very little size difference, however, significant reduction in rate was impractical. Due to the extremely fast rate of the gold reduction a large reduction in rate was convenient for this system. The valeraldehyde concentration was reduced to produce a donor to proton to metal to reducing agent ration of 7:2:1:2, which is an 80% reduction of the concentration of valeraldehyde. While this is a significant reduction the required number of electrons will still be released since each valeraldehyde releases 2 and each gold requires 3 electrons. This results in an electron ratio of 3:4 when analyzing the number required to fully reduce the gold species in relation to those released by the valeraldehyde compound resulting in the desired overall excess of electrons.

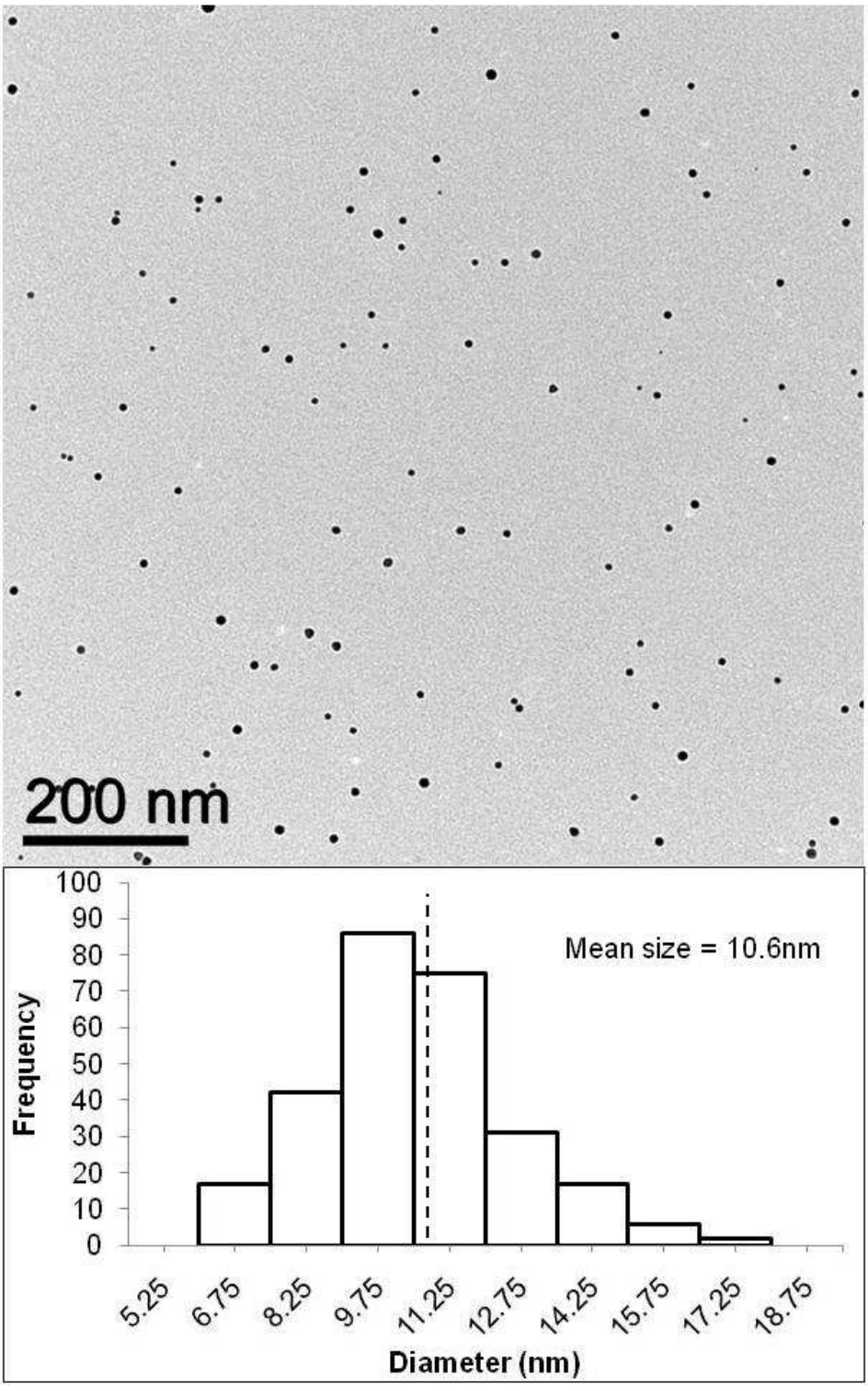

Figure 4. 48 - TEM Analysis of Au Particles Formed from the Reduction of $H[AuBr_4]$ with Valeraldehyde Added Prior to the Metal

$K[AuCl_4]$ was focused on in this set of experiments since succinic acid will be the only source of protons removing any complications that may result from the additional proton in the $H[AuBr_4]$ complex. The decrease in reduction rate was clearly observed as the color change from golden to deep violet took approximately half an hour compared to the five minutes at the previous concentrations. TEM images of the resultant particles indicate a fairly significant change in comparison to the previous reduction rate. Analysis of the particles as well as a representative image are presented in Figure 4. 49. Sizing of the 75 gold particle resulted in an average particle size of 17.0 ± 2.0nm. The distribution of the particle size shows significant high end tailing although the standard deviation is surprisingly low. This indicates that the particle formation is being controlled although there was a tendency for excess particle growth prior to full stabilization by the polymer chains.

The final experiments performed on the gold particle synthesis were to dramatically increase the concentration of the valeraldehyde to increase the reaction rate. In these experiments the reducing agent concentration was tripled to create the donor to proton to metal to reducing agent ratio of 7:2:1:30. After the addition of $K[AuCl_4]$ to the valeraldehyde-PDMAEMA-succinic acid solution, full reduction was immediately observed by evolution of a deep violet color. Figure 4. 50 provides a representative TEM image and analysis of the particles prepared in these experiments. The average size of the 68 particles sized is 11.4 ± 1.7nm and the distribution is slightly abnormal. This size is surprisingly slightly larger and more monodisperse than the particles produced previously with the 7:2:1:10 ratio of donor to proton to gold to valeraldehyde. However, it appears that a particle size around 10-11nm is generally produced in a well controlled manner at high reduction rates.

4.7.3 Conclusions

The method developed in Section 4.5 was successfully applied to the synthesis of gold and palladium nanoparticles. While the palladium complexes studied in this section are very similar to the platinum species employed in a majority of the reactions in this manuscript. Results comparable to the platinum particles were obtained with very small particles being produced. On

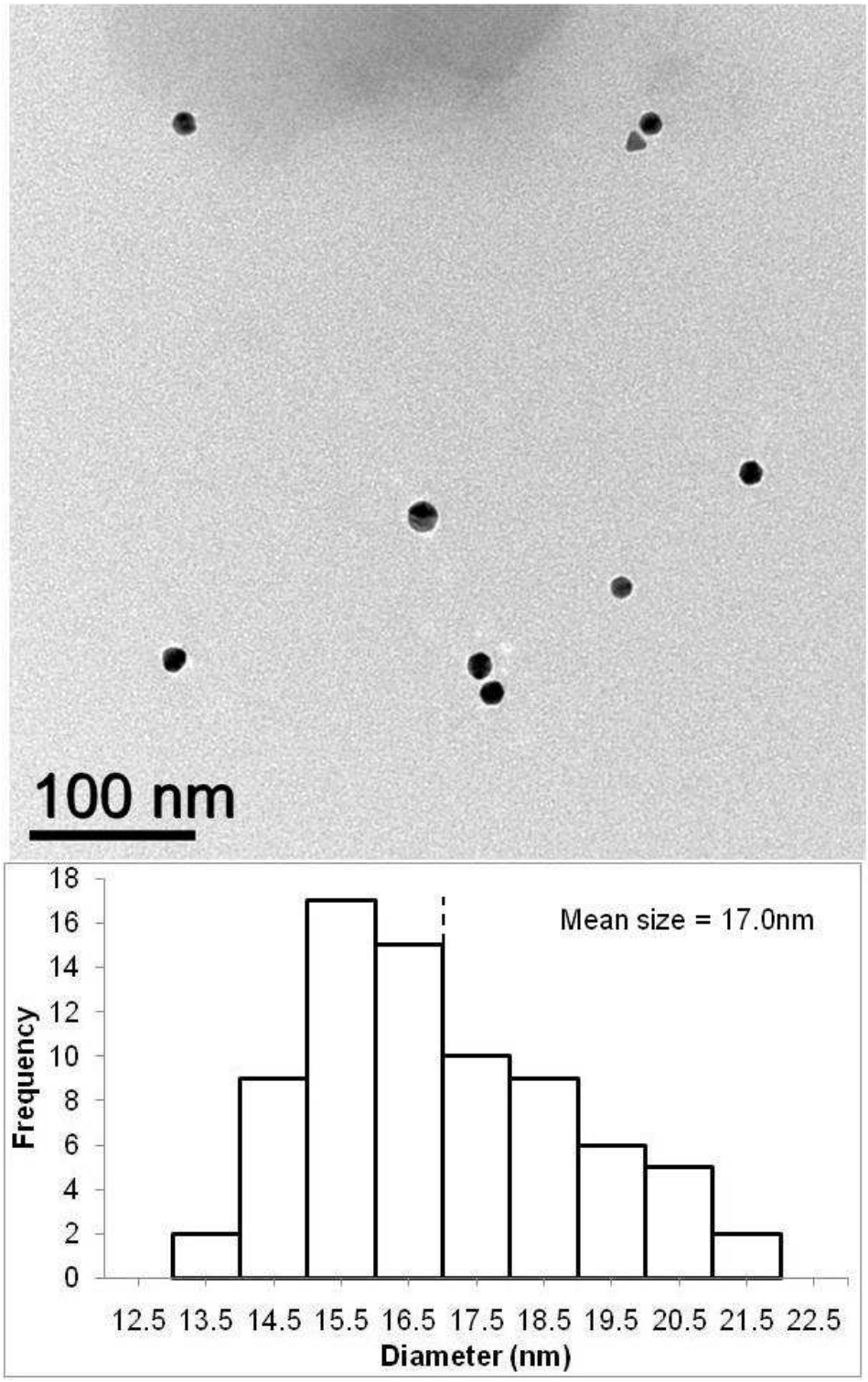

Figure 4. 49 - Reduction of $K[AuCl_4]$ with 20% of the Typical Valeraldehyde Concentration

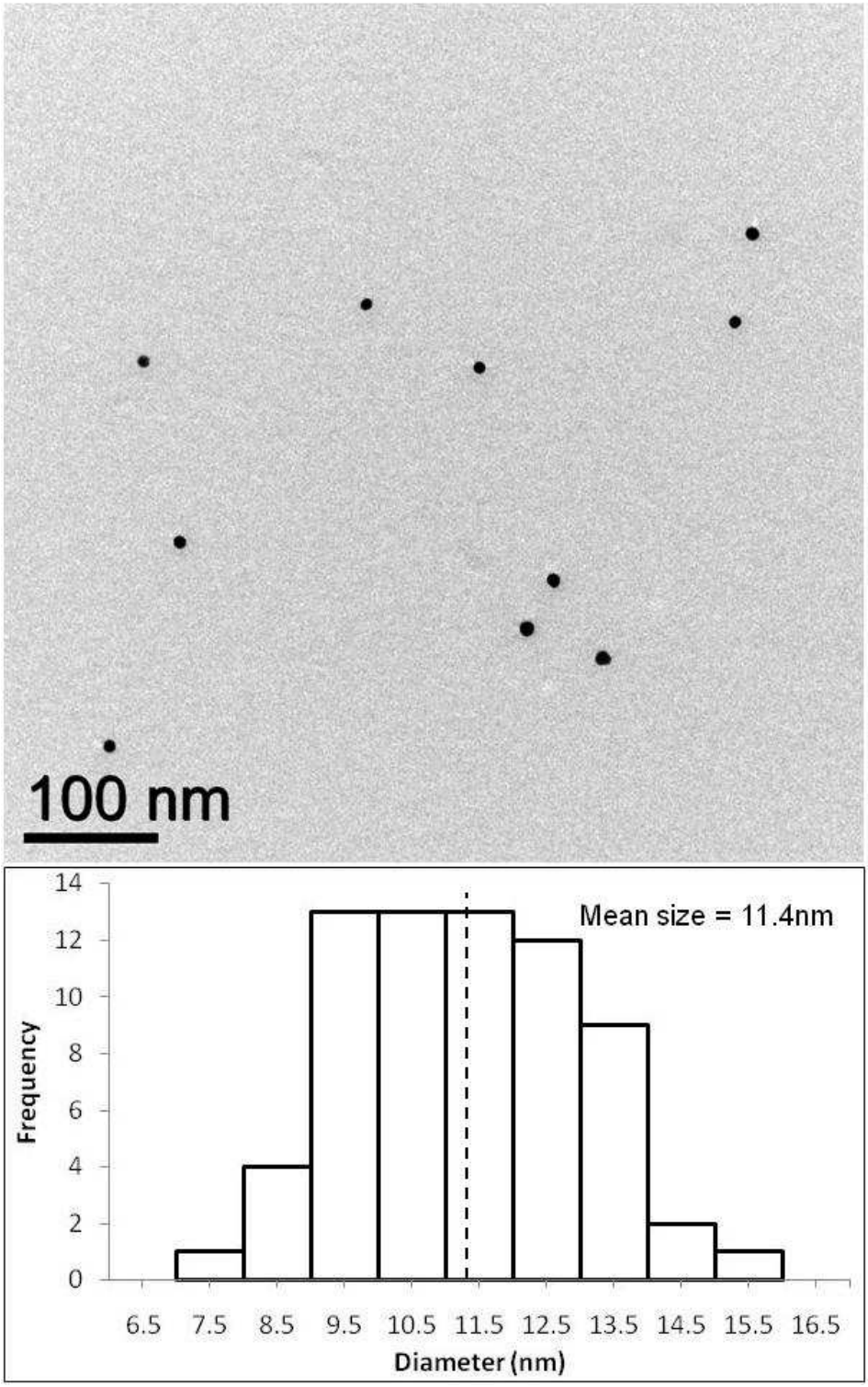

Figure 4. 50 - Reduction of $K[AuCl_4]$ with 3 Times of the Typical Valeraldehyde Concentration

the other hand, the gold species utilized form monoanions which is a significant departure from the previous systems. In these cases the crosslinking is provided exclusively by the succinate anion and any displacement by the monogold anions will result in a looser nanogel. It appears as though this effect is responsible for the formation of particles that are approximately ten times the size of the platinum and palladium particles which have been synthesized. The synthesis of gold particles was ideal for studying the effect of reduction rate on particle size since the reaction progresses much more quickly than for the other metal species. A significant increase is seen for this system when the reducing agent is significantly decreased, indicating that during the reduction process there is a longer time available for continued particle growth before the particle is fully stabilized and growth is halted. The most important consequence of these studies is that the methods of nanoparticle synthesis developed in the manuscript are applicable to systems other than those utilizing platinum complexes. Therefore, it is highly likely that it will useful for a variety of other metals systems which will be useful for a wide range of applications.

4.8 Conclusions

A new technique for the synthesis of well defined metal nanoparticles was developed. The most import aspect of this method is the formation of a crosslinked polymer system which has been labeled a nanogel. In this work, PDMAEMA is used as the polymer where the amines on the side chains are protonated and then crosslinked via dianionic species. Several reducing agents, ascorbic acid; citric acid; D-glucose; and valeraldehyde, were evaluated. Ascorbic and citric acid were both found to be detrimental to the nanogel causing it to break apart and were considered to be less useful than D-glucose and valeraldehyde which are also inactive in the UV-vis region while citric and ascorbic acid are not. The particles formed which had the lowest dispersity were formed using D-glucose and valeraldehyde.

Increase in the size of particles was obtained to some degree for the platinum particles. However, only a doubling of size was able to be achieved while additional equivalents of platinum complexes results in an increase in the number of particles rather than their size. It is important to note that the increase in platinum concentration must be obtained by using a mixture of

$H_2[PtCl_6]$ and $K_2[PtCl_6]$ to maintain a 7:2 donor to proton ratio. In all of these cases, the acidic metal species was employed as the crosslinker. Studying the effect of mono and di acids confirmed the crosslinking mechanism since superstructure formation of the polymer was only observed for the dianionic species.

Demonstration of this method's ability to control the synthesis of metal nanoparticles for systems other than platinum is important for improving the technique's overall usefulness. However, if a dianionic acidic species is necessary the system will be severely limited, The determination that nonmetallic diacids can be used to crosslink the PDMAEMA prior to the addition of the metal complex was extremely important for broadening the use of this technique. Utilizing succinic acid as the crosslinker control of both palladium and gold nanoparticles was accomplished. From these results it appears as though further research should result in controlled synthesis of a wide variety of metal nanoparticles through application of the methods developed in this manuscript.

4.9 Experimental

4.9.1 Synthesis of Poly(2-(Dimethylamino)ethyl methacrylate)

4-Cyano-4(dodecylsulfanylthiocarbonyl)sulfanyl pentanoic acid (RAFT 2.2) was synthesized via the reported method[23] on a reduced scale. RAFT 2.2 was used as the charge transfer agent in the synthesis of homopolymers of PDMAEMA. DMAEMA was run through a neutral alumina column to remove the inhibitor and AIBN was recrystallized from methanol. Solutions of RAFT2.0 and AIBN, 1×10^{-1}M and $2 \times 10^{*2}$M were prepared in acetone. The reaction mixtures were prepared in vacuum adapted bulbs in a RAFT:initiatior:monomer ratio of 1:0.2:1000. Degassing of the solution was performed by three or four freeze-pump-thaw cycles on a high vacuum line. The reactions were carried out in an 80℃ oil bath for varying amounts of time depending on the degree of polymerization desired.

Following the polymerization the reaction is quenched by immersion of the reaction vessel in cold water. Small aliquots are removed and the solvent is removed to prepare the sample for GPC analysis. The sample is dissolved in THF and filtered through a 0.45μm PTFE

filter before injection. Size exclusion chromatography was used to measure the molecular weight of the polymers. THF was the eluent and standardization of the instrument was performed with polystyrene standards. The measurements were made with Shimadzu RID-10A and SPD-10AV detectors. Every run was performed at 1mL min^{-1} at 40℃.

If the samples were not the desired weight, the solution was freeze-pump-thawed for 3 cycles and returned to the oil bath. When the desired molecular mass was achieved, the solvent is removed by vacuum. The solid was then dissolved in a small amount of acetone and reprecipitated in methanol. After collecting the solids via vacuum filtration, the solid was dried on the high vacuum line. The solid PDMAEMA was stable at room temperature with exposure to air.

4.9.2 Synthesis of Polymer Nanogels

2.86 x 10^{-5} M solutions of PDMAEMA were prepared in deionized water. PDMAEMA solution was mixed with solutions of diacid reagents. These reaction mixtures were prepared in various combinations to produces ratios ranging up to 7 donor sites, amine groups from the polymer, per 2 protons, from the diacids. Each of these trials were mixed for approximately 20min before being analyzed. DLS was employed to determine the hydrodynamic radius of the nanogels with the different diacids and the different donor to proton ratios. These samples were prepared by taking approximately 0.1mL of the solution and diluting to about 2mL with deionized water. Several trials consisting of 10-30 runs were taken and the results were averaged. TEM was performed on several of the samples. Samples were deposited on 200 mesh carbon coated copper TEM grids from Electron Microscopy Sciences. Single drops of each solution were deposited on the grid and the extra liquid was wicked away with filter paper. This process was repeated until 5-20 drops of the solution have been deposited. Images were then obtained using a JEOL JEM-1400 TEM operating at 120kV.

4.10 References

1. Pachón, L. D.; Rothenberg, G., *Applied Organometallic Chemistry* **2008,** *22* (6), 288-299.

2. Murray, C. B.; Kagan, C. R.; Bawendi, M. G., *Annu. Rev. Mater. Sci.* **2000,** *30*, 545-610.

3. Oishi, M.; Miyagawa, N.; Sakura, T.; Nagasaki, Y., *Reactive & Functional Polymers* **2007,** *67* (7), 662-668.

4. Egorova, E. M.; Revina, A. A., *Colloids and Surfaces a-Physicochemical and Engineering Aspects* **2000,** *168* (1), 87-96.

5. Mukerjee, S.; McBreen, J., *Journal of Electroanalytical Chemistry* **1998,** *448* (2), 163-171.

6. Jiang, S. P.; Liu, Z.; Tang, H. L.; Pan, M., *Electrochimica Acta* **2006,** *51* (26), 5721-5730.

7. Wang, Y.; Herron, N., *J. Phys. Chem.* **1991,** *95* (2), 525-532.

8. Yan, X. P.; Liu, H. F.; Liew, K. Y., *Journal of Materials Chemistry* **2001,** *11* (12), 3387-3391.

9. Lowe, A. B.; Sumerlin, B. S.; Donovan, M. S.; McCormick, C. L., *Journal of the American Chemical Society* **2002,** *124* (39), 11562-11563.

10. Chiang, Y.; Turkevich, J., *Journal of Colloid Science* **1963,** *18* (8), 772-783.

11. Wiley, B.; Sun, Y. G.; Xia, Y., *Accounts Chem. Res.* **2007,** *40* (10), 1067-1076.

12. Sidorov, S. N.; Bronstein, L. M.; Valetsky, P. M.; Hartmann, J.; Colfen, H.; Schnablegger, H.; Antonietti, M., *Journal of Colloid and Interface Science* **1999,** *212* (2), 197-211.

13. Chen, C. W.; Tano, D.; Akashi, M., *Colloid and Polymer Science* **1999,** *277* (5), 488-493.

14. Mayer, A. B. R.; Mark, J. E.; Hausner, S. H., *Journal of Applied Polymer Science* **1998,** *70* (6), 1209-1219.

15. Vamvakaki, M.; Papoutsakis, L.; Katsamanis, V.; Afchoudia, T.; Fragouli, P. G.; Iatrou, H.; Hadjichristidis, N.; Armes, S. P.; Sidorov, S.; Zhirov, D.; Zhirov, V.; Kostylev, M.; Bronstein, L. M.; Anastasiadis, S. H. In *Micellization in pH-sensitive amphiphilic block copolymers in aqueous media and the formation of metal nanoparticles*, 2005; pp 129-147.

16. Duff, D. G.; Edwards, P. P.; Johnson, B. F. G., *J. Phys. Chem.* **1995,** *99* (43), 15934-15944.

17. Swihart, D. L.; Mason, W. R., *Inorganic Chemistry* **1970,** *9* (7), 1749-1757.

18. Davies, J. A.; Anderson, G. K.; Beveridge, T. J.; Clark, H. C., *J. Bacteriol.* **1983,** *156* (2), 837-845.

19. Krueger, S.; Olson, G. J.; Johnsonbaugh, D.; Beveridge, T. J., *Appl. Environ. Microbiol.* **1993,** *59* (12), 4056-4064.

20. Beveridge, T., *Biotechnic & Histochemistry* **2001,** *76* (3), 111-118.

21. Beveridge, T. J.; Schultze-Lam, S., *Microbiology* **1996,** *142* (10), 2887-2895.

22. Link, S.; El-Sayed, M. A., *The Journal of Physical Chemistry B* **1999,** *103* (21), 4212-4217.

23. Farnham, W. B.; Farnham, W. Synthesis of bis(alkylsulfanylthiocarbonyl) disulfides useful for preparing trithiocarbonate RAFT agents involves reacting thiol, sequentially with sodium or potassium t-butoxide, carbon disulfide and iodine in a solvent mixture. WO2005113493-A1, 11 May 2005.